UNIVERSITY OF WESTMINSTER

WestminsterResearch

http://www.westminster.ac.uk/westminsterresearch

The Global Navigation System Scope (GNSScope): a toolbox for the end-to-end modelling simulation and analysis of GNSS.

Renan Kazazoglu

School of Electronics and Computer Science

The Global Navigation System Scope (GNSScope)

A Toolbox for the End-to-End Modelling

Simulation and Analysis of GNSS

University of Westminster

Renan Kazazoglu

A thesis submitted in partial fulfillment of the requirements of the University of Westminster for the degree of Doctor of Philosophy

May 2010

I dedicate this thesis to three very important people in my life. To my father, who instilled a curiosity for science and engineering in me from a very young age, and my mother, whose unconditional love and caring heart has always found a place for all my endeavors. You have always been my role models and my best friends at the same time, always providing me the support that I need. I can never thank you enough for all the sacrifices you have both made for me over the years. And to my dearest partner, best friend and soul mate in life, without whose infinite patience, understanding and constant support, this work would never have come into completion. You have given me nothing but love and caring, always providing me with the courage to continue on my path. I only hope that I can make you feel just as special.

I hereby certify that the research work presented in this thesis is, to the best of my knowledge and belief, original except as referenced in the thesis. I hereby declare that I have not submitted this material, either whole or in part, for a degree at this or any other institution.

Abstract

The thesis provides a detailed overview of the work carried out by the author over the course of the research for the award of the degree of Doctor of Philosophy at the University of Westminster, and the performance results of the novel techniques introduced into the literature. The outcome of the work is collectively referred to as the Global Navigation System Scope (GNSScope) Toolbox, offering a complete, fully reconfigurable platform for the end-to-end modeling, simulation and analysis of satellite navigation signals and systems, covering the signal acquisition, tracking, and range processing operations that take place in a generic Global Navigation Satellite System (GNSS) receiver, accompanied by a Graphical User Interface (GUI) providing access to all the techniques available in the toolbox. Designed and implemented entirely in the MATLAB mathematical programming environment using Software Defined Radio (SDR) receiver techniques, the toolbox offers a novel new acquisition algorithm capable of handling all Phase-Shift Keying (PSK) type modulations used on all frequency bands in currently available satellite navigation signals, including all sub-classes of the Binary Offset Carrier (BOC) modulated signals. In order to be able to process all these signals identified by the acquisition search, a novel tracking algorithm was also designed and implemented into the toolbox to track and decode all acquired satellite signals, including those currently intended to be used in future navigation systems, such as the Galileo test signals transmitted by the GIOVE satellites orbiting the Earth. In addition to the developed receiver toolbox, three novel algorithms were also designed to handle weak signals, multipath, and multiple access interference in GNSScope. The Mirrored Channel Mitigation Technique, based on the successive and parallel interference cancellation techniques, reduces the hardware complexity of the interference mitigation process by utilizing the local code and carrier replicas generated in the tracking channels, resulting in a reduction in hardware resources proportional to the number of received strong signals. The Trigonometric Interference Cancellation Technique, used in cross-correlation interference mitigation, exploits the underlying mathematical expressions to simplify the interference removal process, resulting in reduced complexity and execution times by reducing the number of operations by 25% per tracking channel. The Split Chip Summation Technique, based on the binary valued signal modulation compression technique, enhances the amount of information captured from compressing the signal to reveal specific filtering effects on the positive and negative polarity chips of the spreading code. Simulation case studies generated entirely using the GNSScope toolbox will be used throughout the thesis to demonstrate the effectiveness of the novel techniques developed over the course of the research, and the results will be compared to those obtained from other techniques reported in the literature.

Acknowledgements

Table of Contents

List of Figures

List of Tables

List of Abbreviations

AM	Amplitude Modulation
ASIC	Application Specific Integrated Circuit
ASK	Amplitude Shift Keying
BOC	Binary Offset Carrier
BPSK	Bi-Phase Shift Keying
C/A	Coarse Acquisition
CASM	Coherent Adaptive Sub-Carrier Modulation
CDM	Code Division Multiplexing
CDMA	Code Division Multiple Access
CPU	Central Processing Unit
CRC	Cyclic Redundancy Check
CW	Continuous Wave
DC	Direct Current
DFT	Discrete Fourier Transform
DGPS	Differential GPS
DLL	Delay Locked Loop
DPIC	Delayed Parallel Interference Cancellation
DS-CDMA	Direct Sequence Code Division Multiple Access
DSP	Digital Signal Processing
DSSS	Direct Sequence Spread Spectrum
DTFT	Discrete Time Fourier Transform
ECEF	Earth Centered Earth Fixed
ECI	Earth Centered Inertial
EGNOS	European Geostationary Navigation Overlay Service
ESA	European Space Agency
FDM	Frequency Division Multiplexing
FDMA	Frequency Division Multiple Access
FHSS	Frequency Hopping Spread Spectrum
FM	Frequency Modulation
FPGA	Field Programmable Gate Array
FSK	Frequency Shift Keying
FT	Fourier Transform

GAGAN	GPS Aided Geo Augmentation Navigation
GBAS	Ground Based Augmentation System
GIOVE	Galileo In-Orbit Validation Element
GLONASS	GLObal NAvigation Satellite System
GNS	Global Navigation System
GNSS	Global Navigation Satellite System
GNSScope	Global Navigation System Scope
GPGPU	General Purpose Graphics Processing Unit
GPS	Global Positioning System
GPU	Graphics Processing Unit
GSM	Global System for Mobile Communications
GUI	Graphical User Interface
HOW	Hand Over Word
HPF	High Pass Filter
IDFT	Inverse Discrete Fourier Transform
IDTFT	Inverse Discrete Time Fourier Transform
IF	Intermediate Frequency
IFT	Inverse Fourier Transform
IRNSS	Indian Regional Navigation Satellite System
LAAS	Local Area Augmentation System
LFSR	Linear Feedback Shift Register
LoS	Line of Sight
LPF	Low Pass Filter
MAI	Multiple Access Interference
MSAS	Multi-functional Satellite Augmentation System
NCO	Numerically Controlled Oscillator
OS	Open Service
PC	Personal Computer
PDI	Post Detection Integration
PIC	Parallel Interference Cancellation
PLL	Phase Locked Loop
PM	Phase Modulation
PRN	Pseudo-Random Noise
PRS	Public Regulated Service

PSK	Phase Shift Keying
QAM	Quadrature Amplitude Modulation
QPSK	Quad-Phase Shift Keying
QZSS	Quasi-Zenith Satellite System
RF	Radio Frequency
SAR	Search and Rescue
SBAS	Satellite Based Augmentation System
SDR	Software Defined Radio
SIC	Successive Interference Cancellation
SNR	Signal to Noise Ratio
SoL	Safety of Life
SVn	Space Vehicle Number
TDM	Time Division Multiplexing
TDMA	Time Division Multiple Access
TLM	Telemetry Word
ToA	Time of Arrival
ToF	Time of Flight
TOW	Time of Week
UHF	Ultra High Frequency Band
UTC	Universal Corrected Time
VCO	Voltage Controlled Oscillator
WAAS	Wide Area Augmentation System
WAGE	Wide Area GPS Enhancement System
WGS-84	World Geodetic System - 1984
XOR	Exclusive OR

Chapter 1 Introduction

Since the launch of the first ever Global Navigation Satellite System (GNSS) satellite in 1978, the NAVSTAR 1 used by the NAVSTAR Global Positioning System (GPS), satellite navigation systems and the signals employed in these systems have undergone many changes. Following the launch of the first ten GPS satellites, referred to as the Block I satellites, each new generation of satellites launched thereafter introduced new signals into the system, in some cases on new frequency bands with new modulation schemes, requiring modifications in the receiver designs to be able to cope with these new and improved signals. In the years following the launch of the Block I GPS satellites, new systems were also conceived and put into operation. Development of the Russian GLObal NAvigation Satellite System (GLONASS) began in 1976, with the first satellites being launched as early as 1982 and global coverage being achieved by 1995. Even now, the next generation GPS-M and GLONASS-K satellites carrying the new and improved signals being transmitted on current and new frequency bands are being prepared for operation, some planned to be activated as early as 2011 [1][2][3].

Although the GPS and GLONASS systems are currently the only systems offering global coverage, there are other systems offering regional coverage, some with the aim of achieving global coverage in the near future. The Chinese Beidou-1 navigation system offers regional coverage using a small constellation of geostationary satellites. Currently the system is being updated and new satellites being designed with the aim of offering global coverage in the future using the new Beidou-2 navigation system, also known as the Compass navigation system. With all the activity in the satellite navigation industry, the European Space Agency (ESA) took the initiative to design and develop its own navigation system offering global coverage. Intended to be fully operational by 2013, the Galileo satellite navigation system is currently in the testing phase with two satellites already in orbit and transmitting test signals for validation. In addition to these global navigation systems, regional systems utilizing currently available satellite navigation signals in addition to a small constellation of satellites offering coverage over specific regions are also under development, where the performance of the global navigation system is enhanced over desired regions on earth. The Indian government has taken the initiative to design and develop such a system, the Indian Regional Navigation Satellite System (IRNSS), with the first satellite expected to be launched by 2010. Another such system is the Japanese Quasi-Zenith Satellite System (QZSS), which is expected to be fully operational by the end of 2013. With so many systems already under development and such high demand for satellite based navigation applications from the public sector as well as the private and military sectors, it can be seen that the future will bring many new navigation signals and systems, offering improved performance with more complex modulation schemes and data structures, requiring more efficient receivers which are capable of handling more than one navigation system signal [1] [2] [3].

Following the launch of the first navigation satellites almost thirty years ago, the very first GNSS receiver designs were conceived entirely using analogue signal processing techniques, where primitive microprocessors were used solely for the calculation of the user coordinates. With the rapid developments in Application Specific Integrated Circuits (ASICs) and the industry designing and developing ever faster and more powerful microprocessors, over the years receiver processing technology has shifted from the analogue domain to the digital domain, introducing smaller more compact receivers,

consuming less power and producing faster results. The use of fast and efficient digital signal processing techniques in GNSS receivers has also led to many new receiver architectures to be developed over time. Although ASICs have come a long way since they were first introduced into GNSS receiver designs, the fact that they cannot be altered once the design has been finalized, coupled with the high costs associated with the fabrication processes involved in producing new ASICs, has forced receiver designers to seek alternative techniques for new receiver designs. With the prospect of having a multitude of navigation signals in multiple frequency bands in the near future, being transmitted by different satellites belonging to different navigation systems, indicates that current GNSS receiver technology will have to adapt to accommodate all the changes being introduced, requiring a more flexible architecture for processing current and future navigation signals [2] [3].

Although more than a decade has passed since their first introduction into receiver designs, Software Defined Radio (SDR) techniques have recently come into the spotlight due to the vast improvements in processor technologies offering parallel processing capabilities and very high speed memory access, deeming real time SDR GNSS receiver operation possible. In addition, the high flexibility and low costs associated with reconfiguring an SDR receiver has made them particularly attractive to receiver designers. In light of these new developments, the Global Navigation System Scope (GNSScope) toolbox was designed and developed in MATLAB, utilizing the flexibility, versatility and fast prototyping times offered by SDR receiver techniques, in response to the predicted demand for a fully configurable GNSS receiver toolbox offering end-to-end modeling, simulation and analysis capabilities for current and future satellite navigation signals operating on a multiple frequency multiple constellation setup [4] [5].

1.1 Current State of Art in SDR GNSS Receivers

At the time of the start of the research project, the only publicly available SDR GNSS receiver was the GPS receiver designed by J. Tsui and described in [2]. This single frequency receiver is limited to processing signals from GPS satellites transmitting on the L1 band using only the encryption-free C/A code. Although this set the benchmark for SDR GNSS receivers at the time, its basic design methodology meant that it did not include any

advanced signal processing techniques, such as weak signal processing and multiple access interference mitigation. As this is a single frequency receiver, it is also not capable of processing the more complex signals being transmitted on the other GNSS frequencies, such as the L1 and L5 frequency bands. Finally, as this receiver was designed before the announcement of the European Galileo and the Chinese Beidou-2 satellite navigation systems, it also cannot process the new signals being transmitted from GNSS satellites using the new offset carrier modulation schemes.

A second SDR GNSS receiver was made available to the public domain during the course of the research project, designed by K. Borre and D. Akos, and described in [3]. In this approach there are noticeable improvements made to the receiver described in [2], however once again it is a single frequency SDR GNSS receiver capable of processing satellite signals transmitted only on the L1 band. Although [3] provides information on offset carrier modulation schemes, the accompanying receiver is only capable of processing GPS signals. Finally, similar to the SDR GNSS receiver described in [2], it only contains the basic acquisition and tracking algorithms necessary for the computation of a user position, with no algorithms to handle weak signals, multipath and multiple access interference mitigation in GNSS.

There are several other state of the art GNSS receivers that are commercially available, including the NAMURU platform designed and developed at the University of New South Wales, however they mainly target low-power ASICs, and as such fall out of the scope of this research project.

1.2 Objectives of the Research Project

Given the current state of the art in SDR GNSS receivers, the main objective of the research project was to design and implement a receiver platform for the end-to-end modeling, simulation and analysis of satellite navigation signals, focusing on enhancing the performance of the signal processing aspects associated with GNSS receivers, mainly covering the acquisition and tracking algorithms. In contrast to the current state of the art where only the C/A code GPS signals transmitted on the L1 band are processed, the new receiver would need to be able to carry out time and frequency domain acquisition on all

current and future satellite navigation signals, including the offset carrier modulated signals planned for the upcoming navigation systems, such as the European Galileo and Chinese Beidou-2 systems, on all available frequency bands. The receiver would also need to be able to maintain a successful lock on all acquired satellite signals using novel tracking algorithms capable of processing current and future satellite navigation signals.

Since most of these future signals have not been fully specified, the acquisition and tracking algorithms would need to be highly reconfigurable, to allow for future expansion to cover any new satellite signals being transmitted. Although the main focus of the research project was on the acquisition and tracking algorithms and the associated signal processing techniques, basic point positioning algorithms would also need to be implemented for the evaluation of the results, and to provide a complete solution.

Another objective of the research project was to investigate the performance of existing algorithms dealing with the issues of weak signals and multipath that commonly occur in satellite navigation systems, and to design and implement novel algorithms in response to these findings to enhance receiver performance under such scenarios. As mentioned in the previous section, the receivers described in [2] and [3] do not contain such signal processing techniques, resulting in reduced performance under typical satellite navigation scenarios due to the reduced number of successfully decoded satellite signals.

The final objective of the research project was to design and implement novel techniques for the detection, identification and mitigation of cross-correlation interference, including continuous wave interference, inherent in all multiple-access based communication systems. Once again, classical techniques available in the literature were to be investigated to provide a benchmark for comparing the results obtained from these new algorithms.

1.3 Characteristics of the GNSScope Platform

With these objectives in mind, the GNSScope platform was designed to offer receiver designers a test-bed to analyze their systems and a reference design to benchmark the performance of their own algorithms [5]. Being a complete end-to-end GNSS receiver toolbox, GNSScope also provides an overview of the operations that take place in each

stage of the processing chain, providing valuable insight to new receiver designers. The toolbox is capable of, but not limited to [6] [7]:

- *Time and frequency domain signal acquisition:* In contrast to the current state of the art where only the C/A code GPS signals transmitted on the L1 band are acquired, the GNSScope toolbox was designed to acquire all available signal content on all frequency bands, including the new offset carrier modulated signals being planned for upcoming regional and global satellite navigation systems. As the specifications for most of these new signals have not been finalized, the acquisition algorithm was designed to process all possible modulation schemes on all possible frequency bands. This highly parameterized algorithm can then be configured to acquire any desired satellite signal, without any further coding.

- *Signal tracking based on Costas loop observables:* Once again, the limitation of the current state of the art SDR GNSS receivers to process only the C/A code GPS signals transmitted on the L1 band led to the design of a new tracking algorithm for the GNSScope toolbox to maintain a lock on all acquired satellite signals, including the offset carrier modulated signals being planned for future satellite navigation systems. Similar to the new acquisition algorithm, this highly parameterized tracking algorithm can be configured to track any desired satellite signal without further coding, to accommodate changes to the specifications of the new offset carrier modulated signals.

- *Point positioning using pseudo-range measurements:* Although out of the scope of this research project, basic positioning algorithms necessary to generate a user position on or above the surface of the Earth were also implemented into the GNSScope toolbox in order to provide a complete end-to-end solution rivaling the current state of the art in SDR GNSS receivers. These algorithms were based on pseudo-range measurements made to four or more satellites to provide the final user coordinates expressed in latitude, longitude and altitude, and the receiver clock bias.

- *Carrier phase measurements for advanced positioning algorithms:* Over the course of the research project, advanced techniques of determining more accurate user position solutions based on carrier phase measurements of the satellite signals

were introduced into the literature. Even though the positioning algorithms fell out of the scope of this research project, carrier phase measurement capabilities were implemented into the tracking algorithm in response to the advancements in the field.

In addition to the main characteristics described above, novel new algorithms designed over the course of the research project were also implemented into the GNSScope toolbox, to cope with various signal degrading scenarios. As the state of the art SDR GNSS receivers described in [2] and [3] do not deal with these scenarios, state of the art signal processing techniques from the literature were also investigated for use in benchmarking the novel new techniques introduced into the literature. These can be summarized as follows:

- *Weak signals:* Coherent and non-coherent integration techniques from classical communication theory were adopted for use in the GNSScope toolbox, to improve receiver performance under weak signal conditions. In addition, novel new techniques developed over the course of the research project were also implemented for processing these weak signals.

- *Multipath processing:* Novel new techniques capable of the detection, identification, and mitigation of signals on the multipath were designed and implemented into the receiver toolbox, to further increase the performance of the acquisition and tracking algorithms.

- *Multiple access interference:* In addition to the serial and parallel interference cancellation techniques adopted from classical communication theory, current state of the art in interference detection, identification and removal were implemented into the toolbox to test and benchmark the performance of the novel new algorithms developed over the course of the research project.

Finally, as the GNSScope SDR receiver toolbox was also designed as a signal analysis platform for receiver designers, functions for observing the status of the signals being processed were also designed and implemented into the toolbox. Due to the SDR GNSS receivers described in [2] and [3] mainly focusing on obtaining accurate position

solutions, these features are unique to the GNSScope receiver toolbox. They can be summarized as:

- *Satellite observable analysis:* Functions for observing changes in satellite observables such as position drift, clock analysis and Doppler shift were designed and implemented into the toolbox, providing an insight into the dynamics of the transmitting satellite. This information, coupled with the signal quality analysis results, can be used to enhance the performance of the acquisition and tracking algorithms.
- *Signal quality analysis:* Functions to observe the data rate and duty cycle, and to analyze chip waveform deformations were also designed and implemented into the toolbox, providing valuable information regarding changes in the signal environment, leading to further enhancement of the performance of the acquisition and tracking algorithms.

1.4 Novel Contributions to the State of Art

The GNSScope toolbox and the associated work described in this thesis are the culmination of four years of research into the state of the art of GNSS receiver technologies, and the resulting novel acquisition and tracking algorithms, weak signal and multipath processing techniques, and interference detection and mitigation techniques that were designed, developed and implemented into the toolbox during the research project. The novel contributions to the state of the art GNSS receiver technology can be listed as follows:

- The GNSScope Receiver Design and Development Toolbox for the end-to-end modeling, simulation and analysis of GNS signals, which includes a fully parameterized and reconfigurable generic GNSS receiver offering the following [8]
  - o an easy to use, interactive user interface to control the majority of the algorithms implemented into the toolbox
  - o in-operation parameter fine tuning through reconfigurable acquisition and tracking loops, offering an increased dynamic range and enhanced performance under low signal-to-noise ratio conditions

- the ability to handle weak signals, signals on the multipath, and multiple access interference on the recorded satellite signals using classical techniques as well as novel techniques developed throughout the course of this project

- multiple frequency and multiple standard operation capable of handling not only all currently available satellite navigation signals, but also future planned signals

- A fully parameterized generic GNSS acquisition block capable of handling all current and future navigation signals on all frequency bands, including the new modulation schemes being developed for future navigation systems [9]

- A fully parameterized generic GNSS tracking channel model capable of handling all current and future navigation signals on all frequency bands, including the new modulation schemes being developed for future navigation systems [6]

- The Mirrored Channel Mitigation technique, designed as a unified local interference generation and removal algorithm, forms the basis for most of the classical communication theory based techniques that were implemented into the GNSScope receiver toolbox [7]

- The Trigonometric Interference Cancellation technique for the mitigation of Continuous Wave (CW) and cross-correlation interference effects during the acquisition and tracking operations with minimal overheads and high efficiency [10]

- The Split Chip Summation technique used for the detection and identification of deformations in the underlying chipping waveforms of the spreading codes to improve the match rate of the locally generated and received signals [11]

1.5 Thesis Organization

This thesis is organized to describe each stage in the GNSScope processing chain along with the relevant background information necessary for the understanding of GNSScope's operation. It should be noted that the work described herein focuses solely on the frequency domain processing of satellite navigation signals. However, acknowledging the need for time domain processing capabilities, the toolbox also tracks and stores

information necessary for time domain operations such as accurate carrier phase information for every frame, obtained in the tracking channels. These and other capabilities of the GNSScope toolbox will be described in the relevant chapters, which are organized as follows.

Following the introduction chapter, Chapter 2 will introduce the principles of satellite based navigation, where the concept of positioning will be explored in three dimensional space. In order to be coherent, the position of an object would need to be defined in a well defined coordinate system, which will also be provided in the chapter. Once the reference coordinate system is determined, the Keplerian mathematics used to find the position of a point on the surface of the Earth will be described in detail, including the computation of the satellite positions and perturbations that need to be carried out in order to correct the results for imperfections on the signal path.

Chapter 3 will introduce the characteristics of satellite navigation signals that fall within the scope of this project. First, the fundamentals of signals and systems will be provided to form a coherent basis to understand the equations given throughout this thesis. This will be followed by the specifics of the GPS and Galileo signals, with a short overview of the upcoming global and regional navigation systems provided at the end of the chapter.

Following the background chapters, Chapter 4 will introduce the strong signal operation capabilities of the GNSScope toolbox. An operational overview of a generic GNSS receiver will be given to provide a framework for the rest of the chapter, where a generic receiver is divided into the acquisition, tracking, and range processing blocks. The blocks will be described in detail, with specifics of their novel implementations in GNSScope provided in relevant sections.

Once the strong signal operation of the GNSScope toolbox is completed, Chapter 5 will delve deeper into the more complicated algorithms implemented in the toolbox, where the weak signals, multipath and multiple access interference capabilities of the toolbox will be discussed in detail. This chapter will also introduce all the novel techniques designed and developed throughout this research project, including the mirrored channel

mitigation technique, the trigonometric interference cancellation technique, and the split chip summation technique.

The next chapter, Chapter 6, will provide a case study using a real recorded GNSS signal to present a comprehensive analysis of the performance of the toolbox under real circumstances. Using signals provided by the GPS constellation as well as the GIOVE-A test satellite, the user position will be calculated and located on a map using the Google Maps application. This chapter will also delve into the details of the user interface designed for the toolbox, the responses of the acquisition and tracking channels, and the parameter fine-tuning capabilities of the receiver.

The thesis will end with the conclusions in Chapter 7, where the work presented will be evaluated and conclusions drawn from the results. Work that was out of the scope of this project will also be presented here, with suggestions for future work to be carried out to further improve the efficiency of the algorithms implemented in the toolbox, enabling real-time operation of the receiver.

1.6 Author's Publications and Presentations

Over the course of this research project, certain novel contributions listed in the previous section were published in the open literature to share the accomplishments achieved with the GNSScope toolbox, and to receive feedback and acknowledgement of the effectiveness of these contributions in the public domain. Copies of the publications have been included in the appendix at the end of this thesis document. Each novelty described in these publications will be explained in detail, in their respective sections within the thesis. However, a list of these publications and presentations, along with the publication dates and relevant conference information, is provided below, for the readers' convenience.

- "GNSS Receiver Technologies and Novel Acquisition Algorithms", The Location and Timing Knowledge Transfer Network (KTN) - UK / South Korea Collaborations, KASI, Korea, Dec 2007 [9].
- "A Single Frequency Reconfigurable GNSS Receiver in SDR", The Research Conference, University of Westminster, London, Feb 2008 [12].

- "GNSScope: A Toolbox for End-to-End Modeling, Simulation and Analysis of GNSS", The Navigation Exhibition, The Royal Institute of Navigation, London, Jun 2008 [4].

- "Weak Signal and Multipath Analysis Using GNSScope: A Toolbox for End-to-End Modeling, Simulation and Analysis of GNSS", NAV'08 / ILA'37, The Royal Institute of Navigation, London, Oct 2008 [7].

- "A Low Complexity Cross-Correlation Interference Mitigation Technique for GNSS", European Navigation Conference - Global Navigation Satellite Systems (ENC-GNSS) 2009, Naples, Italy, May 2009 [10].

- "Extending the Applications and Improving the Efficiency of Positioning Through the Exploitation of New GNSS Signals", European Navigation Conference - Global Navigation Satellite Systems (ENC-GNSS) 2009, Naples, Italy, May 2009 [13].

- "Overview of Software Defined Radio GNSS Receivers using GNSScope: A Toolbox for End-to-End Modeling, Simulation and Analysis of GNSS", The GNSS Receiver Design and Signal Processing Workshop 2009, University of Westminster, London, Jun 2009 [5].

- "The GNSScope Toolbox and Novel Tracking Techniques", The ECS Research Conference, University of Westminster, London, Jun 2009 [6].

- "GNSScope and The Split Chip Summation Technique", European Conference on Circuit Theory and Design (ECCTD) 2009, Antalya, Turkey, Aug 2009 [11].

- "GNSScope: A Toolbox for End-to-End Modeling, Simulation and Analysis of GNSS", Thales, Reading, Dec 2009 [8].

In addition to the aforementioned publications, the following journal paper has also been submitted for review to be considered for publication in the GPS Solutions Journal, December 2009.

- "GNSScope: An Extendible Software Defined Radio Receiver System for Multiple Frequency Multiple Constellation GNSS", GPS Solutions Journal, Dec 2009.

Chapter 2 Principles of Satellite Based Navigation

2.1 Introduction

This chapter will introduce the underlying concepts of Global Navigation Systems (GNS). It will give a brief overview of the concept of finding the position of a point in space and the possible complications of such approaches. In order to define a position consistently in any given medium, there is a need for a common coordinate system. The definition of the Earth-Centered Inertial (ECI) and Earth-Centered Earth-Fixed (ECEF) coordinate systems will be followed by the World Geodetic System 1984 (WGS84) reference geode which is used as the standard physical model of the Earth for GNS. This will be followed by the determination of user and satellite positions in the ECEF coordinate system. A brief overview will be given on the satellite orbits and the underlying Keplerian geometry used to compute the positions of the transmitting satellites using the information provided in the navigation data message they transmit. Once the satellite locations are computed, the user position can be determined using pseudo-range measurements made to these satellites. The material presented in this chapter, including the derivations of all the equations are based on references [1], [2], [3], [14], [15] and [16]. Further details regarding the Global Positioning System (GPS) and Galileo were obtained from [17] and [18], respectively.

2.2 The Global Positioning Concept

The global positioning concept relies on the fact that the position of any point in space can be calculated using measurements to beacons with known locations in space. This point can be illustrated using examples in 1D and 2D, extended to 3D positioning. The first case of finding the position of a point along a line is demonstrated in Figure 2.1, below [2]. If a user was to make a measurement to a single beacon with a known location along this line, they would end up with two distinct position solutions: one to the left of the beacon and another to the right of the beacon, with only one of them being the correct solution, as illustrated in the figure. In order to eliminate the incorrect solution a second measurement needs to be made to a second beacon with a known position on this line [2] [3].
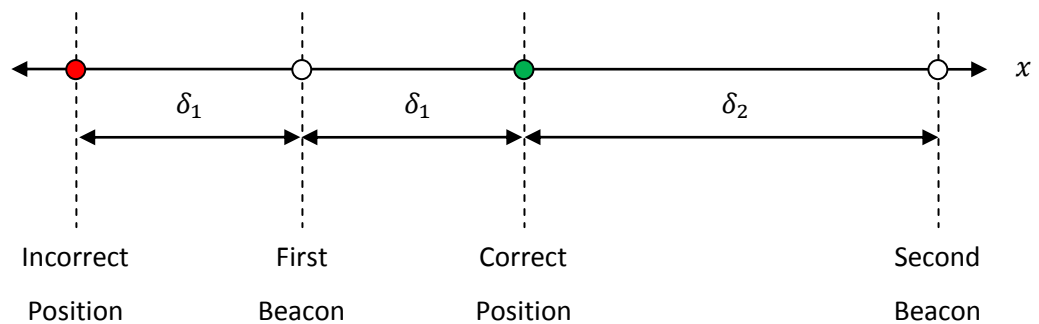
Figure 2.1 - 1D Positioning Example

In the two-dimensional case of finding the position of a point on a plane, using two distances measured to two beacons with known locations, as in the 1D case, would result in two distinct position solutions, since the equidistance trace of a point on a plane results in a circle, with two such circles intersecting at two points. In order to eliminate the incorrect solution a third measurement needs to be made to a third beacon with a known position on this plane, as illustrated in Figure 2.2, below [2].
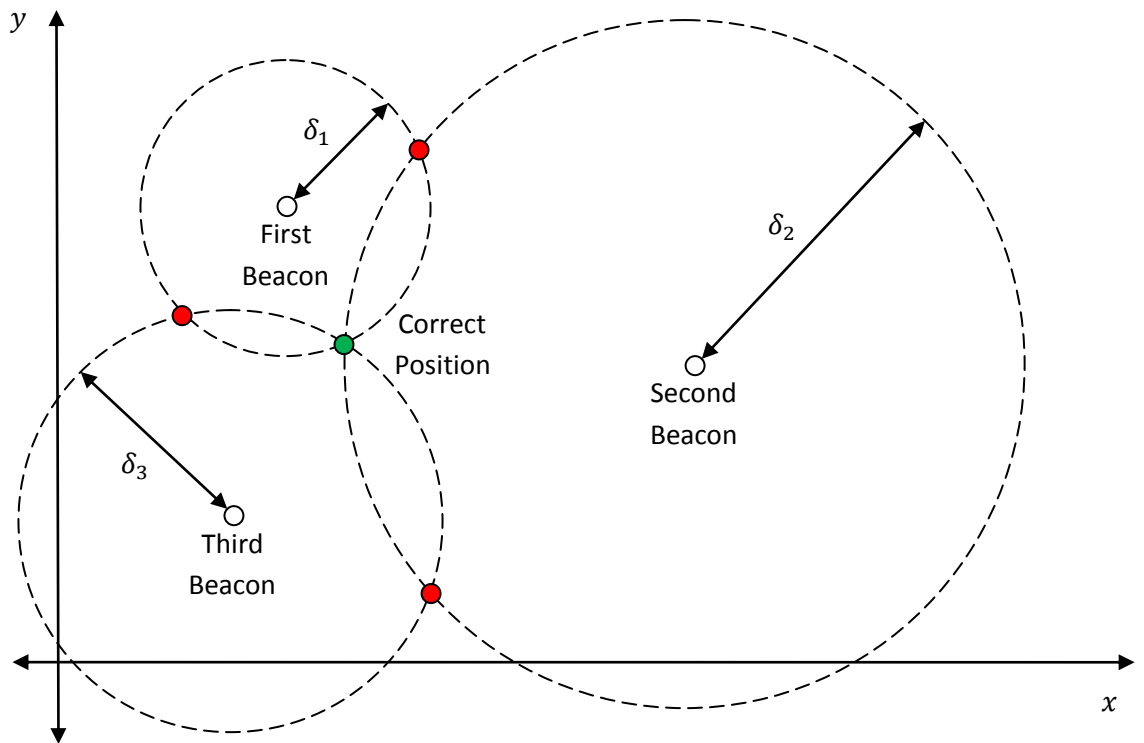
Figure 2.2 - 2D Positioning Example

This technique can be trivially extended to the three-dimensional case of finding the position of a point in space. The equidistance trace of a point in space results in a sphere. The intersection of two such equidistance spheres would result in a circle. The intersection of this circle with a third equidistance sphere would result in two points in space. In order to eliminate the incorrect position solution, a fourth distance measurement must be made to a fourth beacon with a known position in space. In the case of determining the user position on the surface of the Earth using a GNS, this fourth measurement could be avoided by eliminating the solution in space, resulting in the need for only three measurements to determine the users' position. However, this may not be possible in aerial or space based navigation, as the solution in space is not necessarily the incorrect solution [2] [3] [16].

In a Global Navigation Satellite System (GNSS), as the name suggests, satellites are used as the beacons for ranging measurements [1]. The position of these satellites is encoded into the navigation message they transmit, which is continuously updated with new position information. When a user generates a position request, the receiver determines the users distance to visible navigation satellites using pseudo-range measurements to compute a solution. The pseudo-ranges are calculated using Time-of-Arrival (ToA) measurements. This concept relies on the measurement of the Time-of-Flight (ToF) of the navigation message being transmitted from a satellite at a known location. The ToF is calculated by taking the difference between the ToA of the signal and the time it was transmitted from the satellite, which is also encoded into the same navigation data message. As the signal travels at the speed of light, the ToF is multiplied by the speed of light to obtain the required pseudo-range measurement [2] [3].
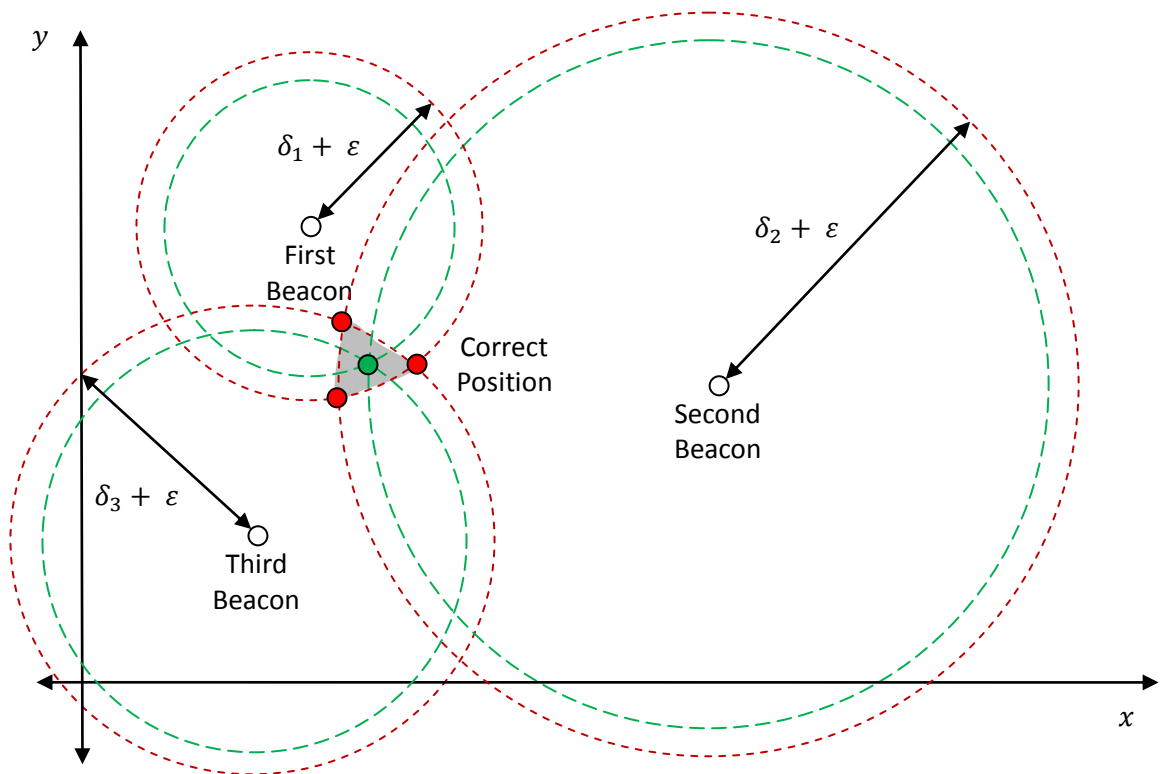
Figure 2.3 - 2D Positioning Example with Clock Bias Effects

The above discussion assumes that the receiver clock and the satellite clocks are synchronous. However, in most practical cases, this assumption does not hold true, resulting in the introduction of a constant bias error, denoted here as ε, on the measured pseudo-ranges to the satellites due to the incorrect ToF measurement. This is illustrated in Figure 2.3, above, for the 2D positioning problem introduced earlier in the section. In this case, rather than having a single intersection point for all three equidistance trace circles, denoted with a green point in the figure, there will be three separate intersection points, denoted with red points in the figure. These three points would converge to the actual position of the user if the clock bias could be compensated for. Thus, in addition to the four satellites (three in the case of finding the position on the surface of the Earth) required to determine the user position, a fifth satellite (fourth in the case of finding the position on the surface of the Earth) is required to compensate for the clock bias error.

In addition to the common receiver clock bias error, there are other factors that affect the pseudo-range measurements, such as errors in the satellite position information included in the navigation data message, ionospheric and tropospheric delays affecting the ToF measurements, and errors introduced from measurement noise in the receiver, which all contribute to inaccuracies in the user position calculations. However, ionospheric errors can be corrected using a dual- or multiple-frequency receiver, while tropospheric errors can be compensated using tropospheric delay models, leaving the receiver clock bias error as the dominant bias on the measured pseudo-ranges [2] [3].

2.3 Determination of User Position in Cartesian Coordinates

In order to determine the user position, as mentioned in the previous section, a minimum of four pseudo-range measurements need to be made to four satellites with known locations in order to handle the receiver clock bias errors in addition to the coordinates in the x, y and z dimensions [1] [2] [3]. Figure 2.4 illustrates this scenario, with the user located at the green point in the figure with coordinates (x_u, y_u, z_u), the four satellites located at the white points in the figure with coordinates (x_i, y_i, z_i) where i denotes the satellite number, and the four pseudo-range measurements to these four satellites denoted by ρ_i.
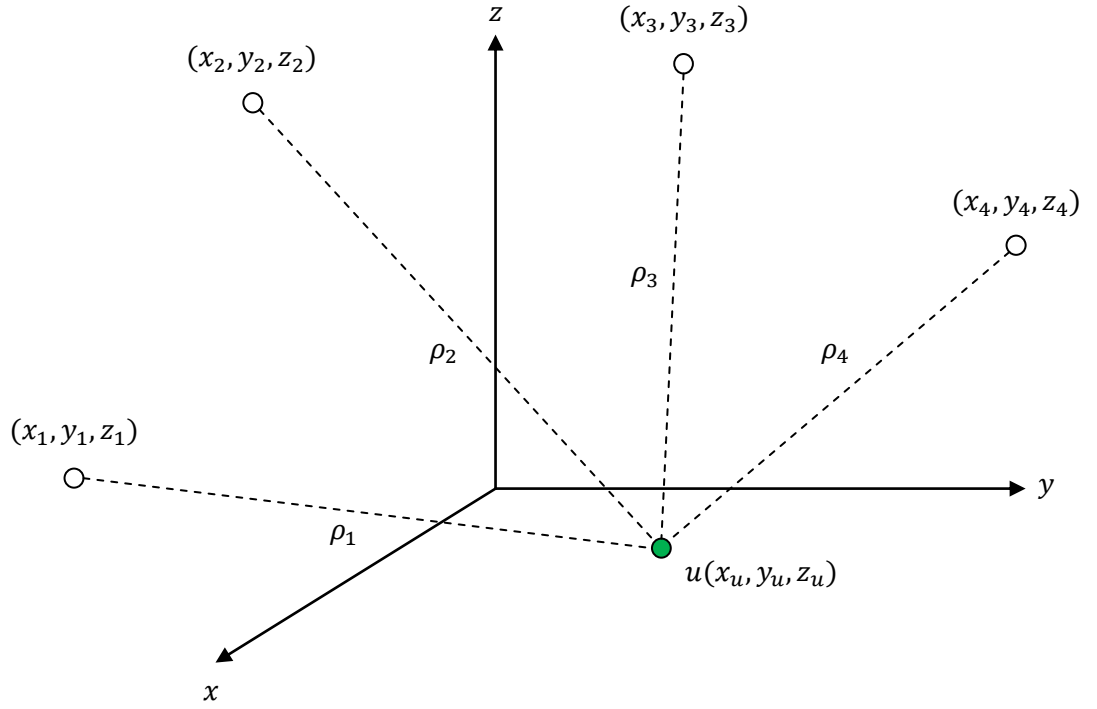
Figure 2.4 - Pseudo-Range Measurements Using Four Satellites

Using the four satellite scenario illustrated above, the measured pseudo-ranges can be related to the satellite and user coordinates as follows [3]:

$$\rho_1 = \sqrt{(x_1 - x_u)^2 + (y_1 - y_u)^2 + (z_1 - z)^2} + b_u$$

$$\rho_2 = \sqrt{(x_2 - x_u)^2 + (y_2 - y_u)^2 + (z_2 - z)^2} + b_u$$

$$\rho_3 = \sqrt{(x_3 - x_u)^2 + (y_3 - y_u)^2 + (z_3 - z)^2} + b_u$$

$$\rho_4 = \sqrt{(x_4 - x_u)^2 + (y_4 - y_u)^2 + (z_4 - z)^2} + b_u$$

Eq. 2.1

where b_u denotes the constant user clock bias, converted to the user range bias through:

$$b_u = c \times b_{ut}$$

Eq. 2.2

where b_{ut}, denotes the user clock bias. This equation set can be rewritten for the generalized case of having $n \geq 4$ satellites, as follows [2]:

$$\rho_i = \sqrt{(x_i - x_u)^2 + (y_i - y_u)^2 + (z_i - z_u)^2} + b_u$$

Eq. 2.3

where $i = 1,2,3 \dots n$. This equation set can be linearized through differentiation to obtain the following [2]:

$$\delta\rho_i = \frac{(x_i - x_u)\delta x_u + (y_i - y_u)\delta y_u + (z_i - z_u)\delta z_u}{\rho_i - b_u} + \delta b_u \qquad \text{Eq. 2.4}$$

In order to obtain the user coordinates x_u, y_u, and z_u, and the clock bias b_u, this equation set needs to be solved iteratively starting from an assumed initial user location, such as the centre of the Earth with no clock bias, making δx_u, δy_u, δz_u, and δb_u the new unknowns. The equation set can be rearranged to reflect this, as follows [2]:

$$\delta\rho_i = \frac{x_i - x_u}{\rho_i - b_u}\delta x_u + \frac{y_i - y_u}{\rho_i - b_u}\delta y_u + \frac{z_i - z_u}{\rho_i - b_u}\delta z_u + \delta b_u \qquad \text{Eq. 2.5}$$

thus becoming a set of linear equations, where the satellite coordinates (x_i, y_i, z_i) are calculated using data extracted from the navigation message. In order to further simplify this linear equation set, new variables can be introduced, as follows [2]:

$$\alpha_{i1} = \frac{x_i - x_u}{\rho_i - b_u}, \qquad \alpha_{i2} = \frac{y_i - y_u}{\rho_i - b_u}, \qquad \alpha_{i3} = \frac{z_i - z_u}{\rho_i - b_u} \qquad \text{Eq. 2.6}$$

Using these new variables, the above linear equation set can be rewritten, as follows [2]:

$$\overrightarrow{\delta\rho} = A\,\overrightarrow{\delta x} \qquad \text{Eq. 2.7}$$

where;

$$A = \begin{bmatrix} \alpha_{11} & \alpha_{12} & \alpha_{13} & 1 \\ \alpha_{21} & \alpha_{22} & \alpha_{23} & 1 \\ \dots & \dots & \dots & \dots \\ \alpha_{n1} & \alpha_{n2} & \alpha_{n3} & 1 \end{bmatrix} \quad \overrightarrow{\delta x} = \begin{bmatrix} \delta x_u \\ \delta y_u \\ \delta z_u \\ \delta b_u \end{bmatrix} \text{ and } \overrightarrow{\delta\rho} = \begin{bmatrix} \delta\rho_1 \\ \delta\rho_2 \\ \delta\rho_3 \\ \delta\rho_4 \end{bmatrix} \qquad \text{Eq. 2.8}$$

Since there are more equations than unknowns for this set of linear equations, the solution can be obtained using the least-squares technique. Since the alpha matrix won't be a square matrix for $n > 4$, its inverse can be obtained using the pseudo-inverse operation, as follows [1] [2]:

$$\overrightarrow{\delta x} = [A^T A]^{-1} A^T \overrightarrow{\delta\rho} \qquad \text{Eq. 2.9}$$

When $n = 4$ the alpha matrix will be a square matrix and its inverse can simply be obtained using the matrix inverse operation. This equation set will then be solved iteratively, starting from an initially assumed user location and clock bias, such as the

centre of the Earth with no receiver clock bias, or synchronous receiver and transmitter clocks. The iteration process will aim to minimize the error function [2]:

$$\varepsilon = \sqrt{\delta x_u^2 + \delta y_u^2 + \delta z_u^2 + \delta b_u^2}$$
Eq. 2.10

2.4 Reference Coordinate Systems

In order to generate the equations determining user position, and express them coherently, there is a need for reference coordinate systems. In general, there are two reference coordinate systems utilized in GNSS. The Earth-Centered Inertial (ECI) coordinate system is used to describe the motion of the satellites and their orbits. The origin of the ECI coordinate system is the center of mass of Earth, while the *xy*-plane coincides with the equatorial plane. The direction of the *x*-axis is fixed in the direction of the vernal equinox, which is defined as the line of intersection of the equatorial plane and the Earth's plane of orbit, and the *z*-axis is normal to the equatorial plane, in the direction of the North Pole. As the *x*-axis is fixed relative to the celestial sphere, the coordinate system is said to be inertial. The Earth-Centered Earth-Fixed (ECEF) coordinate system rotates with the Earth, providing a fixed coordinate system for the computation of the users' position. As in the ECI coordinate system, the origin lies at the centre of mass of the Earth and the *xy*-plane is coincident with the equatorial plane. The *x*-axis points in the direction of 0° longitude, the *y*-axis points in the direction of the 90° east longitude, and the *z*-axis is chosen to be normal to the equatorial plane in the direction of geographical north [3].

2.4.1 World Geodetic System 1984 (WGS-84)

In order to be able to describe the users' position in relation to the surface of the Earth, it is necessary to have a model of the Earth representing its shape and certain other properties for orbital calculations. The World Geodetic System 1984 (WGS-84) is the standard physical model used to describe the Earth in GNSS. WGS-84 defines an ellipsoidal Earth, as shown in Figure 2.5, where cross-sections of the Earth parallel to the equatorial plane are circular [1] [2].
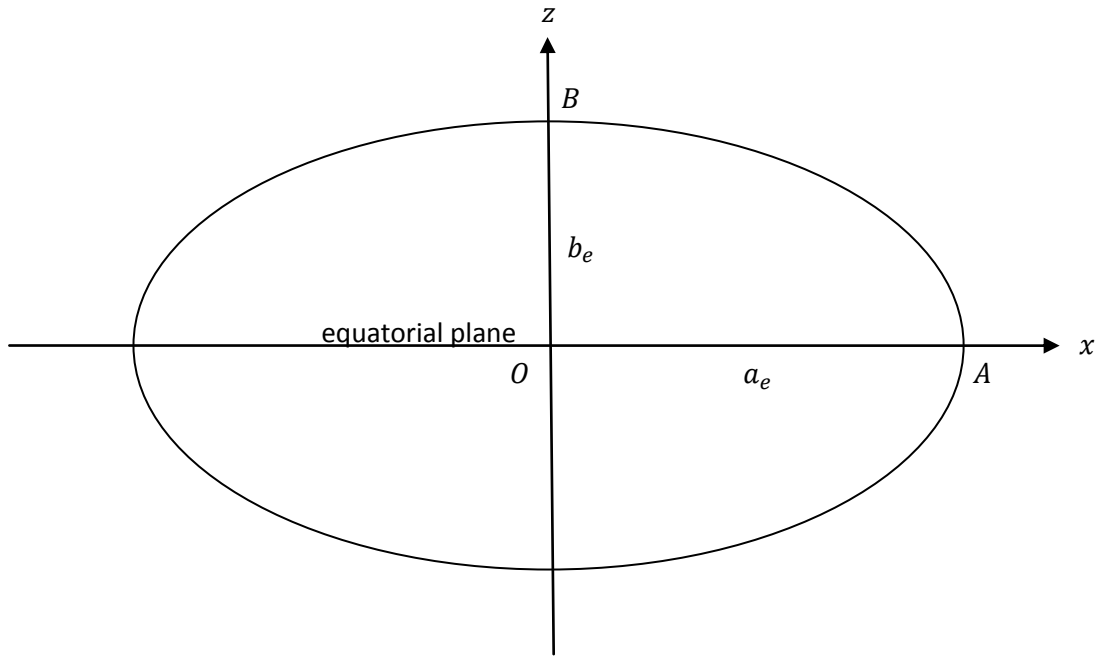
Figure 2.5 - The World Geodetic System 1984 cross-section of the Earth

The governing equations for an ellipsoidal Earth with semi-major axis a_e, semi-minor axis b_e, and focal separation $2c_e$, are given below [2]:

$$\frac{x^2}{a_e^2} + \frac{z^2}{b_e^2} = 1, \qquad a_e^2 - b_e^2 = c_e^2$$

Eq. 2.11

where $a_e = 6378137 \pm 2\ m$ and $b_e = 6356752.3142\ m$ for the Earth in WGS-84. The eccentricity e_e of the Earth can be calculated using [2]:

$$e_e = \frac{c_e}{a_e} = \frac{\sqrt{a_e^2 - b_e^2}}{a_e} = 0.0818191908426$$

Eq. 2.12

The ellipticity e_p, or flattening, of the Earth can be calculated using [2]:

$$e_p = \frac{a_e - b_e}{a_e} = 0.00335281066474$$

Eq. 2.13

The eccentricity and ellipticity are related to each other through the following equation [1] [2]:

$$e_e^2 = e_p(2 - e_p)$$

Eq. 2.14

In addition to the semi-major axis a_e, semi-minor axis b_e, focal separation $2c_e$, eccentricity e_e and ellipticity e_p, the WGS-84 reference geode provides the following constants for the physical model of the Earth [1] [2]:

$$\mu = 3.986005 \times 10^{14} \ m^3/sec^2$$

$$\dot{\Omega}_{ie} = 7.2921151467 \times 10^{-5} \ rad/sec$$

$$\pi = 3.1415926535898$$

Eq. 2.15

$$c = 2.99792458 \times 10^8 \ m/sec$$

where μ is the Earth's universal gravitational parameter, $\dot{\Omega}_{ie}$ is the Earth's rotational rate, and c is the speed of light [2].

2.4.2 Direction Cosine Matrix

The direction cosine matrix is a transformation used to convert coordinates from one system to another. The 2D example presented in Figure 2.6 will be used to explain the underlying geometry, which will then be extended to an n-dimensional case [2].
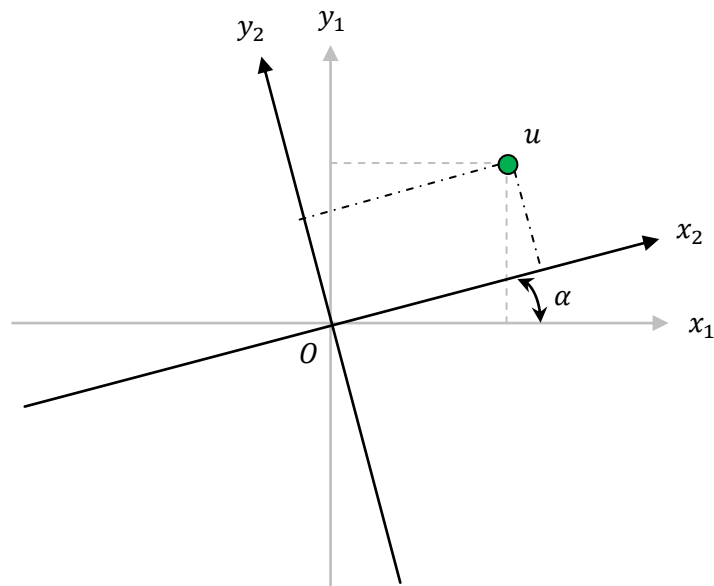
Figure 2.6 - 2D Coordinate Transformation

The figure depicts two coordinate systems, the second one obtained by rotating the first coordinate system by angle α around the origin, O. The point u has the coordinates (X_1, Y_1) in the first coordinate system and (X_2, Y_2) in the second coordinate system. Using simple geometry, (X_2, Y_2) can be related to (X_1, Y_1) as follows:

$$\begin{bmatrix} X_2 \\ Y_2 \end{bmatrix} = \begin{bmatrix} \cos\alpha & \sin\alpha \\ -\sin\alpha & \cos\alpha \end{bmatrix} \begin{bmatrix} X_1 \\ Y_1 \end{bmatrix}$$

Eq. 2.16

In its generalized form, the direction cosine matrix is written as follows:

$$C_1^2 = \begin{bmatrix} \cos\,(X_1\ on\ X_2) & \cos\,(Y_1\ on\ X_2) \\ \cos\,(X_1\ on\ Y_2) & \cos\,(Y_1\ on\ Y_2) \end{bmatrix}$$

Eq. 2.17

where C_1^2 indicates that the coordinate system is transformed from system 1 to system 2, and $\cos\,(X_1\ on\ X_2)$ represents the cosine of the angle between x_1 and x_2, where the direction is taken to be from x_1 to x_2.

The case of transforming three dimensional coordinate systems can be solved by splitting the transformation into its two dimensional transformation components. If a system was to be rotated around its x-axis by angle α, the resulting 3D transformation matrix would be [2]:

$$C_1^2 = \begin{bmatrix} 1 & 0 & 0 \\ 0 & \cos\alpha & \sin\alpha \\ 0 & -\sin\alpha & \cos\alpha \end{bmatrix}$$

Eq. 2.18

Following this, if the system was to be rotated around its y-axis by angle β, the resulting 3D transformation matrix would be [2]:

$$C_2^3 = \begin{bmatrix} \cos\beta & 0 & \sin\beta \\ 0 & 1 & 0 \\ -\sin\beta & 0 & \cos\beta \end{bmatrix}$$

Eq. 2.19

The overall transformation matrix would then be [2]:

$$C_1^3 = C_2^3 C_1^2 = \begin{bmatrix} \cos\alpha & \sin\alpha & 0 \\ -\sin\alpha\cos\beta & \cos\alpha\cos\beta & \sin\beta \\ \sin\alpha\sin\beta & -\cos\alpha\sin\beta & \cos\beta \end{bmatrix}$$

Eq. 2.20

In general, coordinates in any system can be transformed to any other system using [2]:

$$C_1^n = C_{n-1}^n C_{n-2}^{n-1} \dots C_2^3 C_1^2$$

Eq. 2.21

2.5 Determination of User Position on the Surface of Earth

The user coordinates calculated in the previous section are given in the Cartesian coordinate system. However, it is desirable to convert these coordinates into a point on or above the surface of the Earth using spherical coordinates and the WGS-84 reference geode. If the shape of the Earth was assumed to be a perfect sphere, the relationship between the Cartesian user coordinates x_u, y_u, z_u, and the spherical coordinates of geocentric latitude (L_c - the angle between the xy-plane and the line connecting the user to the centre of the Earth), longitude (l - the angle between the x-axis and the projection onto the xy-plane of the line connecting the user to the centre of the Earth), and altitude (h -the height of the user above the surface of the Earth), would be as illustrated in Figure 2.7, below, where the solid lines represent the surface of the Earth and the user is located at the green point in the figure [1][2][3].
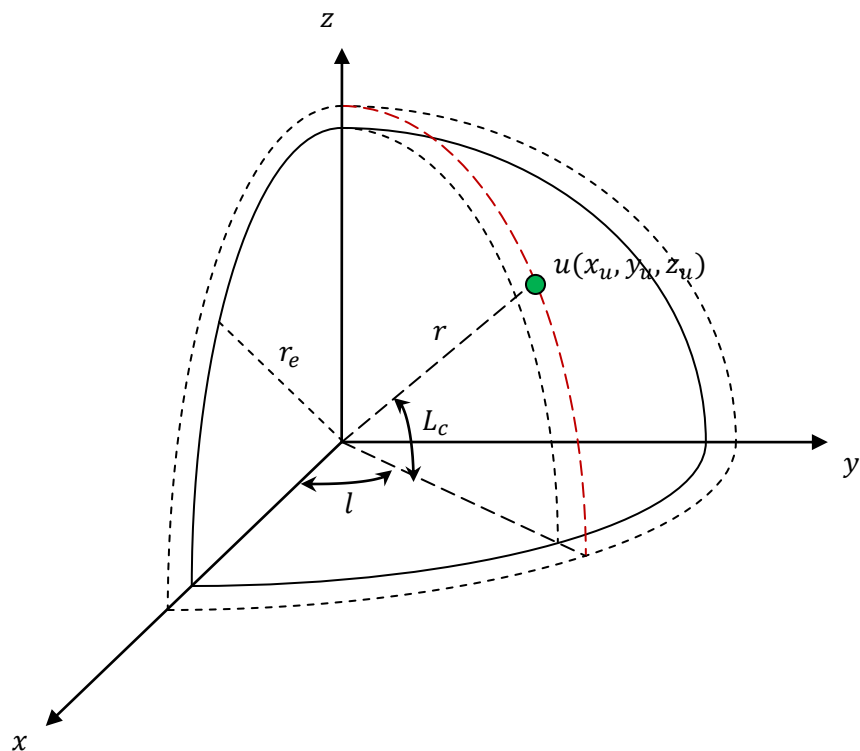
Figure 2.7 - Relationship between Cartesian User Coordinates and Spherical Coordinates

Using the geometry above, the following equations can be derived for converting the Cartesian coordinates into spherical coordinates [2]:

$$L_c = \tan^{-1}\left(\frac{z_u}{\sqrt{x_u^2 + y_u^2}}\right)$$

<div align="right">Eq. 2.22</div>

$$l = \tan^{-1}\left(\frac{y_u}{x_u}\right)$$

<div align="right">Eq. 2.23</div>

$$h = r - r_e$$

<div align="right">Eq. 2.24</div>

where r_e is the radius of the perfect spherical Earth, and r is the distance of the user from the centre of the perfect spherical Earth, obtained using the following equation [2]:

$$r = \sqrt{x_u^2 + y_u^2 + z_u^2}$$

<div align="right">Eq. 2.25</div>

However, the geometry of the Earth is not a perfect sphere, but rather an ellipsoid as described in the WGS-84 reference geode. Hence, even though the equation given for the longitude is correct, the latitude and altitude equations need to be modified to take into account the actual geometry of the Earth. In order to demonstrate this, the geocentric latitude (L_c), geodetic latitude (L), and altitude (h) are illustrated on the cross-section of an ellipsoidal Earth, along with the relevant angles, in Figure 2.8, below [1] [2].
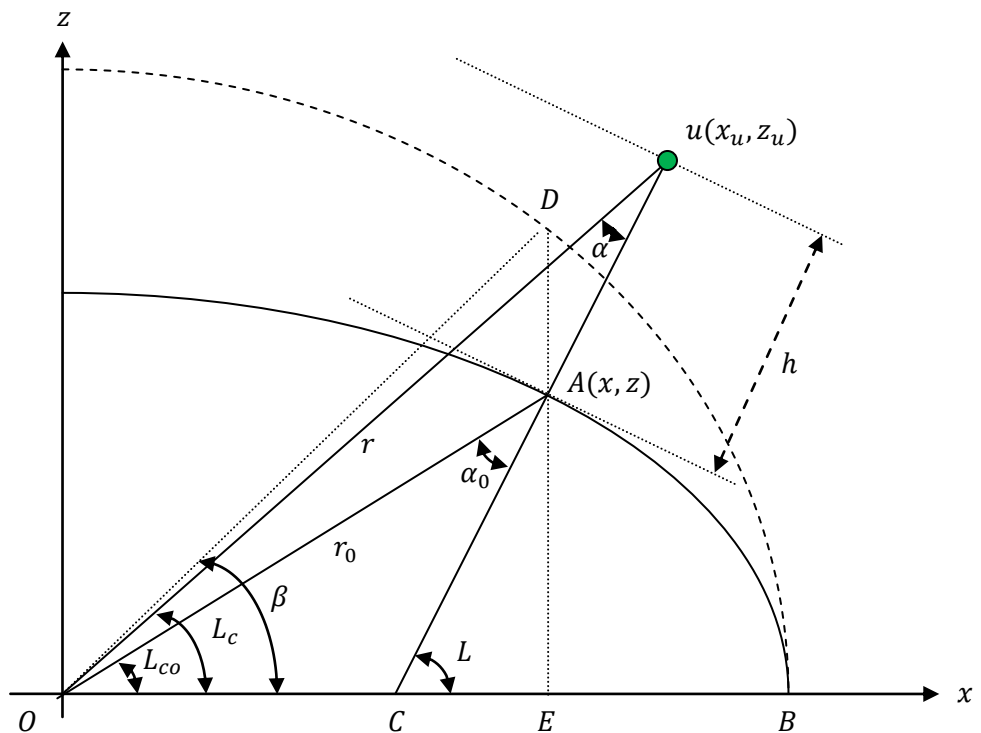
Figure 2.8 - Geometry of Earth Illustrating Geocentric and Geodetic Latitude

In this figure, the line UC is normal to the WGS-84 reference ellipsoid at point A. The line AE is perpendicular to the equatorial plane along the x-axis. D is the projection of the line AE onto a perfect spherical Earth with radius equal to the semi-major axis a_e. Using this geometry, the coordinates $A(x, z)$ of the users' projection on the surface of the Earth can be calculated as follows [2]:

$$x = a_e \cos \beta, \qquad z = b_e \sin \beta$$

<div align="right">Eq. 2.26</div>

Using the above equations, the relationship between the angle β and the geodetic latitude (L) can be found as follows [2]:

$$\tan L = \frac{a_e}{b_e} \tan \beta = \frac{\tan \beta}{\sqrt{1 - e_e^2}}$$

<div align="right">Eq. 2.27</div>

where the final form is obtained using Eq. 2.14 [2] [3].

2.5.1 Determination of Geodetic Latitude

The geodetic latitude (L) can be extracted from Figure 2.8 using the following equation [2]:

$$L = L_c + e_p \sin 2L$$

<div align="right">Eq. 2.28</div>

As this is a non-linear equation, it can be solved iteratively using the following form [2]:

$$L_{i+1} = L_c + e_p \sin 2L_i$$

<div align="right">Eq. 2.29</div>

where $L_0 = L_c$ is taken as the initial condition of the iteration and the equation is solved until the iteration difference $(L_i - L_{i-1})$ is below a predetermined threshold. The value of L_c is calculated using the geocentric latitude equation given in Eq. 2.22 [2] [3].

2.5.2 Determination of Altitude

Assuming the angle $\propto$ will be relatively small when the satellites are above the user, the following relationship can be derived using the AOU triangle [1] [2]:

$$r \cong r_0 + h$$

<div align="right">Eq. 2.30</div>

Thus, the altitude (h) can be found using the following equation [1] [2]:

$$h = r - r_0$$

<div align="right">Eq. 2.31</div>

The value of r_0 is determined using the equation of an ellipse, as given below [1] [2]:

$$r_0 \approx a_e\left(1 - e_p \sin^2 L\right)$$

<div align="right">Eq. 2.32</div>

The resulting equation for the user altitude is [1] [2]:

$$h = r - r_0 = \sqrt{x_u^2 + y_u^2 + z_u^2} - a_e\left(1 - e_p \sin^2 L\right)$$

<div align="right">Eq. 2.33</div>

A more detailed overview of these equations can be found in [1] [2] [3].

2.6 Determination of the Satellite Position

In order to obtain the user position using pseudo-range measurements, the positions of the satellites need to be determined. Although each satellite transmits supplementary information regarding its position at the time of transmission, such as the mean anomaly, this information is not sufficient to calculate the exact position of the satellite. In order to determine the exact position of the satellite, the elliptical orbit it traverses and Kepler's Laws need to be taken into consideration.

2.6.1 Kepler's Laws

There are three basic laws used in orbital mathematics that were laid out by Kepler, which are listed below [2].

1st Law   The orbit of each planet is an ellipse with its parent star at a focus.

2nd Law   The line joining the planet to its parent star sweeps equal areas in equal times.

3rd Law   The square of the period of a planet is proportional to the cube of its mean distance from its parent star.

These laws also apply to the orbits of GNSS satellites, with the orbiting satellite acting like a planet, and the Earth at one of the foci of its elliptical orbit. This is illustrated in Figure 2.9, below [1] [2]. The satellite, S, traverses the elliptical orbit illustrated using dashed lines. The Earth is located at the prime focus, F, of this orbit. The point V is the closest point to the prime focus on the satellite orbit and is referred to as the perigee, while the apogee is defined as the farthest point. The angle v is defined as the true anomaly at time t, and the angle E is defined as the eccentric anomaly at time t. The point P is the

projection of satellite S onto the x-axis, while the point Q is the projection of satellite S onto a circular orbit with a radius equal to a_s, the semi-major axis of the actual orbit.
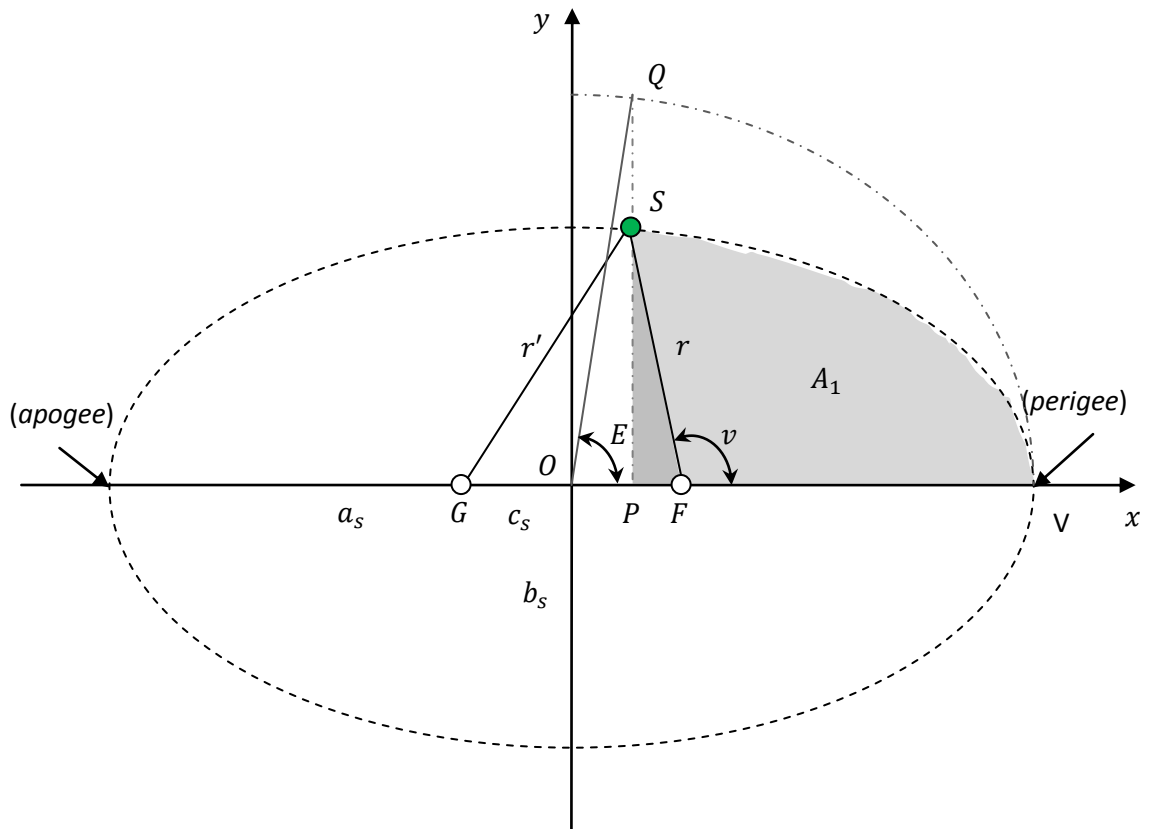
Figure 2.9 - Geometry of the Satellite Orbit

Using the geometry in Figure 2.9 and Kepler's Second Law, the following equation can be derived[2]:

$$\frac{t - t_p}{T} = \frac{A_1}{\pi a_s b_s}$$

Eq. 2.34

where t is the time at which the satellite is at position S, t_p is the time the satellite was at the perigee, T and $\pi a_s b_s$ are the period and area of the elliptical satellite orbit. A_1 is the shaded area of the orbit covered by the satellite during the time $t - t_p$, which is calculated using the following expression [2]:

$$A_1 = \frac{a_s b_s}{2} (E - e_s \sin E)$$

Eq. 2.35

2.6.2 Mean Anomaly

Mean anomaly, M, is defined as follows [1] [2]:

$$M \equiv (E - e_s \sin E) = \frac{2\pi}{T}(t - t_p)$$

<div align="right">Eq. 2.36</div>

Based on this equation, the mean motion, n, can be defined as the average angular velocity of the satellite, as follows [1] [2]:

$$n = \frac{2\pi}{T} = \sqrt{\frac{\mu}{a_s^3}}$$

<div align="right">Eq. 2.37</div>

Hence, the final equation for the mean anomaly, also referred to as Kepler's Equation, becomes [1] [2]:

$$M \equiv (E - e_s \sin E) = n(t - t_p)$$

<div align="right">Eq. 2.38</div>

From Kepler's Equation it can be seen that M and t are linearly related, which is the reason for this term being called mean anomaly [1] [2] [3].

2.6.3 True Anomaly

The true anomaly, v, is used in determining the true position of the satellite. In order to calculate the true anomaly, it is necessary to determine the value of the eccentric anomaly, E, as follows [2]:

$$E = M + e_s \sin E$$

<div align="right">Eq. 2.39</div>

where the mean anomaly, M, and the eccentricity, e_s, of the elliptical satellite orbit are obtained from the navigation data message transmitted by the satellite. This equation is solved iteratively until the difference between successive approximations becomes sufficiently low. Once the value of the eccentric anomaly is determined, the unambiguous value of the true anomaly can be obtained using the following expression [2]:

$$v = v_1 \, \text{sign} \, v_2$$

<div align="right">Eq. 2.40</div>

where,
$$v_1 = \cos^{-1}\left(\frac{\cos E - e_s}{1 - e_s \cos E}\right), \quad v_2 = \sin^{-1}\left(\frac{\sqrt{1 - e_s^2}\sin E}{1 - e_s \cos E}\right) \qquad \text{Eq. 2.41}$$

It can be seen from that the true anomaly depends only on e_s and E, where e_s is obtained from the navigation data message transmitted by the satellite, and E is calculated from M using Eq. 2.39, which is also obtained from the navigation data message [1] [2] [3].

2.6.4 Satellite Orbit Frame to ECEF Transform

In the above discussion, the satellite position is calculated in the satellite orbit frame, where the origin is at the Earth's center of mass, the x-axis is in the direction of the perigee, the z-axis is perpendicular to the satellite orbit plane, and the y-axis is in the direction forming a right-hand coordinate system, as illustrated in Figure 2.10, below [2]. The coordinates of the satellite in this reference frame are as follows [2]:

$$x = r\cos v, \qquad y = r\sin v, \qquad z = 0 \qquad \text{Eq. 2.42}$$

where the value of r is computed using the following expression [2]:

$$r = a_s(1 - e_s \cos E) \qquad \text{Eq. 2.43}$$

and E is computed using Eq. 2.39, while a_s and e_s are obtained from the navigation data.
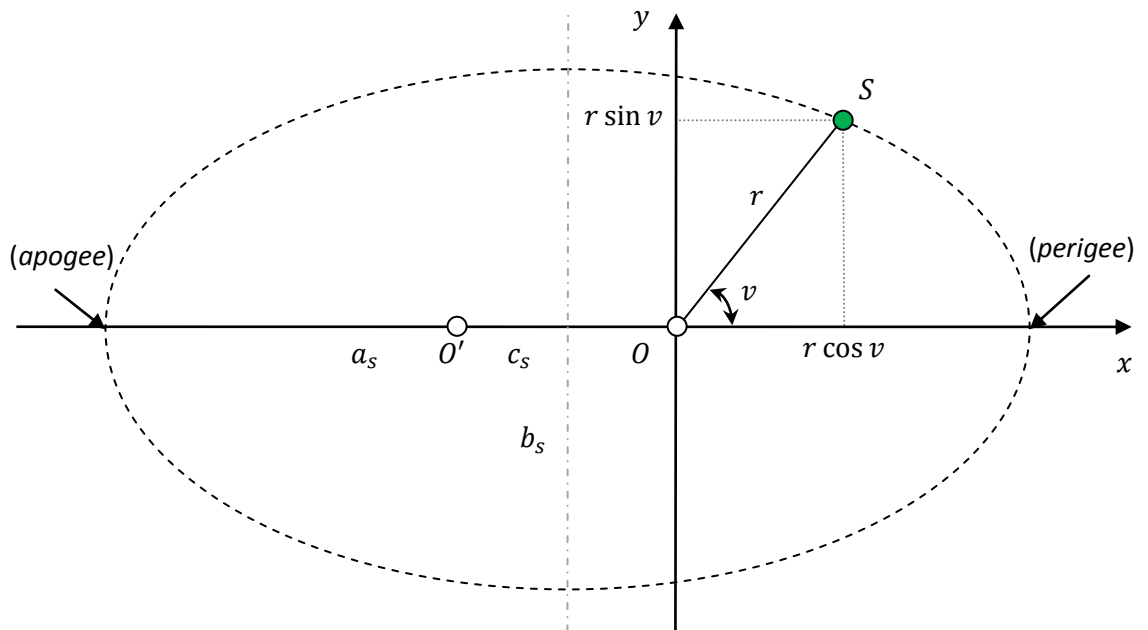
Figure 2.10 - The Satellite Orbit Frame

However, in order to be able to compute the user position, it is necessary to determine the satellite positions in the ECEF coordinate system. To convert the satellite coordinates from the satellite orbit frame to the ECEF coordinate system, the direction cosine matrix transformation, mentioned earlier in the chapter, is used. The set of intermediate transformations necessary to complete the conversion are illustrated including the relevant angles used in transforming from one frame of reference to another, in Figure 2.11, below [1] [2].
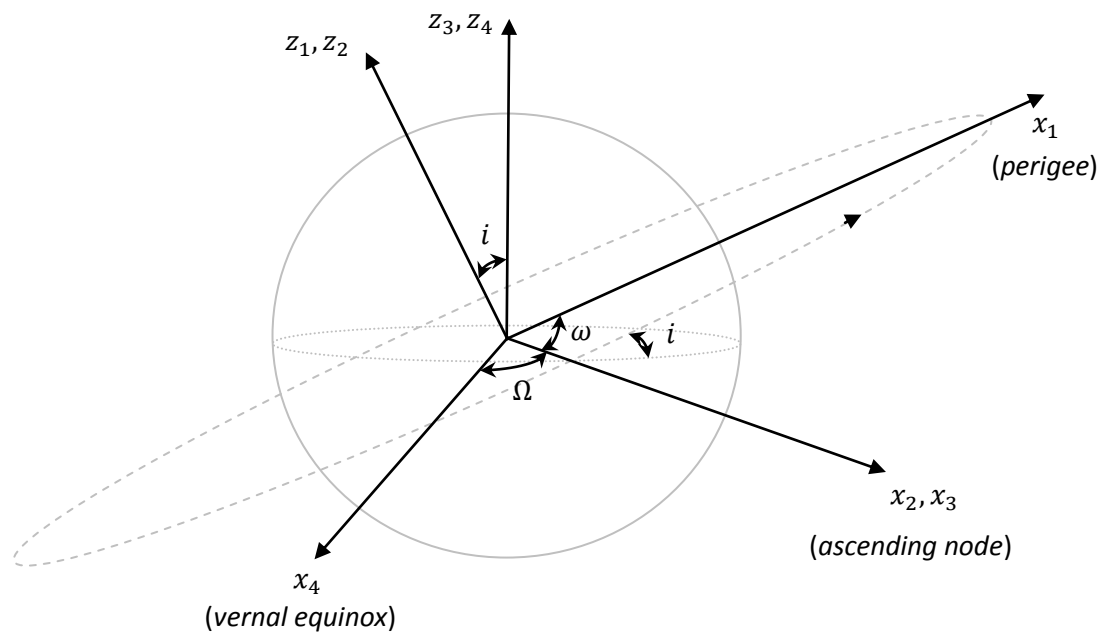
Figure 2.11 - Orbit Frame to ECEF Transformation Geometry

The first transformation brings the *x*-axis from the direction of perigee to the ascending node, which is defined as the point where the satellite crosses the equatorial plane in the north direction. The angle ω is the angle between the direction of perigee and the ascending node, and is referred to as the argument of the perigee. The argument of the perigee is obtained from the navigation message transmitted by the satellite. The second transformation aligns the *z*-axis to be normal to the equatorial plane. The angle i between the two *z*-axes, or alternatively between the satellites orbit plane and the equatorial plane, is referred to as the inclination angle. The final transformation rotates the *x*-axis from the direction of the ascending node to the direction of the vernal equinox. The angle Ω between these two axes is referred to as the right ascension [2].

However, this transformation is not enough to account for Earth's rotation rate, $\dot{\Omega}_{ie}$, defined in the WGS-84 reference geode and given in Eq. 2.15. Thus, the satellite coordinates will be in the ECI frame rather than the ECEF frame. In order to reference a point on or above the surface of the Earth, it is necessary to align the *x*-axis with the Greenwich meridian, as defined in the ECEF coordinate system. The effect of the rotation of the Earth is illustrated in the equatorial plane, with the vernal equinox and the ascending node, in Figure 2.12, below [1] [2].
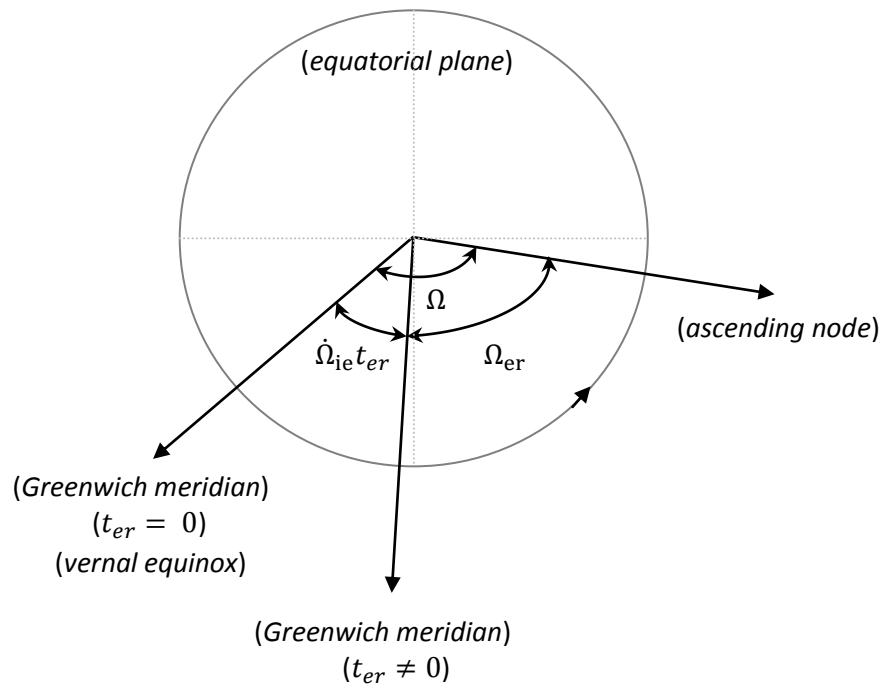
Figure 2.12 - Earth's Rotation in the Equatorial Plane

In order to account for the rotation of the Earth, it is necessary to define a new time reference, t_{er}, so that at $t_{er} = 0$ the Greenwich meridian and vernal equinox are aligned, and the angle Ω_{er} between the ascending node and Greenwich meridian is equal to the right ascension. Looking at Figure 2.12, it can be seen that [2]:

$$\Omega_{er} = \Omega - \dot{\Omega}_{er}t_{er}$$

Eq. 2.44

In order to calculate the value of Ω_{er} using Eq. 2.44, the time reference t_{er} must be expressed in terms of the base time, t, of the atomic clock on board the satellite, which is

48

obtained from the navigation message. The bias between t and t_{er} can be expressed as follows [2]:

$$t_{er} = t + \Delta t$$

<div align="right">Eq. 2.45</div>

where Δt represents the time bias of t_{er}. Thus, Eq. 2.44 can be written as follows [2]:

$$\Omega_{er} = \Omega_e - \dot{\Omega}_{er} t$$

<div align="right">Eq. 2.46</div>

where

$$\Omega_e = \Omega - \dot{\Omega}_{er} \Delta t$$

<div align="right">Eq. 2.47</div>

is referred to as the longitude of the ascending node at weekly epoch, and is obtained from the navigation data message. The final transformation from the satellite orbit frame to the ECEF frame can be obtained using the direction cosine matrix, as follows [1] [2]:

$$\begin{bmatrix} x_s \\ y_s \\ z_s \end{bmatrix} = \begin{bmatrix} r\cos\Omega_{er}\cos(\varphi) - r\sin\Omega_{er}\cos i \sin(\varphi) \\ r\sin\Omega_{er}\cos(\varphi) + r\cos\Omega_{er}\cos i \sin(\varphi) \\ r\sin i \sin(\varphi) \end{bmatrix}$$

<div align="right">Eq. 2.48</div>

where

$$\varphi = v + \omega$$

2.6.5 Perturbations to the Satellite Coordinates

The calculations carried out above assume perfect elliptical orbits and point mass objects, while ignoring the effects of other celestial objects such as the sun and the moon. Although this simplifies the calculations, if not compensated for, it will result in inaccuracies in the calculated coordinates. To this end, several constants are transmitted in the navigation message, given in Table 2.1, below [2] [17].

<div align="center">Table 2.1 - Ephemeris Parameters Used in the Perturbations to the Satellite Coordinates</div>

Symbol	Definition
M_0	Mean anomaly at reference time
Δn	Mean motion difference term
$\sqrt{a_s}$	Square root of the semi-major axis of the satellite orbit
e_s	Eccentricity of the satellite orbit
T_{GD}	Group delay differential for the satellite
$t_{oc}, a_{f0}, a_{f1}, a_{f2}$	Clock correction parameters
t_{oe}	Reference time of ephemeris
C_{us}	Amplitude of the sine harmonic correction term to the argument of latitude

C_{uc}	Amplitude of the cosine harmonic correction term to the argument of latitude
C_{rs}	Amplitude of the sine harmonic correction term to the orbit radius
C_{rc}	Amplitude of the cosine harmonic correction term to the orbit radius
C_{is}	Amplitude of the sine harmonic correction term to the angle of inclination
C_{ic}	Amplitude of the cosine harmonic correction term to the angle of inclination
Ω_e	Longitude of the ascending node at weekly epoch
$\dot{\Omega}$	Rate of the right ascension
i	Inclination angle at reference time
$idot$	Rate of inclination angle
ω	Argument of perigee at reference time

Using these ephemeris parameters, the following perturbations need to be carried out in order to obtain the correct satellite coordinates. The right ascension, Ω, is corrected as [2] [17]:

$$\Omega = \Omega + \dot{\Omega}(t - t_{oe})$$

Eq. 2.49

Resulting in the corrected form of Eq. 2.46 as follows [2] [17]:

$$\Omega_{er} = \Omega_e + \dot{\Omega}(t - t_{oe}) - \dot{\Omega}_{er}\Delta t$$

Eq. 2.50

The mean motion in Eq. 2.37 is corrected as follows [2] [17]:

$$n = \sqrt{\frac{\mu}{a_s^3}} + \Delta n$$

Eq. 2.51

The mean anomaly in Eq. 2.38 is corrected as follows [2] [17]:

$$M = M_0 + n(t - t_{oe})$$

Eq. 2.52

The orbital transformation angle φ, defined in Eq. 2.48, is corrected as follows [2] [17]:

$$\varphi = \varphi + \delta\varphi$$

Eq. 2.53

where,
$$\delta\varphi = C_{us} \sin 2\varphi + C_{uc} \cos 2\varphi$$

Eq. 2.54

The satellite distance, r, to the center of mass of the Earth in Eq. 2.43 is corrected as follows [2] [17]:

$$r = r + \delta r$$

where,
$$\delta r = C_{rs} \sin 2\varphi + C_{rc} \cos 2\varphi$$

The inclination of the satellite orbit frame, i, is corrected as follows [2] [17]:

$$i = i + \delta i$$

where,
$$\delta i = C_{is} \sin 2\varphi + C_{ic} \cos 2\varphi$$

The satellite time, t, is corrected as follows [2] [17]:

$$t = t_c - \Delta t$$

where t_c is the coarse system time at time of transmission, obtained from the navigation message, and,

$$\Delta t = a_{f0} + a_{f1}(t_c - t_{oc}) + a_{f2}(t_c - t_{oc})^2 + \Delta t_r - T_{GD}$$

where,
$$\Delta t_r = \frac{-2\sqrt{\mu}}{c^2} e_s \sqrt{a_s} \sin E$$

2.7 Conclusions

This chapter has provided an overview of the basic concepts necessary to solve the user positioning problem introduced by the use of satellite navigation systems. It has been shown through examples that, determining position in three dimensional space using unsynchronized clocks requires the knowledge of the position of and distance to at least four beacons in space. As the name suggests, in satellite navigation these beacons are satellites orbiting the Earth. As they aren't stationary, their positions need to be relayed to the user through a message transmitted by each satellite. This message contains parameters necessary for the determination of the position of these satellites. Once the positions of the satellites are known, the user position can be calculated in terms of latitude, longitude, altitude and receiver clock bias using Keplerian geometry. Further corrections are carried out on the calculated user coordinates reflecting the true geometry of the Earth, to calculate the exact user position.

Chapter 3 Characteristics of Satellite Navigation Signals

3.1 Introduction

This chapter will introduce the properties of the signals used in GNSS. The discussion will focus on the GPS and Galileo signals, and provide a brief overview of other up and coming global and regional satellite navigation systems. In order to understand these signals, a brief background will be given, regarding basic signal processing operations, modulation schemes, and multiplexing and multiple access techniques forming a basis for the signal processing techniques commonly employed in GNSS. Most of the discussion on signal processing is based on references [19] and [20], where more detailed information can be found. This will be followed by the GPS and Galileo signal structures, providing details relevant to the scope of this research work, based on the information provided in the [17] and [18] documents.

3.2 Fundamentals of Signals and Systems

This section will provide a brief overview of relevant signal processing operations, as a reference for the expressions used throughout the thesis. A more detailed description of these signal processing techniques can be found in [19] and [20]. Some sample signals that will be used throughout the thesis are given in Table 3.1, below.

Table 3.1 - Sample Signals

Signal	Classification	
$x(t) = A\cos(\omega_0 t + \varphi)$	Continuous-Time	Real
$x(t) = Ae^{(j\omega_0 t + \varphi)}$	Continuous-Time	Complex
$x[k] = A\cos(\omega_0 k + \varphi)$	Discrete-Time	Real
$x[k] = Ae^{(j\omega_0 k + \varphi)}$	Discrete-Time	Complex

Basic signal processing operations in continuous and discrete-time are given in Table 3.2 .

Table 3.2 – Basic Signal Processing Operations

Operation	Continuous Time	Discrete Time
Scaling	$y(t) = \alpha x(t)$	$y[k] = \alpha x[k]$
Addition	$y(t) = x_1(t) + x_2(t)$	$y[k] = x_1[k] + x_2[k]$
Multiplication	$y(t) = x_1(t)x_2(t)$	$y[k] = x_1[k]x_2[k]$
Differentiation / Differencing	$y(t) = \dfrac{\delta x(t)}{\delta t}$	$y[k] = x[k] - x[k-1]$
Integration / Accumulation	$y(t) = \displaystyle\int_{-\infty}^{t} x(\tau)\delta\tau$	$y[k] = \displaystyle\sum_{n=-\infty}^{k} x[n]$

In order to analyze the frequency content of satellite signals, the continuous and discrete Fourier transform pairs given in Table 3.3 are used [19].

Table 3.3 - The Fourier Transform

	Fourier Transform	Inverse Fourier Transform
Continuous Time	$X(\omega) = \displaystyle\int_{-\infty}^{+\infty} x(t)e^{-j\omega t}\delta t$	$x(t) = \dfrac{1}{2\pi}\displaystyle\int_{-\infty}^{+\infty} X(\omega)e^{j\omega t}\delta t$
Discrete Time	$X[k] = \displaystyle\sum_{n=0}^{N-1} x[n]e^{-j2\pi kn/N}$	$x[n] = \dfrac{1}{N}\displaystyle\sum_{k=0}^{N-1} X[k]e^{j2\pi kn/N}$

While the scaling and addition of two signals in the Fourier domain carries through to the time domain, the multiplication of two signals in the Fourier transform domain is referred to as the convolution operation in the time domain, as given in Table 3.4 [19].

Table 3.4 - The Convolution Operation

	Expression
Linear Convolution in Continuous Time	$X_1(\omega)X_2(\omega) = x_1(t) * x_2(t) = \int_{-\infty}^{+\infty} x_1(t)x_2(t-\tau)\delta\tau$
Circular Convolution in Discrete Time	$X_1[k]X_2[k] = x_1[n] \circledast x_2[n] = \sum_{m=0}^{N-1} x_1[m]x_2[\langle n-m \rangle_N]$

Finally, the correlation operation is used to compare two signals and determine how similar they are. The correlation of two different signals is referred to as their *cross-correlation function*, while the correlation of a function with itself is referred to as its *auto-correlation function*, as given in Table 3.5 [19].

Table 3.5 - The Correlation Operation

	Cross-Correlation Function	*Auto-Correlation Function*
Continuous Time	$r_{xy}(\tau) = \int_{-\infty}^{+\infty} x(\tau)y^*(t-\tau)$	$r_{xx}(\tau) = \int_{-\infty}^{+\infty} x(t)x^*(t-\tau)$
Discrete Time	$r_{xy}[k] = \sum_{n=-\infty}^{+\infty} x[n]y^*[n-k]$	$r_{xx}[k] = \sum_{n=-\infty}^{+\infty} x[n]x^*[n-k]$

3.2.1 Modulation

The process of varying an aspect of a signal, such as its amplitude, frequency or phase, with respect to another waveform of interest is called modulation. In communication theory, the waveform of interest is referred to as the message, and the signal being modified is referred to as the carrier signal. Satellite navigation systems utilize spread spectrum modulation techniques to spread the frequency domain content of the signal in order to achieve a wider bandwidth. These techniques are generally used to establish secure communications, increase resistance to interference and jamming, and prevent detection and interception of communications. In satellite navigation systems, spread

spectrum is also used to limit the power flux density on satellite downlinks. There are two main techniques employed in spread spectrum: direct sequence and frequency hopping, referred to as Direct Sequence Spread Spectrum (DSSS) and Frequency Hopping Spread Spectrum (FHSS), respectively. Both techniques utilize noise-like Pseudo Random Number (PRN) sequences to determine the spreading pattern in the allocated bandwidth, in essence encrypting the message content with this sequence. Hence, users without prior knowledge of the spreading pattern are essentially unable to intercept the communications. The message is then decrypted by the receiver through correlation with the spreading sequence.

3.2.2 Multiplexing and Channel Access Techniques

In communication theory, multiplexing is the process of combining more than one message, be it analog or digital, into one signal to be transmitted over a shared medium, such as a communication channel. In essence, multiplexing is used to divide the capacity of a low level communication channel, such as the coupled copper wires used in telephone communications, into multiple higher level channels, in the case of telephone communications, enabling the use of the same coupled copper wires by multiple customers simultaneously. The complementary process of recovering the individual messages from the multiplexed signal is referred to as demultiplexing.

There are three basic multiplexing techniques commonly used in communications: Time Division Multiplexing (TDM), Frequency Division Multiplexing (FDM) and Code Division Multiplexing (CDM). In TDM, the channel is divided into multiple recurring fixed-length time slots, where each signal is assigned its own time slot to transmit in, hence, enabling the usage of the same channel by multiple signals seamlessly. Once all the signals have transmitted one block of information, the cycle is repeated in the same order, continuously. An application of this technique is the Global System for Mobile Communications (GSM) network, where users time-share the wireless channel. In contrast to TDM where the channel is divided into non-overlapping segments in the time domain, FDM divides the frequency spectrum into non-overlapping frequency ranges for individual signals to be transmitted in. In order to utilize FDM, the signals need to be frequency modulated to the designated frequency band prior to transmission.

Applications of this technique include the FM radio transmissions and first and second generation satellites of the Russian GLObal NAvigation Satellite System (GLONASS). This is illustrated in Figure 3.1, below, with a time / frequency chart of three signals to be transmitted in the figure.
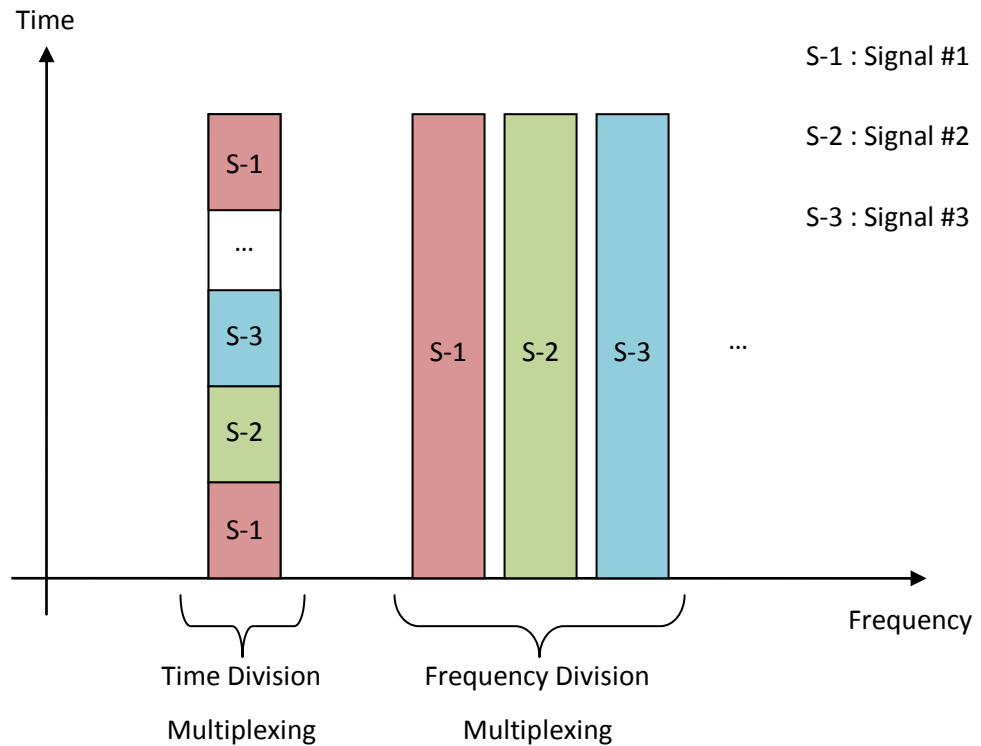
Figure 3.1 - TDM vs. FDM Comparison

The third multiplexing technique, CDM, is an extension of the spread spectrum methods introduced in the previous section, where rather than spreading only one message using a PRN sequence to increase its performance, n messages are spread using n unique and orthogonal PRN sequences, and transmitted over the same channel. In contrast to the turn-taking method of TDM and multiple band approach of FDM, CDM allows the use of the same band by providing unique "signatures" for each message being transmitted in the channel. In order to be able to receive a desired message, the receiver need only correlate the signature of the desired message with the channel to obtain the encoded data. Applications of this technique include the 3G cellular phone networks and most current satellite navigation system signals.

Channel access methods, or multiple access techniques, are extensions based on the multiplexing techniques described above, allowing multiple users to connect and share the capacity of a communication medium, such as a wireless communication channel or a bus network. There are three basic multiple access techniques based on the multiplexing schemes described above: Time Division Multiple Access (TDMA), based on the TDM scheme where each user is assigned a time slot in a cyclical manner, Frequency Division Multiple Access (FDMA), based on the FDM scheme where each user is assigned a frequency band to transmit in, and Code Division Multiple Access (CDMA), based on the CDM scheme where each user is assigned a unique signature in the form of a unique PRN code.

3.3 GNSS Signal Spectra

In order to understand the processing that takes place in a GNSS receiver, it is necessary to know the relevant details of the signals in question. These signals are transmitted on several frequencies in the UHF band, spanning the 500 MHz to 3 GHz frequency range, and are illustrated in Figure 3.2, below, [17] and [18]. The following sections will provide details regarding the modulation techniques, coding schemes and frame formats of the GPS and Galileo signals, followed by a brief overview of up and coming GNSS signals.
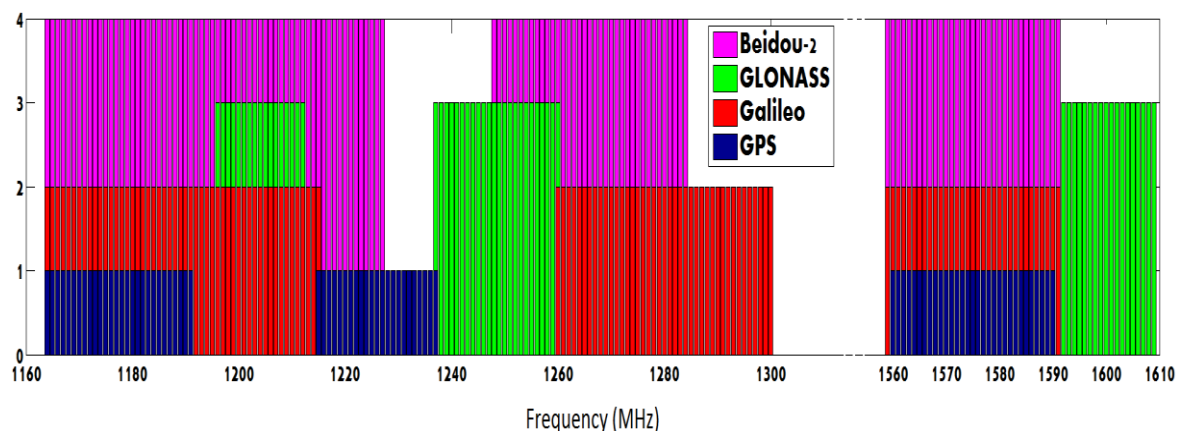
Figure 3.2 - Frequency Spectrum of current GNSS Signals

3.4 GPS Signal Characteristics

The GPS signals are transmitted on the L1, L2 and L5 bands, as illustrated in Figure 3.2, which are obtained from a common 10.23 MHz onboard atomic frequency standard clock, using the following clock multipliers [22];

$$L1 = 154 \times 10.23 \, MHz = 1575.42 \, MHz$$

$$L2 = 120 \times 10.23 \, MHz = 1227.6 \, MHz$$

Eq. 3.1

$$L5 = 115 \times 10.23 \, MHz = 1176.45 \, MHz$$

Although the signals are transmitted on the above frequencies, the motions of the satellite and the receiver can produce a Doppler effect, causing the center frequency to shift by up to ±10 KHz at the receiver. These signals are composed of the carrier wave, the spreading sequences and the navigation data containing orbital parameters and correction terms necessary for the computation of the satellite and user positions. There are two unique PRN sequences transmitted from each satellite: the Coarse Acquisition (C/A) code with a period of 1 millisecond, and the encrypted Precision (P(Y)) code with a period of 1 week, which is a military code not available for civilian use. The two codes are phase locked at the satellite, which enables the receiver to compute the phase of the long P(Y) code through the phase of the C/A code. The block diagram illustrating the signal generation process on the L1 and L2 frequencies can be seen in Figure 3.3, below[1].
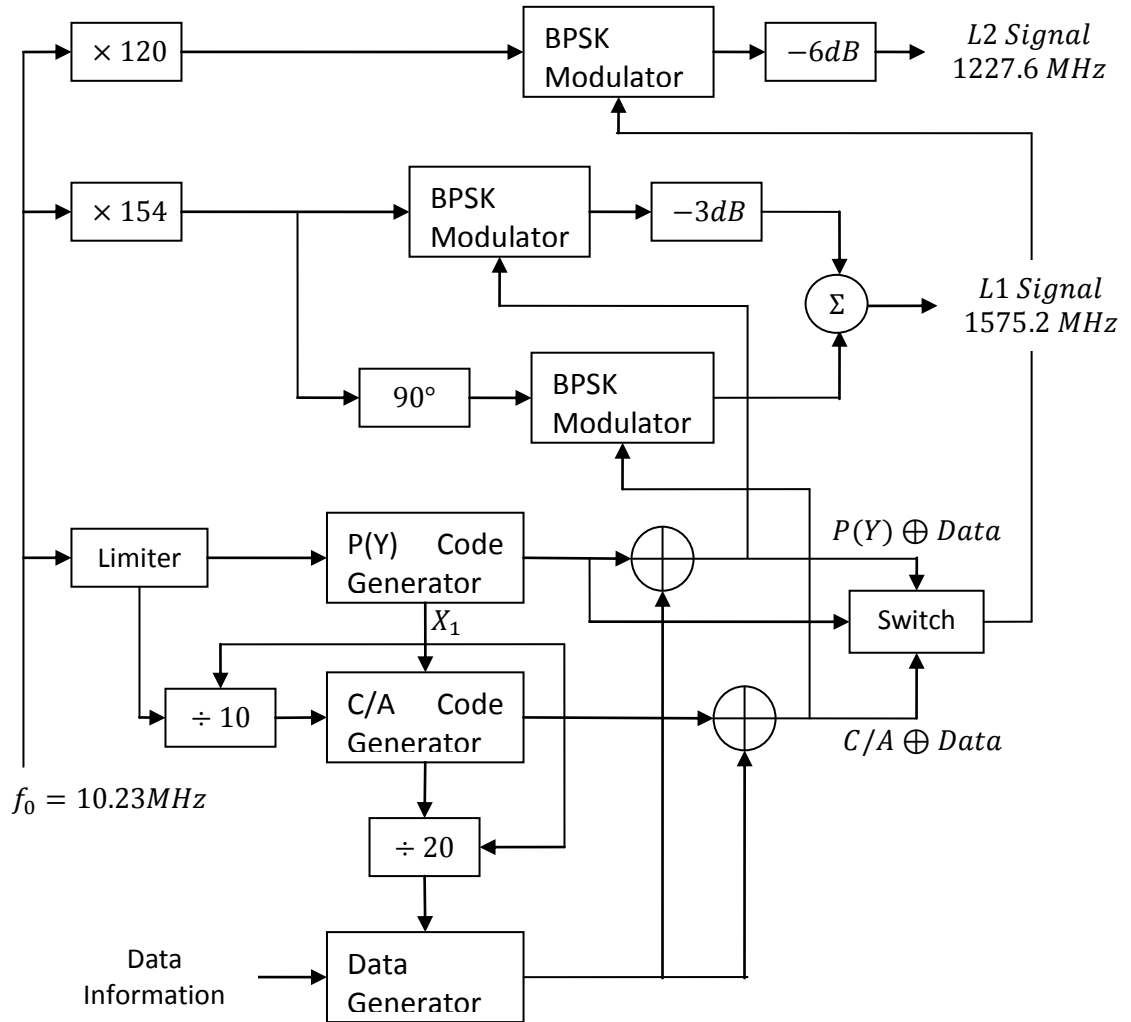
Figure 3.3 - GPS Satellite Signal Generation

Although the effective atomic frequency standard clock observed from the receiver is $f_0 = 10.23 \, MH$, the exact frequency of the onboard clock is $f_0 = 10.22999999543 \, MHz$ which accounts for relativistic effects. The first step of the signal generation process is to provide the L1 and L2 frequencies that will be used in the modulation process. This is accomplished by the $\times 154$ and $\times 120$ clock multipliers, respectively. The clock limiter in the block diagram is used to stabilize the satellite clock before generating the PRN sequences for the C/A and P(Y) signals. The correction terms and supplementary information contained in the navigation message are produced by the data generator block, and are identical for the C/A and P(Y) signals. The X_1 signal obtained from the P(Y) code generator block is used to synchronize the data generator, C/A code generator and the P(Y) code generator blocks in order to keep these signals in phase-lock at all times.

Once generated, the data is spread with the PRN sequences using the Exclusive-OR (XOR) operator in accordance with the DSSS technique, forming a CDMA system which is referred to as Direct Sequence CDMA (DS-CDMA).

The next step in the processing chain is the modulation of the $C/A \oplus Data$ and $P(Y) \oplus Data$ DS-CDMA signals onto a carrier, using the Bi-Phase Shift Keying (BPSK) modulation technique. BPSK, also known as 2-PSK, is a form of PSK where there are only two phases in the modulation: 0 and π. Observing the signal generation block diagram, it can be seen that the two signals are in phase quadrature of each other on the L1 frequency. The overall expression for the combined signals transmitted from satellite i, can be written as follows:

$$
\begin{aligned}
s^i(t) = \sqrt{2P_C} &\left(C^i(t) \oplus D^i(t) \right) \cos(2\pi f_{L1} t) \\
&+ \sqrt{2P_{PL1}} \left(P^i(t) \oplus D^i(t) \right) \sin(2\pi f_{L1} t) \\
&+ \sqrt{2P_{PL2}} \left(P^i(t) \oplus D^i(t) \right) \sin(2\pi f_{L2} t)
\end{aligned}
$$

Eq. 3.2

where P_C, P_{PL1} and P_{PL2} represent the power levels of the C/A and P(Y) signals, C^i is the C/A code of satellite i, P^i is the P(Y) code for satellite i, D^i is the navigation data message for satellite i, and f_{L1} and f_{L2} are the carrier frequencies corresponding to the L1 and L2 bands, respectively. The modulation stages along with the final signal are illustrated in Figure 3.3, below. The C/A code has a period of 1 millisecond and each data bit is spread by 20 C/A code periods, resulting in a 50 Hz data rate for the navigation data message. When a transition occurs in the spread data, the carrier phase is shifted instantaneously by 180°, resulting in the final BPSK signal given in Figure 3.3.
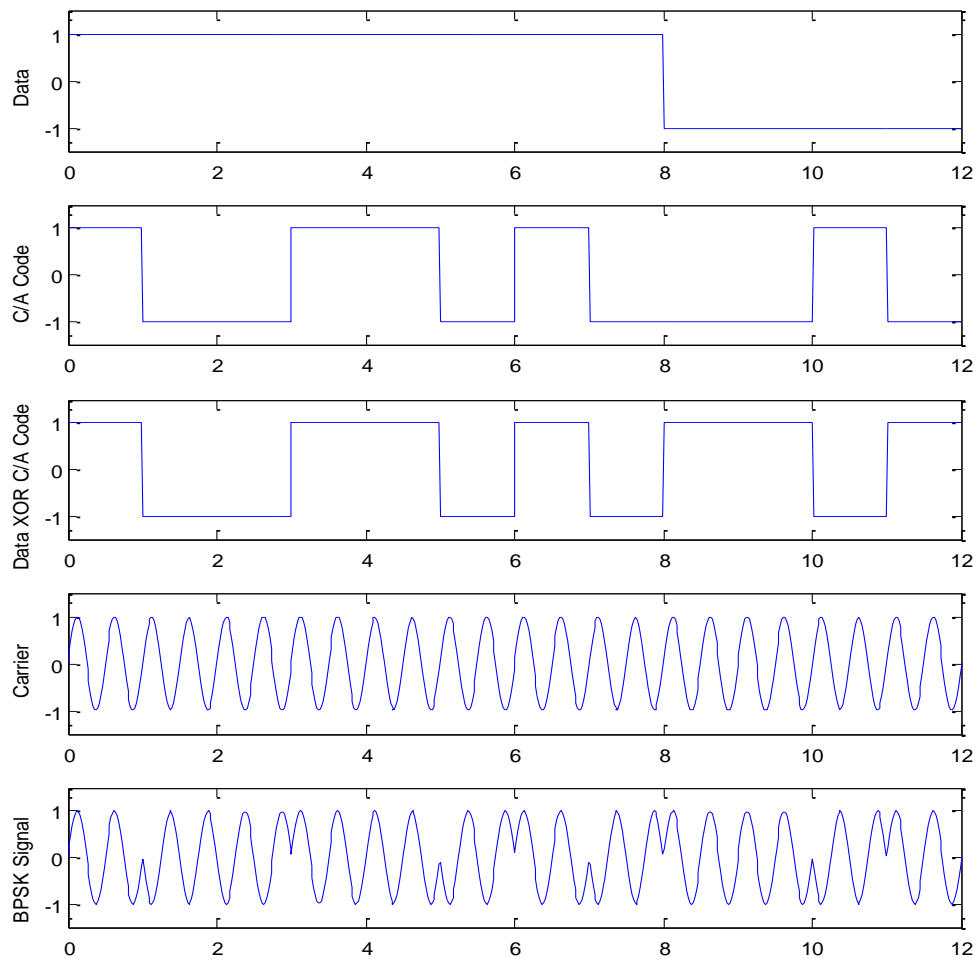
Figure 3.4 - BPSK Signal Generation

3.4.1 The C/A Code and Gold Sequence Generation

The C/A and P(Y) codes used in spreading the navigation data transmitted from the satellites belong to a group of PRN sequences referred to as Gold Codes. These codes are generated using tapped Linear Feedback Shift Registers (LFSR) and are deterministic sequences exhibiting noise like behavior. The discussion in this section will focus on the properties of the C/A codes, as the P(Y) codes are encrypted and not available for civilian use, [1] and [2].

Gold Codes are maximum-length sequences of length $N = 2^n - 1$ generated from the sum of two maximum-length sequences. The C/A codes used in GPS use $n = 10$ to generate sequences of length $N = 1023$. The two polynomials used in the generation process are:

$$G1(x) = 1 + x^3 + x^{10}$$

Eq. 3.3

$$G2(x) = 1 + x^2 + x^3 + x^6 + x^8 + x^9 + x^{10}$$

Eq. 3.4

where $G1$ and $G2$ are the governing polynomials for the two shift registers in the LFSR, given in Figure 3.5, below.
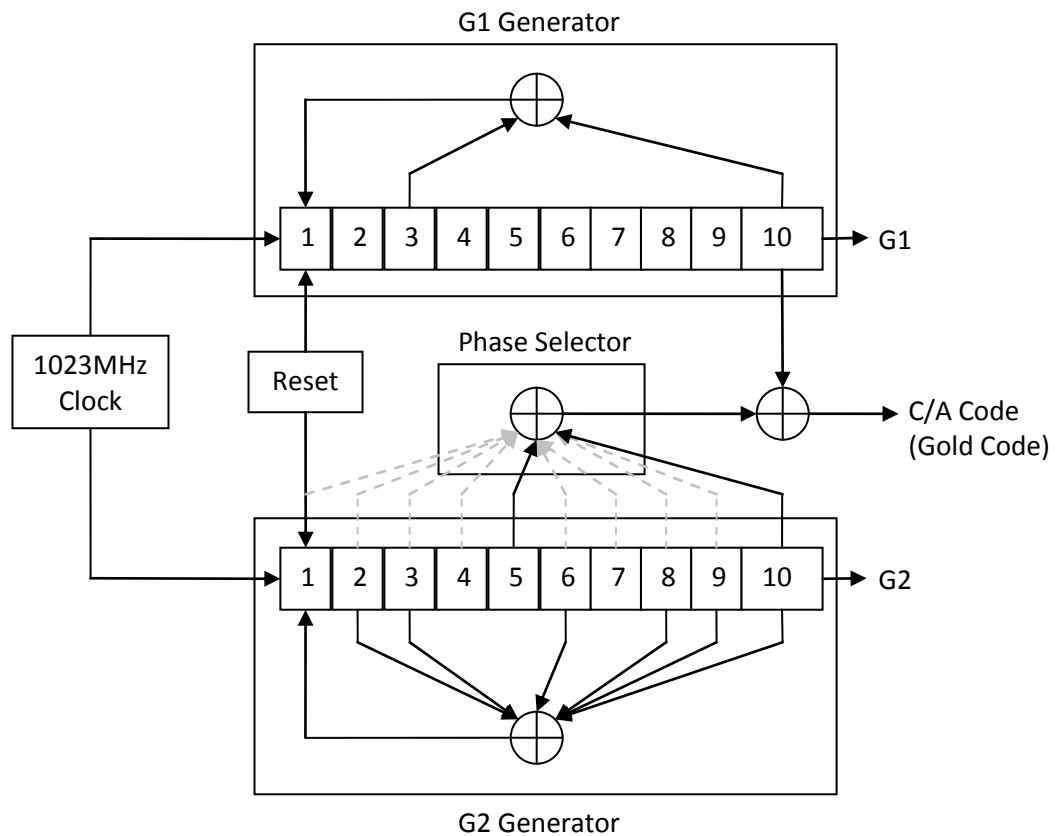
Figure 3.5 - C/A Code Generator (LFSR)

Using this structure, there are 37 unique Gold Codes that can be generated using various inputs to the phase selector block, which is used to determine the amount of shift to be applied to the $G2$ sequence before being modulo-2 added to the $G1$ sequence. The

possible combinations and the amount of delays they introduce are given in Table 3.6, below.

Table 3.6 - C/A Code Phase Selection

Satellite ID	GPS PRN Number	Phase Selector Setup	Code Chip Delay
1	1	$2 \oplus 6$	5
2	2	$3 \oplus 7$	6
3	3	$4 \oplus 8$	7
4	4	$5 \oplus 9$	8
5	5	$1 \oplus 9$	17
6	6	$2 \oplus 10$	18
7	7	$1 \oplus 8$	139
8	8	$2 \oplus 9$	140
9	9	$3 \oplus 10$	141
10	10	$2 \oplus 3$	251
11	11	$3 \oplus 4$	252
12	12	$5 \oplus 6$	254
13	13	$6 \oplus 7$	255
14	14	$7 \oplus 8$	256
15	15	$8 \oplus 9$	257
16	16	$9 \oplus 10$	258
17	17	$1 \oplus 4$	469
18	18	$2 \oplus 5$	470
19	19	$3 \oplus 6$	471
20	20	$4 \oplus 7$	472
21	21	$5 \oplus 8$	473
22	22	$6 \oplus 9$	474
23	23	$1 \oplus 3$	509
24	24	$4 \oplus 6$	512
25	25	$5 \oplus 7$	513
26	26	$6 \oplus 8$	514
27	27	$7 \oplus 9$	515
28	28	$8 \oplus 10$	516
29	29	$1 \oplus 6$	859
30	30	$2 \oplus 7$	860
31	31	$3 \oplus 8$	861
32	32	$4 \oplus 9$	862
*	33	$5 \oplus 10$	863
*	34	$4 \oplus 10$	950
*	35	$1 \oplus 7$	947
*	36	$2 \oplus 8$	948
*	37	$4 \oplus 10$	950

It can be seen that GPS PRN numbers 34 and 37 have the same C/A code as they have the same phase selection and delay value. The first 32 codes are assigned to the GPS satellites and recycled as older satellites are replaced with newer ones. The last 5 codes are reserved for other uses, such as ground transmitters and control stations.

3.4.2 The C/A Code Correlation Properties

One of the most important properties of the spreading sequences used in GPS lies in their auto-correlation and cross-correlation characteristics. If the Gold codes were infinite length random sequences, they would result in orthogonal codes with no cross-correlation between the sequences, and no auto-correlation except at zero lag. However, the codes used in GPS are finite length approximations generating pseudo-random sequences with close to ideal characteristics, resulting in almost orthogonal codes. As a result, their cross-correlations and non-zero lag auto-correlations are not exactly zero. This can be seen in the auto-correlation plot of PRN 1 and the cross-correlation plot of PRN 1 and PRN 2, in Figure 3.6 and Figure 3.7, respectively.
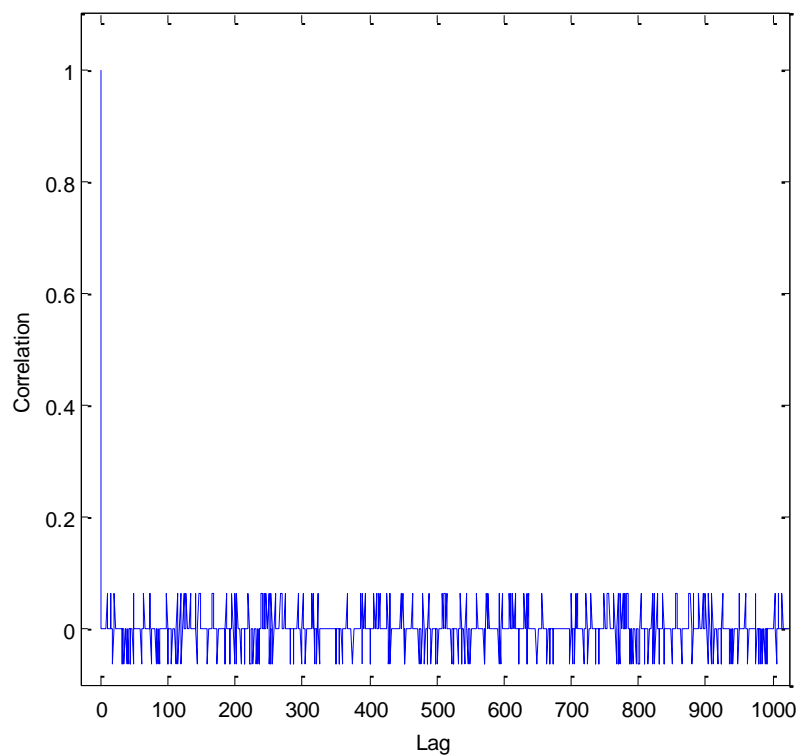
Figure 3.6 - Auto-Correlation Plot of PRN 1
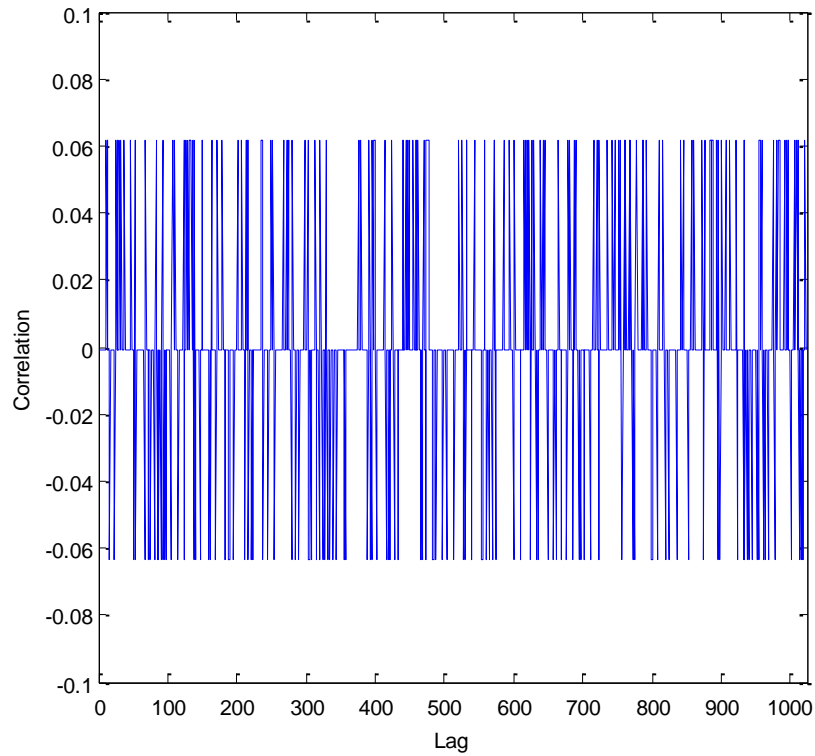
Figure 3.7 - Cross-Correlation Plot of PRN 1 and PRN 2

The cross-correlations and non-zero lag auto-correlations of these Gold codes satisfy the following relationship:

$$|r_{kk}| \leq 2^{(n+2)/2} + 1$$

Eq. 3.5

where r_{kk} is the value of the correlation, and $n = 10$ for GPS C/A codes, resulting in the following expression:

$$|r_{kk}| \leq 65$$

Eq. 3.6

3.4.3 Navigation Data Structure

The GPS navigation data is transmitted at a rate of 50 bps, as mentioned earlier in the chapter. This data is divided into pages, frames, sub-frames and words in order to simplify the decoding process. There are 25 frames, each containing 5 sub-frames. Each sub-frame contains 10 words of 30 bits, resulting in a 300 bit sub-frame that takes 6 seconds to transmit using the 50 bps transmission rate. The time it takes to transmit each frame is 30

seconds. The total time it takes to transmit the 25 frames contained in the navigation message is 12.5 minutes. The first three sub-frames are repeated in each frame and contain clock corrections, satellite data accuracy information, and ephemeris parameters necessary for the computation of the user position. The last two sub-frames are used to transmit additional data referred to as the almanac, which contains ionospheric, tropospheric and Universal Coordinated Time (UTC) parameters for use in additional correction models, and health indicators for the determination of ranging accuracy. This data is spread over the last two sub-frames of the 25 frame navigation message, also referred to as the 25 pages of almanac data, and repeats every 12.5 minutes. While each satellite only transmits its own ephemeris data, the almanac data is the same for all satellites and contains information relevant to all satellites. The general structure of a frame containing 5 sub-frames can be seen in Figure 3.8, below [2].

1	TLM	HOW	Clock correction parameters, Satellite health and User range accuracy
2	TLM	HOW	Ephemeris data
3	TLM	HOW	Ephemeris data
4	TLM	HOW	Almanac data
5	TLM	HOW	Almanac data

Figure 3.8 - Frame Structure indicating the Sub-Frames

It can be seen from this figure that each sub-frame begins with the same two special words: Telemetry (TLM) and the Hand Over Word (HOW). These words are used for frame synchronization and contain the synchronization preamble, sub-frame ID, the truncated Time of Week (TOW) count and parity bits. The structure of these two words can be seen in Figure 3.9, below. Further details regarding the structure of each sub-frame and its contents can be found in [17].

TLM Word

0 1	0 2	0 3	0 4	0 5	0 6	0 7	0 8	0 9	1 0	1 1	1 2	1 3	1 4	1 5	1 6	1 7	1 8	1 9	2 0	2 1	2 2	2 3	2 4	2 5	2 6	2 7	2 8	2 9	3 0

Preamble   Reserved   Parity

HOW Word

0 1	0 2	0 3	0 4	0 5	0 6	0 7	0 8	0 9	1 0	1 1	1 2	1 3	1 4	1 5	1 6	1 7	1 8	1 9	2 0	2 1	2 2	2 3	2 4	2 5	2 6	2 7	2 8	2 9	3 0

Truncated TOW   ID   Parity

Reserved

Figure 3.9 - The TLM and HOW Word Formats

3.5 Galileo Signal Characteristics

The Galileo signals are transmitted on the L1, E1, E2, E5 (containing the E5a and E5b sub-bands) and E6 bands, as illustrated in Figure 3.2, where the Open Service (OS) signal is transmitted on the L1 band for ease of use with current single frequency GPS receiver hardware [18]. These signals are DS-CDMA signals using sub-classes of a new modulation technique referred to as the Binary Offset Carrier (BOC) modulation technique. There are three signals within the transmitted L1 signal, referred to as the L1A, L1B and L1C signals. The L1A signal is also referred to as the Public Regulated Service (PRS) and is a limited access signal, where the spreading codes are encrypted. The L1B signal contains the navigation data message and is used to extract the parameters necessary for the computation of the satellite and user positions. The L1C signal is a data-free pilot channel which is used to improve the acquisition and tracking performance of the L1 OS receiver. These signals are multiplexed into the L1 signal using the Coherent Adaptive Subcarrier Modulation (CASM) technique.

The spreading sequences used in the L1B and L1C signals have the same chipping rate as the GPS L1 signal, $1.023\ MHz$, and are 4092 chips long giving them an acquisition time of 4 milliseconds. As the pilot channel doesn't contain any data, it is modulated by a

secondary code of 25 chips to extend the length of the code to 100 milliseconds, providing a highly accurate synchronization resource under low signal quality conditions. This final code is referred to as the tiered pilot code, as it can be acquired using the shorter 4092 chip spreading sequence under high signal quality conditions where the secondary chipping sequence is treated as data modulation, while the long code can be used under low signal quality conditions.

The following sub-sections will provide details of the Coherent Adaptive Subcarrier Modulation technique used to combine the individual signals in each frequency band, and the Binary Offset Carrier modulation technique used to modulate the signals on each band. This will be followed by the overall signal transmitted on the L1 band overlaid with the GPS L1 signal. Further details regarding the specifics of the spreading sequences and modulation techniques used on individual frequency bands can be found in [18].

3.5.1 Coherent Adaptive Subcarrier Modulation

The Galileo L1A, L1B and L1C signals are combined to generate the composite L1 signal, using the Coherent Adaptive Subcarrier Modulation (CASM) technique, also referred to as the tricode hexaphase or interplex modulation technique, in accordance with the block diagram given in Figure 3.10, below [3].
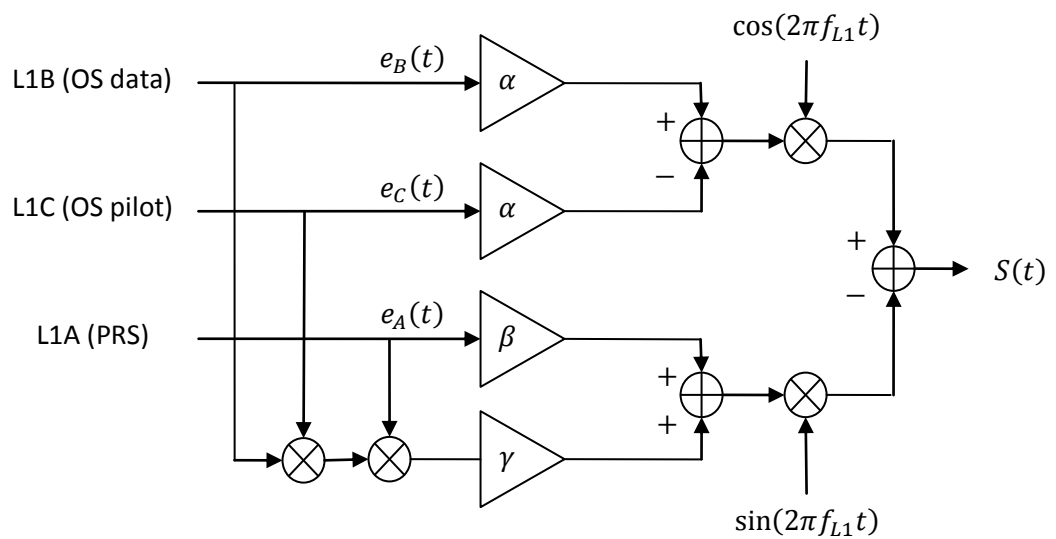
Figure 3.10 - Coherent Adaptive Subcarrier Modulation Scheme

Referring to the block diagram, the combined L1-band signal can be expressed as follows:

$$S(t) = \alpha\big(e_B(t) - e_C(t)\big)\cos(2\pi f_{L1}t)$$
$$- \big(\beta e_A(t) + \gamma e_A(t)e_B(t)e_C(t)\big)\sin(2\pi f_{L1}t) \qquad \text{Eq. 3.7}$$

where the L1 OS data and pilot channels are modulated onto the in-phase component of the multiplexed signal while the L1 PRS channel is modulated onto the quadrature component. In order to guarantee a constant power envelope on the overall signal and equal power levels for the L1 OS and L1 PRS signals, the gain factors are chosen as:

$$\alpha = \frac{\sqrt{2}}{3}$$

$$\beta = \frac{2}{3} \qquad\qquad \text{Eq. 3.8}$$

$$\gamma = \frac{1}{3}$$

3.5.2 Binary Offset Carrier Modulation

Next generation signals being planned for the up and coming navigation systems, including the Galileo GNSS, utilize a new modulation technique referred to as the Binary Offset Carrier (BOC) modulation technique, where the navigation message or data content is modulated by a binary sub-carrier in addition to the spreading code and carrier present in classical PSK modulation schemes. This is illustrated in Figure 3.11, below, using the same data and chipping sequence as the BPSK example given in Figure 3.4, above.
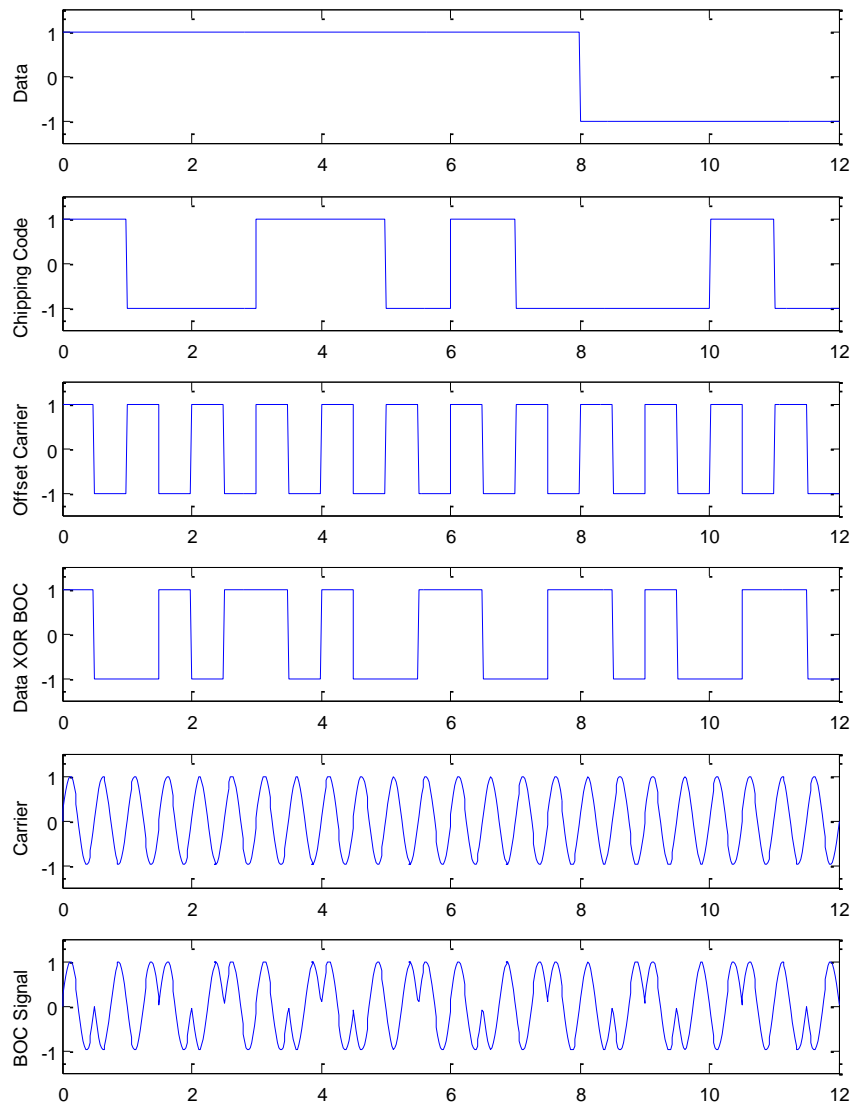
Figure 3.11 - Binary Offset Carrier Modulation Example

Modulating the signal with this additional sub-carrier splits the signal spectrum into two symmetrical lobes containing no signal power on the carrier frequency. This enables the re-use of current frequency bands without disrupting the operation of currently available signals in the same bands. This is demonstrated with the power spectral density plot of the L1 band GPS and Galileo signals, using the Welch method, in Figure 3.12, where the red plot represents the GPS signal and the blue plot represents the Galileo signal.
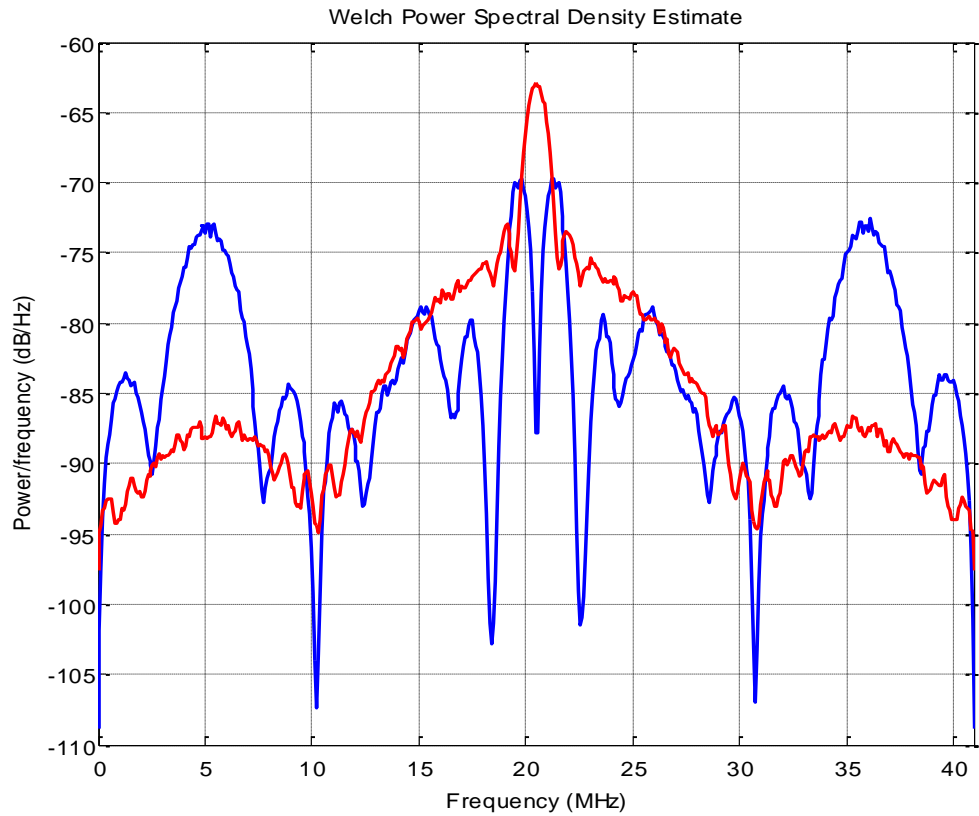
Figure 3.12 - Welch Power Spectral Density Spectrum of L1 GPS (Red) and Galileo Signals (Blue)

Binary Offset Carrier modulated signals are represented using the following notation:

$$BOC(m, n)$$

Eq. 3.9

where m represents the sub-carrier to reference frequency ratio and n represents the spreading sequence to reference frequency ratio, with the reference frequency being $f_0 = 1.023 MHz$. This work will focus on the $BOC(n, n)$ type modulations where the sub-carrier and chipping sequence have the same frequency, as the Galileo In-Orbit Validation Element (GIOVE) satellites currently utilize these signals.

3.6 Other GNSS Signals

In addition to the GPS and Galileo GNSSs, there are several other up and coming global and regional navigation systems. The Russian GLONASS system had achieved global coverage by the end of 1995; however, it ended up disintegrating following the collapse of the Russian economy. The system is now being updated with a view to achieving global coverage using FDMA signals by the end of 2011. Although the GPS-GLONASS Interoperability and Compatibility Working Group meetings between the US and Russia hinted at the system being moved to DSSS, no announcements have since been made by either government. The Chinese Compass/Beidou navigation system is being developed as an independent GNSS similar to the GPS and Galileo systems. Currently further information regarding the system is unavailable as standardization documents have not been released to the public [21].

In addition to these global navigation systems, there are regional navigation systems being developed to provide enhanced performance over specific regions. The first of these is the Japanese Quasi Zenith Satellite System (QZSS), consisting of three satellites to enhance the performance of the GPS system in urban areas in Japan. Fully operational status is scheduled to be achieved by the end of 2013. The second regional system is the Indian Regional Navigation Satellite System (IRNSS) being developed by the Indian Space Research Organization. The first satellite is expected to be launched by the end of 2009, with the full constellation scheduled to be completed by 2012.

Finally, there are several augmentation systems in operation and being developed to support the operation of current and future GNSS signals in demanding applications. The US operated Local Area Augmentation System (LAAS) and Differential GPS (DGPS) are Ground Based Augmentation Systems (GBAS) enhancing the performance of GPS using ground stations to report on the performance and accuracy of the transmitted signals. The US operated Wide Area Augmentation System (WAAS) and Wide Area GPS Enhancement (WAGE) systems, the European Geostationary Navigation Overlay Service (EGNOS) operated by the European Space Agency (ESA), the Japanese Multi-functional Satellite Augmentation System (MSAS) and the GPS Aided Geo Augmentation Navigation (GAGAN) system proposed by India are Satellite Based Augmentation Systems (SBAS)

aiming to provide vital enhancements to the accuracy of the signals in Safety of Life (SoL) and Search and Rescue (SAR) applications.

3.7 Conclusions

This chapter has provided a brief overview of the signals currently used in satellite navigation systems. Concepts and definitions fundamental to signals and systems, such as the Fourier transform, filtering and convolution operations, correlation, modulation and multiplexing operations, have been explained in order to form a coherent understanding of the signal definitions and mechanisms used to generate them. An overview of currently available and upcoming satellite navigation signals and their spectra has been given before delving into the details of the GPS and Galileo satellite signals and the phase-shift keying and binary offset carrier modulation techniques utilized in generating these signals. Finally, a brief overview of current and upcoming ground and space based regional and global navigation signals has been given to conclude the chapter.

Chapter 4 Strong Signal Operation of the GNSScope Toolbox

4.1 Introduction

With the development of up and coming satellite navigation systems such as the European Galileo and the Chinese Compass/Beidou systems, as well as the enhancements planned for the American GPS system mentioned in the previous chapter, new receiver designs will be required to cope with the improved signaling schemes and services being deployed by these systems. Having access to more than one satellite navigation signal across several frequency bands will also require these new receiver designs to be capable of operating on multiple satellite navigation standards and multiple frequency bands. As most of these signals and navigation standards are still under development and are subject to change before being finalized, GNSS receiver designers will be required to alter their designs to accommodate changes being made to the standards. In light of this, the Global Navigation System Scope (GNSScope) was designed and developed as a toolbox in MATLAB, utilizing the flexibility, versatility and fast prototyping times offered by Software

Defined Radio (SDR) design techniques. GNSScope is a complete end-to-end modeling, simulation and analysis environment covering the reception model for the GPS L1/L2C and GIOVE-A L1/E5 satellite navigation signals, offering receiver designers a test-bed to analyze their systems and a reference design to benchmark the performance of their designs. Details of the basic operation of the GNSScope toolbox will be given in this chapter, covering general receiver operation overview, and the acquisition, tracking, and range processing blocks, using examples and results generated entirely in GNSScope.

4.2 Operational Overview of a GNSS Receiver

This chapter will present the basic operation of GNSScope using examples generated in the toolbox, covering the acquisition, tracking, and range processing operations. As satellite navigation systems consist of multiple satellites transmitting signals over a multitude of frequency bands, a channelized architecture is utilized, where each signal being observed is processed in a separate tracking channel. The block diagram illustrating this relationship is given in Figure 4.1, below, where GNSScope covers the Acquisition, Tracking, and Range Processing blocks[2] [3] [23] [24] [25].
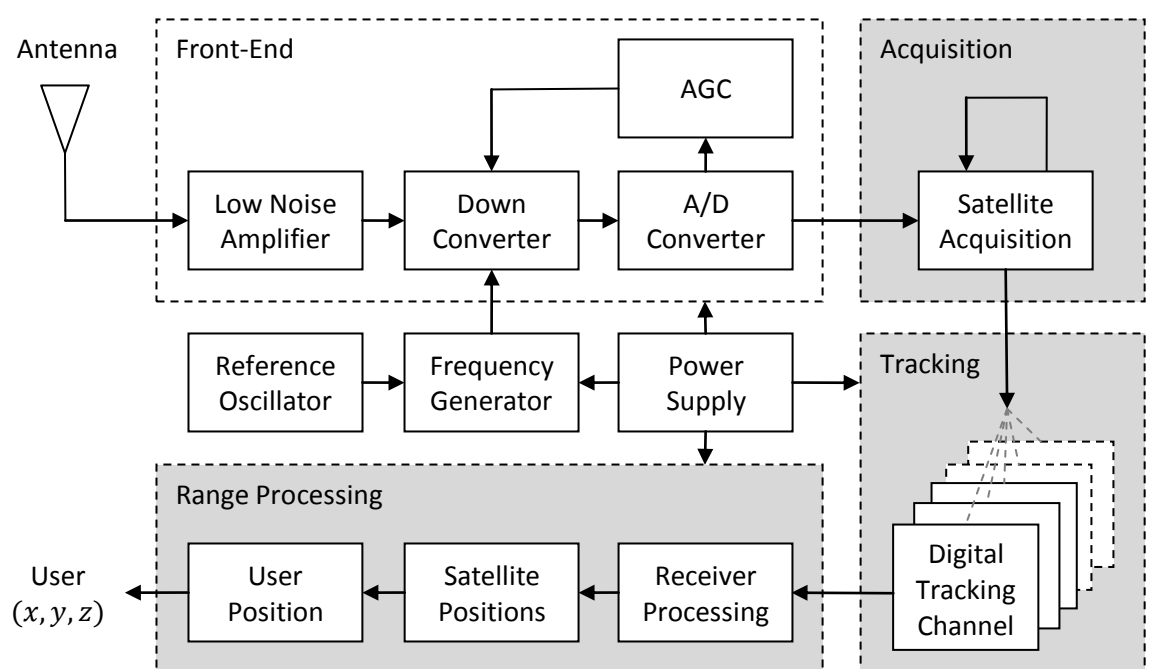
Figure 4.1 - Operational Block Diagram of a Generic GNSS Receiver

The composite Radio Frequency (RF) signal being received from the antenna is passed through the Front-End block for amplification, down conversion to an Intermediate Frequency (IF) and digitization into a binary sequence. This provides the remaining blocks with a digital IF signal, reducing the number of operations necessary in each stage, as the sampling rate is much lower than the Nyquist rate required by the UHF band signals being transmitted from the satellites. This is followed by the acquisition block, where the signal is searched for visible satellite signals. The acquisition process is repeated until all the visible satellite signals are acquired or the minimum signal requirement is satisfied. The information obtained from the acquisition process is used to initialize digital tracking channels for each satellite signal available in the received composite signal. As the acquisition process is a computationally intensive and time consuming operation, it is important for the digital tracking channels to keep a lock on all acquired signals. When a lock is established on the visible satellite signals, the digital tracking channels begin extracting the binary coded navigation data necessary for the computation of the satellite and user positions, which is carried out in the range processing block [26]. The extracted navigation data is searched for frame preambles in order to synchronize the frames and extract the necessary parameters to be used in the computations given in Chapter 2. Once these parameters are obtained, the positions of the satellites are computed and corrected for clock bias and Ionospheric and Tropospheric errors. Once the positions of the satellites and the pseudo-ranges to each satellite are known, the user position can be calculated using the equations given in Chapter 2.

The following sections will provide details regarding the basic operational capabilities of GNSScope, consisting of the Acquisition, Tracking, and Range Processing blocks, under good signal conditions where the received signals are of relatively high strength with no interferers or multipath effects. Further capabilities of GNSScope such as weak signal operation, multipath tracking and interference removal, will be discussed in the following chapter.

4.3 Acquisition

The aim of signal acquisition is to detect all visible satellite signals coming from all available satellite navigation systems present in the incoming IF signal and provide the navigation signal type and PRN code information of the detected satellites in addition to coarse estimates of the carrier frequency and PRN code phase offset necessary for the initialization of the digital tracking channels [2][3]. The navigation system type is necessary to determine the modulation scheme used in encoding the data in the signal. Currently, GNSScope supports the GPS, Galileo and GIOVE signals which are multiplexed using the CDMA technique, with the ability to acquire up and coming navigation signals such as the Compass/Beidou, IRNSS and QZSS signals once the spreading codes are made available to the public. As multiple satellites share the same frequency bands in CDMA systems, it is also necessary to determine the PRN code, or signature, of the satellite being acquired in order to uniquely determine the transmitting satellite.

In addition to these parameters, coarse estimates of the carrier frequency and code phase offset need to be determined to initialize the digital tracking channels. Even though the carrier IF center frequency corresponding to each frequency band can be determined from the band in question and the mixers used in the down conversion process, there can be up to a $\pm 10\ KHz$ shift from this frequency due to the relative motion between the user and the transmitting satellite. It is up to the acquisition process to determine this Doppler shift to be used in the tracking channels. The last parameter to be established is the code phase offset. Due to the correlation properties of the Gold codes used to spread the satellite signals, there is almost no auto-correlation of the PRN codes except at zero lag. Once the PRN codes are perfectly aligned, the incoming signal can be de-spread and the navigation data can be extracted. Thus, the correct starting point of the PRN codes must also be determined by the acquisition process for the initialization of the digital tracking channels [2][3].

In general there are three methods of acquisition when processing signals in the frequency domain: serial search acquisition, parallel frequency space search acquisition and parallel code phase space search acquisition. Details regarding these techniques will be given in the following sub-sections with examples generated entirely in GNSScope.

4.3.1 Serial Search Acquisition

The serial search acquisition algorithm is one of the lowest complexity acquisition algorithms for CDMA signals. As the name suggests, the acquisition algorithm searches through all possible Doppler frequencies and code phase offsets in a sequential manner, where each frequency bin is searched for all possible code phase shifts before progressing to the next frequency bin. This is illustrated in Figure 4.2, below, where the spreading code is n chips long and the Doppler search range is split into k frequency bins [1].
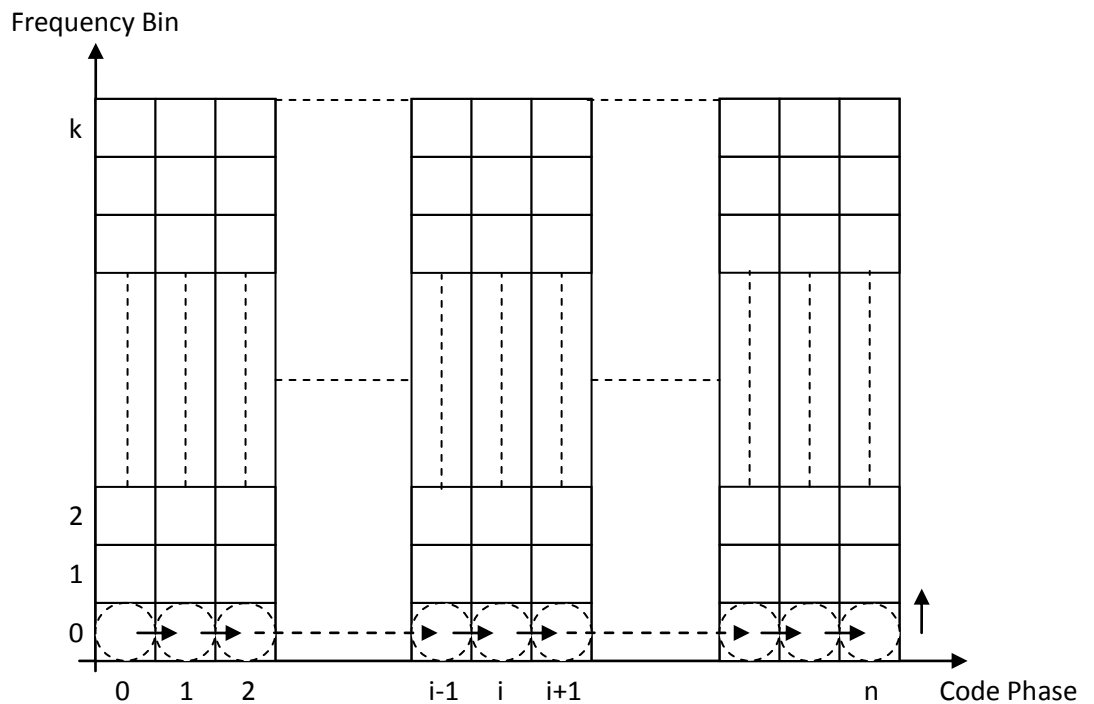
Figure 4.2 - Serial Search Acquisition Illustration

It can be seen from the figure that the serial search acquisition algorithm has to compute the correlation of n different code phase offsets for each of the k frequency bins, resulting in $k \times n$ operations to complete the search operation. If the Doppler search range was split into $500 \, Hz$ frequency bins, searching for a GPS L1 satellite signal using the serial search acquisition algorithm would result in:

$$\left(\frac{20000}{500} + 1\right) \times 1023 = 41943 \; operations$$

Eq. 4.1

This requires a large number of operations to complete the acquisition process; however, the tradeoff in the large number of operations is justified by its ease of implementation and low complexity. A block diagram representing the implementation of the serial search acquisition algorithm is given in Figure 4.3, below[3].
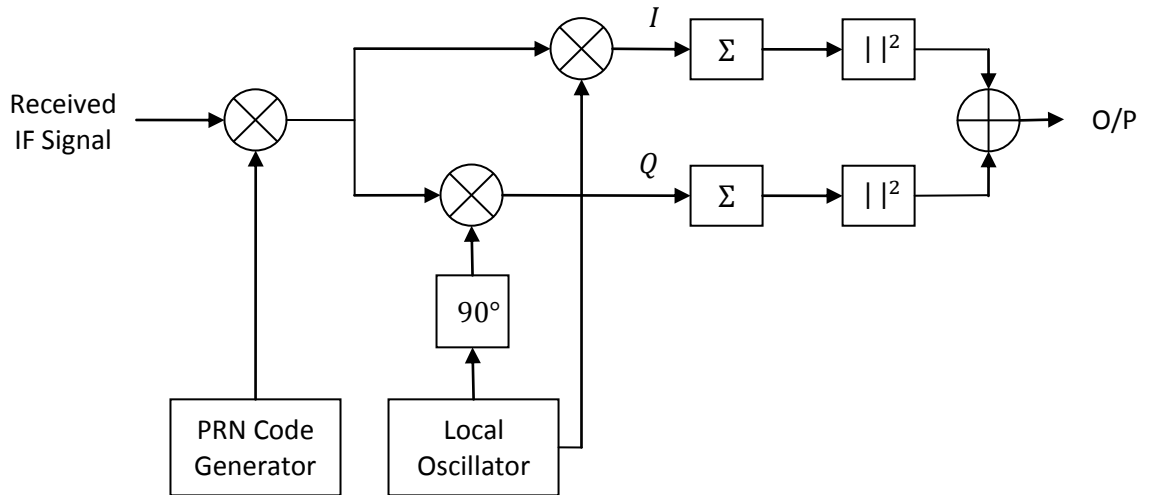
Figure 4.3 - Block Diagram of Serial Search Acquisition

The local PRN code generator generates the spreading code corresponding to a certain code phase for despreading the received IF signal, while the local oscillator generates the carrier wave corresponding to a certain frequency bin for carrier wipe-off. A 90° phase shifter is used to generate the quadrature phase carrier from the local oscillator. The in-phase and quadrature signals, represented by I and Q respectively, are obtained once the signal is despread and the carrier is removed. Samples corresponding to one PRN code period are then integrated and squared to obtain the in-phase and quadrature correlation results of the received IF signal. If the incoming signal and the locally generated carrier wave were in-phase with each other, all the energy would be in the in-phase arm, making the quadrature arm redundant. However, in general this isn't the case, and the energy in the quadrature arm must be included in determining whether a satellite signal is present in the received IF signal. If there is a satellite signal present in the incoming IF signal and the locally generated carrier and code replicas are well aligned with this signal, the output

of the serial search acquisition algorithm will show a peak in the results, which can be detected using a simple thresholding logic.

Figure 4.4 shows the results of the serial search acquisition algorithm carried out in GNSScope using real GPS data recorded from an antenna and front-end. The sampling frequency for the data is $38.192.000\ Hz$ with an IF center frequency of $9.550.000\ Hz$. The peak in the first plot indicates successful acquisition of PRN 3, while the absence of any peaks in the second plot indicates no acquisition of PRN 4, which is not visible in the recorded data.
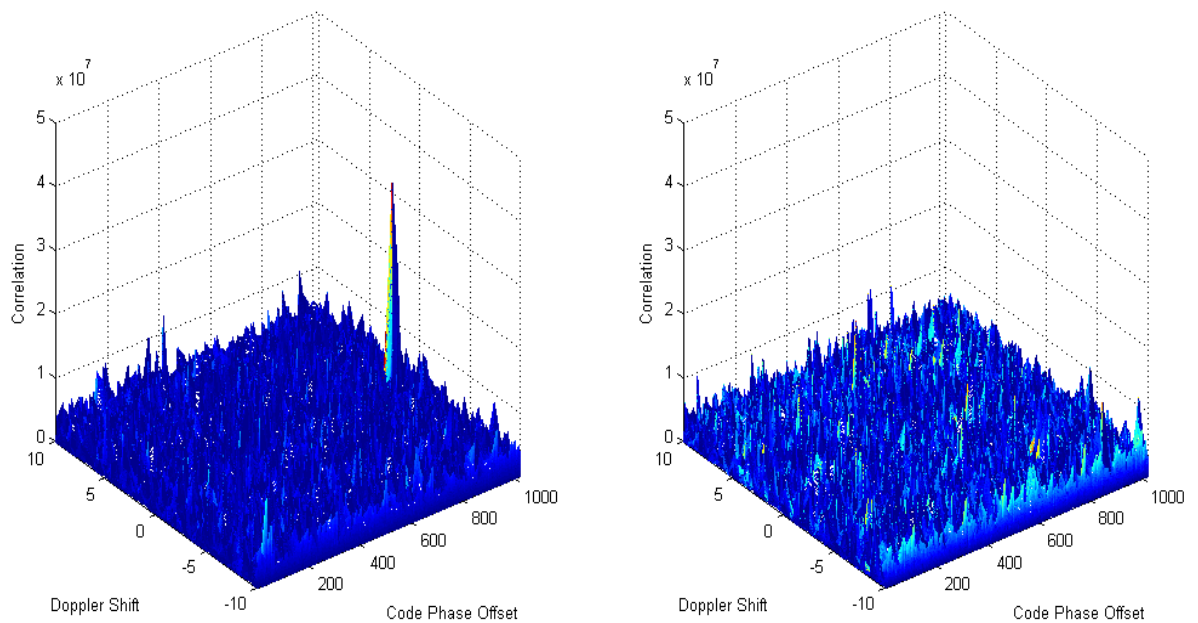
Figure 4.4 - Serial Search Acquisition of PRN 3 and PRN 4

4.3.2 Parallel Frequency Space Search Acquisition

Although the serial search acquisition algorithm successfully detects visible satellites in the incoming signal with a low complexity implementation, searching through each code phase offset for each frequency bin results in a large number of operations and a time consuming search process. The parallel frequency space search acquisition algorithm, as the name suggests, aims to reduce the number of operations involved by parallelizing the search process in the frequency dimension. This is achieved by carrying out the search procedure in the frequency domain, as opposed to the time domain as in the serial search

acquisition algorithm, through the Fourier transform operation. This reduces the time it takes to complete the search procedure, as only the code phase dimension needs to be searched through, at the cost of increased complexity in the form of the Fourier transform operation. A block diagram representing the parallel frequency space search acquisition algorithm can be seen in Figure 4.5, below [1] [3].
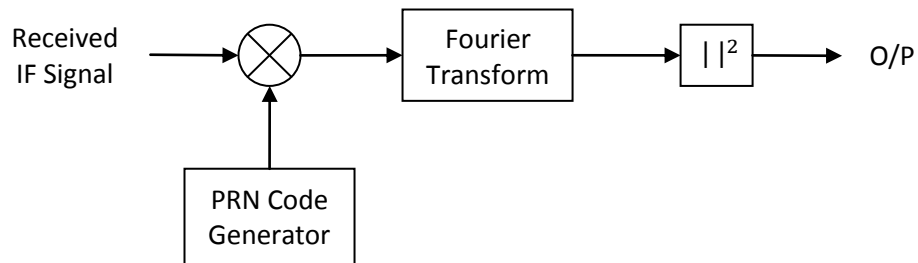
Figure 4.5 - Block Diagram of Parallel Frequency Space Search Acquisition

As seen in the figure, the incoming signal is first despread by multiplying with a locally generated PRN code set at a specific code phase. The resulting signal is then transferred to the frequency domain using the Fourier transformation for the detection of the carrier frequency. When the locally generated PRN code is perfectly aligned with the code in the incoming signal, it is despread and the result becomes a continuous wave signal at the frequency of the carrier with the Doppler shift. The Fourier transform of this continuous wave signal will then show a peak at the corresponding frequency in the frequency domain, indicating the existence of a satellite signal. This removes the need to search each frequency bin to discover the frequency of the carrier wave, parallelizing the process of carrier frequency acquisition and reducing the time taken to complete the acquisition process.

Figure 4.6 shows the results of the parallel frequency space search acquisition algorithm carried out in GNSScope using the same recorded real data signal as in the serial search acquisition example. Both plots correspond to the acquisition of PRN 3, showing the importance of the perfect alignment of the locally generated PRN code. The peak seen in the second plot indicates the exact frequency of the carrier including the Doppler shift,

while the absence of a peak in the first plot indicates that the PRN code is misaligned, causing incorrect removal of the spreading sequence.
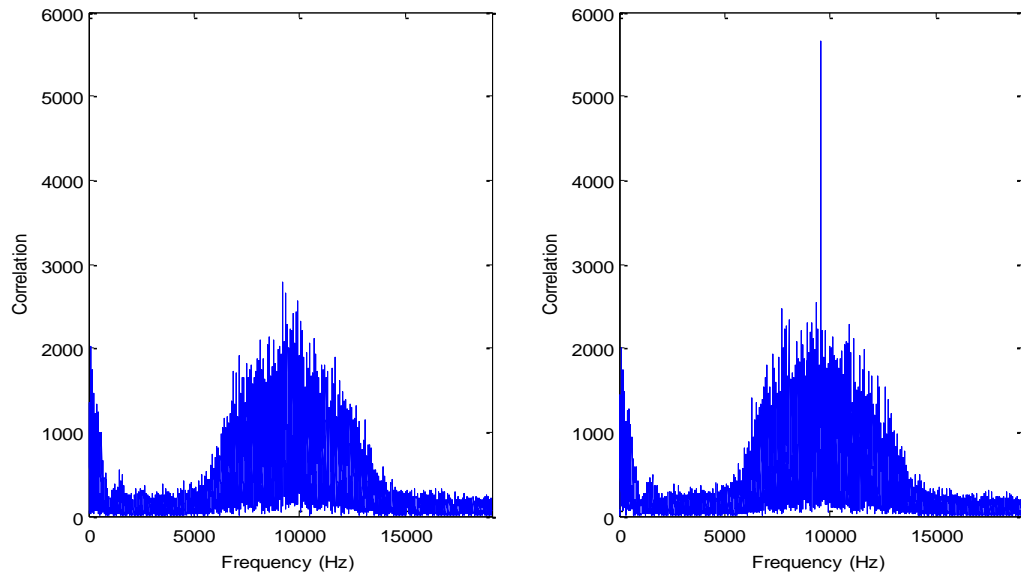
Figure 4.6 - Parallel Frequency Space Search Acqusition of PRN 3

4.3.3 Parallel Code Phase Space Search Acquisition

The parallel frequency space search acquisition technique parallelizes the search process in the frequency dimension, removing the need to search through the 41 frequency bins necessary to cover the $\pm 10\,KHz$ Doppler search range in $500\,Hz$ steps. While this reduces the number of operations to a certain extent, the large number of steps necessary to cover the code phase dimension creates a bottleneck in the search process. The parallel code phase space search acquisition technique addresses this issue by parallelizing the search procedure in the code phase dimension, resulting in only 41 iterations to search through all the frequency bins in the acquisition, further reducing the time required to complete the acquisition at the cost of increased complexity [1][2] [3]. The block diagram representation of the technique is given in Figure 4.7, below.
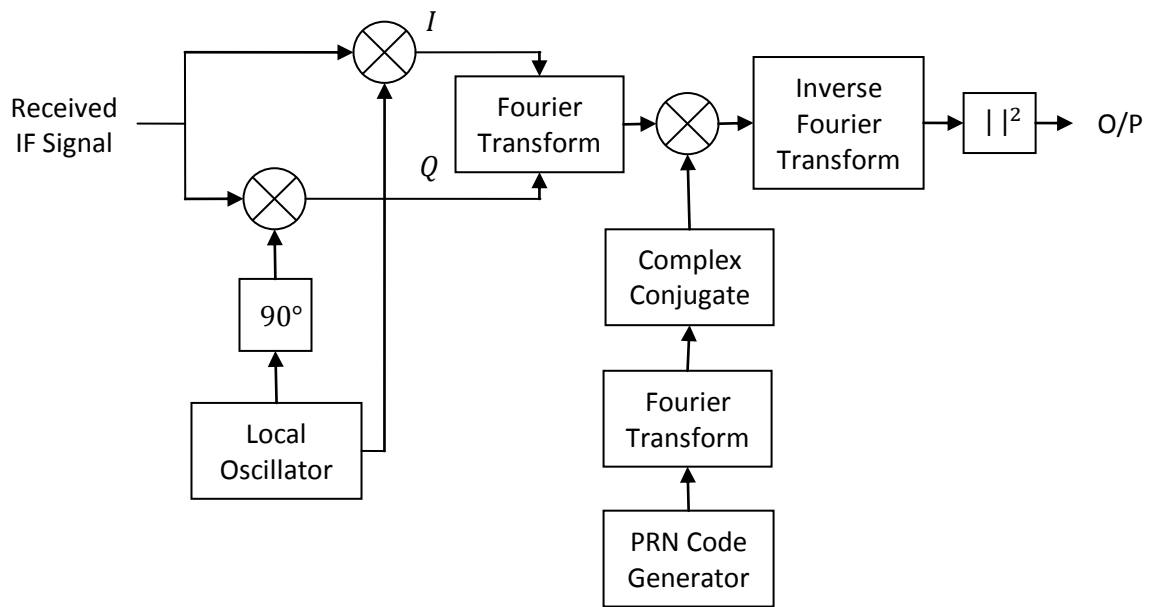
Figure 4.7 - Block Diagram of Parallel Code Phase Space Search Acquisition

As seen in the figure, the first step is to remove the carrier from the received IF signal by multiplying with the locally generated carrier corresponding to a specific frequency bin. This produces the in-phase and quadrature signals which are combined to generate the following complex signal:

$$s[n] = I[n] + jQ[n]$$

Eq. 4.2

This complex signal is transferred to the frequency domain using the Fourier transformation. The locally generated PRN code is also transferred to the frequency domain using the Fourier transformation followed by complex conjugation. These two signals are then multiplied in the frequency domain to carry out the time domain equivalent circular correlation operation. The results are then converted back to the time domain through an inverse Fourier transform followed by a squaring operation to obtain the correlation results expressed in terms of signal energy. When the locally generated carrier wave and PRN code are perfectly aligned with the received IF signal, the output will present with a peak, indicating successful detection of a satellite in the signal.

4.3.4 Acquisition of the New GNSS Signals

As mentioned in Chapter 3, up and coming navigation signals as well as the modernized signals for GPS utilize the new BOC type modulations in place of the PSK type modulations currently in use. This requires certain modifications to be made to the acquisition algorithms in order to handle these new signals. In addition to the spreading code and carrier wave, in BOC type modulations the spreading code is modulated by an additional square-wave sub-carrier. Acquiring these signals requires the PRN code generator to be modified to include the relevant square-wave sub-carrier, which is sine or cosine oriented depending on the specific type of BOC modulation in use. Treating the new offset carrier as part of the PRN code spreading the navigation message enables the above mentioned acquisition techniques developed for PSK type modulations to be reused for the acquisition of BOC type modulations, without complicating the acquisition algorithms any further. The new PRN code generator block diagram is given in Figure 4.8, below [18] [27] [28].
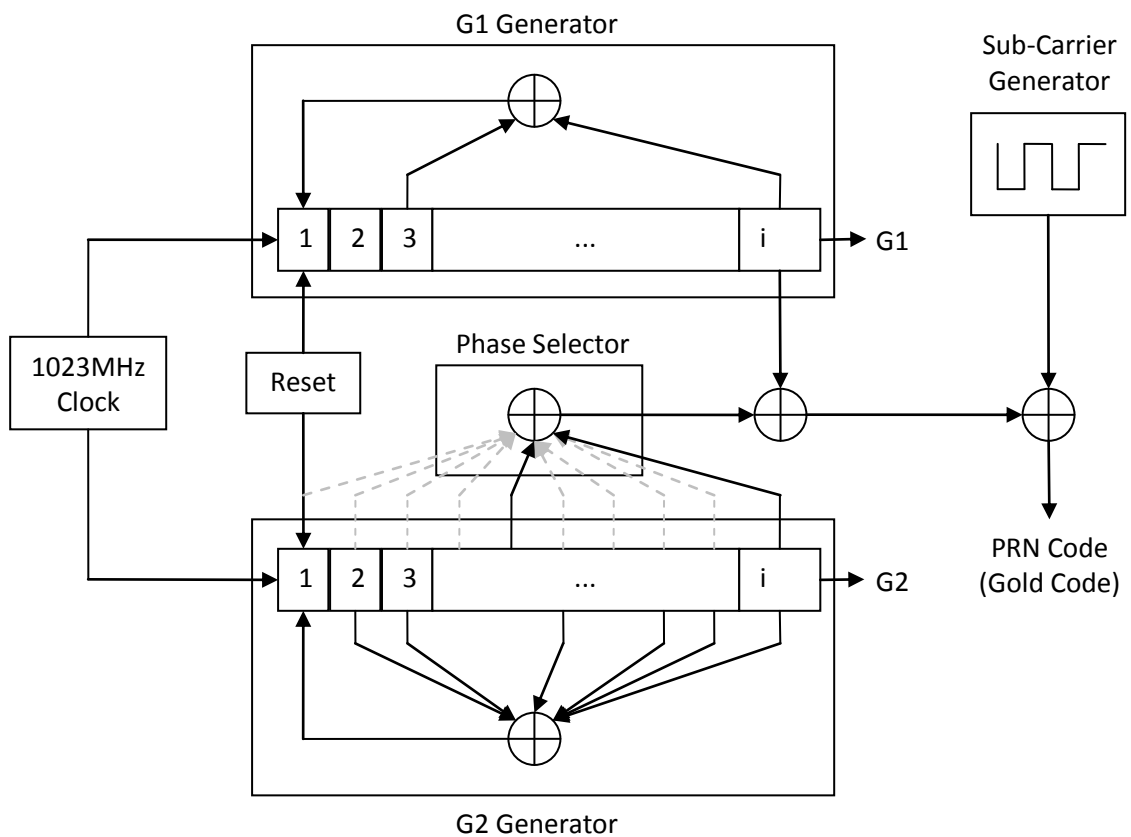
Figure 4.8 - Modified PRN Code Generator for BOC Type Modulations

Figure 4.9 shows the results of the parallel code phase space search acquisition algorithm carried out in GNSScope using real GIOVE-A data recorded from an antenna and front-end. The sampling frequency for the data is $16.367.600\ Hz$ with an IF center frequency of $4.130.400\ Hz$. The first plot is the complete results of the acquisition search with the peak indicating successful acquisition of the GIOVE-A signal. The second plot is a cross-section of the first plot along the code phase dimension, with an enlarged version of the peak in the inlay plot displaying the characteristic BOC auto-correlation [5] [8].
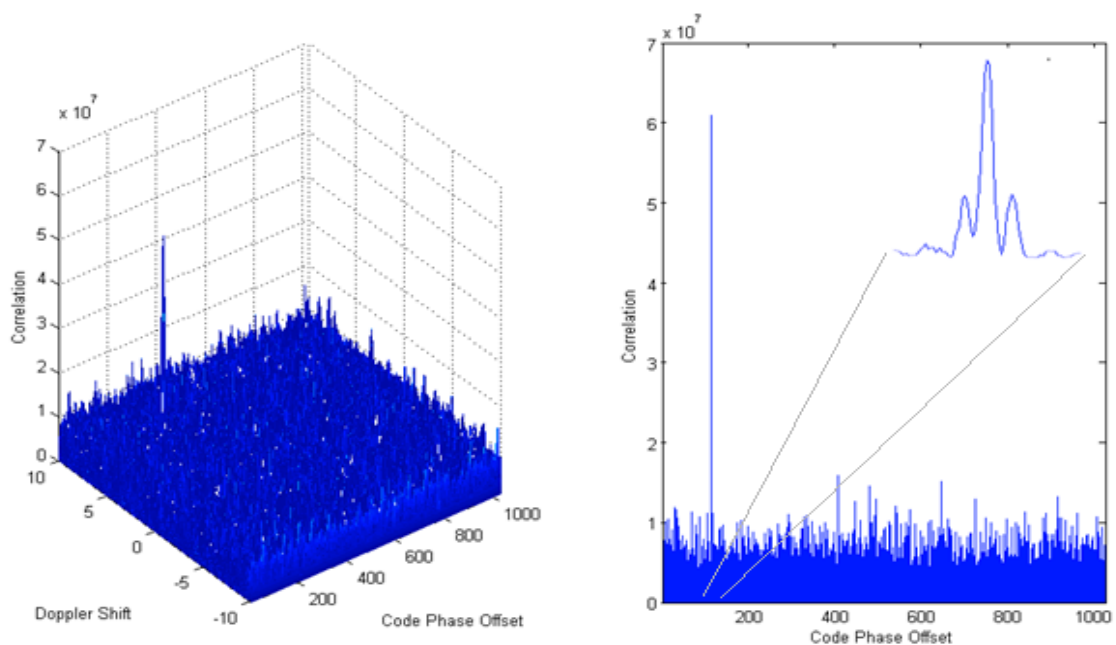
Figure 4.9 - Parallel Code Phase Space Search Acquisition of the GIOVE-A Signal

4.4 Tracking

The coarse carrier frequency and code phase offset estimates computed by the acquisition process for each visible satellite are used as initial conditions for the digital tracking channels, with each acquired satellite being assigned its own digital tracking channel. Once these estimates are computed, the tracking channels need to keep a lock on acquired satellites and decode the navigation data message from the received IF signal, to be used in calculating satellite and user positions. In order to accomplish this,

the digital tracking channels must accurately estimate the carrier frequency and carrier phase for carrier wipe-off, and the code phase offset for code stripping and despreading the satellite signal [1][2]. This basic tracking concept is illustrated in the block diagram given in Figure 4.10, below.
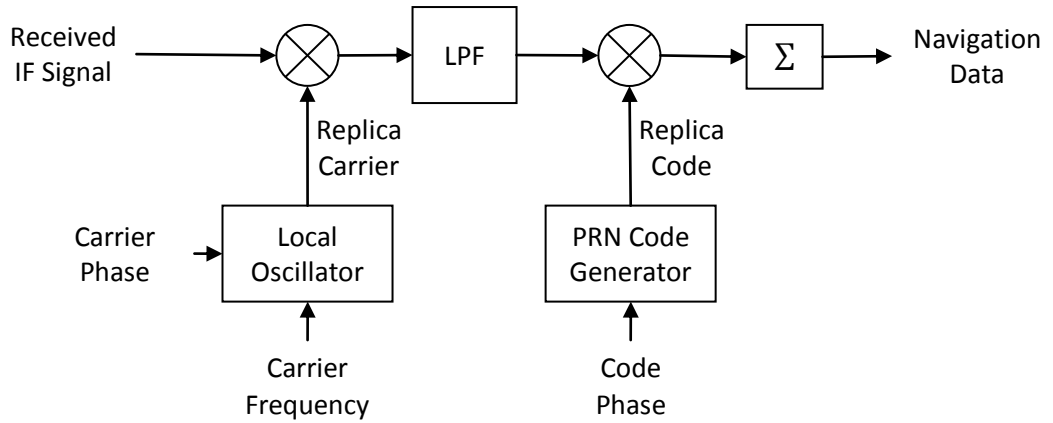
Figure 4.10 - Basic Tracking Concept

The received IF signal, containing the signal of interest, can be represented as follows:

$$s^i[n] = PRN^i[n]D^i[n] \cos(2\pi f_{IF} n) + \varepsilon[n]$$

Eq. 4.3

where $s^i[n]$ is the signal component representing the ith satellite, PRN^i is the corresponding spreading sequence, including the offset carrier in the case of BOC modulated signals, D^i is the navigation data contained in the signal, $\cos(2\pi f_{IF} n)$ is the carrier corresponding to the signal of interest, and $\varepsilon[n]$ is the noise or error in the received IF signal due to various sources including cross-correlations from other satellite signals, while n depicts the signal is in discrete time. Following the concept in Figure 4.10, carrier wipe-off is achieved by multiplication with the locally generated carrier wave. If the incoming and locally generated carriers are perfectly aligned in frequency and phase, the resulting signal can be expressed as follows:

$$s^i[n] \cos(2\pi f_{IF} n) = PRN^i[n]D^i[n] \cos(2\pi f_{IF} n) \cos(2\pi f_{IF} n)$$

Eq. 4.4

Using the simple trigonometric expansion for the multiplication of two cosines, the resulting signal can be expressed as follows:

$$s^i[n]\cos(2\pi f_{IF}n) = \frac{1}{2}PRN^i[n]D^i[n] + \frac{1}{2}PRN^i[n]D^i[n]\cos(2\pi 2f_{IF}n)$$

Eq. 4.5

where the first term is the signal of interest with the carrier wiped-off, and the second term is the same signal at double IF. The double IF term can be filtered out using a simple low pass filter, leaving the spread signal of interest, $PRN^i[n]D^i[n]$.

The second stage in the demodulation process is the despreading of this signal, which is accomplished by multiplication with the locally generated PRN code. As each data bit is spread across the full length of the PRN code, the resulting signal must also be accumulated for the full length of the PRN code in order to obtain the maximum energy from the received IF signal. If the incoming and locally generated PRN codes are perfectly aligned, the resulting signal can be expressed as follows:

$$\sum_{n=0}^{N-1} PRN^i[n]PRN^i[n]D^i[n] = ND^i[n]$$

Eq. 4.6

where N is the length of the spreading code, including the offset carrier in the case of BOC modulated navigation signals. Thus, when the digital tracking channel is locked onto the satellite signal, the output is the navigation data message.

As the acquisition process is a time and resource consuming process, it is important that once a lock is established on a satellite, it is not lost by the digital tracking channels as long as it remains visible. However, as the satellite and receiver dynamics change over time, so do the parameters of the satellite signals of interest. In order to achieve a successful lock on these signals, it is necessary to use a feedback loop structure to follow the carrier frequency and code phase offset. This is accomplished with a carrier tracking loop and a code tracking loop, to track the carrier frequency and code phase offset, respectively. As both of these feedback loops are based on digital Phase Locked Loops (PLL), the principles and basic operation of digital PLLs will be given in the following sub-section, followed by the details of the carrier and code tracking loops.

4.4.1 Principles of Digital Phase Locked Loops

Phase Locked Loops are used to control the frequency of a local oscillator in order to track the frequency of an input signal, also referred to as the reference signal. They are based on a phase comparator used to measure the phase difference between the incoming and locally generated signals until a match is achieved. A detailed analysis of analog PLLs can be found in [29], with details regarding digitization of the analog PLL model in [1], [2] and [30]. A generalized block diagram of an analog PLL can be seen in Figure 4.11, below, where frequency domain representations of the Numerically Controlled Oscillator (NCO) and Low Pass Filter (LPF) are given in the figure.
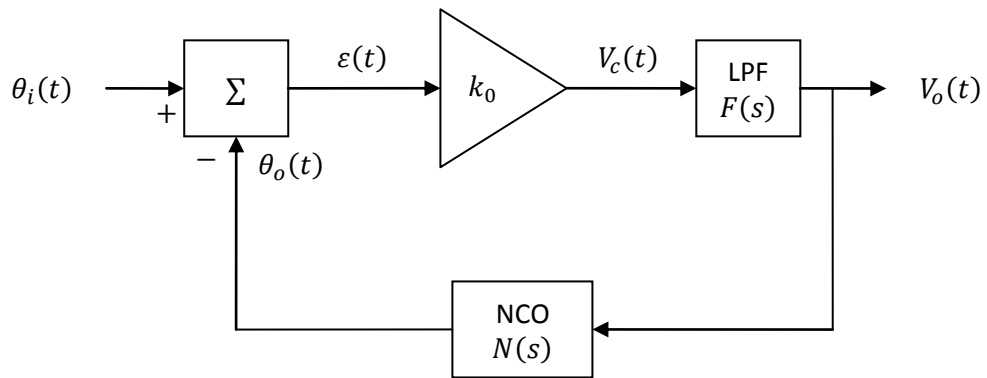
Figure 4.11 - Generalized Analog PLL Block Diagram

The two inputs to the phase comparator are $\theta_i[n]$, representing the input signal to the digital PLL, and $\theta_o[n]$, representing the output of the NCO, the digital equivalent of an analog Voltage Controlled Oscillator (VCO). The output of the phase comparator is the error term $\varepsilon[n]$ representing the phase difference between these two signals. The amplifier in the block diagram is a representation of the internal gain factor, k_0, of the phase comparator, and is not implemented as a separate amplifier. The overall output of the phase comparator is represented by the voltage $V_c[n]$. The LPF is used to limit the noise in the loop and is represented in the frequency domain by the function $F(z)$. The output of the LPF is the voltage $V_o[n]$, and is used to control the frequency of the NCO. The expressions for a digital PLL will be derived from the expressions for an analog PLL. Further details regarding these derivations and further details can be found in [1] [2] [3].

The transfer function of an analog VCO can be expressed in the Laplace domain as follows:

$$N(s) = \frac{k_1}{s}$$

<div align="right">Eq. 4.7</div>

The order of the transfer function of the LPF also determines the order of the PLL. Of particular interest to this work are first and second order PLLs, utilizing zero order and first order transfer functions from the following analog LPFs in the Laplace domain:

$$F(s) = 1$$

<div align="right">Eq. 4.8</div>

$$F(s) = \frac{s\tau_2 + 1}{s\tau_1}$$

<div align="right">Eq. 4.9</div>

Using these s-domain representations, the overall transfer function of a second order analog PLL can be expressed in the Laplace domain as follows:

$$H(s) = \frac{2\zeta\omega_n s + \omega_n^2}{s^2 + 2\zeta\omega_n s + \omega_n^2}$$

<div align="right">Eq. 4.10</div>

where ζ is referred to as the damping ratio and ω_n is referred to as the natural frequency of the PLL, and are obtained from the following expressions:

$$\zeta = \tau_2\omega_n/2$$

<div align="right">Eq. 4.11</div>

$$\omega_n = \sqrt{(k_0 k_1)/\tau_1}$$

<div align="right">Eq. 4.12</div>

Another important parameter of a PLL is the noise bandwidth B_n, which is expressed as:

$$B_n = \frac{\omega_n}{2}\left(\zeta + \frac{1}{4\zeta}\right)$$

<div align="right">Eq. 4.13</div>

These three parameters, the damping ratio, the natural frequency and the noise bandwidth, are used to characterize analog and digital PLLs in general.

The block diagram of a digital PLL is given in Figure 4.12, below.
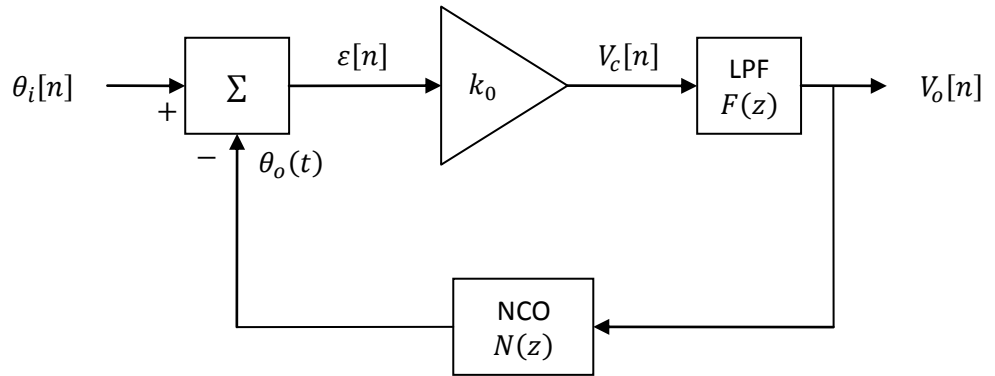
Figure 4.12 - Generalized Digital PLL Block Diagram

In order to derive the expressions for a digital PLL, the z-domain equivalents of the above expressions must be derived. The transfer function of the NCO can be expressed as:

$$N(z) = \frac{k_1 z^{-1}}{1 - z^{-1}}$$

Eq. 4.14

where k_1 is the gain factor of the NCO. The analog LPFs given above can be transformed from the continuous s-domain to the discrete z-domain using the bilinear transformation, as follows:

$$F(z) = C_0 \frac{1 - z^{-1}}{1 + z^{-1}}$$

Eq. 4.15

$$F(z) = \frac{(C_1 - C_2) - C_1 z^{-1}}{1 - z^{-1}}$$

Eq. 4.16

The constants C_0, C_1 and C_2 are expressed as:

$$C_0 = \frac{2}{t_s}$$

Eq. 4.17

$$C_1 = \frac{2\tau_2 - t_s}{2\tau_1}$$

Eq. 4.18

$$C_2 = \frac{t_s}{\tau_1}$$

Eq. 4.19

where t_s represents the sampling interval, and τ_1 and τ_2 are the LPF constants. The transfer function of the digital PLL can be expressed as:

$$H(z) = \frac{\theta_o(z)}{\theta_i(z)} = \frac{k_0 F(z) N(z)}{1 + k_0 F(z) N(z)}$$

Eq. 4.20

Substituting the transfer functions for the LPF and NCO into this expression, the transfer function of a second order digital PLL can be expressed as:

$$H(z) = \frac{k_0 k_1 (C_1 + C_2) z^{-1} - k_0 k_1 C_1 z^{-2}}{1 + [k_0 k_1 (C_1 + C_2) - 2] z^{-1} + (1 - k_0 k_1 C_1) z^{-2}}$$

Eq. 4.21

The expressions for the constants C_1 and C_2 are obtained by applying the bilinear transformation to the transfer function of the analog PLL and equating it to the transfer function of the digital PLL, and can be expressed as follows:

$$C_1 = \frac{1}{k_0 k_1} \frac{8\zeta \omega_n t_s}{4 + 4\zeta \omega_n t_s + (\omega_n t_s)^2}$$

Eq. 4.22

$$C_2 = \frac{1}{k_0 k_1} \frac{4(\omega_n t_s)^2}{4 + 4\zeta \omega_n t_s + (\omega_n t_s)^2}$$

Eq. 4.23

GNSScope was designed with fully configurable PLL implementations capable of on-the-fly reconfiguration to adapt the performance of the receiver as the digital tracking channels obtain a stronger lock on the satellites being tracked. Reducing the noise bandwidth once a strong lock is obtained enables higher precision estimation of the carrier and code parameters necessary for the decoding process. The nominal values of the PLL parameters are given below, and are fully configurable by the user / designer through the user interface of GNSScope:

$$\zeta = \frac{\sqrt{2}}{2}$$

Eq. 4.24

$$B_n = 25 \ Hz$$

4.4.2 The Carrier Tracking Loop

The purpose of the carrier tracking loop is to generate an exact replica of the carrier wave in the incoming IF signal to be able to correctly wipe-off the carrier. As mentioned above, the carrier tracking loop is based on the PLL architecture, and is modified to be insensitive to 180° phase shifts due to the navigation data present in the incoming IF signal. This modified phase locked loop is referred to as the Costas carrier tracking loop, and is given in Figure 4.13, below [1].
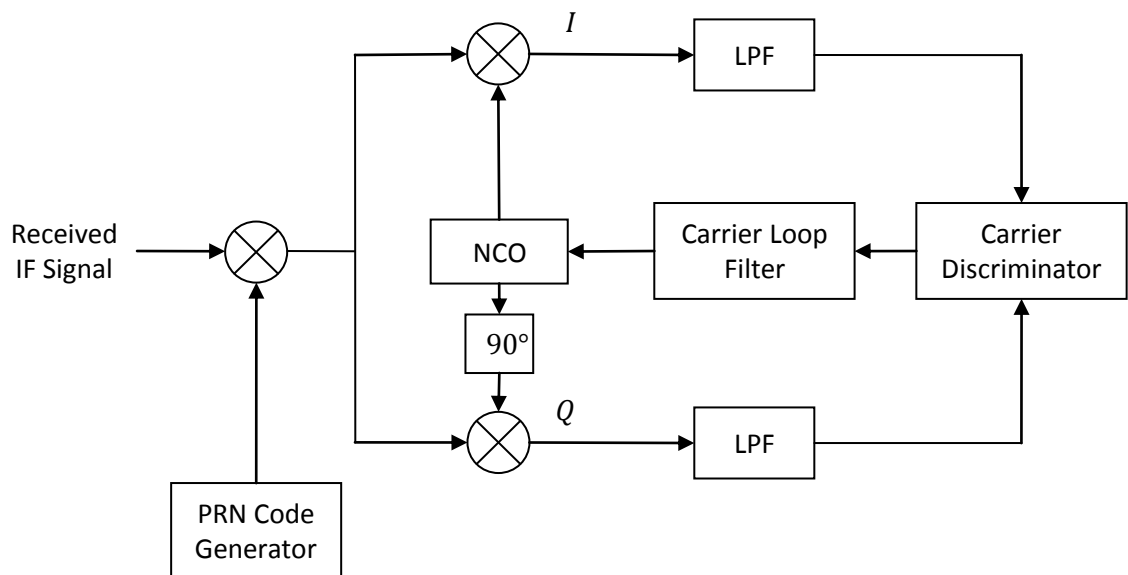
Figure 4.13 - The Costas Carrier Tracking Loop

The Costas carrier tracking loop assumes that the spreading code generated by the PRN code generator is perfectly aligned with that of the incoming IF signal, in order to successfully despread the signal. Assuming for simplicity, that the incoming signal doesn't contain any noise, the despread signal can be expressed as:

$$s^i[n] = D^i[n]\cos(2\pi f_{IF}n)$$

Eq. 4.25

This is followed by the modified PLL which is made insensitive to 180° phase shifts with the addition of the quadrature phase arm. Following multiplication by the locally

generated carrier wave, the signals in the in-phase and quadrature phase arms can be expressed, respectively, as:

$$I^i[n] = D^i[n] \cos(2\pi f_{IF} n) \cos(2\pi f_{IF} n + \varphi)$$

$$= \frac{1}{2} D^i[n] \cos(\varphi) + \frac{1}{2} D^i[n] \cos(2\pi 2 f_{IF} n + \varphi) \qquad \text{Eq. 4.26}$$

$$Q^i[n] = D^i[n] \cos(2\pi f_{IF} n) \sin(2\pi f_{IF} n + \varphi)$$

$$= \frac{1}{2} D^i[n] \sin(\varphi) + \frac{1}{2} D^i[n] \sin(2\pi 2 f_{IF} n + \varphi) \qquad \text{Eq. 4.27}$$

The double-IF term is then filtered out using the LPFs in the in-phase and quadrature arms of the PLL. The carrier discriminator acts as a phase detector in the PLL, providing the carrier loop filter with the phase error between the incoming and locally generated carrier wave. The phase error can be obtained from Eq. 4.26 and Eq. 4.27, as follows:

$$\frac{Q^i[n]}{I^i[n]} = \frac{\frac{1}{2} D^i[n] \sin(\varphi)}{\frac{1}{2} D^i[n] \cos(\varphi)} = \frac{\sin(\varphi)}{\cos(\varphi)} = \tan(\varphi) \qquad \text{Eq. 4.28}$$

$$\varphi = \tan^{-1}\left(\frac{Q^i[n]}{I^i[n]}\right) \qquad \text{Eq. 4.29}$$

The phase error is then passed through the carrier loop filter and the output is used to control the frequency of the locally generated carrier wave to match that of the incoming IF signal. When the energy is concentrated in the in-phase arm, the phase error approaches zero, indicating that the incoming and locally generated carrier waves are matched. Although the arctangent discriminator given in Eq. 4.29 provides the precise phase error between the incoming and locally generated carrier waves, it also has high computational complexity, resulting in lengthy computation times. Alternative carrier discriminators with reduced complexity are given in Table 4.1, below.

Table 4.1 - Costas Carrier Loop Discriminators

Discriminator Function	Discriminator Output
$D = \tan^{-1}(Q^i/I^i)$	Proportional to phase error φ
$D = \text{sign}(I^i) Q^i$	Proportional to $\sin \varphi$
$D = I^i Q^i$	Proportional to $\sin 2\varphi$

4.4.3 The Code Tracking Loop

The purpose of the code tracking loop is to generate an exact replica of the spreading code in the incoming IF signal to be able to correctly despread the coded signal. Similar to the carrier tracking loop, the code tracking loop is also based on the principles of PLLs. However, rather than multiplying with the locally generated replica as in the carrier tracking loop, the incoming IF is correlated with delayed locally generated replicas of the spreading code, in order to despread the signal. This modified loop is referred to as the Delay Locked Loop (DLL), as it uses different delays of the same signal rather than different phases, and is given in Figure 4.14, below [1].
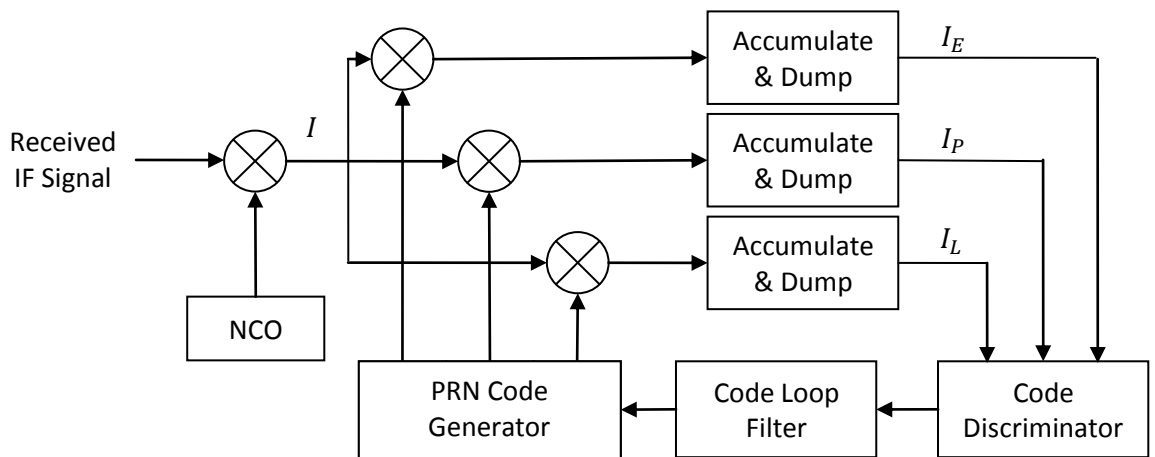
Figure 4.14 - Basic DLL Block Diagram

Following carrier wipe-off, the baseband signal is correlated with three replicas of the locally generated PRN code; the early, prompt and late replicas. Due to the characteristics of the spreading codes, when the locally generated PRN code is one chip out of phase, the correlation result will approach zero, indicating no match. The early, prompt and late correlation outputs are input to the carrier discriminator, which acts as a phase detector in the DLL. The output of the carrier discriminator is used to adjust the phase of the PRN code generator. One common discriminator used in GNSS for this basic DLL is $I_E - I_L$, where I_E and I_L refer to the early and late in-phase correlations, respectively. Although this is a very basic discriminator with a simple implementation, in order to perform well, it requires that the locally generated carrier is in perfect phase alignment with the incoming

IF signal. However, this may not always be the case, due to interference, jamming and noise on the incoming IF signal. In order to make the code tracking loop insensitive to phase shifts in the signal, a quadrature phase arm is added to the processing loop, similar to the carrier tracking loop. This modified code tracking loop is referred to as the Costas code tracking loop, and is given in Figure 4.15, below [1].
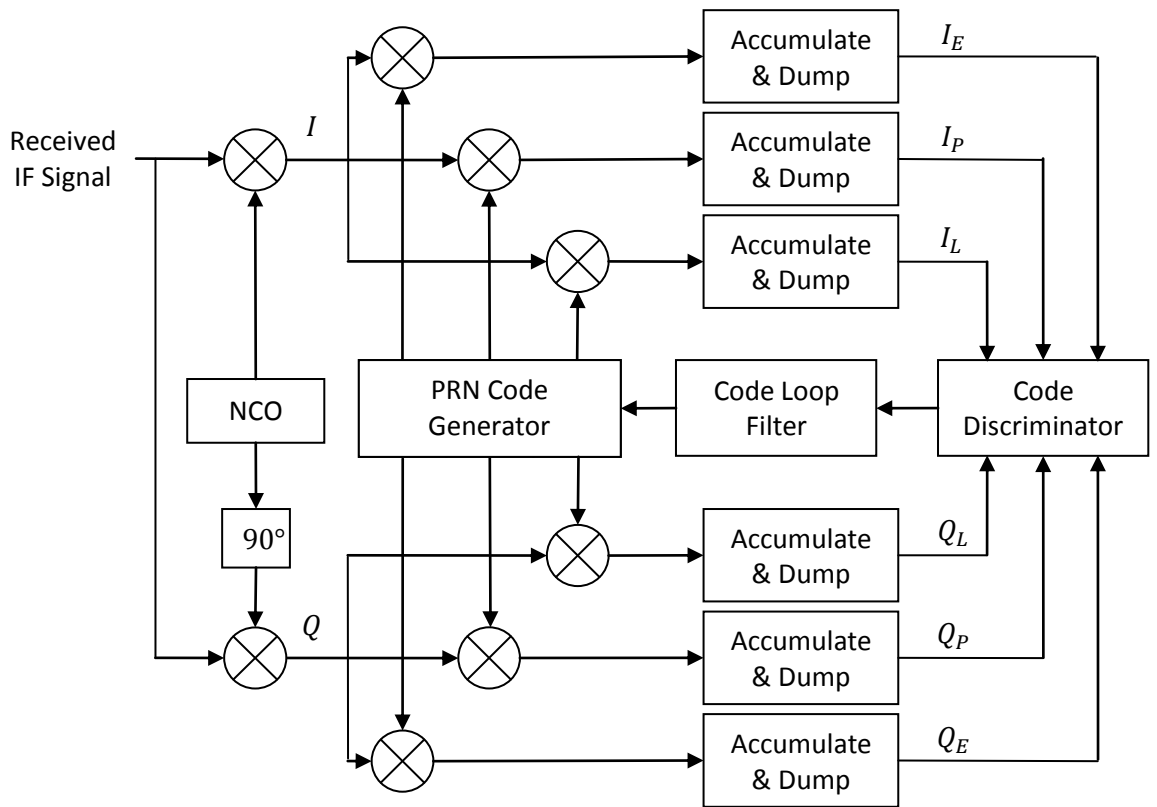
Figure 4.15 - The Costas Code Tracking Loop

When the locally generated carrier wave and PRN code are perfectly aligned, the prompt in-phase correlation output, I_P, will give the data bit encoded into the signal. When there are errors in the locally generated carrier wave and PRN code sequence, the energy in the accumulator outputs will shift between the in-phase and quadrature phase arms of the tracking loop. Common discriminators used in this Costas code tracking loop are given in Table 4.2, below. Of these discriminators, the normalized early minus late power discriminator provides a good estimate of the phase error while being independent of the SNR of the incoming signal due to the normalization, or the performance of the carrier tracking loop due to its use of the quadrature phase results.

Table 4.2 - Costas Code Tracking Loop Discriminators

Discriminator Name	Discriminator Function
Early minus Late Power Discriminator	$D = (I_E^2 + Q_E^2) - (I_L^2 + Q_L^2)$
Normalized Early minus Late Power Discriminator	$D = \dfrac{(I_E^2 + Q_E^2) - (I_L^2 + Q_L^2)}{(I_E^2 + Q_E^2) + (I_L^2 + Q_L^2)}$
Dot Product Discriminator	$D = I_P(I_E - I_L) + Q_P(Q_E - Q_L)$

4.4.4 The Combined Costas Code and Carrier Tracking Loop

The two Costas tracking loops described above are combined to form the Costas code and carrier tracking loop, also referred to as the Costas loop, which is given in Figure 4.16, below [1], where the individual code and carrier tracking loops given in the preceding sections are combined in a feedback loop configuration.
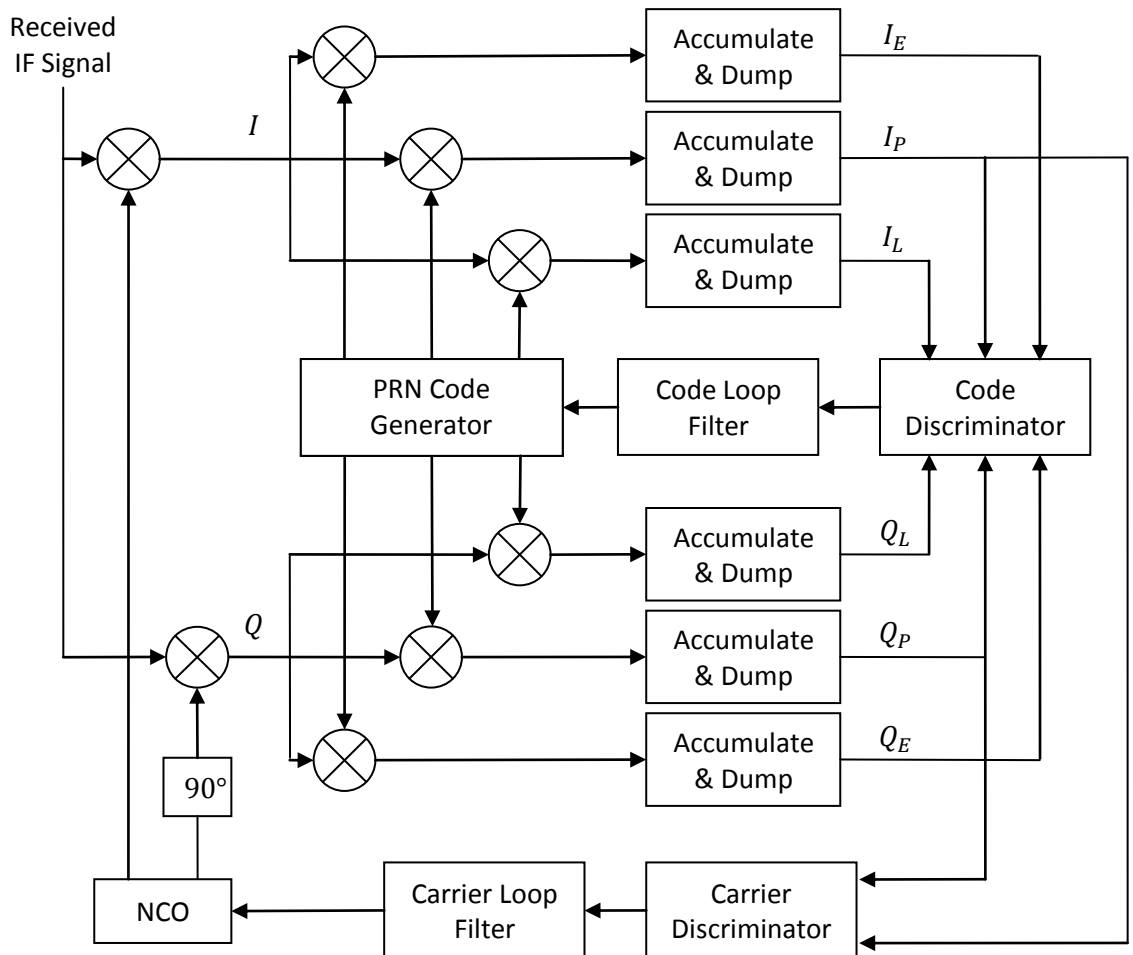
Figure 4.16 - The Costas Code and Carrier Tracking Loop

Combining the two loops achieves two goals; first of all it ensures that the locally generated PRN code used to despread the incoming IF signal in the carrier tracking loop and the locally generated carrier wave used to wipe-off the carrier in the code tracking loop are in good phase alignment with the incoming IF signal. Secondly, by combining the two loops, the number of operations necessary to complete the tracking operation is reduced, leading to faster operation times and simpler hardware implementations.

4.4.5 Tracking of the New GNSS Signals

While the combined Costas code and carrier tracking loop is good at tracking signals with PSK type modulations such as the currently available GPS signals, it requires further modifications in order to cope with the new BOC type modulated navigation signals [27]. To this end several new tracking techniques have been implemented in GNSScope. The simplest of these implementations is to treat the new offset carrier wave as being part of the PRN code spreading the navigation data sequence, as done in the acquisition technique for the BOC type modulations described in this chapter. This is achieved by modifying the PRN code generator in the Costas tracking loop to include the offset carrier, as shown in Figure 4.8. The resulting autocorrelation function for the GIOVE-A satellite signal generated in GNSScope is given in Figure 4.17, below, along with the autocorrelation function of a PSK modulated signal for reference [5] [31].
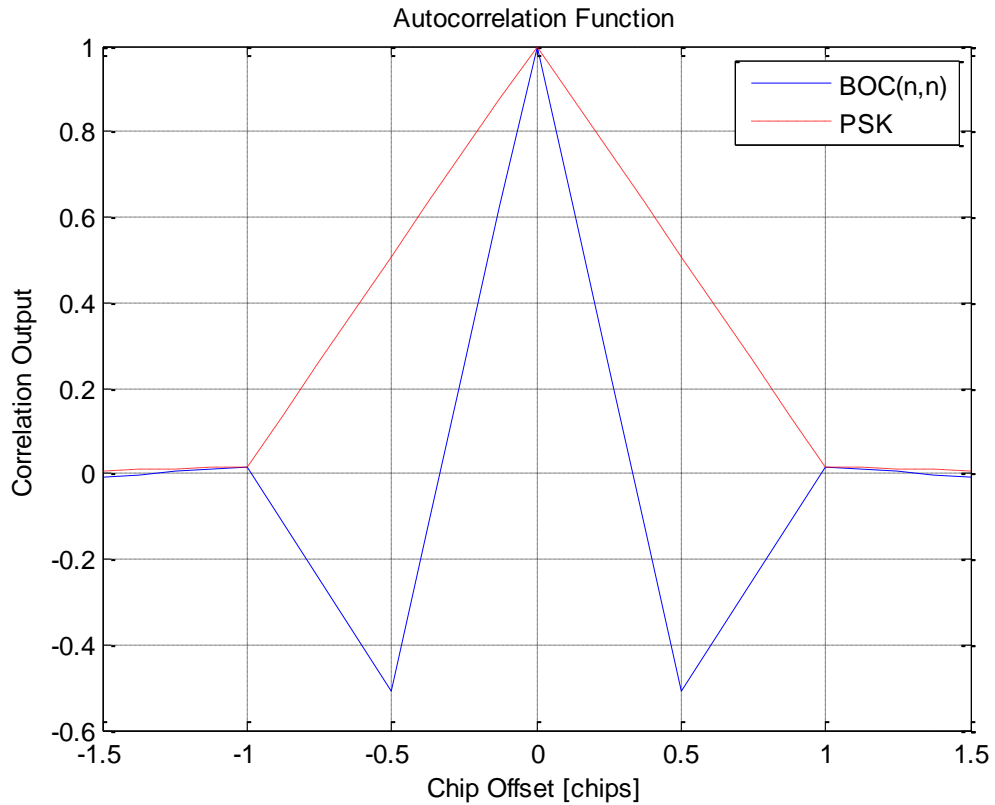
Figure 4.17 - Autocorrelation Function of the GIOVE-A BOC Code

It can be seen from the figure that this approach results in an autocorrelation function presenting with one stable peak representing the correct alignment of the PRN codes, similar to PSK modulated signals, and two unstable peaks at half a chip offset from the correct alignment. The effect of these unstable peaks caused by the offset carrier can be further analyzed by observing the response of the discriminators to these BOC type modulations. For simplicity, the coherent early minus late discriminator will be used as it provides linear responses making it easier to compare discriminator gain in the prime interval. Figure 4.18, below, illustrates the discriminator responses in GNSScope when using 0.25 chip, 0.5 chip and 1 chip spacing between the early and late correlator arms. The discriminator response when presented with a PSK modulated signal using 0.5 chip spacing is also included in the figure in order to provide a frame of reference.
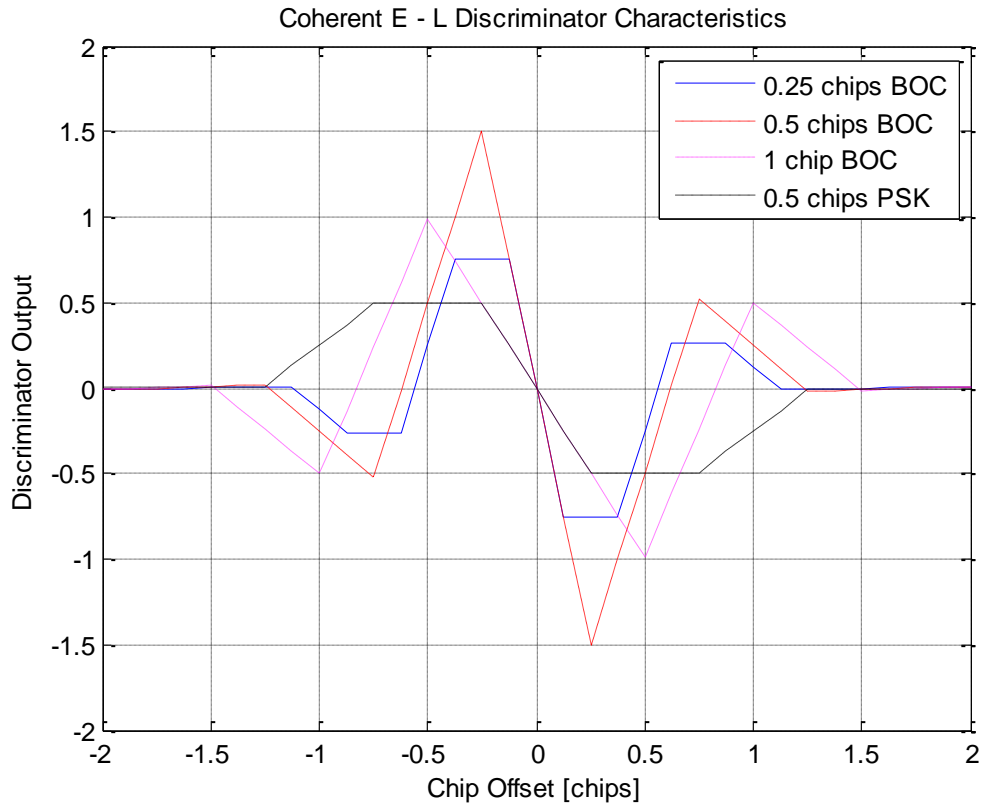
Figure 4.18 - Discriminator Characteristics for BOC and PSK Modulations

It can be seen that, while providing a similar response to the PSK modulated signals, the 1 chip spacing coherent discriminator negates any gains obtained from the use of the offset carrier in BOC modulated signals, resulting in the same slope, or gain, in the neighborhood of the stable node. In contrast, the half-chip and quarter-chip spacing coherent discriminator responses display improved gain at the cost of reducing the linear operation range of the discriminator by around a third, due to the unstable nodes introduced from the offset carrier.

The linear operation range of this technique can be increased by introducing additional correlators into the tracking loop. In GNSScope, this is done by the addition of the very early and very late correlator arms, as indicated in Figure 4.19, below. When set to track the unstable peaks in the autocorrelation characteristics, the information provided by these correlators can be used to move the tracking estimation towards the stable peak when it locks onto one these unstable peaks while tracking a signal, hence improving receiver performance and ensuring perfect code alignment [5] [8].
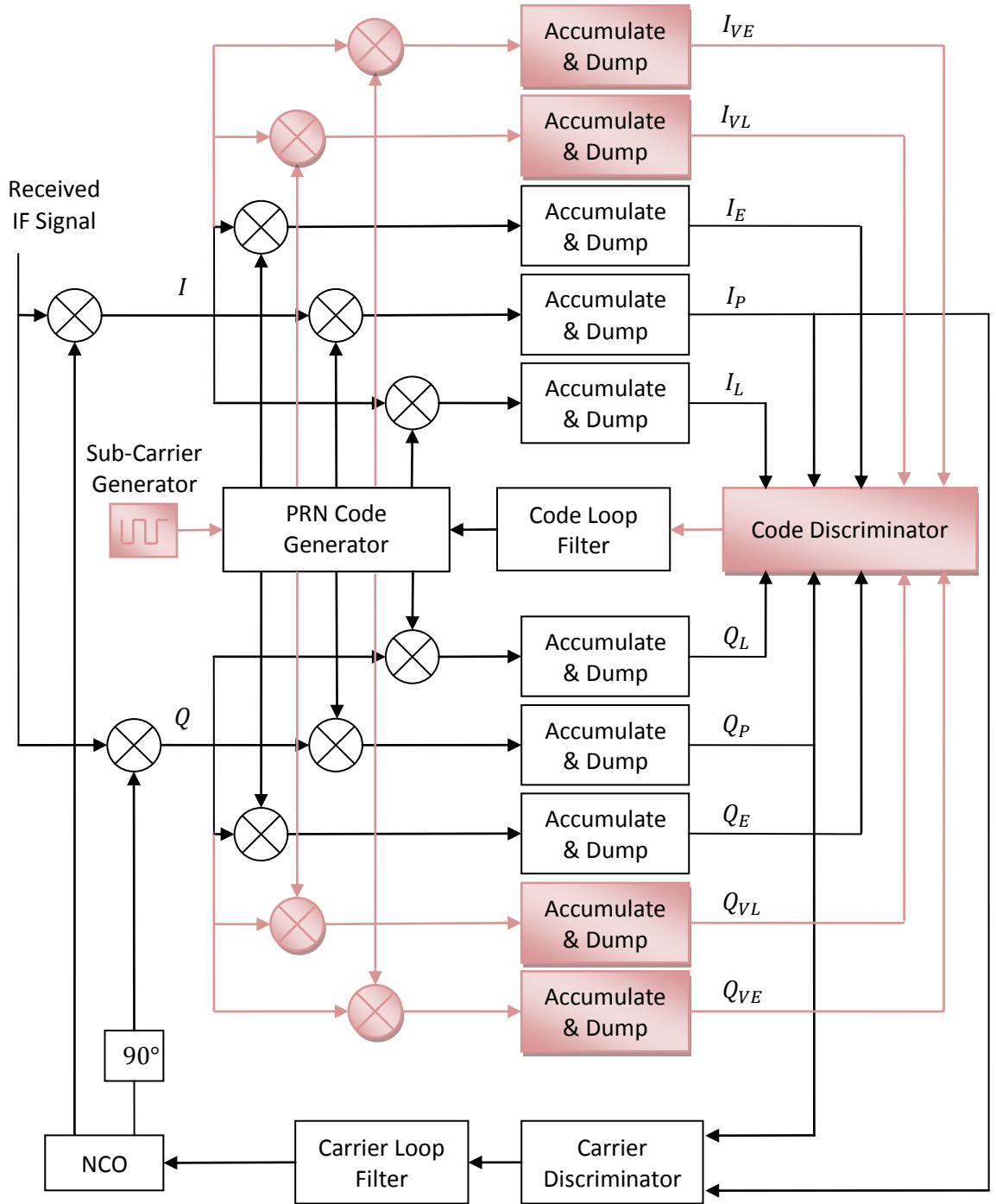
Figure 4.19 - Block Diagram of the Modified Costas Code and Carrier Tracking Loop

An alternative technique developed in GNSScope utilizes the fact that the PRN code and the offset carrier present in BOC type modulations are synchronized at the satellite prior to being transmitted. Thus, rather than tracking the composite BOC code, the tracking loop can be configured to track the underlying PRN code only, simplifying the tracking

loop and resulting in a new cross-correlation characteristic, presented in Figure 4.20, below.
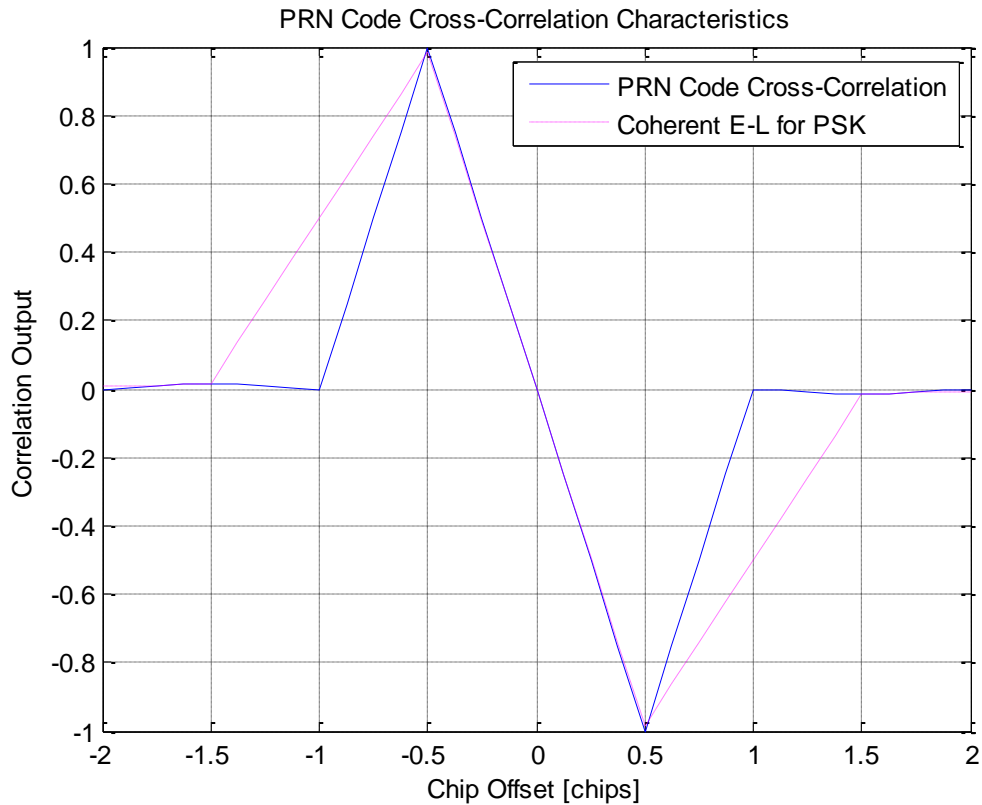
Figure 4.20 - PRN Code Cross-Correlation Characteristic

Comparing the cross-correlation output when the composite BOC spreading code is treated as a PRN code, with the coherent early minus late discriminator characteristics of PSK type modulations, it can be seen that they return identical phase errors in the ± 0.5 chip range. This cross-correlation characteristic in itself is used in GNSScope as a discriminator in determining the code phase offset during tracking operation, removing the need for the additional correlator arms in the tracking loops, thus reducing complexity and operation time. However, as this is a coherent type discriminator which is not inherently normalized, care must be taken to measure available signal power to renormalize the results obtained from cross-correlation. This is done in GNSScope by tracking the prompt in-phase and quadrature correlation outputs of the tracking loop to determine the data bit phase and available signal power [5].

4.5 Range Processing

The range processing block is responsible for the frame synchronization, parameter extraction, and satellite and user position calculation operations. The prompt in-phase output of the code and carrier tracking block containing the down-converted and despread navigation data consists of the correlation results between the incoming and locally generated signals, as seen in Figure 4.21, below [5] [8].
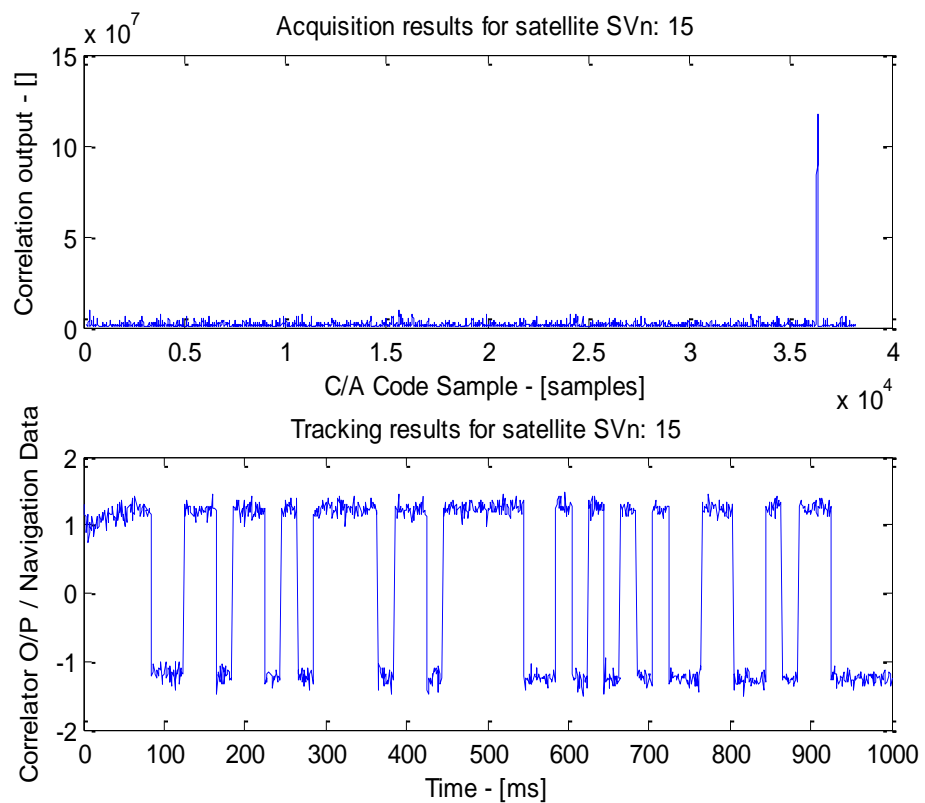
Figure 4.21 - Normalized outputs from the Acquisition and Tracking blocks (for GPS SVn:15)

In order to be processed by the range processing block, these results need to be converted into a binary sequence representing the navigation data bits transmitted by the satellites. This is accomplished by thresholding the correlation outputs with respect to zero to generate a binary sequence containing the navigation message. As each navigation data bit transmitted from the satellite is repeated over several PRN code epochs within the navigation message, further error correction is carried out on the binary sequence to resolve any inconsistencies caused by phase errors in the tracking

loop. This is done by checking the widths of each data bit to ensure that the data bit transitions occur at the correct points in the navigation message, with each data bit repeating over the same number of PRN code epochs [17].

Once the outputs of the tracking loop are converted into the navigation data bits, it is necessary to determine the starting point of the sub-frames in the navigation message, in order to correctly identify and extract the parameters necessary for the computation of the satellite and user positions. As mentioned in Chapter 3, each sub-frame contains two words, the TLM and HOW, used in detecting and identifying the sub-frames in the navigation message. These two words are correlated with the navigation message to determine possible starting points of the sub-frames. It should be noted that the Costas carrier and code tracking loops inherent insensitivity to 180° phase shifts could cause the TLM and HOW words to be inversed, resulting in a negative correlation in the navigation data sequence, which should also be accounted for. As these words are short in length and are not unique sequences in the navigation message, the correlation operation will result in more than one possible starting point for each sub-frame. However, as the sub-frames are of a fixed length and repeat periodically, the ambiguity in the starting points of the sub-frames is resolved by checking the length and order of the sub-frames detected by the correlation operation.

Following successful identification of the sub-frames, a parity check algorithm is applied to correct the polarity of the received data and detect any corruption in the received sub-frames. If the parity check succeeds, the necessary parameters for the computation of the satellite and user positions are extracted from each sub-frame. These parameters are given in Table 4.3, Table 4.4, and

Table 4.5, below, for sub-frames 1, 2 and 3. Once the necessary parameters are extracted from the navigation message, the satellite and user positions are calculated using the equations and methodology described in Chapter 2.

Table 4.3 - Ephemeris Data - Sub-Frame 1

Symbol	Definition
WN	Week Number
TOW	Time of Week
T_{GD}	Group delay differential for the satellite
t_{oc}	Clock correction parameter t_{oc}
a_{f0}	Clock correction parameter a_{f0}
a_{f1}	Clock correction parameter a_{f1}
a_{f2}	Clock correction parameter a_{f2}
$IODC$	Issue of Data, Clock

Table 4.4 - Ephemeris Data - Sub-Frame 2

Symbol	Definition
Δn	Mean motion difference term
M_o	Mean anomaly at reference time
e_S	Eccentricity of the satellite orbit
t_{oe}	Reference Time, Ephemeris
$\sqrt{a_S}$	Square root of the semi-major axis of the satellite orbit
C_{rs}	Sine harmonic correction term to the orbit radius
C_{us}	Sine harmonic correction term to the argument of latitude
C_{uc}	Cosine harmonic correction term to the argument of latitude
$IODE$	Issue of Data, Ephemeris

Table 4.5 - Ephemeris Data - Sub-Frame 3

Symbol	Definition
ω	Argument of perigee
Ω_o	Longitude of the ascending node
$\dot{\Omega}$	Rate of right ascension
i_0	Inclination angle at reference time
$idot$	Rate of inclination angle
C_{rc}	Cosine harmonic correction term to the orbit radius
C_{is}	Sine harmonic correction term to the angle of inclination
C_{ic}	Cosine harmonic correction term to the angle of inclination
$IODE$	Issue of Data, Ephemeris

4.6 Conclusions

This chapter has outlined the basic operation of GNSScope, a toolbox designed and developed in MATLAB for end-to-end modeling, simulation and analysis of current and upcoming GNSS signals. The operational overview of a GNSS receiver has been briefly described to provide a basis for the contents of the chapter. Following the overview, basic acquisition techniques implemented in GNSScope have been detailed, with examples captured from the toolbox itself showing successful detection and identification of GNSS signals. Once acquired, the satellite signals require tracking over time in order to extract the navigation message encoded in the signal. The fundamentals of digital PLLs have been given to provide a basis for understanding the underlying techniques utilized in the tracking loops. The evolution of the combined Costas carrier and code tracking loop has been demonstrated through the principles of individual code and carrier tracking loops. Once the individual satellite signals are extracted from the received signal, it is necessary to decode the message and extract the parameters necessary to compute the satellite and user positions. These have been detailed in the range processing section to complete the basic operational overview of GNSScope.

Chapter 5 Weak Signals, Multipath and Multiple Access Interference in the GNSScope Toolbox

5.1 Introduction

The previous chapter has provided an overview of the basic operational capabilities of GNSScope, covering strong signal acquisition and tracking, and the parameter extraction and range processing operations. This chapter will build on these foundations to delve into the advanced operational capabilities of GNSScope. These include improved acquisition and tracking techniques developed to cope with the up and coming ground and space based navigation signals, post detection integration techniques used in the acquisition of weak signals, weak signal acquisition and tracking techniques, multiple access interference removal in the acquisition and tracking loops, and multipath handling capabilities built into GNSScope. Prior to elaborating on these techniques, a brief introduction into the issues of weak signals, multipath, and multiple access interference will be given. This will be followed by a detailed description of the techniques developed in GNSScope, accompanied by results and analyses generated in GNSScope using both recorded and generated signals. This chapter will conclude with a case study, taking the reader through the whole process of satellite navigation, from signal acquisition to the handling of weak signals, from tracking to range and rage-rate processing, and finally the determination of the users' position on a map of the Earth.

5.2 Weak Signals, Multipath and Multiple Access Interference in GNSS

While the previous chapters dealt with signal generation at the satellite and the general processing that takes place in a GNSS receiver under good signal conditions, this chapter will deal with the issues relating to the reception of weak signals and signals with interference. By design, satellite navigation signals belonging to the same navigation system are transmitted at equal power levels from each satellite. As these satellites orbit the Earth at approximately the same distance, the signals would be expected to reach the receiver at similar power levels. However, due to the satellites transmitting their signals from different locations across the visible sky, the signals experience different paths when travelling to the receiver, resulting in varying levels of received signal power. When the received power level of a satellite signal drops below the cross-correlation peaks introduced by another satellite signal, it is referred to as a weak signal. For GPS L1 signals using 10-bit PRN codes, this is equivalent to a 24dB power difference between the two satellite signals, which will be used as a benchmark for strong and weak signal processing throughout the thesis. This problem of varying signal power levels is referred to as the "near-far" problem in classical DS-CDMA based communication systems, as signals reaching the receiver from ground based transmitters at varying distances would also cause the received signal power levels to vary at the receiver, affecting the performance of the receiver. Acquiring and tracking such weak signals requires further processing to be carried out in the receiver to improve the detectable signal content, which will be discussed in the following sections [2] [3] [32].

Another problem inherent in satellite navigation is the multipath problem, where signals reach the receiver from two or more paths which may or may not contain the direct LoS signal, due to the satellite signal being reflected from the surfaces of obstructions in the environment, such as the windows of tall buildings. As the shortest distance between two points in space is a straight line, the distance travelled by the multipath signal will always be greater than that of the direct LoS, resulting in an increased travel time, as all signals travel at the speed of light. This increased travelling time will result in the pseudo-ranges calculated by the receiver not converging to the correct user position, as the relevant equidistance sphere mentioned in Chapter 2 will have a larger radius than expected. It is

important to distinguish these signals on the multipath to improve receiver performance. The issue of multipath and its effects on acquisition and tracking will be discussed in the following sections[2] [3].

The final problem of particular interest to this work is the issue of Multiple Access Interference (MAI) [33]. As mentioned in Chapter 3, navigation signals being transmitted from different satellites share the same frequency band through the use of the CDMA multiplexing technique. Spreading the signals using orthogonal codes ensures that signals being transmitted from one satellite won't interfere with another. However, as the PRN codes used in spreading these satellite signals are of finite length, they are not perfectly orthogonal, but rather a close approximation. Thus, the cross-correlation characteristics of these PRN codes deviate from the ideal case of having no cross-correlation to presenting with non-zero peaks in the cross-correlation plots. Under weak signal conditions, these non-zero cross-correlation peaks could mask out the satellite signal of interest, resulting in non-detection or false detection of a particular satellite signal. This problem is referred to as MAI, and is of particular importance to weak signal acquisition and tracking, which will also be discussed in the following sections [3].

The following section will provide details of the advanced signal processing techniques in the literature implemented in the toolbox to improve the acquisition and tracking performance of GNSScope in the presence of weak signals, multipath, and multiple access interference. These techniques will also form a basis for the novel techniques developed in GNSScope, which will be presented later in the chapter.

5.3 Advanced Signal Processing Techniques

In Chapter 4, the basic acquisition techniques of serial search, parallel frequency space search, and parallel code phase space search acquisition, and the PLL based concepts of code and carrier tracking loops leading to the combined Costas code and carrier tracking loop were described. While these techniques are successful at acquiring relatively strong signals, and maintaining a successful lock following the acquisition process, when presented with undesirable signal conditions such as obstructions on the signal path, bad weather conditions, or having strong interferers present such as other navigation signals

or jamming, these techniques often fail to detect the presence of available satellite signals, reducing receiver performance which could lead to incorrect user position solutions or no position solution at all due to not being able to acquire a sufficient number of satellites. Even if a satellite is acquired, when the signal conditions deteriorate, the tracking loops may fail to maintain a lock on the acquired signals, requiring re-acquisition of the satellite in order to re-initiate the tracking loops with updated code and carrier information. As the operations necessary for the acquisition of a satellite are computationally demanding, it is desirable to avoid any failures in maintaining a lock on acquired satellite signals [23] [33].

This section will provide details of techniques from classical communication theory applied to satellite navigation systems and implemented in GNSScope, to cope with such circumstances. The coherent and non-coherent post-detection integration techniques used to improve acquisition performance under weak signal conditions will be explained in the next subsection, followed by details regarding weak signal tracking in GNSScope, with examples generated using the toolbox. This will be followed by the successive and parallel interference cancellation techniques from CDMA based communication systems, applied to GNSS, with examples illustrating successful operation in the presence of multipath and multiple access interference. The last subsection will provide a brief overview of several techniques from the current literature that are based on the successive and parallel interference cancellation techniques and implemented in GNSScope to provide a comprehensive simulation and analysis environment.

5.3.1 Weak Signal Acquisition

In parallel code phase space search acquisition, while the resolution of the code phase dimension of the search space is typically in the order of a fraction of a chip, the frequency dimension has a much lower resolution due to being split into a small number of frequency bins, typically around 500 Hz in size. Although this resolution is sufficient for the tracking loops to maintain a lock under strong signal conditions with no interference, in the presence of weak signals or interference, this might not be good enough for the tracking loop to continue tracking the signal after being acquired. Additionally, some weak signals may present with a very weak peak in their acquisition results not strong

enough for unambiguous identification of the satellite parameters. In order to improve the acquisition performance of the receiver and refine the frequency resolution of the acquisition results under such circumstances, the correlation results can be accumulated over multiple code epochs. This technique is referred to as Post-Detection Integration (PDI), and can be accomplished through the coherent or non-coherent integration of the acquisition results [2] [34].

In the coherent integration technique, a frame size corresponding to several code epochs is chosen for processing. The size of the frame is limited by the number of code repetitions in an individual data bit of the navigation message, as a navigation data bit transition would degrade the output power. A common choice for the frame size is half the number of code repetitions in a navigation data bit, as this would ensure that in two consecutive frames one would be free of any data bit transitions, producing the highest output. Once the frame size is determined, the signal is despread using a locally generated PRN code of matching frame size, leaving a continuous wave signal in the form of the data bit modulated by the carrier. Since the remaining signal is a continuous wave signal, its frequency can be determined from its spectral content, as the correct frequency of this continuous wave signal will present with a peak in the spectral content. The gain of this technique is dependent on the number of PRN code epochs present in the input frame, and can be calculated using the following equation [2]:

$$G_c = 10 \log(n)$$

Eq. 5.1

where n is the number of code epochs present in the input frame. Thus, applying coherent integration to a weak GPS signal over 10 milliseconds would result in a 10 dB gain in the acquisition outputs. This is illustrated in Figure 5.1 and Figure 5.2 below, where a real recorded GPS signal is used to demonstrate the processing gain obtained from the coherent integration technique over a 10 millisecond integration window. The first plot illustrates the signals spectral content prior to applying coherent integration to the GPS satellite SVn:15, while the second plot illustrates the results after applying coherent integration on the signal. Both plots were normalized as the magnitudes of the spectral content is directly proportional to the integration window, and would distort the results when compared to each other.
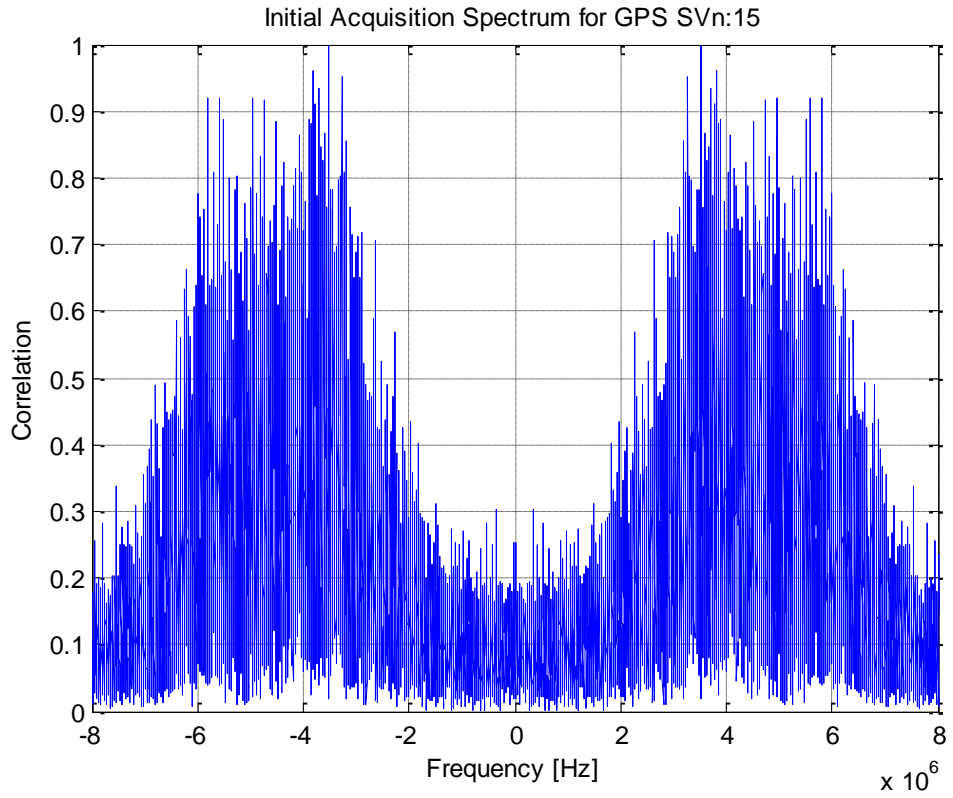
Figure 5.1 - Normalized Frequency Spectrum for GPS SVn:15 prior to Coherent Integration
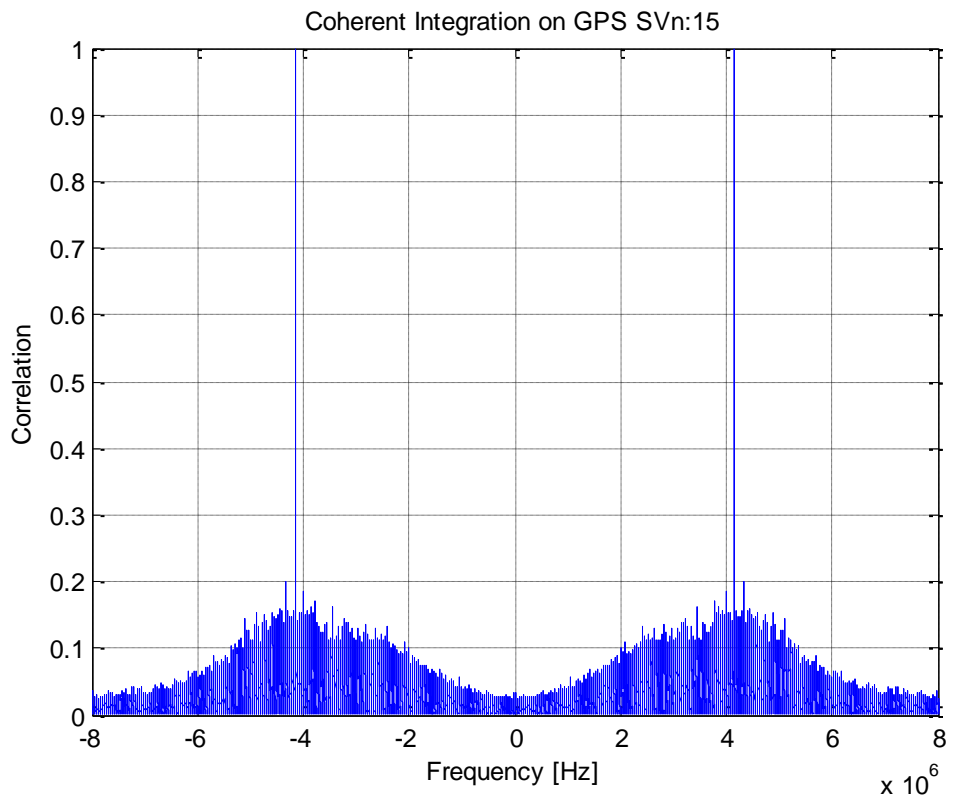
Figure 5.2 - Normalized Frequency Spectrum for GPS SVn:15 following Coherent Integration

While the coherent integration technique seeks to improve the results by extending the processing window, it is limited by the number of PRN code epochs used to encode each navigation data bit in the system, where optimal gains are obtained when the technique is applied to frame lengths half that of each data bit in order to avoid losses caused by data bit transitions. However, this integration time might not be sufficient enough to improve the correlation outputs to a level where the weak satellite signal will become detectable. Under such circumstances, further gains can be obtained by the use of non-coherent integration, where the results of consecutive coherent integrations are accumulated over longer periods of time to further improve the processing gains of satellite acquisition. When non-coherent is carried out, the effect of Doppler shift on the frequency of the signal must be taken into account in order not to degrade the acquisition results. Figure 5.3, below, presents the composite overall acquisition search results for GPS satellite SVn:15, with the coherent and non-coherent integration techniques applied to the acquisition search results to further refine the signal parameters for the tracking loops. Further details regarding coherent and non-coherent integration techniques can be found in [1] and [2].
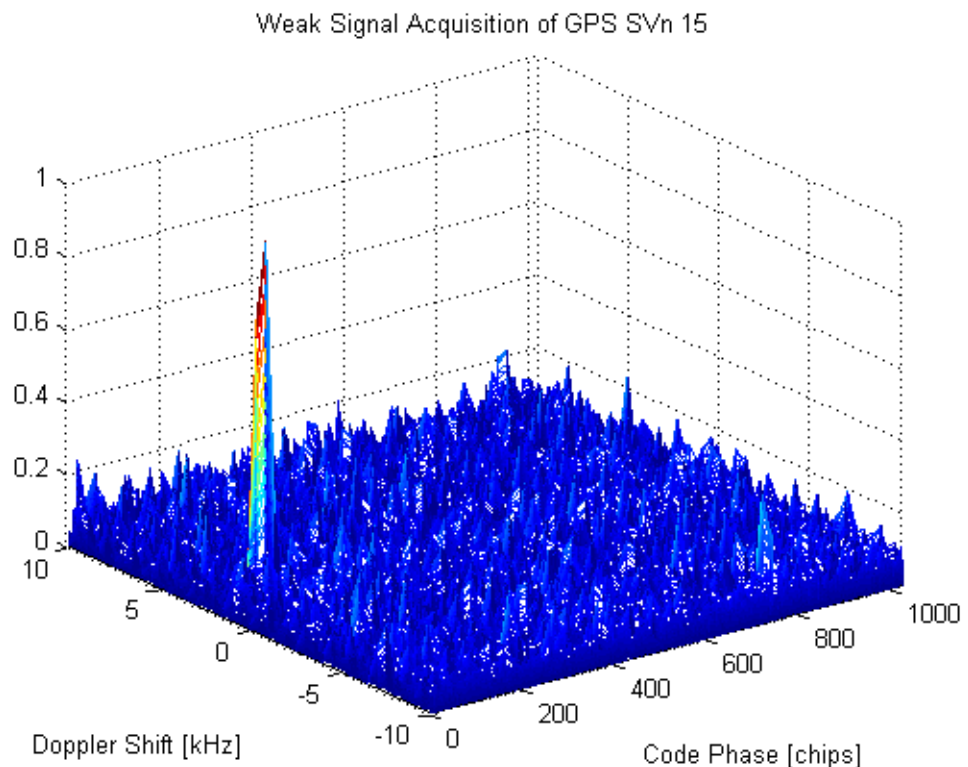
Figure 5.3 - Weak Signal Acquisition of a GPS Satellite (SVn:15)

5.3.2 Weak Signal Tracking

In strong signal tracking, as described in Chapter 4, estimating the carrier frequency and the initial starting point of the underlying PRN code are sufficient to correctly wipe-off the carrier and despread the signal to obtain the navigation data bit. However, when presented with weak signals, this estimation is not enough to maintain a successful lock on the acquired signal, requiring additional processing to improve the loop performance. In order to handle these weak signal conditions, the tracking loop in GNSScope is modified to accommodate the guidelines presented in [2], where, in addition to the carrier frequency and the initial starting point of the PRN code, the carrier phase and PRN code phase are also tracked for improved alignment of the locally generated carrier and code replicas with the received IF signal. In order to track the exact phase of the PRN code, it is necessary take into account the effect of Doppler frequency shift on the exact length of one PRN code period. In GNSScope, this is accomplished by recalculating the number of samples per PRN code chip to establish the length of the frame. As the sampling frequency is not an integer multiple of the carrier frequency, the estimated frame length will not match the actual frame length. This difference is calculated and stored to be used in the frame length computation process in the next iteration. In contrast to the frame length estimation process, tracking the carrier phase is accomplished through a simple phase computation on the generated carrier wave at the end of each frame to establish the phase offset of the new carrier wave to be generated for the next iteration.

In addition to these parameters, in the GNSScope toolbox, the base frequency used to generate the PRN code is also tracked to take into account the relativistic effects of satellite and receiver motion on the effective chipping frequency. Although the dynamics of the chipping frequency are much more stable in real scenarios compared to some of the other parameters used in the tracking process, this technique results in the closest match of the locally generated code and carrier waves possible within the limitations of the sampling rate of the incoming signal. The first 300 milliseconds of the normalized weak signal tracking output for the GPS satellite SVn:15 is given in Figure 5.4, below, where the navigation data can be seen to be present with a large amount of noise on the

output due to the weak signal conditions. Figure 5.5 presents the chipping rate data obtained from weak signal tracking of the same satellite with a larger one second window to better present the underlying changes in the chipping rate during weak signal tracking, where the blue curve represents a cubic curve fitting applied to the chipping rate data.
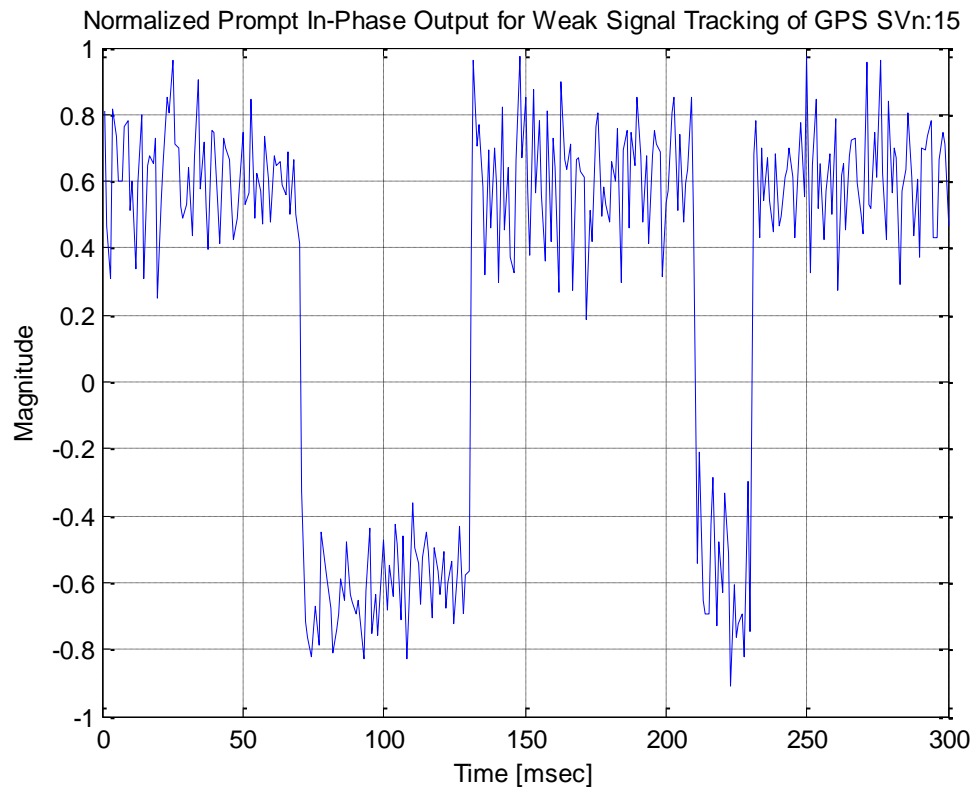
Figure 5.4 - Normalized Prompt In-Phase Output for Weak Signal Tracking of GPS SVn:15
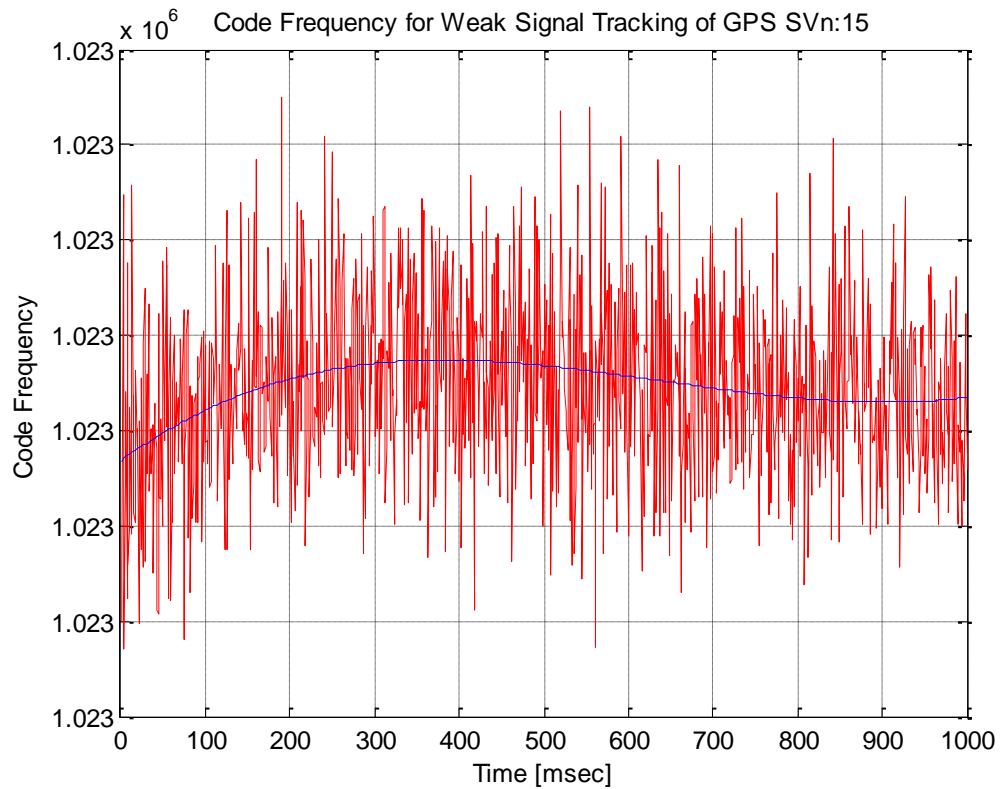
Figure 5.5 - The Code Frequency for Weak Signal Tracking of GPS SVn:15

5.3.3 Successive Interference Cancellation

Successive Interference Cancellation (SIC) is a cross-correlation interference mitigation technique in which the strongest satellite signals are reconstructed and removed from the received signal successively, each time re-acquiring to obtain the new strongest satellite signal in the received IF. The technique relies on the notion of selectively cancelling out individual signals from a composite by subtracting locally generated replicas of identified signals. Figure 5.6 shows a basic block diagram representation of the implementation of the SIC technique in the GNSScope toolbox [1][3] [35] [36].
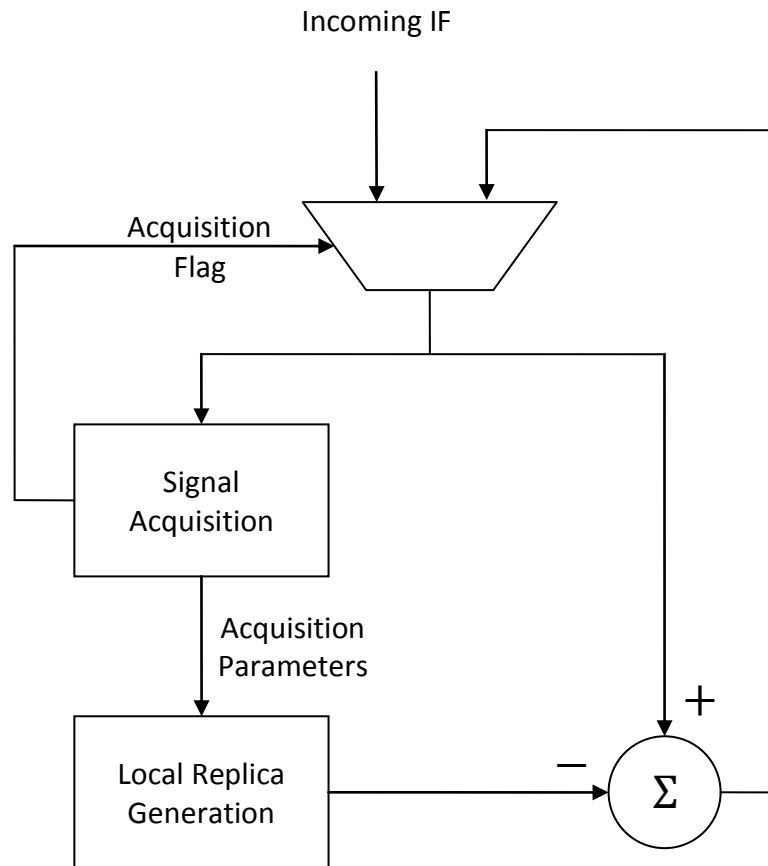
Figure 5.6 - Successive Interference Cancellation Technique Block Diagram

The acquisition flag is used to determine whether there are any other signals left in the file to be searched for. As long as the acquisition search identifies a satellite signal in the input data, it will continue to attempt to remove it in order to reveal any weak signals being masked by stronger signals due to MAI. The incoming IF is only used for the first stage of the acquisition process. From then on, the buffered output of the subtraction operation is used for the acquisition search. The acquisition parameters of each successfully acquired satellite are used to initiate a tracking channel to start tracking the satellite.

The SIC technique comes with certain advantages and disadvantages. Starting the reconstruction process from the strongest signal and working down has the advantage of removing the destructive effects of the strongest interfering signal in each stage, hence

reducing MAI in all the subsequent stages. It is important that the reconstruction parameters of code phase, carrier phase, carrier frequency, sign and amplitude are estimated based on the signal with the highest SNR in each stage, as any deviation from actual signal parameters could cause the SIC technique to further increase the interference on the weak signals. Also, as the SIC method requires re-acquisition of all the remaining satellites in each stage, it is computationally intensive and, in the presence of multiple strong interferes, could result in significantly larger processing times.

Figure 5.7, below, presents the results of applying the SIC technique to a sample weak GIOVE-A signal generated in GNSScope, 34dB below the received signal power level. The upper mesh plot presents the initial acquisition results of this satellite while the lower cross-section plot presents the re-acquisition results following interference removal using SIC. It can be seen from the first plot that there are no significant peaks in the acquisition results, indicating non-detection of the available GIOVE-A signal. However, following the first pass of the SIC technique, it can be seen in the second plot that there is a weak correlation peak present in the acquisition cross-section, indicating successful detection of the weak GIOVE-A signal [7].
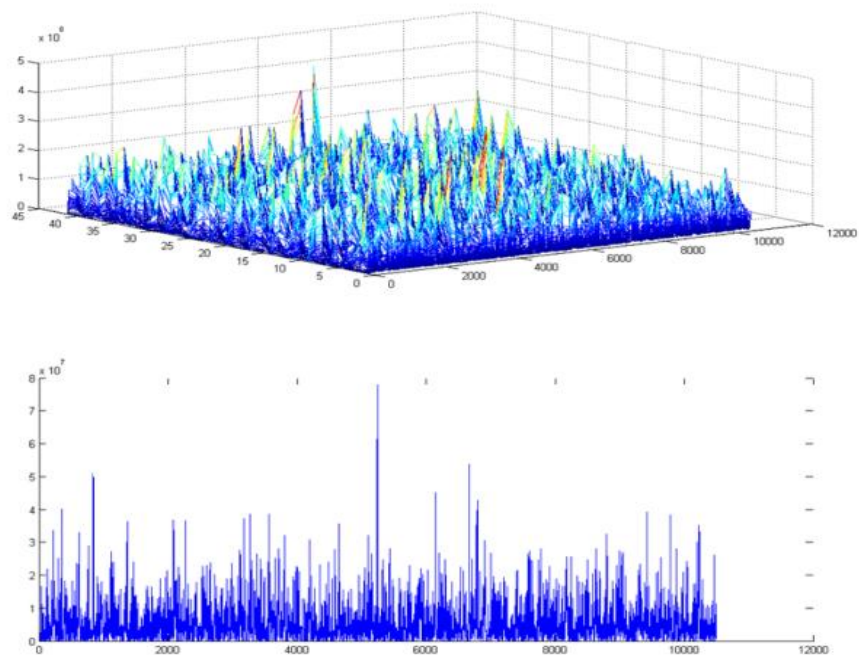
Figure 5.7 - Serial Interference Cancellation Acquisition Results Prior to Mitigation

5.3.4 Parallel Interference Cancellation

The Parallel Interference Cancellation (PIC) technique, which is based on the same notion of cancelling interfering signals by subtracting locally regenerated replicas from the incoming IF, deals with the processing time problem of SIC by processing all the strong interferers simultaneously. Once an estimate of all the strong interferers is established, they are all subtracted from the received signal followed by re-acquisition for the detection of the weak signals. This process is repeated until all desired satellite signals are acquired. The trade off for achieving this reduced processing time is in the significantly increased software and hardware complexity, especially when signal power levels vary widely requiring multiple stages to acquire all visible satellites. In GNSScope, this trade off is minimized by utilizing iterative search techniques coupled with multiple object instantiation to handle the strong signal replica generation in one stage. These generated replica interferers are then summed and subtracted from the incoming IF for weak signal acquisition to recover any remaining visible satellites in the signal. The overall block diagram of the PIC techniques implementation in GNSScope can be seen in Figure 5.8, below [1][3][35].
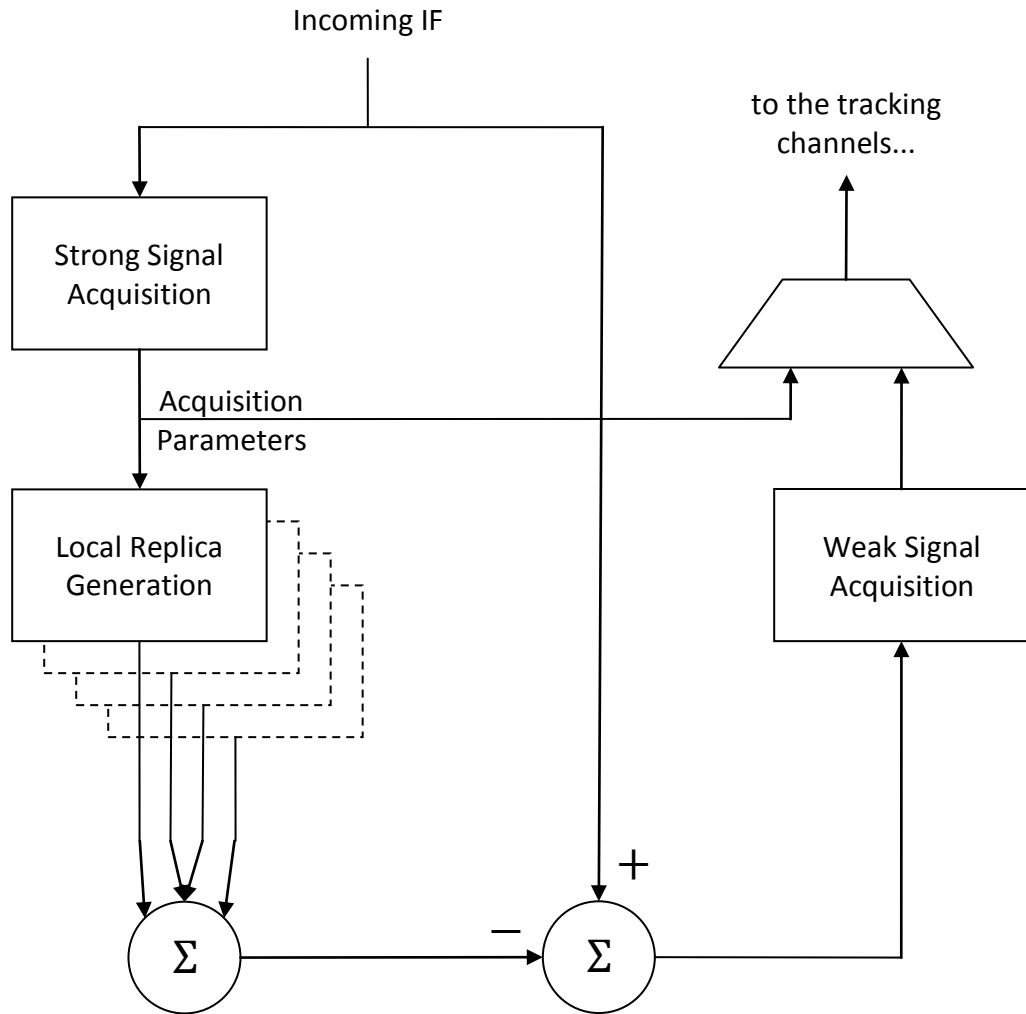
Figure 5.8 - Parallel Interference Cancellation Technique Block Diagram

The results of the PIC technique applied to an input file containing three strong GPS signals accompanied by one weak GPS signal can be seen in Figure 5.9, below. The lack of a strong peak in the upper mesh plot indicates that the weak signal is being masked out by the MAI introduced from the three strong signals. These strong signals were acquired and removed from the input IF using the PIC technique to reveal the weak signal in the file. In order to improve on the performance of the results, 10 milliseconds of coherent integration was applied to obtain the lower plot in Figure 5.9 representing the acquisition cross-section along the code phase dimension [7].
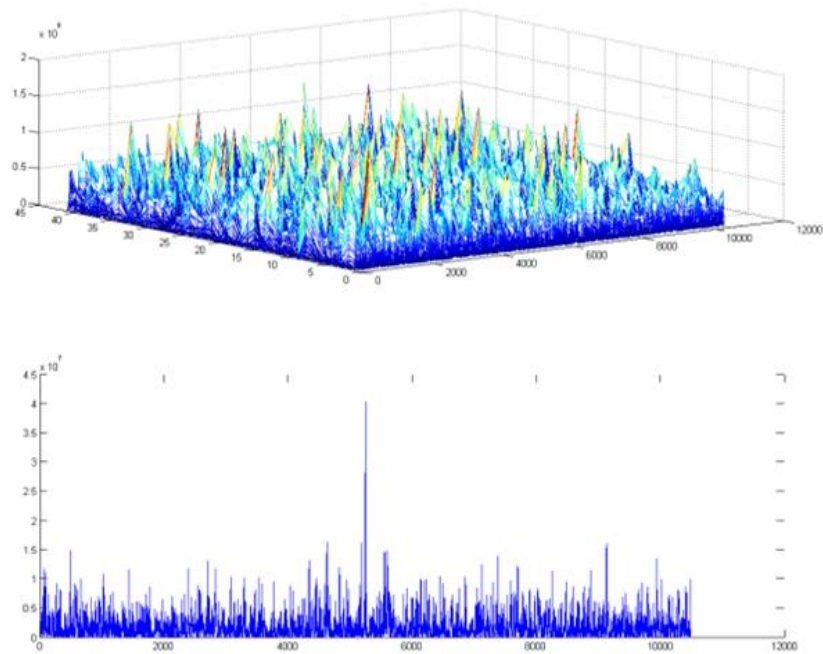
Figure 5.9 - Parallel Interference Cancellation Acquisition Results with Coherent Integration

5.3.5 SIC / PIC Based Interference Cancellation Techniques

Both the SIC and the PIC techniques don't come without disadvantages. Whether due to multipath, obstacles on the signal path or channel fading, the channel profile may change over time, resulting in a change in the received signal power levels. The need to process the strongest signal first would require an SIC receiver to be reconfigurable. Since this process brings an overhead, a clever decision making mechanism is necessary to minimize the amount of changes to the system. The serial nature of processing in SIC also results in varying amounts of delay being introduced into the system, increasing processing time and storage requirements depending on the number of strong interferers in the data. The PIC technique was devised mainly to overcome this issue of large delays in the system. In return for increased hardware complexity, it offers fixed delay with reduced processing times as long as the visible satellite constellation doesn't change vastly. However, due to sampling resolution limitations of most GNSS front-ends, the subtraction process becomes an issue possibly introducing destructive quantization noise into the system.

Since their introduction into GNSS, several variants of the SIC and PIC techniques have been developed. The Delayed Parallel Interference Cancellation (DPIC) technique deals with the quantization noise issue by creating matched correlator channels to track the incoming and reconstructed signals in parallel, then performing the subtraction operation on the outputs of the integrate-and-dump filters of the tracking channels, where the results have a much higher resolution as they are typically accumulated over a whole frame of the underlying spreading code [37] [38]. This method deals with the resolution issue at the cost of added correlator channels. Another method uses the sinc(Δf) relationship of the cross-correlation properties of PRN codes to create an estimate of the strong signal interferer. Although this reduces hardware complexity, it could produce incorrect estimates of the strong signal due to incorrect handling of the effects of relative Doppler frequency. Further details regarding these techniques can be found in [39] and [40]. The following section will delve into the details of novel signal processing techniques developed in GNSScope for the processing of weak signals, multipath and multiple access interference in GNSS.

5.4 Novel New Signal Processing Techniques in GNSScope

The previous section provided details of the SIC and PIC techniques from classical communication theory applied to satellite navigation systems, which kick started work in the area of multiple access interference cancellation in GNSS. Examples generated in GNSScope were used to illustrate the effectiveness of these techniques under weak signal and multipath conditions, including minor modifications that were made to the algorithms to improve their performance in a software defined radio GNSS receiver scenario, where the operations are carried out on a generic PC. The section concluded with SIC and PIC based techniques from the literature that were implemented in GNSScope to provide a comparative basis for further research in the issue of cross-correlation interference in GNSS.

This section will provide the details of novel techniques designed and developed in GNSScope for handling weak signals, multipath and multiple access interference in multi-standard multi-frequency GNSS receiver operation. The first of these novel techniques is based on the SIC, PIC and DPIC techniques described in the previous section, where the

amount of overhead generated by the interference removal operation is minimized to simplify the process. This will be followed by the trigonometric interference cancellation technique, where the locally generated replicas of the interfering signals are simplified using trigonometric equivalences. The last of these novel techniques, the split-chip compression technique, will be described in the final section. In order to provide a basis for the technique, the binary valued signal modulation compression technique will also be introduced, with examples generated in GNSScope.

5.4.1 Mirrored Channel Mitigation Technique

The mirrored channel mitigation technique is a cross-correlation interference mitigation technique designed and implemented in GNSScope based on the PIC, DPIC and sinc(Δf) techniques described in the previous section, whereby the effects of the interference is computed in a matched correlator channel and the cancellation to recover the signal of interest is carried out on the in-phase and quadrature outputs of the integrate-and-dump filters of the correlator channels. However, rather than using the exact estimate of the strong signal amplitude during the scaling operation prior to signal wipe-off; a heavily quantized amplitude can be used to simplify the scaling operation without degrading weak signal recovery. This is due to the fact that in order to cause multiple access interference between satellite navigation signals, the interferer needs to be above a certain threshold in comparison to the received power level of the signal of interest, in the case of the PRN codes used in GPS this value is 24dB. Once the majority of the strong signal interferer is mitigated, the remaining signal power is comparable to that of the weak signal of interest, removing the cross-correlation interference, hence resulting in successful acquisition and tracking of the weak signals. Using a heavily quantized amplitude also leads itself to a simpler implementation of the technique in a GNSS receiver, as the amplitude scaling operation in this case can be carried out with adders rather than multipliers, reducing hardware complexity and increasing operation speeds in the case of SDR GNSS receivers, such as the GNSScope toolbox [7].

In addition to the reduced complexity, using heavily quantized amplitude for the scaling of the strong signal interferers enables batch processing of multiple strong signal interferers that fall into the same amplitude bin in the reconstruction process, reducing

the number of mirrored channels necessary to carry out the interference mitigation process. In contrast to the PIC and DPIC techniques, this technique results in an overhead of only N_w additional correlator channels as opposed to the $N_s \times N_w$ additional correlator channels; where N_w is the number of weak signals and N_s is the number of strong signals being processed by the receiver. Furthermore, as signals with relatively low received power levels will not contribute to the MAI on the weak signal of interest, there is no need to apply mitigation techniques to these signals, resulting in significantly reduced overheads when processing weak signals, and signals containing multipath and cross-correlation interference from other satellites.

A block diagram representation of the mirrored channel mitigation technique can be seen in Figure 5.10, below. The block diagram is represented for the case of the effects of one strong signal interferer being mitigated from a weak signal of interest. The interference regeneration block seen in the figure uses the information regarding the initial starting point of the PRN code, the actual phase PRN code, the frequency of the carrier wave and the actual phase of the carrier wave obtained from the relevant strong signal tracking channel to locally reconstruct the strong signal found within the received IF. This signal is then processed by the amplitude scaling block to determine how many amplitude bins are needed for the successful mitigation of the strong signal interference. This scaled reconstructed signal is then processed in the mirrored interference cancellation channel to reproduce the cross-correlation interference caused by the strong signal interferer on the weak signal of interest in the received IF. The final in-phase and quadrature phase outputs of the weak signal tracking channel are calculated by subtracting the computed interference from the results of the weak signal processing of the received IF.
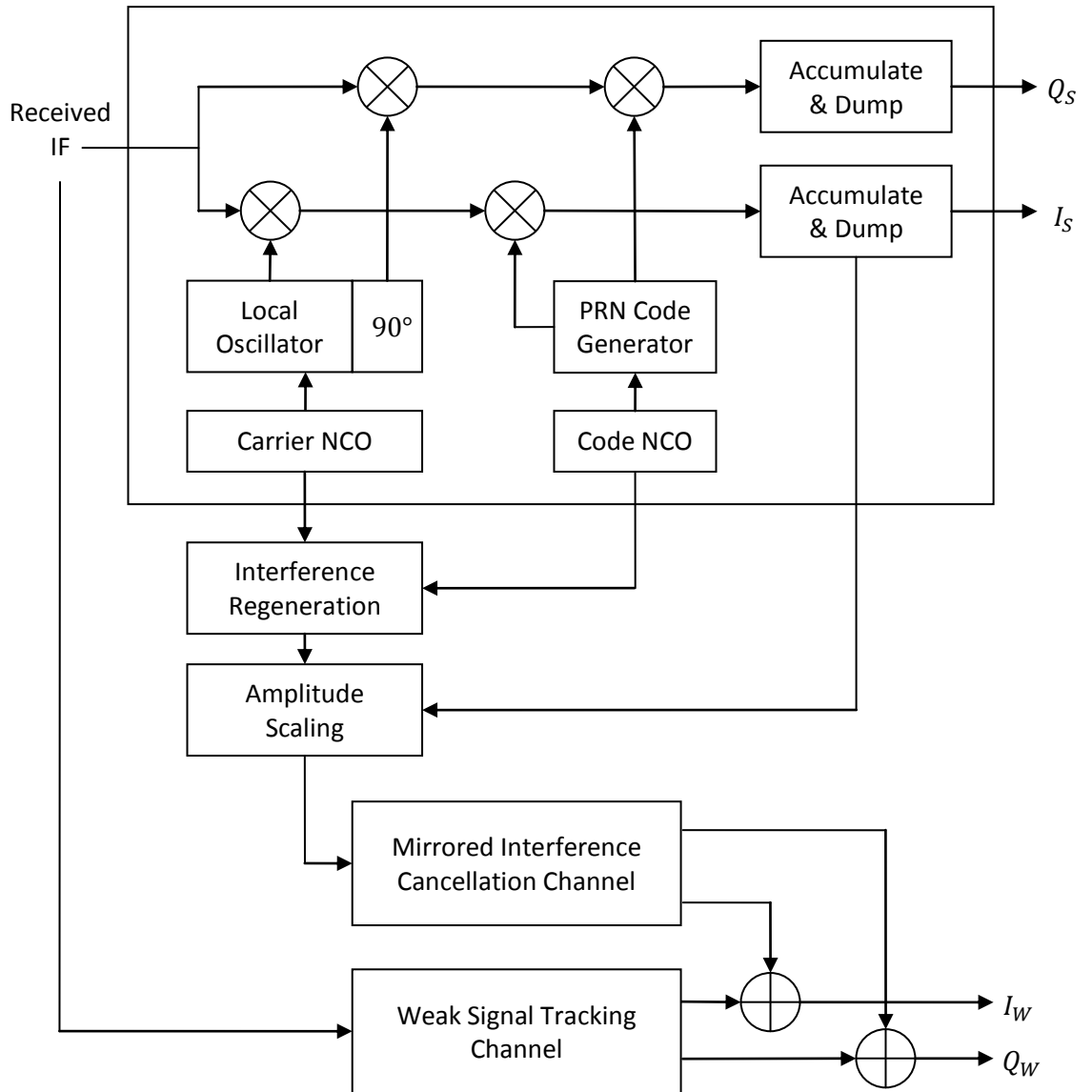
Figure 5.10 - Block Diagram Representation of the Mirrored Channel Mitigation Technique

The proposed technique was implemented in GNSScope with added flexibility in the form of reconfigurable word lengths and look up tables for the scaling operation during strong signal reconstruction, resulting in controllable performance depending on the signal dynamics of the received IF. Figure 5.11, below, presents the results of the technique applied to the recovery of signals on the multipath. The top figure presents the initial strong signal acquisition results of a generated signal with three multipath components with decreasing signal power levels. Although the multipath components are not detectable in the initial acquisition results, once the strong signal is mitigated using the

mirrored channel mitigation technique, they are clearly detectable in the cross-sectional re-acquisition plots of the same strong signal given in the second and third plots in the figure. The residue seen in the center of the third plot is what remains of the strong signal that was initially present in the received IF, which is an artifact of the quantization process used in the amplitude scaling operation. This technique is also used to form a basis for the trigonometric interference cancellation technique, which is described in the following section [5].
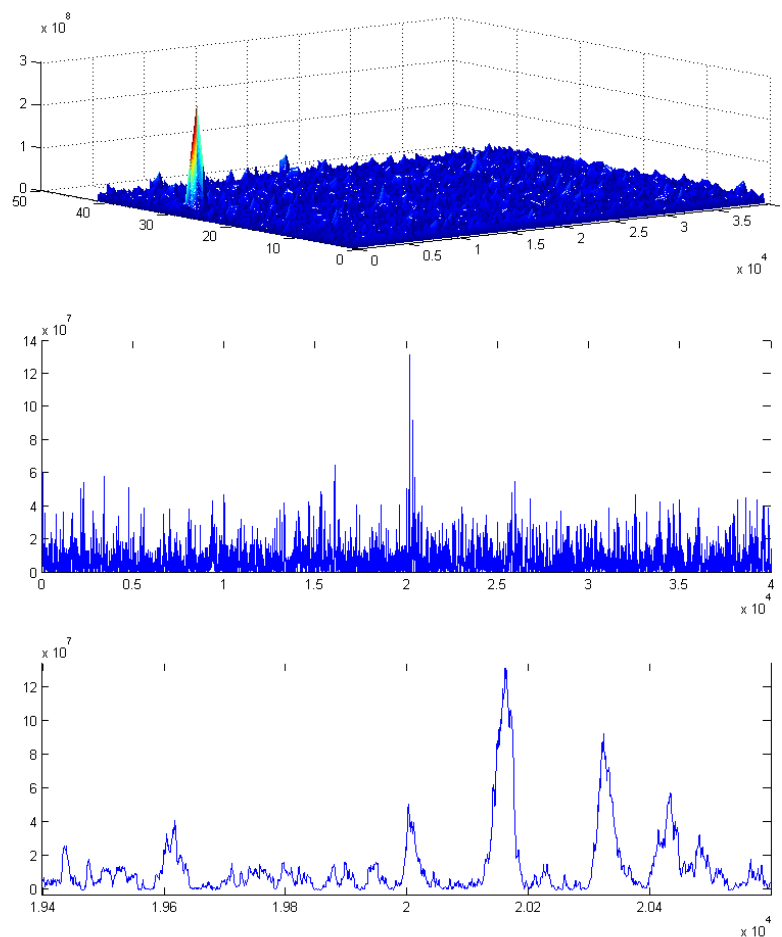
Figure 5.11 - Mirrored Channel Mitigation Technique Used to Recover Signals on the Multipath

5.4.2 Trigonometric Interference Cancellation Technique

The trigonometric interference cancellation technique is a cross-correlation interference mitigation technique whereby the underlying mathematical expressions are exploited to simplify the interference removal process in the mirrored channel mitigation technique, reducing the execution time and the overall complexity of the receiver at the cost of slightly increased storage requirements. The technique was designed and developed in GNSScope, and incorporated into the toolbox for testing under a variety of signal conditions. Results from these tests indicating successful acquisition of a very weak signal using the trigonometric interference cancellation technique will be given at the end of the section, following an explanation of the technique with the derivation of relevant expressions [5] [10] [13].

Assuming, for simplicity, that there is one weak signal and one strong interferer in the incoming IF, the locally generated replica of the strong interferer being tracked in the receiver can be expressed as follows:

$$I_S = A_S \times PRN_S \times \cos(f_c + f_d^S)$$

<div align="right">Eq. 5.2</div>

where I_S is the reconstructed in-phase component of the strong signal, A_S is the amplitude of the strong signal that is being tracked, obtained from the integrate-and-dump filter outputs of the tracking channels, PRN_S is the associated Gold code for the strong signal interferer, f_c is the centre frequency of the carrier wave and f_d^S is the Doppler frequency offset of the strong signal interferer. When processed in a standard correlator channel searching for the weak signal of interest, the in-phase tracking output of the receiver could be expressed as:

$$I = \left[A_S \times PRN_S \times \cos(f_c + f_d^S)\right] \times \left[PRN_W \times \cos(f_c + f_d^W)\right]$$

<div align="right">Eq. 5.3</div>

where I is the in-phase correlator output for the weak signal of interest, PRN_W is the associated Gold code for the weak signal and f_d^W is the Doppler frequency offset of the weak signal of interest. Rearranging these variables, this equation can be re-written as follows:

$$I = A_S \times [PRN_S \times PRN_W] \times \left[\cos(f_c + f_d^S) \times \cos(f_c + f_d^W)\right]$$

<div align="right">Eq. 5.4</div>

It can be seen that A_S is a scale-factor and $[PRN_S \times PRN_W]$ is the cross-correlation of the Gold codes of the strong interferer and weak signal of interest. This equation can be further simplified using the following trigonometric expression:

$$\cos(\alpha) \times \cos(\beta) = \frac{1}{2}[\cos(\alpha - \beta) + \cos(\alpha + \beta)]$$

<div align="right">Eq. 5.5</div>

resulting in the following expression for the in-phase correlator output of the weak signal tracking channel:

$$I = \frac{A_S}{2} \times [PRN_S \times PRN_W]$$
$$\times \left[\cos(f_d^S - f_d^W) + \cos(2 \times f_c + f_d^S - f_d^W)\right]$$

<div align="right">Eq. 5.6</div>

It can be seen from Eq. 5.6 that this results in two components: one very low frequency output that is close to DC due to the small range of Doppler frequency shifts possible in civilian and avian navigation, and another double IF component also containing the Doppler difference between the strong and weak signal carrier waves. Simulation case studies have shown that the high frequency component can be ignored as it will be filtered out by the integrate-and-dump filters of the correlator channels, resulting in the following simplified matched correlator channel equation:

$$I = A_S \times [PRN_S \times PRN_W] \times \cos(f_d^S - f_d^W)$$

<div align="right">Eq. 5.7</div>

where the amplitude of the strong signal interferer can be obtained from the associated strong signal tracking channel integrate-and-dump filters, and the cross-correlation of the associated strong and weak signal PRN codes can be stored locally, removing the need to generate the cross-correlations on the fly, resulting in reduced execution times.

This method can be trivially extended to *n* strong signal interferers through *n* matched correlator channels in the GNSScope toolbox. As A_S is obtained from the channel tracking the strong signal interferer, the remaining operation is to simply multiply the cross-correlation of the strong and weak signals with the Doppler difference term $\cos(f_d^S - f_d^W)$, removing the necessity to fully reconstruct the strong interferer as in the PIC and DPIC techniques mentioned earlier in the chapter, reducing the computational load by

25% for each strong interferer on the weak signal. Also, in contrast to the $\text{sinc}(\Delta f)$ technique, the effect of the relative Doppler frequency is computed for every sample, rather than being approximated to a constant scale factor. This results in a low complexity cross-correlation interference mitigation technique targeting practical complexity reduced real-time GNSS receiver architectures, leading to improved processing efficiency and hence increased receiver performance and reduced power consumption.

An added advantage of this technique comes in the form of its ability to remove Continuous Wave (CW) type interference that might be present in the signal bandwidth. A CW signal can be treated as a satellite signal with an underlying spreading code consisting of a single chip, or where all of the chips of the spreading code are the same. Using this representation, Eq. 5.7 can be rewritten as follows:

$$I = A_{CW} \times PRN_W \times \cos\left[f_{CW} - \left(f_c + f_d^W\right)\right]$$

Eq. 5.8

where A_{CW} is the amplitude and f_{CW} is the frequency of the interference. In order to further simplify this expression, the frequency of the CW interference can be rewritten as follows:

$$f_{CW} = f_c + f_d^{CW}$$

Eq. 5.9

where f_d^{CW} is the difference frequency between the CW interference and the center frequency of the carrier in the incoming IF. The resulting expression for the matched correlator channel will be:

$$I = A_{CW} \times PRN_W \times \cos\left(f_d^{CW} - f_d^W\right)$$

Eq. 5.10

Comparing Eq. 5.8 and Eq. 5.10, it can be seen that the same algorithm can be used to remove CW interference as well as MAI. Simulation case studies carried out in GNSScope using both real and simulated strong and weak signal conditions show that the technique is successful at identifying and removing strong signal interferers in a variety of cases including weak signal acquisition / tracking, multipath signal wipe-off / recovery and continuous wave interference removal.
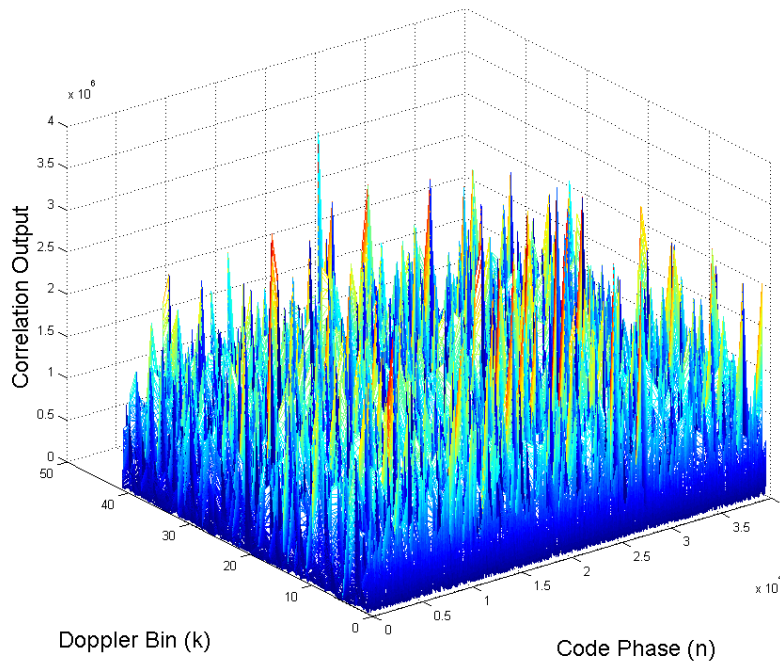
Figure 5.12 - Weak Signal Parallel Code Phase Space Search Acquisition Results prior to MAI Removal

Figure 5.12, above, shows the initial acquisition results of a weak signal of interest being masked out by interference coming from a strong satellite signal present in the incoming IF. The received power level of the weak signal was set to be 34dB below the received power level of the strong signal. The interfering signal was set to have a 1kHz Doppler frequency offset relative to the weak signal, in order to induce worst case conditions during acquisition. It can be seen that this results in the weak signal not being detected during initial acquisition, as the auto-correlation peak for the weak signal of interest is being masked out by the cross-correlation peaks of the strong signal. Using conventional acquisition techniques, the weak signal present in the incoming IF would go undetected, reducing receiver performance. In the event that there aren't sufficient detectable satellites, this could lead to the receiver not being able to get a position fix. Figure 5.13 presents the parallel code phase space search acquisition results for the weak signal of interest following MAI removal using the trigonometric interference removal technique. The strong acquisition peak, which can be seen in more detail in the acquisition cross-section presented in Figure 5.14 indicates successful weak signal acquisition using the proposed method. It can be seen that the acquisition results also provide a good C/N_0, improving the processing gain of subsequent stages.
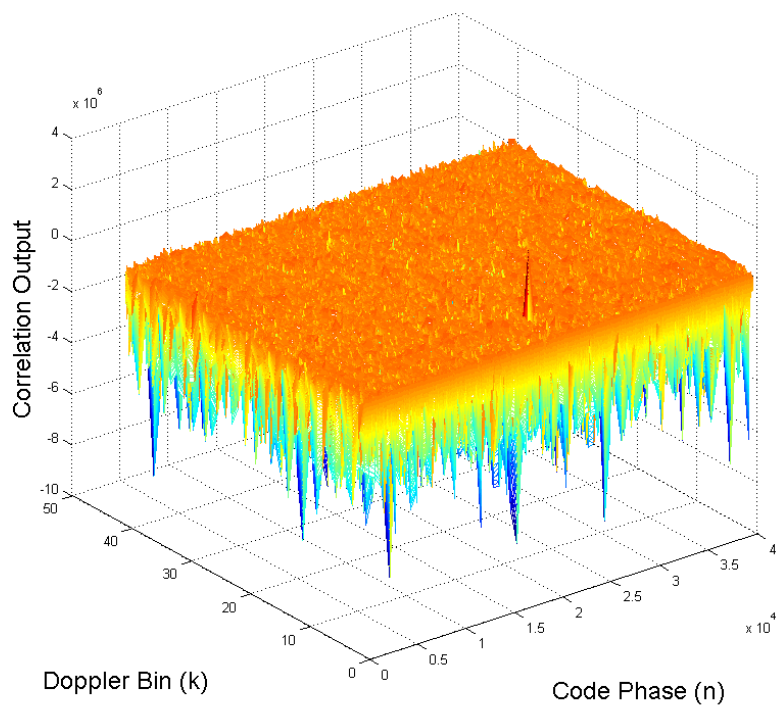
Figure 5.13 - Weak Signal Parallel Code Phase Search Acquisition following MAI Removal
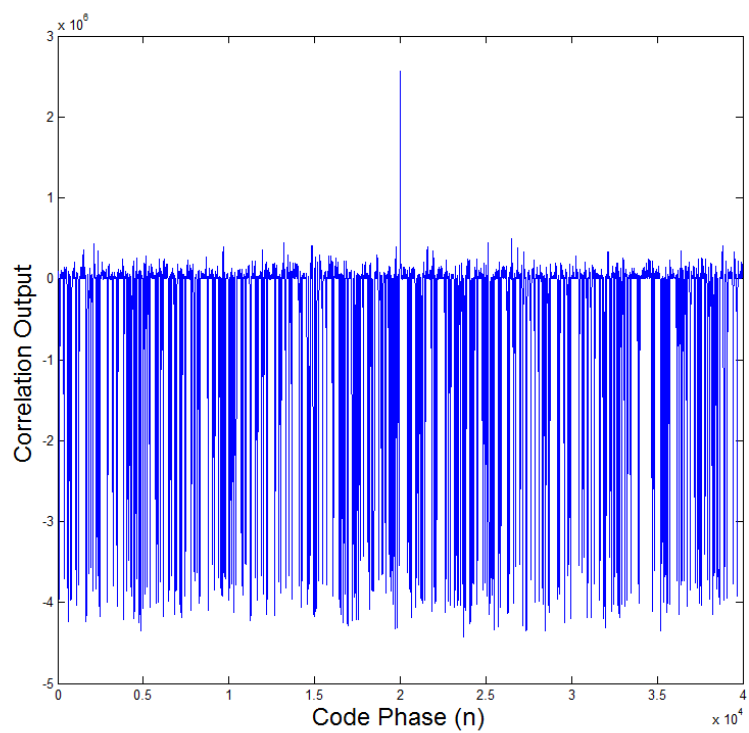
Figure 5.14 - Cross-Section of the Weak Signal Acquisition Results

As mentioned earlier in the section, this technique trivially extends to n strong signal interferers through n matched correlator channels. As an example, the same weak signal was this time accompanied by three strong signal interferers, all set to be 24dB above the received power level of the weak signal. The interfering signals were set to have increasing Doppler frequency offsets relative to the weak signal in 1kHz steps, in order to induce worst case conditions during acquisition. The parallel code phase space search acquisition results for the weak signal following MAI mitigation using the trigonometric interference cancellation technique can be seen in Figure 5.15, while the cross-section of these results along the code phase dimension can be seen in Figure 5.16. Once again, it can be seen that using the technique, strong signal interferers can be removed, revealing any weak satellite signals that might be present in the incoming IF. Comparing Figure 5.14 and Figure 5.16, it can be seen that the increased number of interferers result in more cross-correlation peaks to show up in the acquisition results. However, it can also be seen that the SNR has been preserved, and the same weak signal is present in both results with equal signal power.
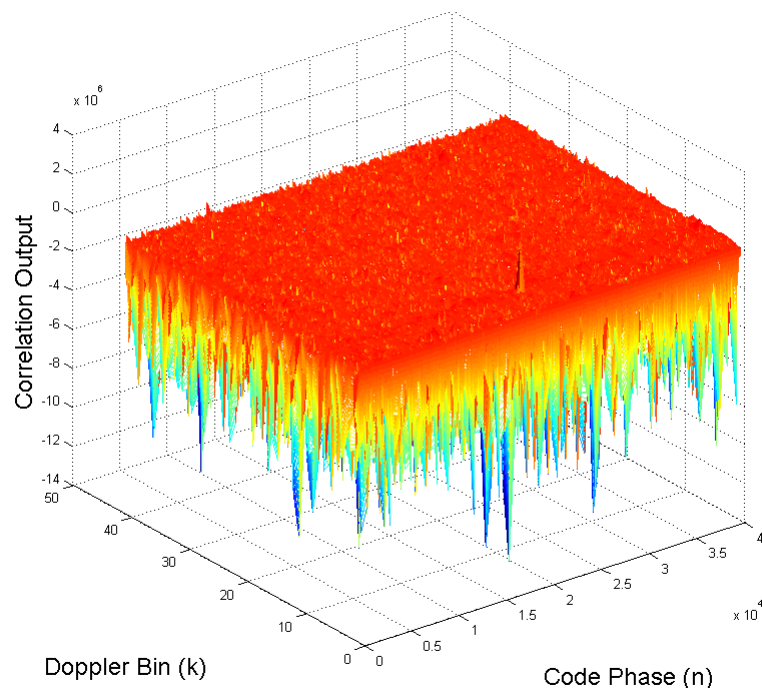
Figure 5.15 - Weak Signal Parallel Code Phase Search Acquisition following MAI Removal
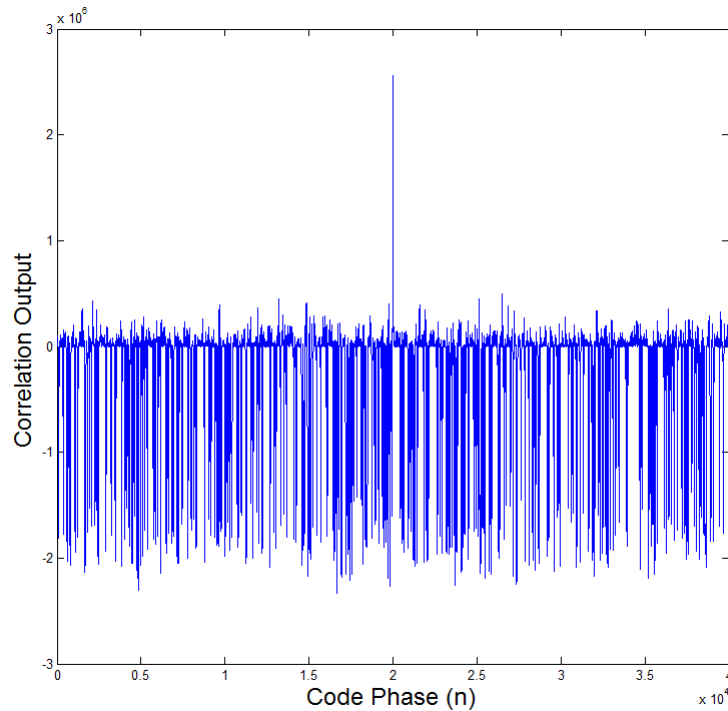
Figure 5.16 - Cross-Section of the Weak Signal Acquisition Results

5.4.3 Split Chip Summation Technique

As advances in high-sensitivity GNSS receiver technologies targeting indoor and urban canyon navigation require higher and higher processing speeds for tasks such as multiple access interference mitigation and multipath compensation, the need for improved processing techniques reducing the number of operations for acquisition and tracking is ever increasing. The computational load in these cases can be significantly reduced by the application of the Binary-Valued Signal Modulation Compression for High Speed Cross-Correlation technique [40]. This is accomplished through the summation of the received signal samples rectified by the polarity of the chipping code, resulting in the samples of a single chip of this code. As this technique can be implemented using only simple additions, it greatly reduces the computational complexity while preserving signal range and phase information in the chip waveform. This technique was implemented in the GNSScope toolbox, with minor modifications made to the acquisition and tracking blocks to accommodate the new compressed chip waveform.

Using this technique, the large number of received signal samples are reduced to a short vector with few samples representing the channel and receiver front-end effects on the chip itself. An example of this, produced using the GNSScope toolbox, can be seen in Figure 5.17 where the compression technique is applied to a generated signal over 100 milliseconds of GPS L1 data containing a multipath component with a 180 degree phase shift with respect to the line of sight signal. The compressed chip waveform clearly indicates the existence of an opposite phase component in the signal, offset from the LoS component by 8 milliseconds. Also, the filtering effects from the satellite, channel and front-end are partially visible on the leading edge of the chip, although greatly attenuated [41] [42].
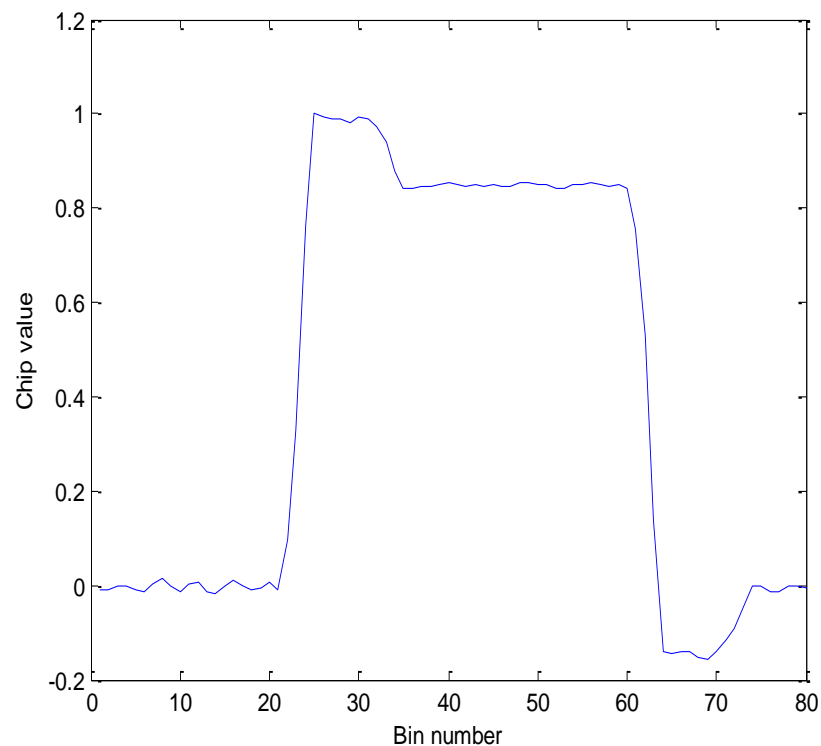
Figure 5.17 - Binary Valued Signal Modulation Compression Applied to a Sample GPS L1 Signal

The Split Chip Compression technique is based on the binary-valued signal modulation compression technique, whereby the samples of the received signal are summed after being rectified by the polarity of the chipping code. However, rather than summing all the chips and compressing the waveform into a single chip of the PRN code, losing most of

the information associated with the specific chip polarities, the technique described here splits the chipping code into its positive and negative chips, accumulating them in two separate vectors [11]. As the Gold codes used for spreading current and upcoming satellite navigation signals are close to being balanced, this technique results in increased sensitivity to perturbations on the chipping waveforms, as specific perturbations that affect the two polarities of the chipping waveform differently are preserved rather than being accumulated and filtered out over time, at the cost of a second short vector for the storage of the two separate chips. The two compressed chips represent the effects of the transmitter, channel and receiver front-end on the chipping waveform and can be used in the detection, identification and compensation of distortions such as multipath, unbalanced chipping code duty cycles and filter ringing, which can then be compensated for using linearization, curve fitting and parameter extraction techniques.

The performance of the technique is demonstrated using a sample satellite signal generated in GNSScope with a 40 MHz sampling frequency and 5 MHz center frequency, in order to demonstrate the results in high resolution. The signal contains transmitter, channel and front-end filtering effects that are present in typical GNSS receivers. In order to provide a frame of reference, the same signal is processed using the binary valued signal modulation compression technique as well as the split chip summation technique, and the resulting compressed chip waveforms are compared for effectiveness in determining the differences in the filtering effects on the positive and negative polarity chips, and how these effects get filtered out during the accumulation process when integrated into a single vector. The simulations were carried out over an accumulation time of 200 milliseconds to account for the response times of the acquisition and tracking channel filters and provide more detailed chip waveforms containing more pronounced distortions while filtering out instantaneous noise effects that might occur on the signal.

The compressed chip waveform obtained from the binary valued signal modulation compression technique is presented in Figure 5.18, below. Observing the chip waveform, it can be seen that the leading and trailing edges of the chip contain the filter ringing effects introduced by the front end of the GNSS receiver. It can also be seen that this effect is more prominent on the trailing edge of the chip. Although these effects are visible on the

leading and trailing edges of the chip waveform, it appears that the chip itself has not been affected by filter ringing, with an almost flat profile for its "true" state.
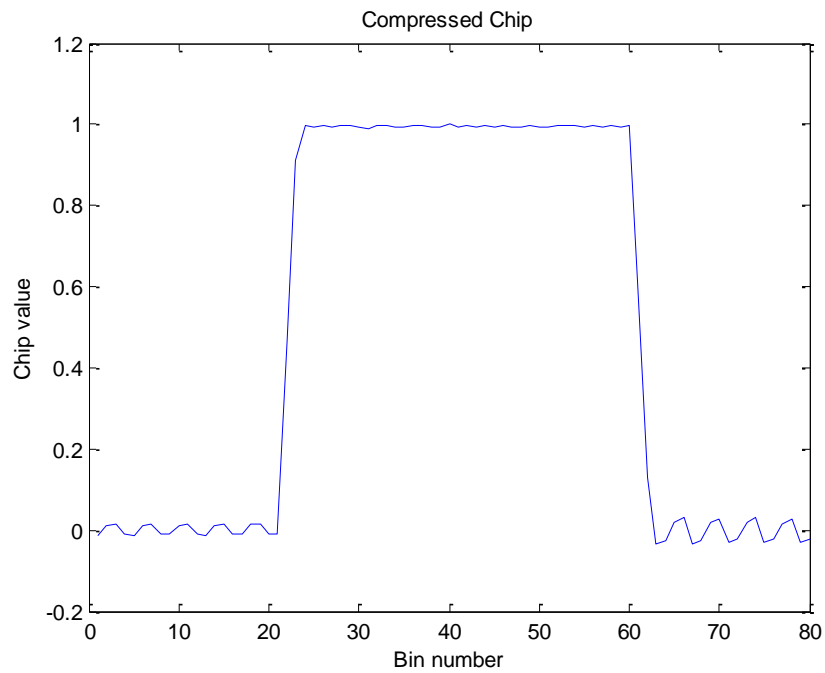
Figure 5.18 - Binary Valued Signal Modulation Compression Results

The positive and negative chip waveforms obtained from the split chip summation technique are presented in Figure 5.19 and Figure 5.20, respectively. Comparing the chip waveform obtained from the binary valued signal modulation compression technique to the positive and negative chip waveforms obtained from the split chip summation technique reveals further information regarding the effects of the transmitter, channel and receiver front end on the signal which were filtered out during the accumulation process in the binary valued signal modulation compression technique. It can now be seen that the "true" states of the chips themselves do not have a flat profile at all, but rather they present with a constant oscillation that continues on both of the chip polarities of the spreading code. Furthermore, it can be seen that the filter ringing effect present on the leading and trailing edges of the chip waveforms is more pronounced on the positive polarity chip compared to the negative one.
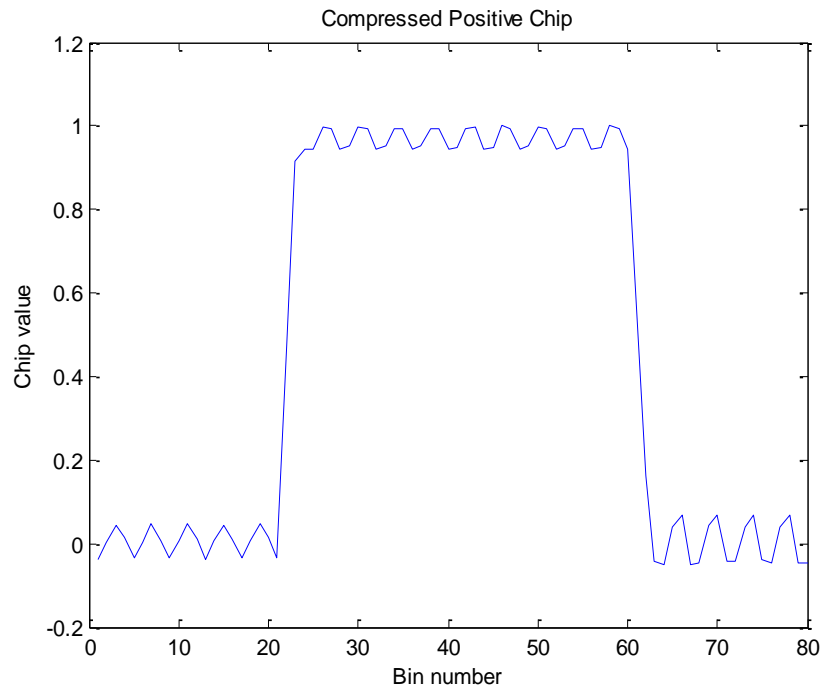
Figure 5.19 - Compressed Positive Chip Obtained from the Split Chip Summation Technique
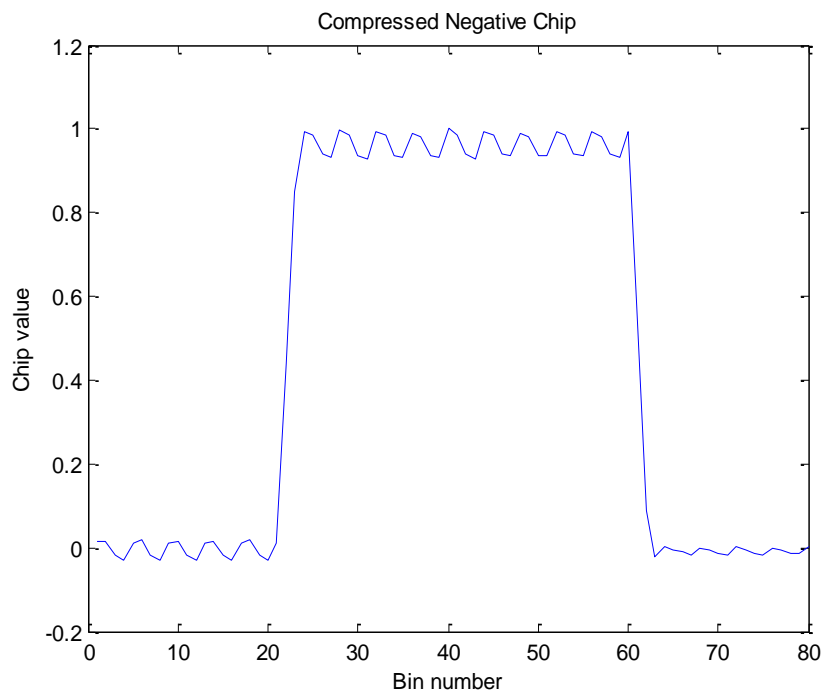
Figure 5.20 - Compressed Negative Chip Obtained from the Split Chip Summation Technique

This technique can also be used to detect and correct for unbalanced duty cycles errors in the underlying spreading code that can be caused by minor errors in the transmitter. In order to demonstrate this capability, as sample satellite navigation signal was generated that contains the transmitter effects only, with no channel or front end effects present in the signal, to draw attention to the unbalanced duty cycle issue alone. The signal was generated with the same 40 MHz sampling frequency and 5 MHz center frequency to provide high resolution results. The compressed positive and negative chip waveforms obtained using the split chip summation technique are presented in Figure 5.21 and Figure 5.22, respectively.
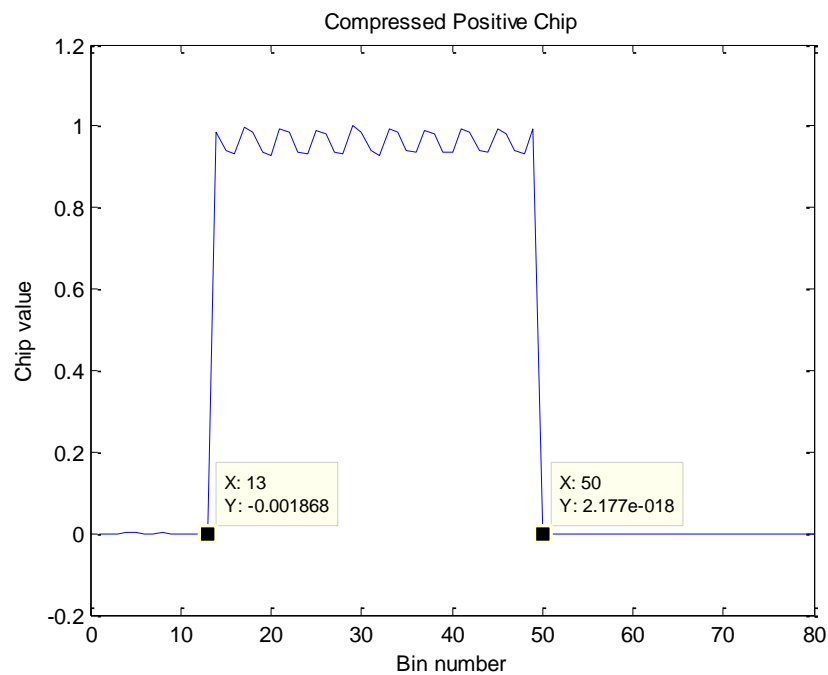
Figure 5.21 - Compressed Positive Chip Obtained from the Split Chip Summation Technique
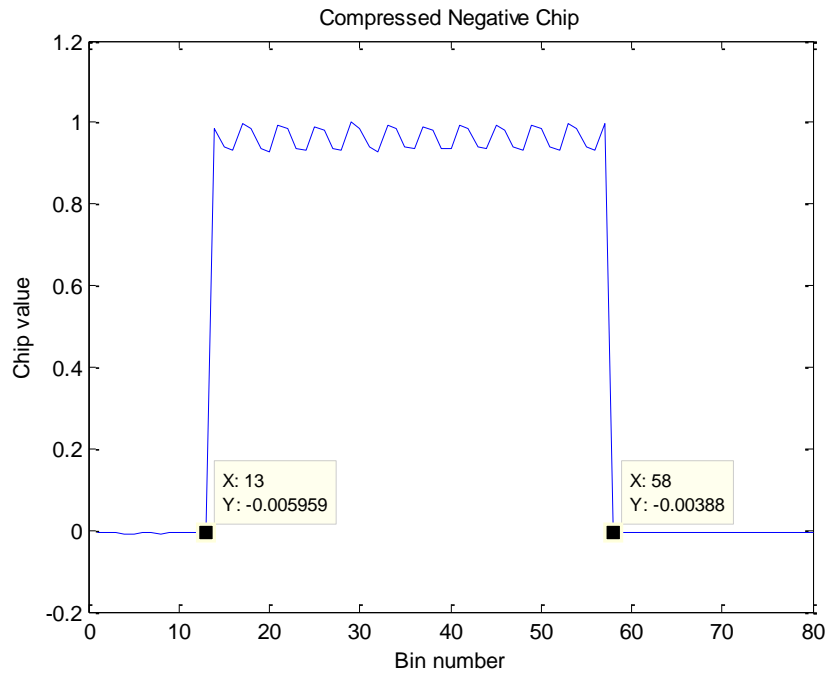
Figure 5.22 - Compressed Negative Chip Obtained from the Split Chip Summation Technique

Closer inspection of the two compressed chip waveforms obtained using the split chip summation technique reveals that the two chips are not balanced, in that the chip widths are not equal. It can be seen that there is a 10% duty cycle imbalance on the two extracted chip waveforms. When processed by a conventional tracking loop, this would result in reduced correlation outputs, as 10% of each chip of the locally generated spreading code will be out of phase with the incoming IF. In the case of tracking a weak signal with interference from stronger signals and multipath present in the incoming IF, this could result in a loss of lock on the acquired satellite signal, degrading receiver performance, leading to reduced accuracy on the estimated position solution. Having knowledge of this duty cycle imbalance, the locally generated spreading code can be altered to match the underlying spreading code in the incoming IF, resulting in improved correlation outputs and enhanced tracking performance under such circumstances.

5.6 Conclusions

This chapter has provided an overview of the advanced processing techniques designed and implemented in GNSScope. Before delving into the details of these techniques, a brief overview on the issues of weak signals, multipath, and multiple access interference that present in satellite navigation systems was presented. This was followed by the details of weak signal acquisition and tracking techniques implemented in GNSScope, with modifications to ensure higher accuracy in the computed results. In order to provide a basis for the techniques described in this chapter, the successive and parallel interference cancellation techniques were briefly described, with an analysis of their shortcomings. This was followed by a brief overview of several SIC and PIC based techniques in the literature, to provide a comparison for the novel techniques developed in the toolbox. The final section of this chapter provided the details of these novel techniques, namely the mirrored channel mitigation technique, the trigonometric interference cancellation technique, and the split chip summation technique. Case studies were also provided for each technique, presenting their performance in the presence of weak signals, multipath, multiple access interference and continuous wave interference, bringing the chapter to an end.

Chapter 6 Performance Analyses of the GNSScope Toolbox

6.1 Introduction

The previous chapter dealt with the advanced signal processing techniques built into the GNSScope toolbox, enhancing receiver performance under weak signal conditions, and in the presence of multipath and multiple access interference. While the performance of these techniques were shown using short case studies looking into their effectiveness, the performance of the GNSScope toolbox as a whole was not considered in a complete end-to-end navigation exercise. This chapter will provide an overall performance analysis of the GNSScope toolbox, where a real recorded signal containing both the GPS and the GIOVE-A satellite transmissions will be processed from acquisition and tracking to the final satellite and user position calculations and placement of the results on a map using Google Maps for a complete solution. Advanced signal processing techniques designed and implemented in the GNSScope toolbox, and detailed in the previous chapters, will be used to improve the overall performance and accuracy of the results. The chapter will begin with the details of the graphical user interface built into the toolbox for easy access to most of its capabilities. This will be followed by detailed analyses of each stage of the receiver processing chain, including signal acquisition, tracking loop responses, bit extraction and frame synchronization, navigation data extraction, and computation of the satellite and user coordinates. The chapter will end with further analysis into the effects of hardware limitations and data path quantization on the results of the acquisition and tracking operations.

6.2 The Graphical User Interface

GNSScope is a comprehensive toolbox designed and implemented in MATLAB for the end-to-end modeling, simulation and analysis of current and future satellite navigation signals, including, but not limited to, those provided by the GPS and Galileo satellite navigation systems. The ability to acquire and track a wide variety of signals from multiple systems and frequency bands, including strong and weak signals, signals on the multipath, and signals containing cross-correlation interference from neighboring satellite signals as well as jamming from CW type signals, requires many tools to be utilized to maximize receiver performance under such conditions. In order to simplify the handling of the vast number of parameters and variables necessary for the correct operation of the toolbox, a Graphical User Interface (GUI) was designed and developed in MATLAB, to accompany the GNSScope toolbox, providing structured access to all the parameters involved in each stage of the processing chain.
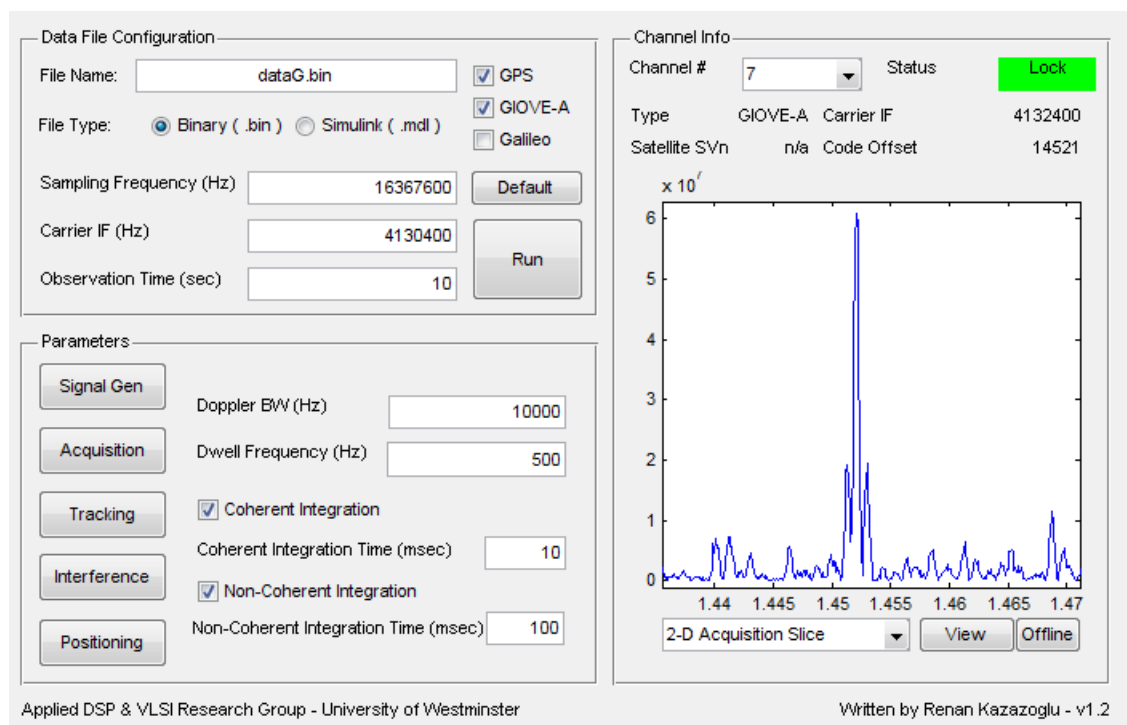
Figure 6.1 - The GNSScope User Interface

A screenshot of the GUI can be seen in Figure 6.1, above [5] [8]. The user interface is split into three panes, namely the data file configuration pane, the parameters pane, and the channel info pane. The data file configuration pane, displayed in Figure 6.2, below, contains the basic parameters necessary for identifying an input IF, which is characterized by the file type, the sampling frequency used in recording the file, the carrier IF without Doppler, and the observation or processing time for the file. Currently the GUI is capable of processing binary files containing recordings of real signals obtained through data acquisition cards or converted from other sources such as hardware signal generators and synthesizers, as well as initializing signal generation capabilities built into the GNSScope toolbox using the Simulink design environment provided in MATLAB.
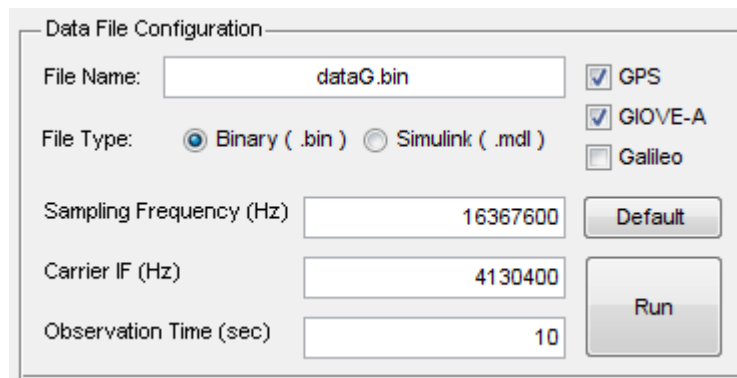
Figure 6.2 - The Data File Configuration Panel

In addition to the parameters defining the input signals, the processing of certain types of signals belonging to individual satellite navigation systems can be enabled or disabled through their respective checkboxes, in order to minimize the processing time involved with the acquisition of all the satellites available through the different navigation systems and provide the ability to focus attention to specific signals and navigation systems. The final components of the data file configuration pane are the *Default* and *Run* buttons. As the name suggests, the *Run* button saves all the parameters and configurations of the receiver and initiates processing the file. The receiver will run continuously until the end of the observation time is reached, whereby the results are uploaded into the user interface for access and analysis by the user. The *Default* button is included in the

interface to provide users with quick and easy access to the default configuration of the receiver, whereby it is set to process all available signals form GPS, GIOVE-A and Galileo satellites in strong signal processing mode with 10 millisecond coherent integration time to improve the results with hindering processing speeds. Non-coherent integration is disabled in this mode. The Doppler search bandwidth is set to 10kHz with a 500 Hz frequency resolution. The cross-correlation interference mitigation techniques and weak signal processing modes are also disabled in the default mode configuration to ensure fast processing times and rapid access to general information regarding the selected input signal. For most general purpose GNSS processing problems, the default settings will provide satisfactory results with minimal overhead.
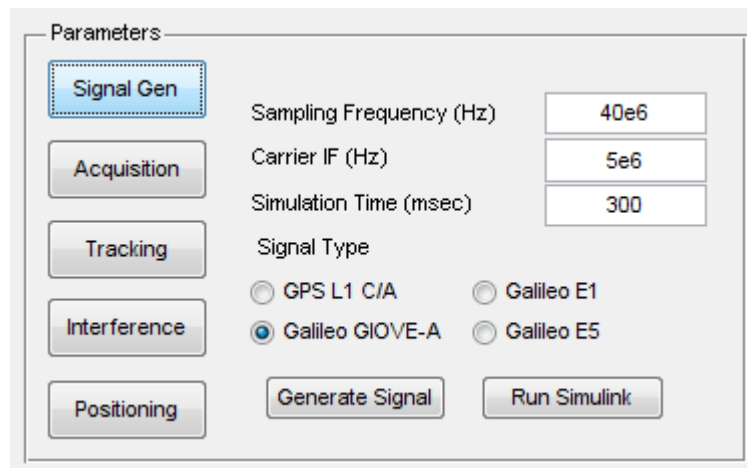
Figure 6.3 - The Signal Generation Panel

The second pane in the user interface is the parameters pane, which is a composite pane containing several sub-panels corresponding to the specific blocks within the GNSScope toolbox, namely the signal generation, acquisition, tracking, interference mitigation, and positioning blocks. The first of these sub-panels is the signal generation panel, which is responsible for handling the signal generation parameters, when a locally generated signal is to be used for processing in the toolbox. This sub-panel can be seen in Figure 6.3, above.

Currently, the GNSScope toolbox offers two options for the generation of satellite signals. The first of these options can be accessed via the *Generate Signal* button, which registers the desired sampling frequency, carrier IF, simulation time and signal type information entered by the user, to generate a simple single satellite signal for testing purposes. The signal types currently supported by the toolbox for signal generation purposes are the GPS L1 C/A code signal, the Galileo GIOVE-A test signal, and the Galileo E1 and E5 signals. Signals generated in this manner contain the appropriate noise levels without cross-correlation interference or weak signals being present in the file. The second option to generate a satellite signal is to use the *Run Simulink* button, which provides the user access to the Simulink environment for custom signal generation, enabling users to tailor the signal to their requirements for use in the GNSScope toolbox.

The second sub-panel of the parameters pane is the acquisition panel, responsible for handling the parameters regarding the acquisition of satellite navigation signals, which can be seen in Figure 6.4, below. It contains settings for the Doppler search bandwidth and the frequency bin size, as well as the options to enable or disable coherent and non-coherent integration on the acquisition results to improve the accuracy of the results and the performance of the receiver. Both the coherent and the non-coherent integration times can be set individually in milliseconds, or alternatively in number of frames by including the letter "f" in the timing information, where a frame is defined as one period of the underlying chipping code used in the satellite signal.
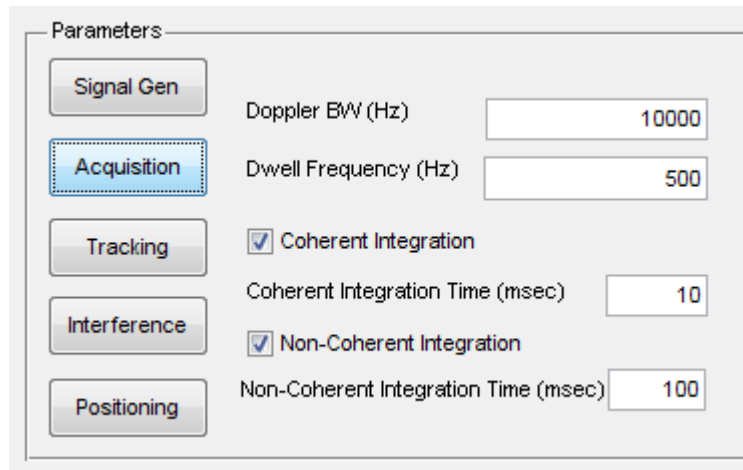
Figure 6.4 - The Acquisition Panel

The third sub-panel of the parameters pane is the tracking panel, given below in Figure 6.5, which handles the configuration of the tracking loops, including the PLL / DLL parameters, discriminator types and the early / late correlator arm spacing to be used in the receiver. These parameters can be set individually for the code and carrier tracking loops through the respective buttons in the panel. Upon initialization, these values are set to their default values to reduce the number of parameters necessary to be input by the user.
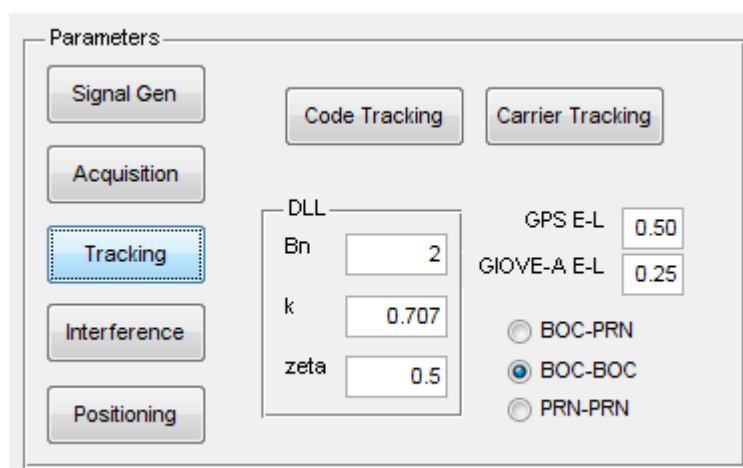
Figure 6.5 - The Tracking Panel

The fourth sub-panel of the parameters pane is called the Interference panel, and is given in Figure 6.6, below. This panel is used to enable or disable some or all of the novel advanced signal processing techniques designed and developed in GNSScope. Enabling multiple interference cancellation techniques in the toolbox will result in the output workspace containing the results of each individual technique separately. These results can then be used for comparative analysis of the effectiveness of the techniques. In order to form a benchmark for all analyses carried out in GNSScope, the SIC and PIC techniques are also included. In addition to these interference cancellation techniques, the user is provided with the option to analyze the multipath content of the received signals. This is done by using the selected interference mitigation techniques to mitigate the strongest signal path in the incoming IF, to reveal any multipath components being received from the same satellite. An example of this type of analysis was given in Figure 5.11.
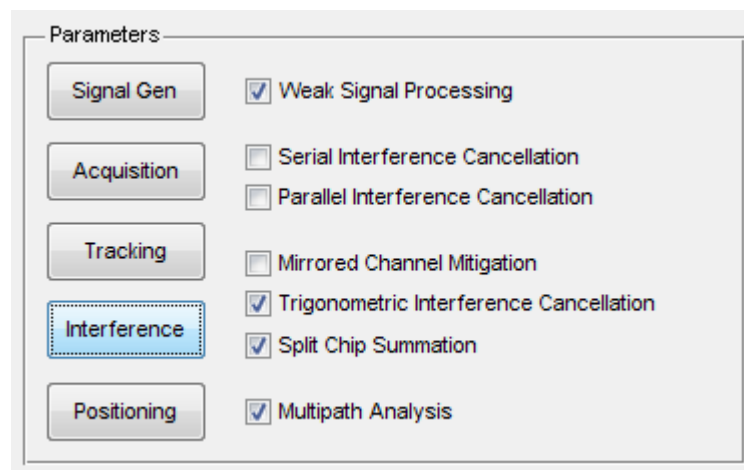
Figure 6.6 - The Interference Panel

The last sub-panel of the parameters pane is the positioning panel given in Figure 6.7, below, which displays the final user coordinates in terms of latitude, longitude and altitude. These are calculated using classical Keplerian geometry and the equations provided in 0, as these positioning algorithms lie beyond the scope of this work. Once the incoming IF has been processed and the user coordinates have been calculated, the *Display User Coordinates in Google Maps* button can be used to view the results on a

map, providing the user with a complete end-to-end solution for the modeling, simulation and analysis of GNSS.
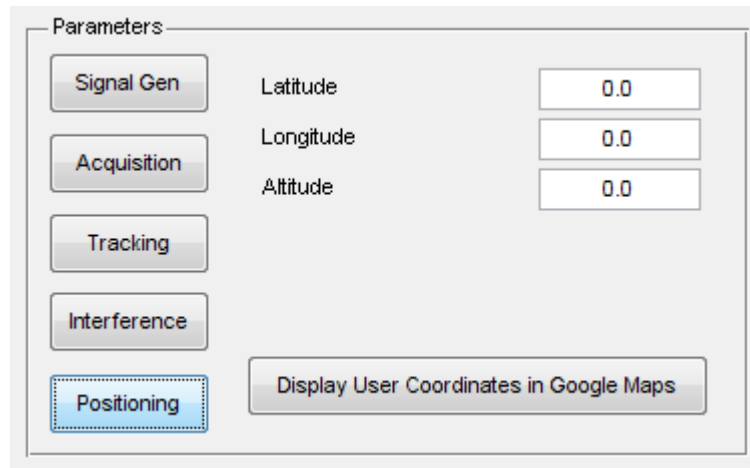
Figure 6.7 - The Positioning Panel

The final panel of the GNSScope GUI is the *Channel Info* panel, which can be seen in detail in Figure 6.8, below. This panel provides the user with an organized layout containing all the results obtained from processing the selected IF signal. When the receiver completes processing this signal, the *Channel #* drop-down box will be populated with all the channels that were created during receiver operation. To the right of this box, the channel status indicator can be seen, which is used to indicate the quality and reliability of the results for the specified channel. This is determined from the PLL and DLL locks of the tracking channels. A green light indicates a strong lock on the signal with narrow band operation, while an orange light indicates a weak lock on the signal with wide band operation, and a red light indicates loss of lock during part or all of the processing of the signal. Each channel in the receiver is assigned a specific satellite signal during initial acquisition. The relevant details of these satellites are also provided in this panel in order to be able to identify the satellites being processed in each channel. The information provided consists of the satellite type, the satellite number in the respective constellation, the carrier IF and the initial code phase offset of the spreading code obtained during initial acquisition.
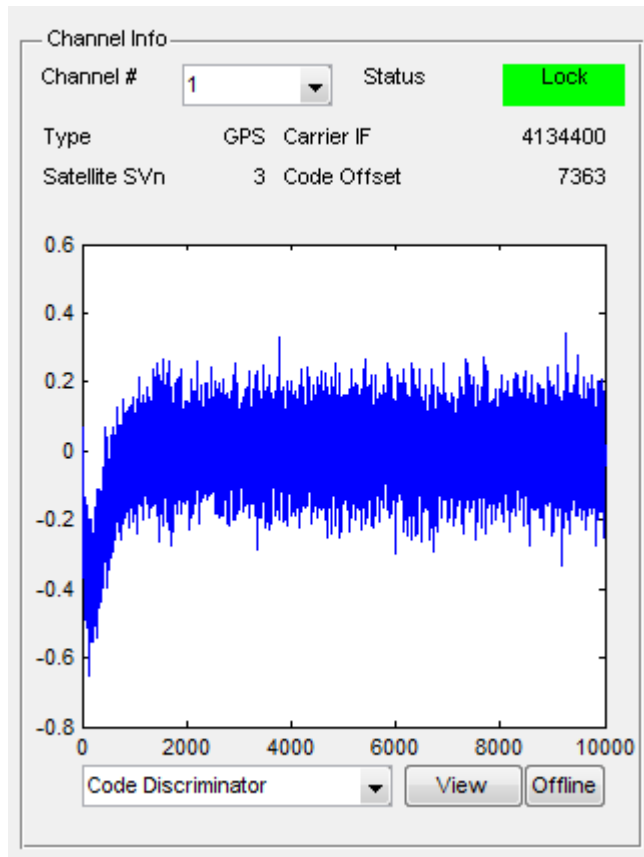
Figure 6.8 - The Channel Info Panel

In addition to the channel details provided above, the channel info pane also provides the user with a comprehensive figure based analysis tool, which can be seen above. Using this tool, many analyses can be completed at the click of a button through the user interface. The plots provided with this tool include the initial acquisition results, cross-sectional views, enhancements obtained from weak signal processing techniques, the carrier and code discriminator responses for the observation time, the carrier frequency and chipping rate accounting for relativistic effects between the satellite and the receiver, the early, prompt and late in-phase and quadrature correlator outputs, results of the novel advanced signal processing techniques applied to the selected IF signal, and the final navigation data message for the observation time. As the tool was designed in MATLAB, further plots and analyses can be carried out using the workspace, and added into the GUI for future use. Once the desired plot is selected, pressing the view button will present the user with the results. The last component of the interface is the *Offline* button at the

lower right corner of the panel. When the receiver has processed the selected signal, pressing this button will save the entire workspace to a file for future processing, removing the necessity to run the whole process each time the toolbox is started and saving large amounts of simulation time. The saved workspace can be later loaded simply by pressing the offline button when the receiver is first initiated, enabling users to continue their work from where they left.

6.3 A User Positioning Case Study in GNSScope

The previous section provided the details of the GUI accompanying the GNSScope toolbox, from initial signal selection to final analysis of the results obtained from processing that file. This section will provide an in-depth analysis of each stage in the processing chain using a real recorded GNSS signal containing signals from GPS satellites as well as the GIOVE-A test satellite which is part of the Galileo navigation system. This will include initial acquisition search results, enhancements obtained from weak signal processing, the PLL / DLL responses in the tracking loops, the discriminator responses, stability analyses, cross-correlation interference and multipath detection, analysis of the prompt correlator outputs, frame synchronization and bit extraction, navigation data decoding, user position calculation, and finally, locating a user on a map, where the results will be provided on a map using the Google Maps application [5].

The signal that will be used throughout this section was recorded at a sampling rate of $16.367.600\ Hz$ with the center frequency of the carrier IF being at $4.130.400\ Hz$. An observation time of $30\ sec$ was chosen, as it is the minimum observation time required to process all five sub-frames of the GPS signal to produce a user position result. The GIOVE-A signal transmitted by the Galileo navigation system will also be processed, with the results being provided in the relevant sections. The results obtained from processing this signal in GNSScope will be broken down into five sections, where the results of each stage of the processing chain are discussed in detail in their respective sections. Analysis will begin with signal acquisition in the next section, where the acquisition search results will be presented. This will be followed by the analysis of the tracking loop responses for each correlator channel that was instantiated during acquisition. Once the correlator channels complete processing all the available signal content in the input IF, their outputs will be

processed for the frame synchronization and bit extraction operations, in the next section. This will be followed by the extraction of the navigation data and parameters necessary for the computation of the user position. The final section will provide the results of the user positioning algorithms and present this information on a map provided by the web-based Google Maps application.

6.3.1 Signal Acquisition

The first step in the receiver processing chain is the acquisition of all available satellite signals in the composite IF input. As there is no prior information concerning the signal of interest, cold start acquisition is carried out on the signal, where all known satellites are searched for sequentially until all the available signals are acquired. In order to improve the accuracy of the results, post detection integration was used during acquisition, in the form of a 10 millisecond coherent integration window for signals transmitted by the GPS satellites and an 8 millisecond coherent integration window for the signal transmitted by the GIOVE-A satellite. Furthermore, non-coherent integration was carried out on the results of 5 consecutive coherent integration bins to minimize the noise content of the results and maximize the carrier-to-noise ratio (C/No) of the correlation peaks.

The acquisition search results for the GPS satellites can be seen in Table 6.1, below, where each detected satellite is listed in the table along with the parameters necessary for the initialization of the tracking channels. The first column in the table presents the PRN code numbers assigned to each detected satellite signal. The next three columns present supplementary information regarding each satellite: the launch date, the atomic frequency standard used on board the satellite, and the orbital plane the transmitting is satellite travelling in. These are followed by the PRN code phase and the carrier frequency of the detected satellite. These two values, along with the associated PRN code number, will be used to initialize the tracking channels in the next stage of the receiver processing chain. Looking at the table, it can be seen that the PRN code phase is not an integer, but rather a fractional number. This is a result of the high sampling rate used during the recording of the signal, which causes each chip of the underlying PRN code to be sampled multiple times, resulting in more accurate results for the PRN code phase. A similar situation can be seen in the carrier frequency column, where the results are once again

fractional, rather than being pulled from one of the finite number of frequency bins used during acquisition. This is due to the post detection integration techniques applied to the results, which are used to increase the frequency resolution of the acquisition search results, improving the initial hold-in performance of the tracking loops.

Table 6.1 - Acquisition Search Results for the GPS Satellites

PRN	Launch Date	Frequency Standard	Orbital Plane	PRN Code Phase [chips]	Carrier Frequency [Hz]	Acquisition C/No [dB]
3	29/03/96	Cs*	C2	460.25	4134404.287	21.646
15	01/10/90	Cs*	D5	93.25	4132086.297	15.243
16	29/01/03	Rb**	B1	129.4375	4131251.196	9.283
18	30/01/01	Rb**	E4	95.5	4132468.726	10.464
19	20/03/04	Rb**	C3	396.25	4136878.370	17.265
22	21/12/03	Rb**	E2	879.625	4134677.450	25.018

*Cs = Cesium Atomic Frequency Standard / **Rb = Rubidium Atomic Frequency Standard

The last column in the table presents the C/No values for the acquired satellites, which were computed based on the results obtained from the coherent and non-coherent integration of the acquisition outputs, and as such, include the processing gains obtained from these PDI techniques [43] [44]. It can be seen that PRN codes 22 and 3 have the strongest acquired signal powers, while 16 and 18 have the weakest acquired signal powers. This can also be seen from the acquisition plots given in Figure 6.9 to Figure 6.14, below, where the upper figures present the acquisition mesh plots while the lower figures present a cross-sectional view along the code-phase dimension providing the outputs of a frequency bin.
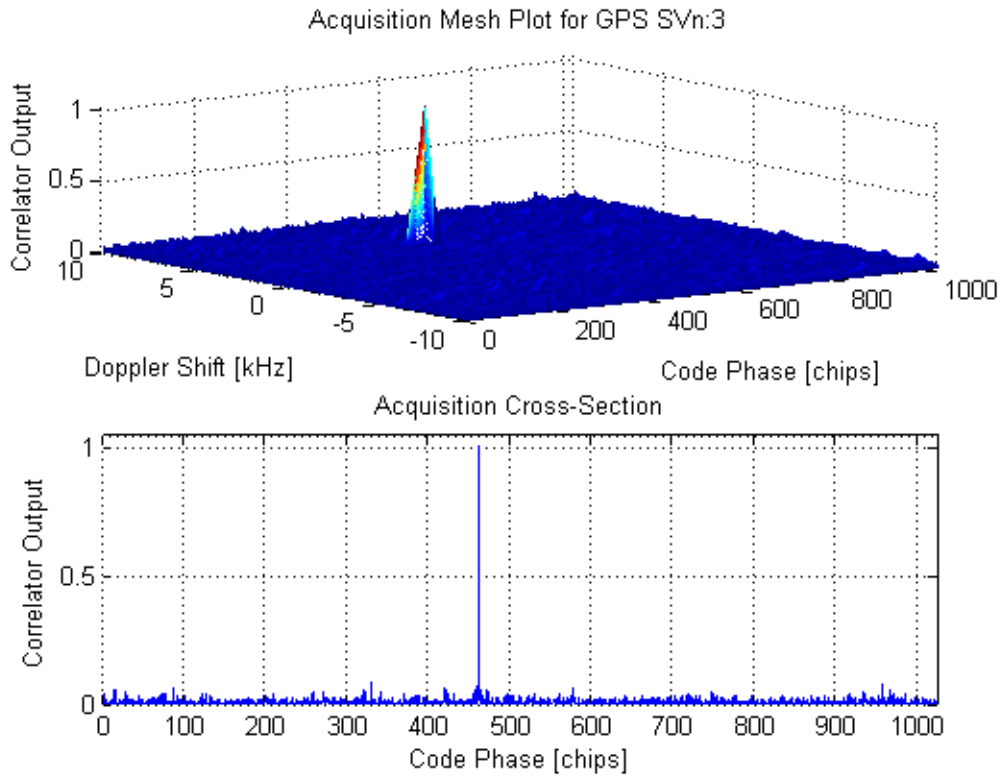
Figure 6.9 - Acquisition Plots for GPS SVn:3
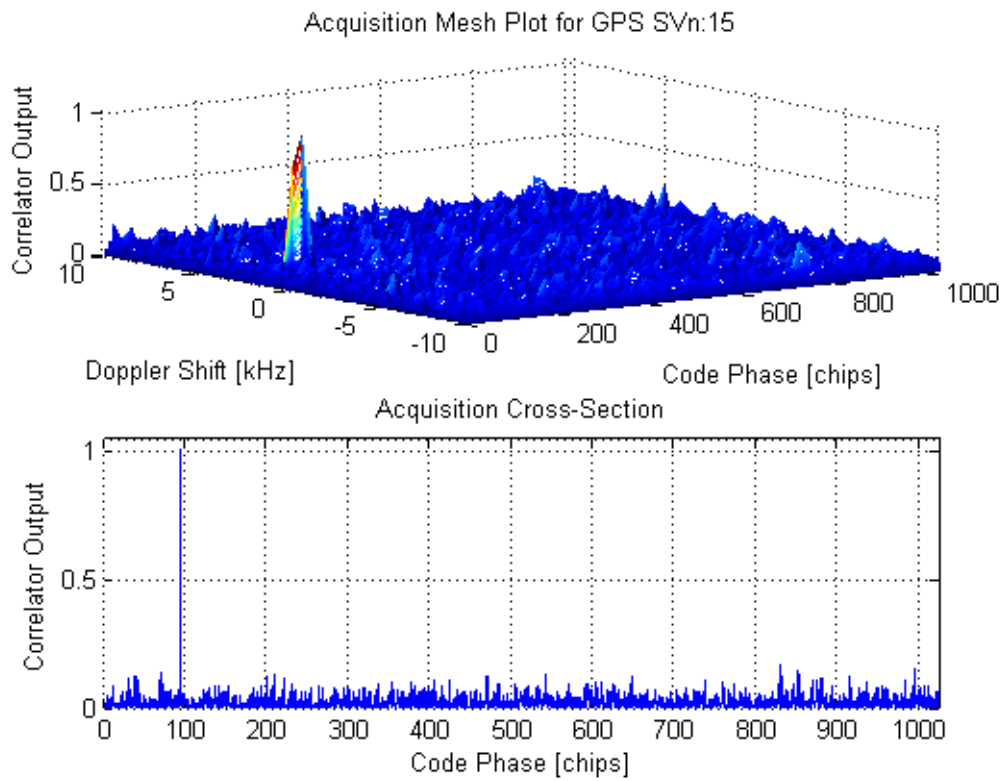
Figure 6.10 - Acquisition Plots for GPS SVn:15
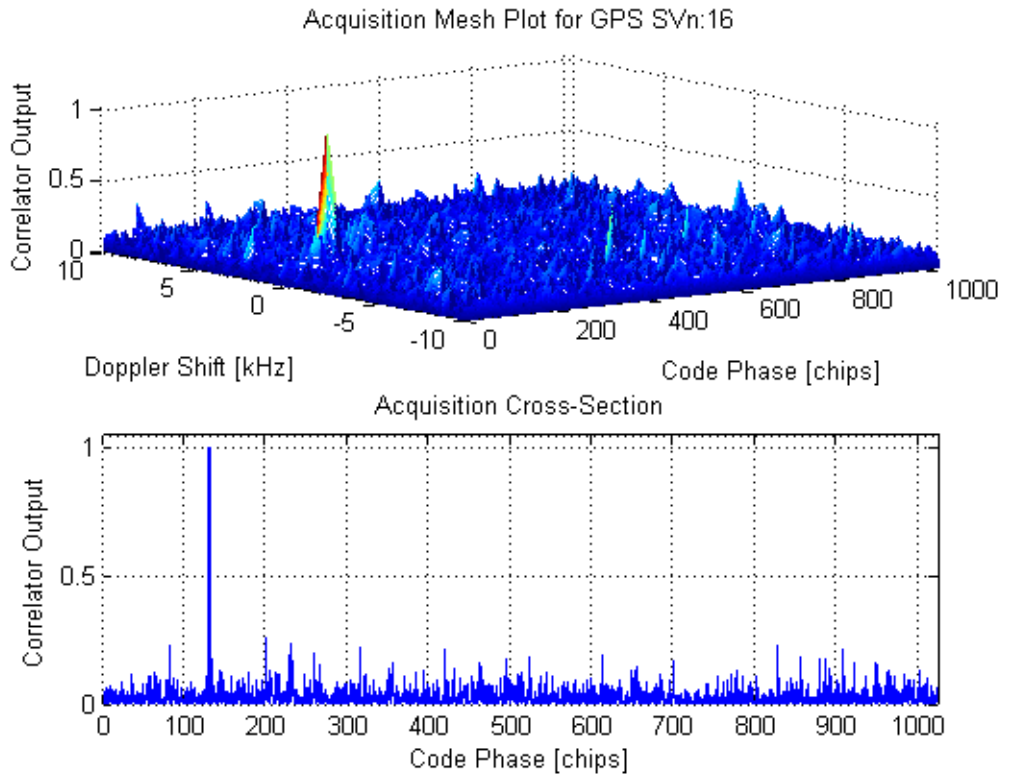
Figure 6.11 - Acquisition Plots for GPS SVn:16
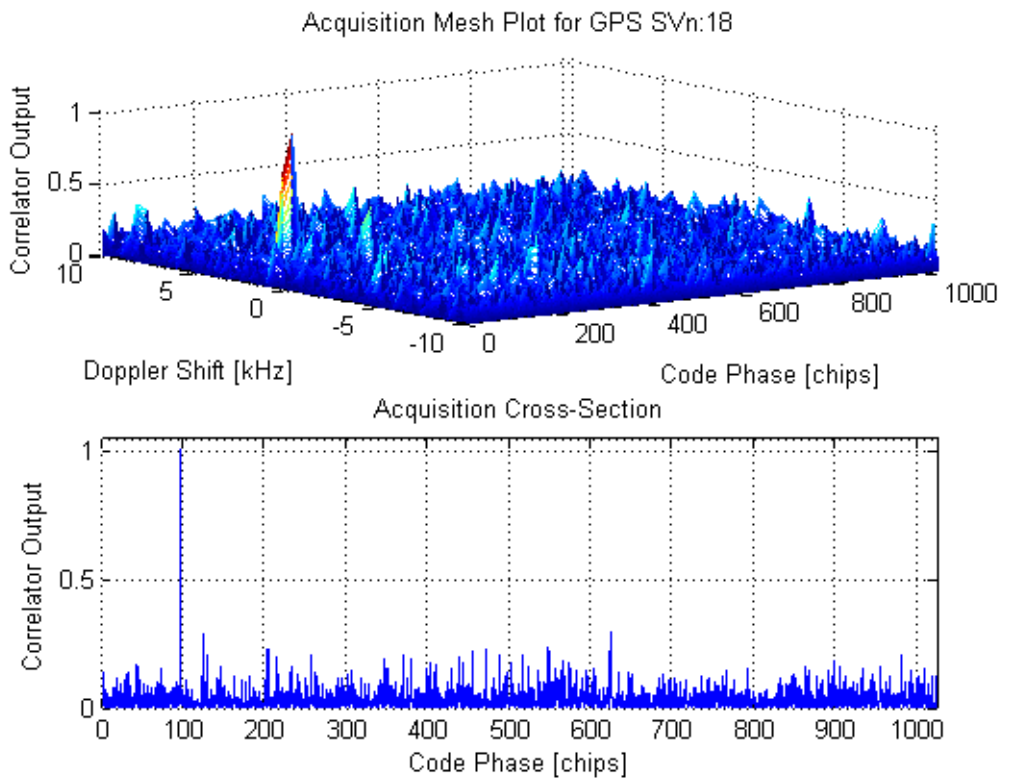
Figure 6.12 - Acquisition Plots for GPS SVn:18
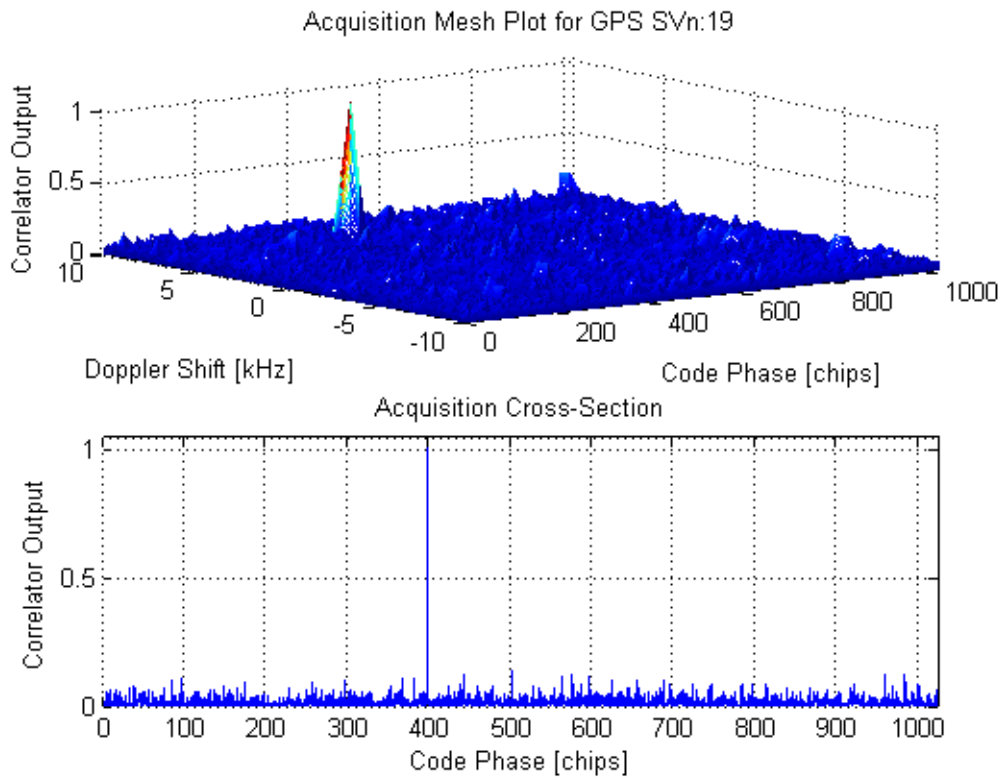
Figure 6.13 - Acquisition Plots for GPS SVn:19
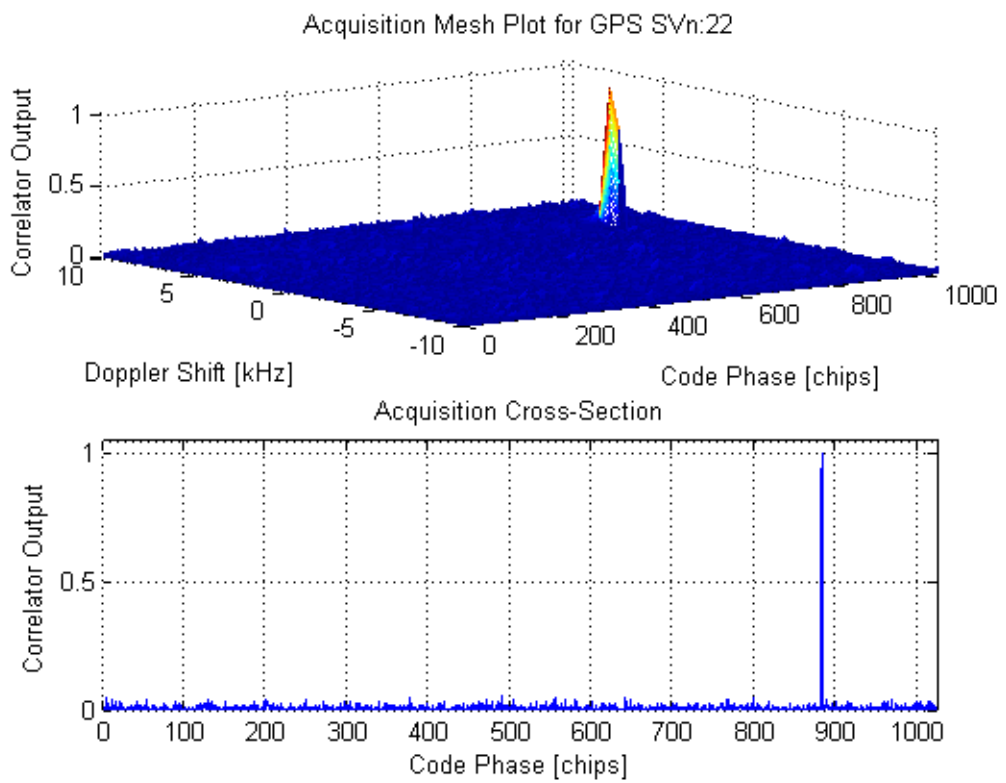
Figure 6.14 - Acquisition Plots for GPS SVn:22

The acquisition search results for the GIOVE-A test satellite can be seen in Table 6.2, below. Once again, due to the high sampling rate used in recording this file, the PRN code phase is fractional, providing an accurate estimate of the exact starting point of the PRN code. Similarly, due to the coherent and non-coherent integration techniques used to increase the accuracy of the results, the carrier frequency is also fractional. These results are also presented in graphical form in Figure 6.15, below, where the characteristic correlation triangle for the BOC modulated signal can be seen in detail in the lower plot.
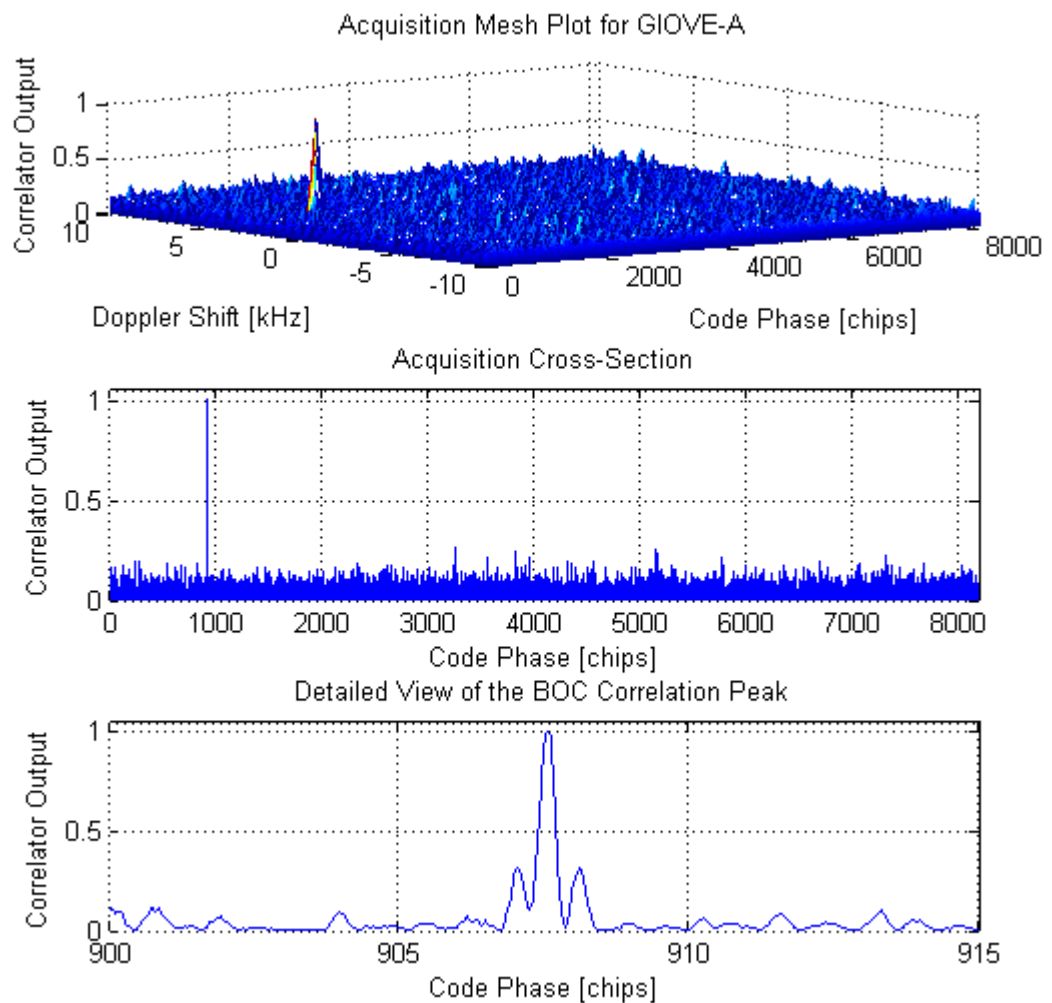
Figure 6.15 - Acquisition Plots for the GIOVE-A Satellite

Table 6.2 - Acquisition Search Results for the GIOVE-A Satellite

PRN	Launch Date	Frequency Standard	PRN Code Phase [chips]	Carrier Frequency [Hz]	Acquisition C/No [dB]
1	28/12/05	Rb*	907.59	4132453.167	14.058
*Rb = Rubidium Atomic Frequency Standard					

6.3.2 Tracking Loop Responses

Once the acquisition search is completed, the second stage of receiver processing in GNSScope takes over. Using the coarse carrier frequency and code phase information obtained from the acquisition search, six GPS channels and one GIOVE-A channel are initiated for tracking the acquired satellite signals. In order to process the navigation data without prior knowledge of the almanac, it is necessary to process a whole navigation data frame, lasting five sub-frames, or 30 seconds. However, as the starting points of these sub-frames are also unknown prior to processing, the tracking loops are set to process 35 seconds of the input IF signal, to ensure that at least five whole sub-frames can be extracted from the outputs of the tracking channels. This section will provide a detailed review of the results obtained from the tracking channels.

The error functions and corresponding outputs for the corrected chipping rates and carrier frequencies of each acquired GPS satellite can be seen in Figure 6.16 to Figure 6.21, respectively, and in Figure 6.22 for the GIOVE-A satellite, for the whole 35 millisecond observation time. It can be seen that the plots corresponding to the GPS satellites all contain a noise spike at the same iteration, hinting at issues with the tracking loops. However, this spike is due an issue with the downloading of the sampled data from the IF front-end to the computer, and is not part of this work. The reason this spike only presents in the GPS channels and not the GIOVE-A channel is that the accumulation window used in the GPS channels is only 1 millisecond wide, while the GIOVE-A channel uses an 8 millisecond wide accumulation window, which filters out most of the effects of the damaged part of the data. Using these figures, the following information can be extracted regarding the acquired satellites.

Table 6.3 - Tracking Loop Observations

	GPS 3	GPS 15	GPS 16	GPS 18	GPS 19	GPS 22	GIOVE-A
Carrier Frequency(Hz)							
Variance	45.9	156.43	259.96	173.64	93.58	42.06	96.09
Standard Deviation	6.78	12.5	16.13	13.18	9.67	6.48	9.8
Code Chipping Rate(Hz)							
Variance	0.07	0.18	0.34	0.23	0.13	0.06	0.42
Standard Deviation	0.26	0.42	0.58	0.48	0.36	0.24	0.65
Satellite Motion							
Doppler Drift	⇩	⇧	⇧	⇧⇩	⇧	⇩	⇧
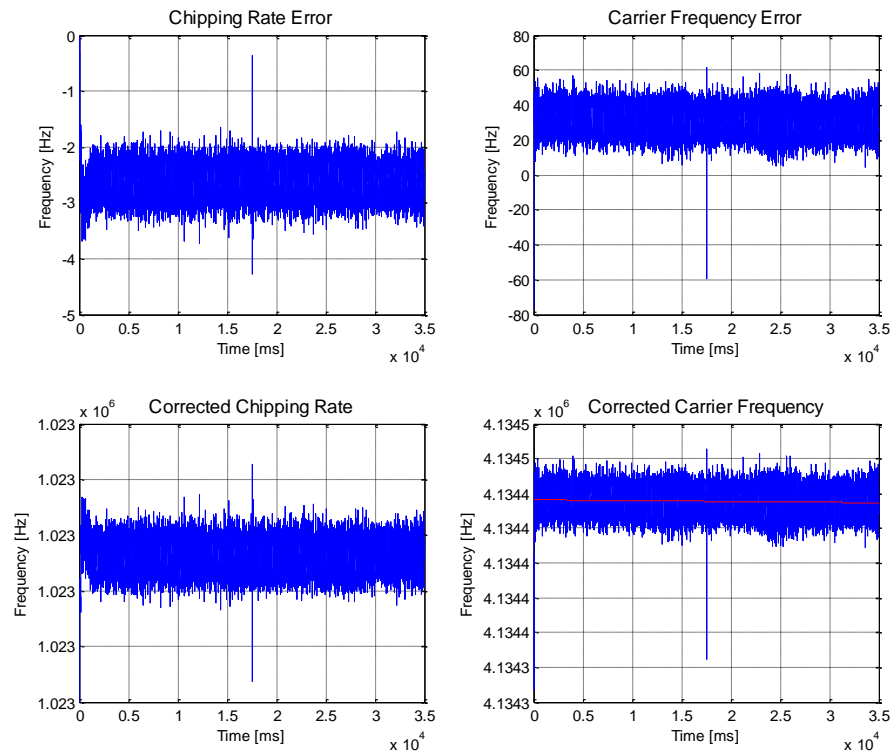
Figure 6.16 - Tracking Results for GPS SVn:3
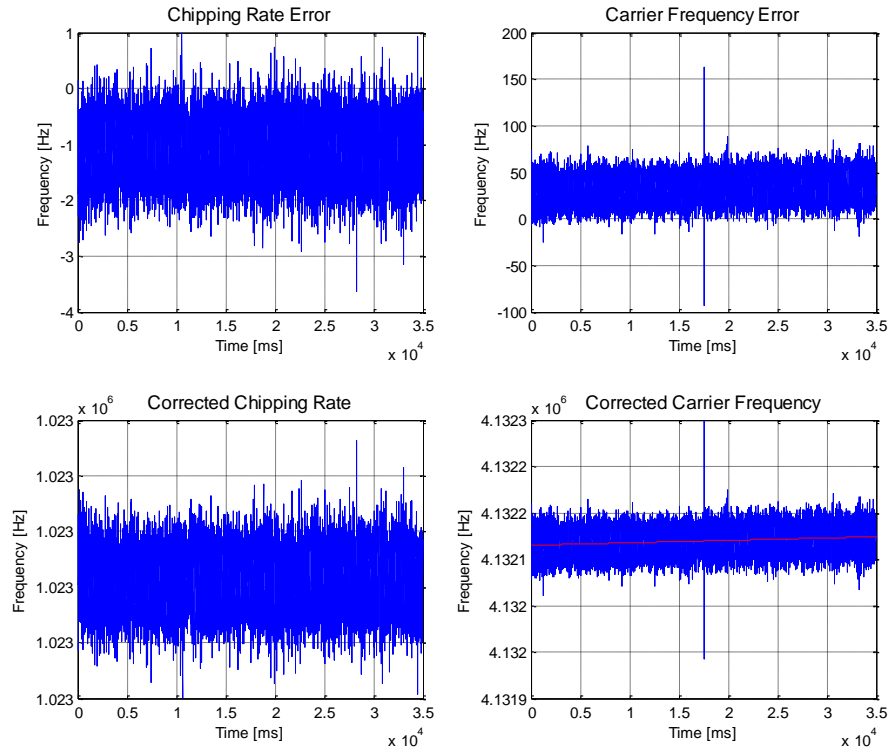
Figure 6.17 - Tracking Results for GPS SVn:15
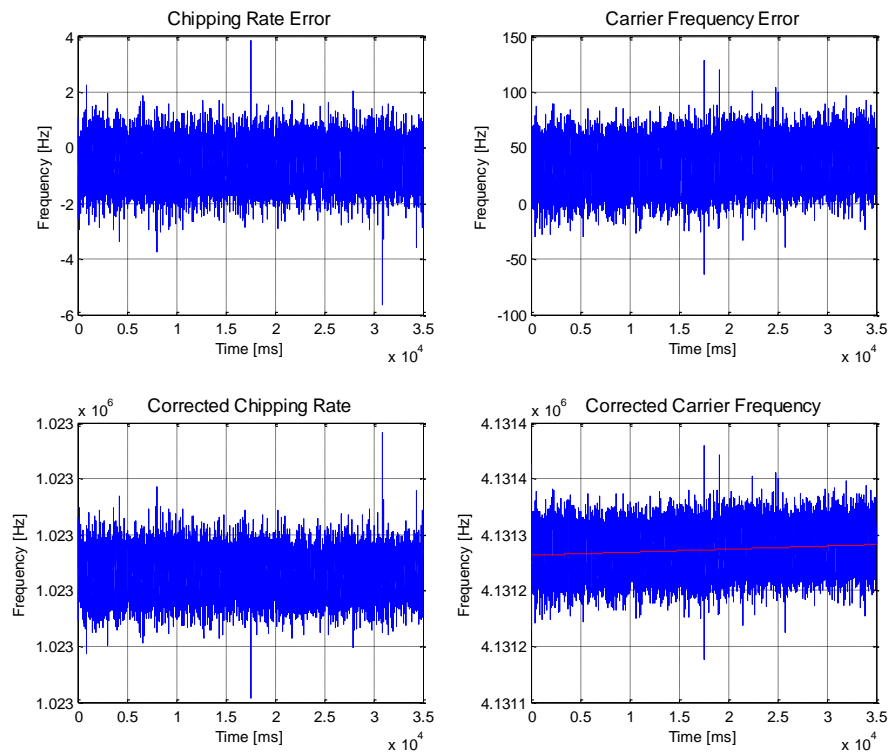
Figure 6.18 - Tracking Results for GPS SVn:16

158
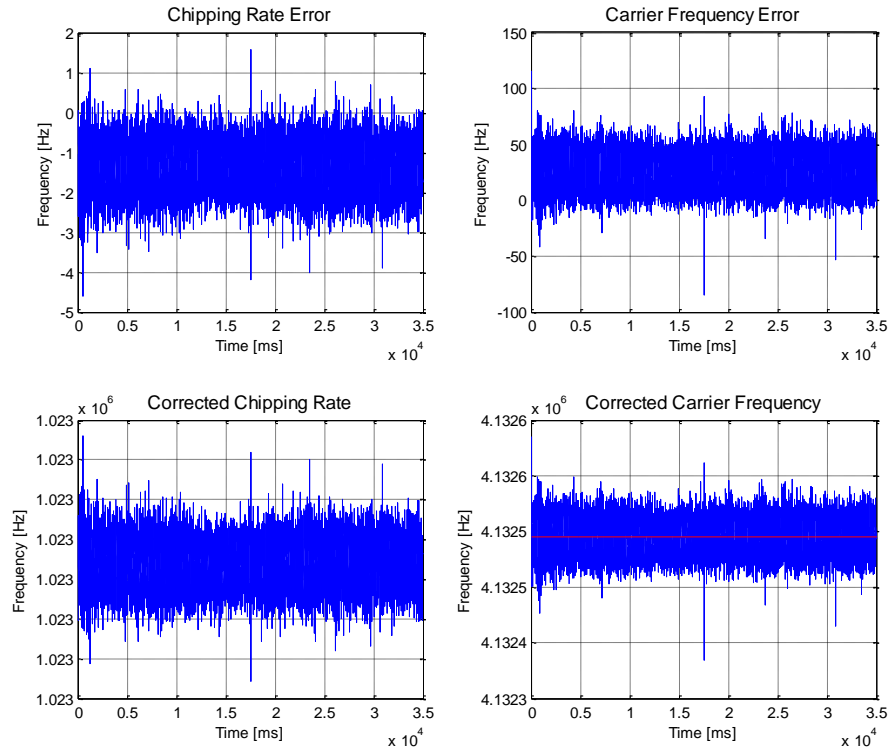
Figure 6.19 - Tracking Results for GPS SVn:18
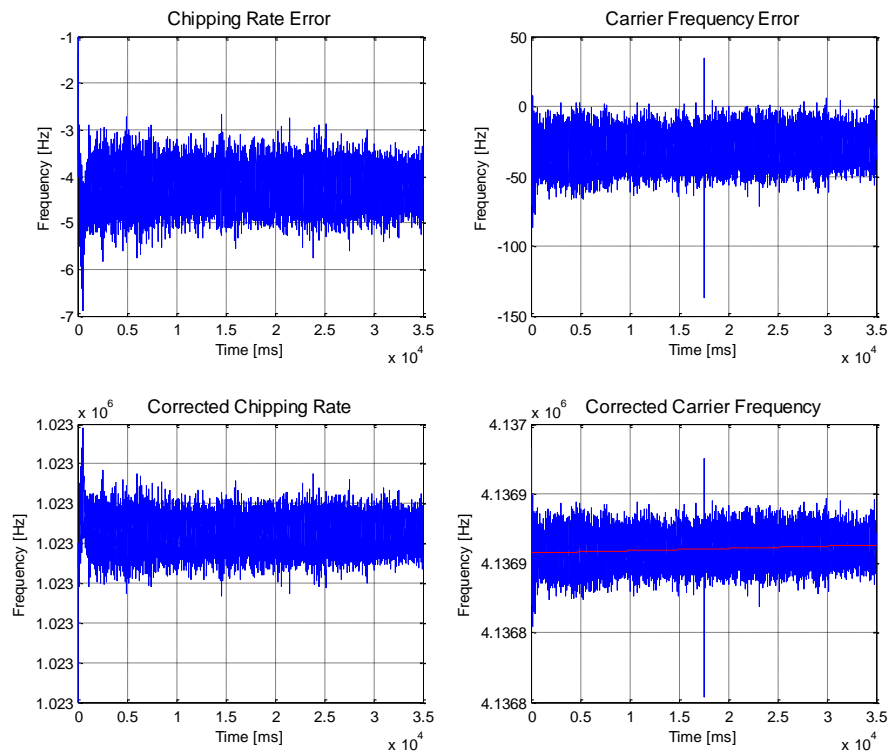
Figure 6.20 - Tracking Results for GPS SVn:19

159
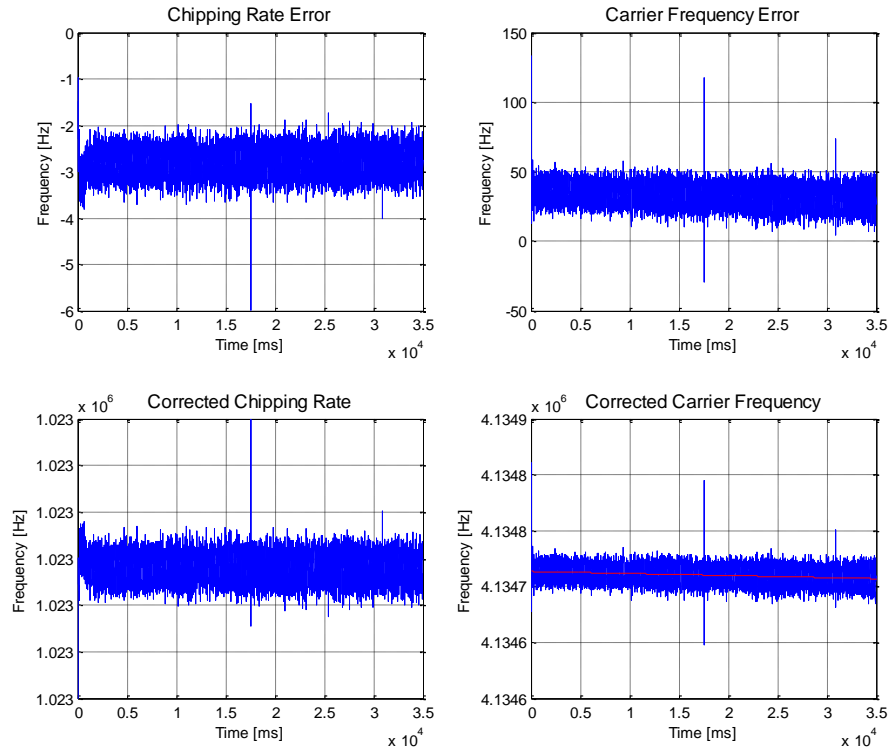
Figure 6.21 - Tracking Results for GPS SVn:22
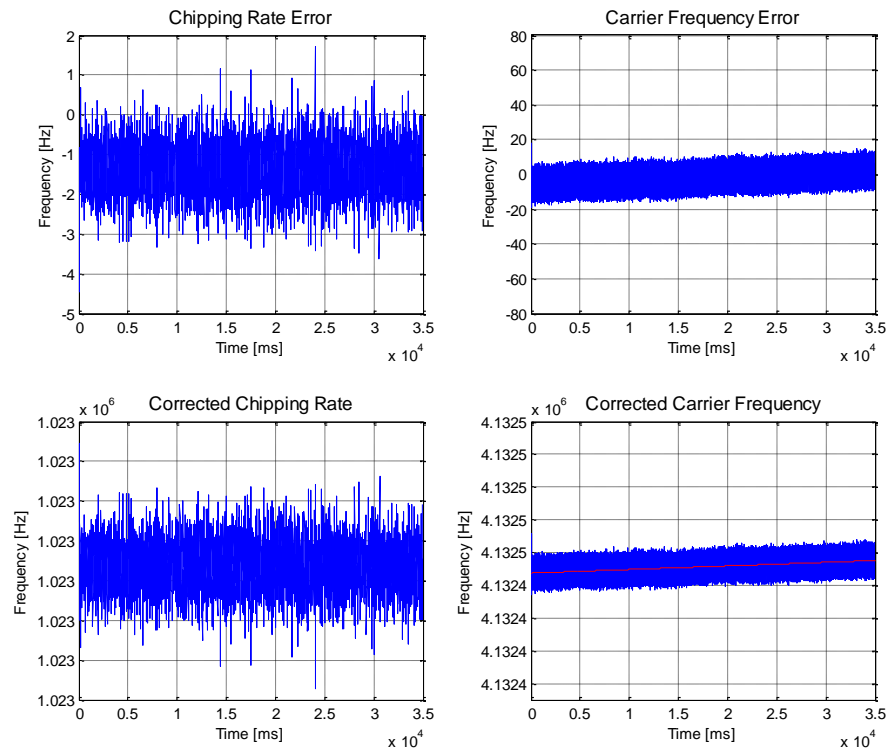
Figure 6.22 - Tracking Results for GIOVE-A

Observing the statistical characteristics for the carrier frequency and code chipping rates given in Table 6.3, it can be seen that the satellite signals which had higher carrier to noise ratios from the acquisition stage, have lower corresponding deviation in their tracking responses, due to having a better lock on the signal parameters. It can also be seen that the mean error in carrier frequency is in the range of 50 Hz, even though the frequency bins used in the cold start acquisition were set to be 500 Hz each. This is due to the 10 frame post detection integration used in acquisition, which increases the frequency resolution of the results. The Doppler drift of the satellites are also provided in the table, and are determined from the trend, or slope, of the corrected carrier frequencies for the satellites, where ⇧ indicates the satellite is moving towards the receiver, ⇩ indicates the satellite is moving away from the receiver, and ⇧⇩ indicates that the satellite appears motionless for the observation period, implying an overhead satellite, as in the case of GPS SVn:18.

In order to improve the performance of the tracking loops in GNSScope, a lock-on time is implemented in the tracking channels to speed up the settling times of the feedback loops at the cost of wider noise bandwidths, which reduces the accuracy of the results. This is accomplished by having two sets of loop parameters each, for the code and carrier tracking loops. When a satellite signal is acquired, the tracking loops initiate in wide-band operation mode. As the tracking loops settle to their final values, the PLL and DLL used in the tracking loops are reconfigured to their narrow-band operation modes, reducing the noise included in the calculations and increasing the accuracy and stability of the results. This effect can be observed in the discriminator responses for the carrier and code tracking loops, which are given in Figure 6.23 to Figure 6.28 for the GPS satellites, and Figure 6.29 for the GIOVE-A satellite, where the upper plots present the code loop responses and the lower plots present the carrier loop responses for the first 1500 milliseconds of the tracking operation. Looking at the figures, it can be seen that the carrier tracking loops settle within the first 10 milliseconds, with narrow-band mode of operation taking place within the first 100 milliseconds. In the cases of GPS satellites 16 and 18, the tracking loops are not able to maintain narrow-band mode of operation, resulting in a relatively high amount of noise in the carrier discriminator outputs due to the low C/No of these satellite signals.

In GNSScope, the reference frequency used for the generation of the Gold codes is also tracked for each acquired satellite, to account for relativistic effects and sampling losses, and precisely match the locally generated spreading codes with those transmitted by the satellites. Looking at the responses, it can be seen that the code tracking loops have a relatively high settling time in comparison to the carrier tracking loops. This is due to the properties of the Gold codes used in spreading the satellite signals, which produces a high correlation output with very little degradation, once the carrier is locked in frequency and phase. Once again, it can be seen that the satellites with low C/No result in larger amounts of variation due to the increased noise in the computations.
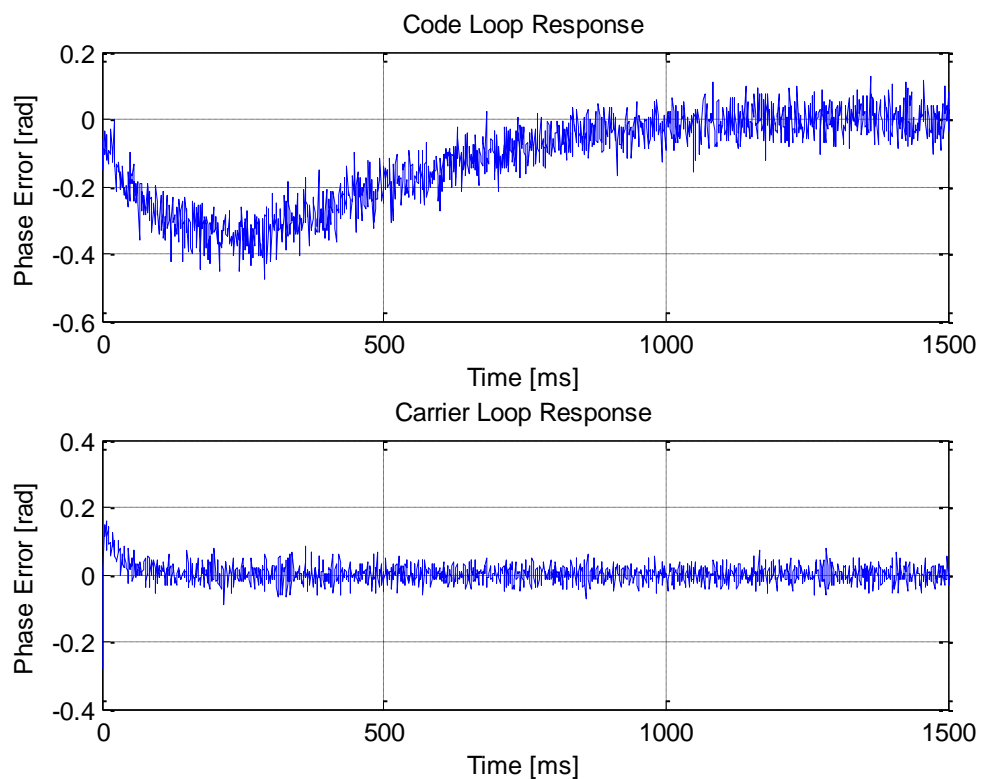
Figure 6.23 - Code and Carrier Loop Responses for GPS SVn:3
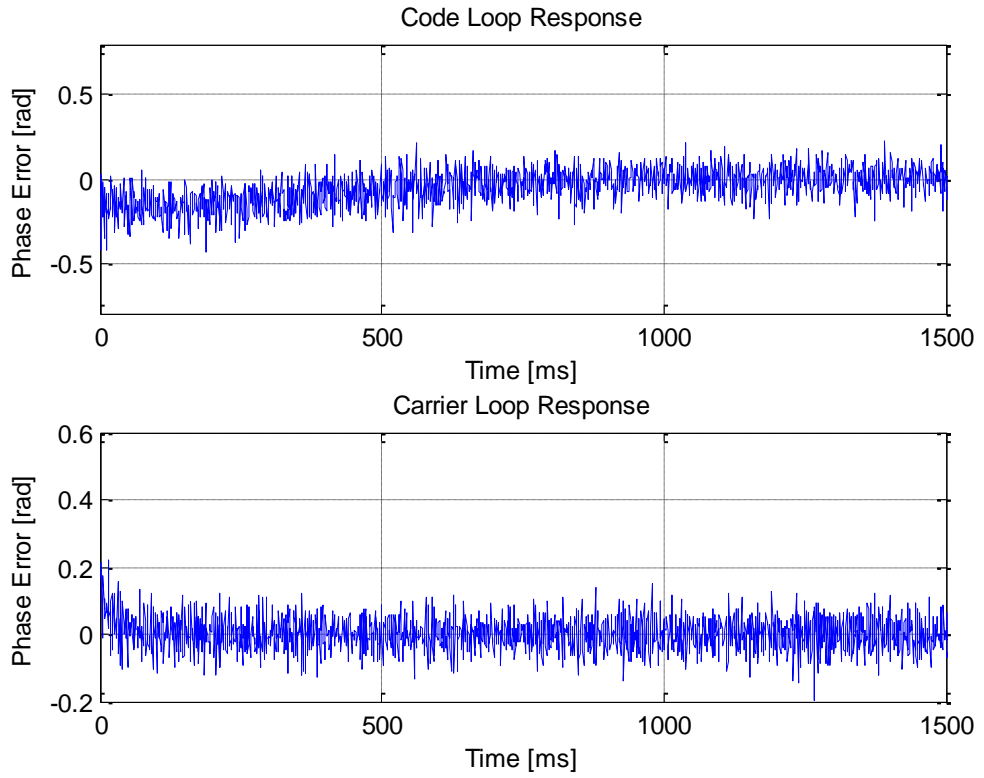
Figure 6.24 - Code and Carrier Loop Responses for GPS SVn:15
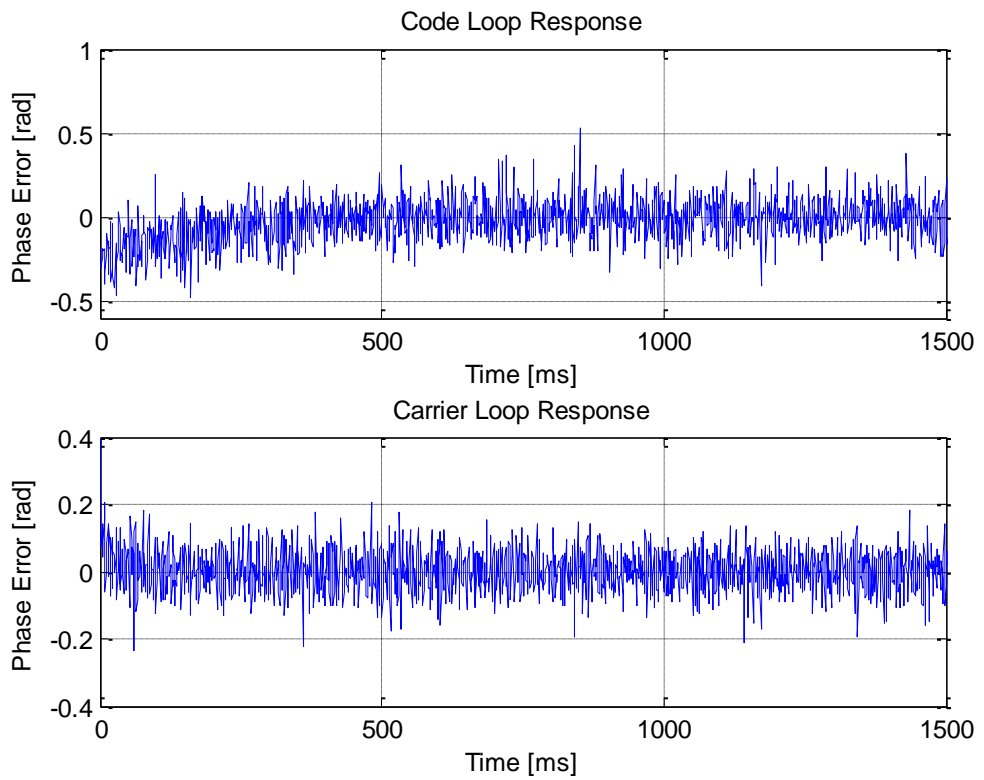
Figure 6.25 - Code and Carrier Loop Responses for GPS SVn:16
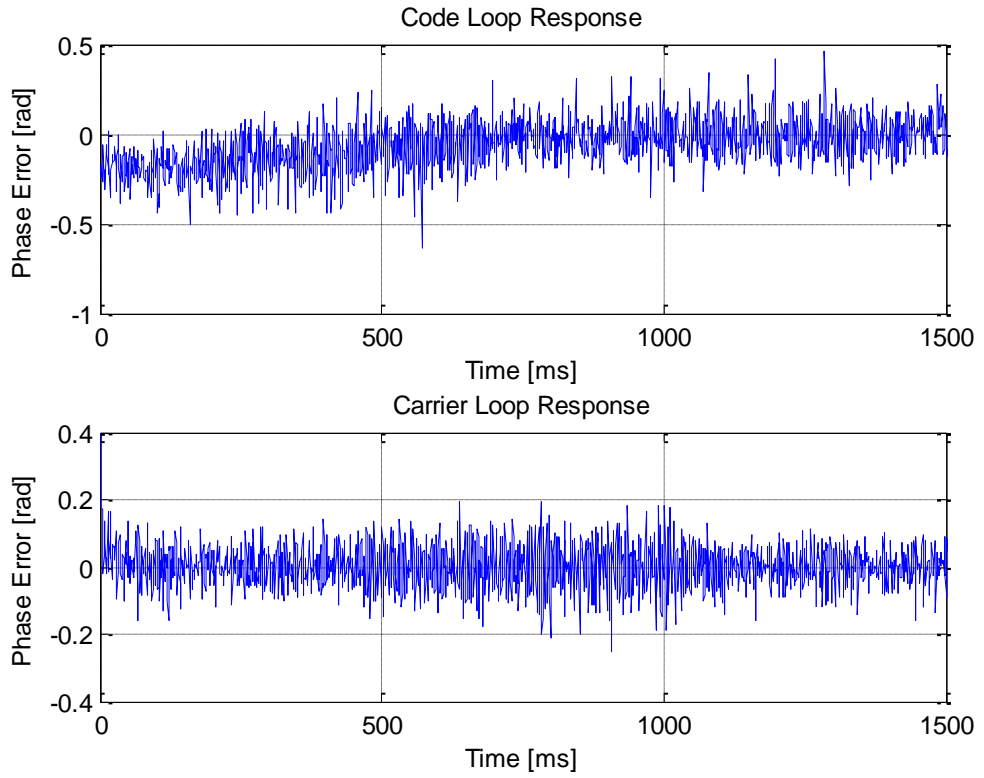
Figure 6.26 - Code and Carrier Loop Responses for GPS SVn:18
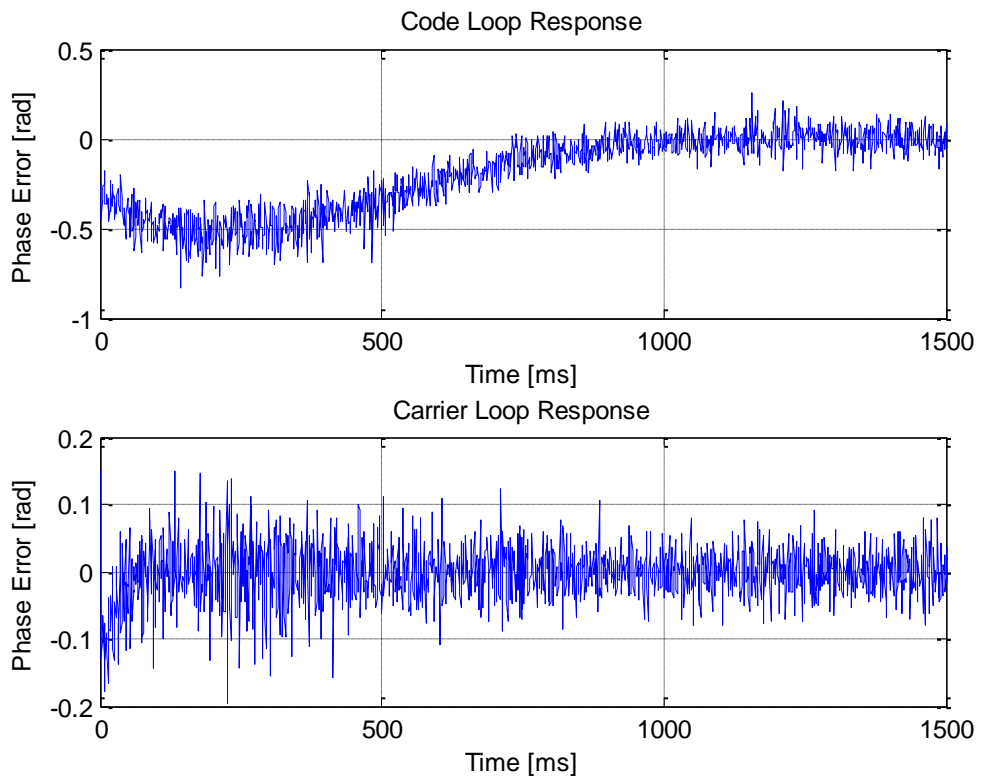
Figure 6.27 - Code and Carrier Loop Responses for GPS SVn:19
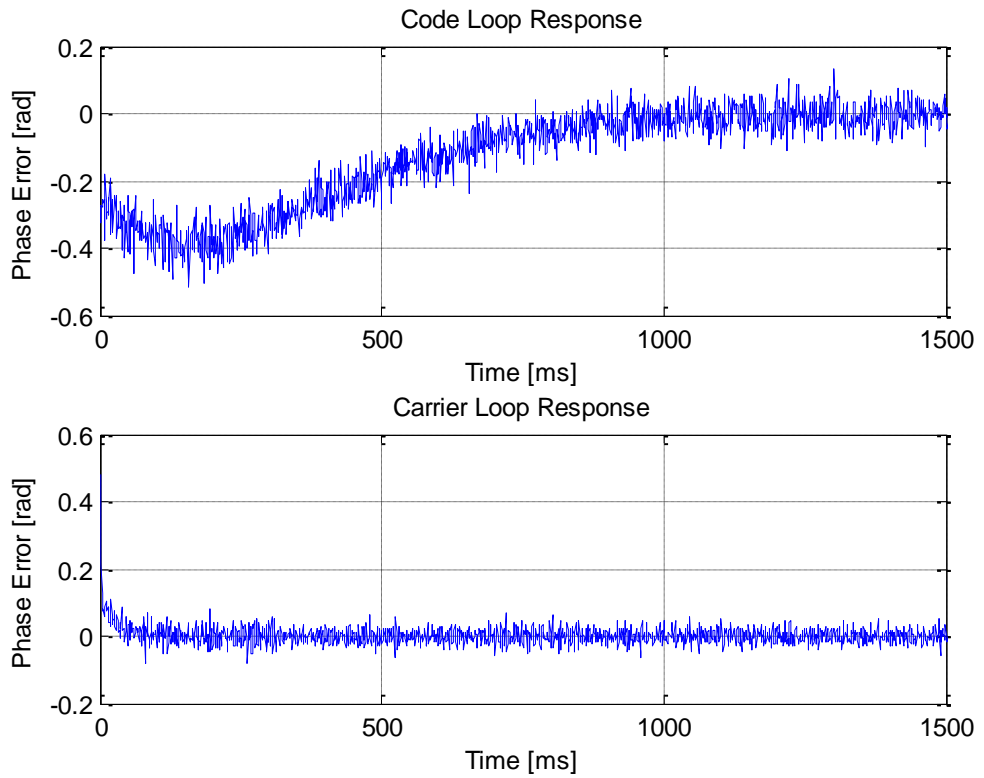
Figure 6.28 - Code and Carrier Loop Responses for GPS SVn:22
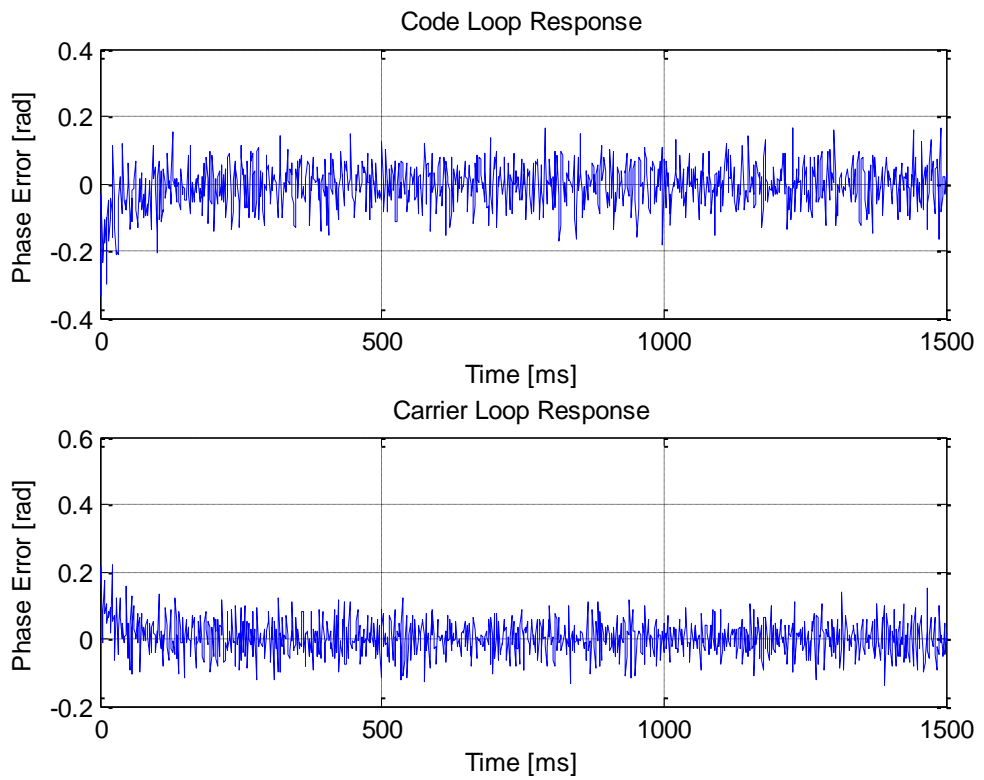
Figure 6.29 - Code and Carrier Loop Responses for GIOVE-A

6.3.3 Bit Extraction and Frame Synchronization

Once the acquisition search identifies all visible satellites, and the tracking channels recover the all the signals for the observation period, the range processing algorithms can begin processing these signals [1][2] [23]. The first stage of processing is to convert the outputs of the tracking channels into binary sequences representing the satellite signals, as these signals are obtained from the tracking channels in the form of the outputs of the prompt in-phase correlators. This is accomplished simply by quantizing the correlator outputs to a single bit, representing the sign of the correlator outputs. However, due to contributions from error sources such as noise, multipath, or interference, the correlator outputs might not always have the same strength. In order to simplify the further stages of processing, during the quantization operation, a second sequence is also generated, representing the strength of the quantized bit, as being a low strength or a high strength bit. Once this is done for all the acquired satellite signals, the binary sequence is checked for any incorrect bits that may have occurred, using the quantized bit strength information obtained from the previous stage and the knowledge of the widths of each transmitted navigation data bit in terms of spreading code repetitions.

The normalized results from the bit extraction process can be seen in Figure 6.30 to Figure 6.35 for the GPS satellites and Figure 6.36 for the GIOVE-A satellite, where the blue data represents the correlator outputs while the red data represents the extracted binary data. Only the first 2000 milliseconds are presented in the figures for ease of readability. It can be seen from these figures that the satellites with higher C/No have stronger correlation outputs with faster settling times and lower variation in the output signal, while the satellites with lower C/No have weaker correlation outputs with slower settling times and higher variation in the output signals, as in the case of GPS satellites 15, 16, 18 and 19. Looking at the navigation message transmitted by the GIOVE-A test satellite, the repeating symbols of the secondary code carrying no navigation information can be seen in the figure. This secondary code alternates in phase every period, representing the test message being transmitted by the GIOVE-A satellite, which is a simple square wave.
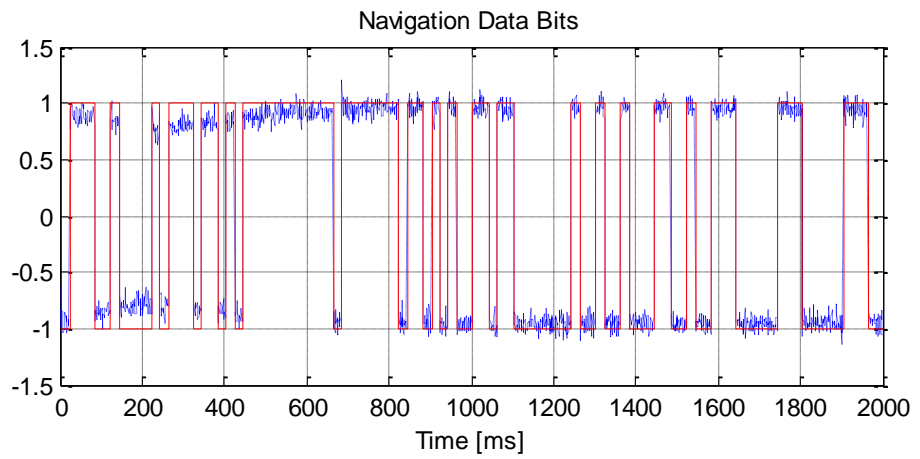
Figure 6.30 - Bit Synchronization Outputs for GPS SVn:3
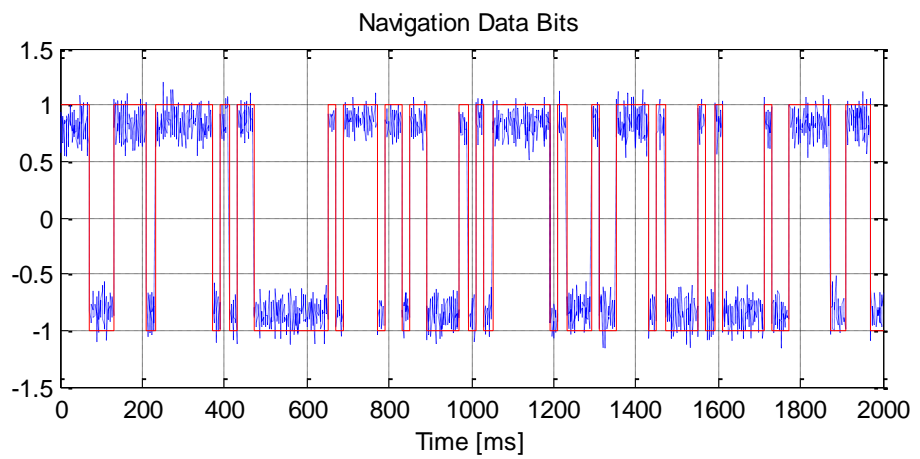
Figure 6.31 - Bits Synchronization Outputs for GPS SVn:15
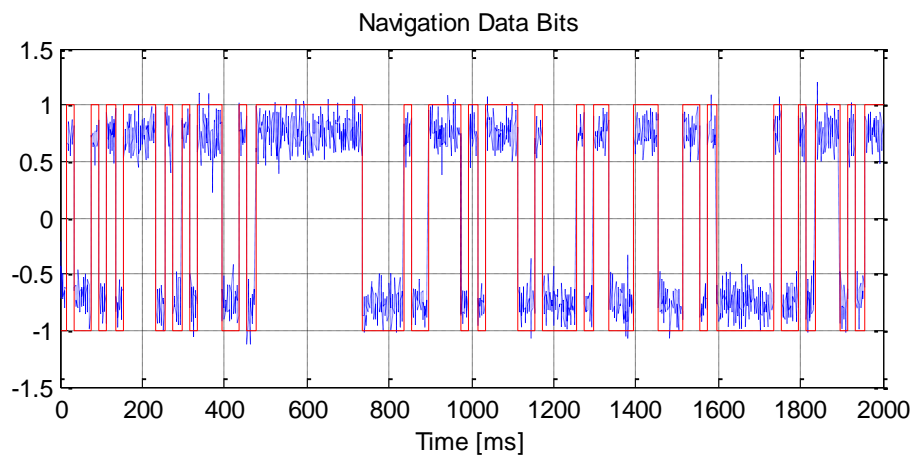
Figure 6.32 - Bit Synchronization Outputs for GPS SVn:16
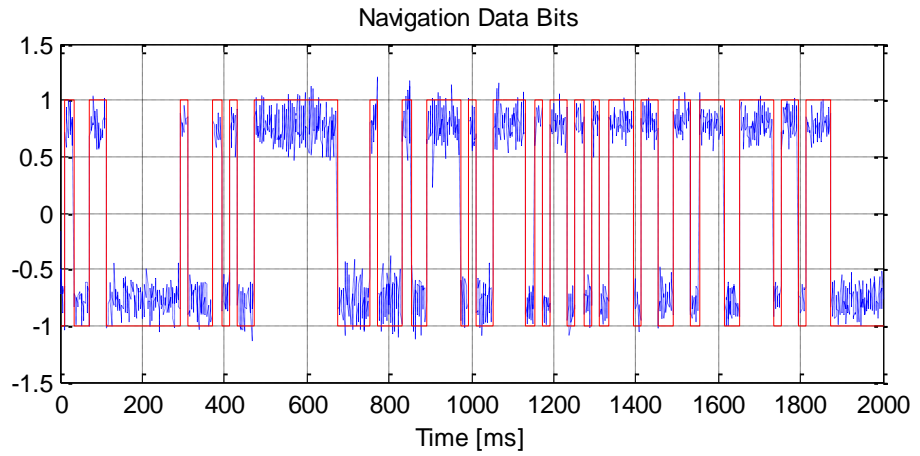
Figure 6.33 - Bit Synchronization Outputs for GPS SVn:18
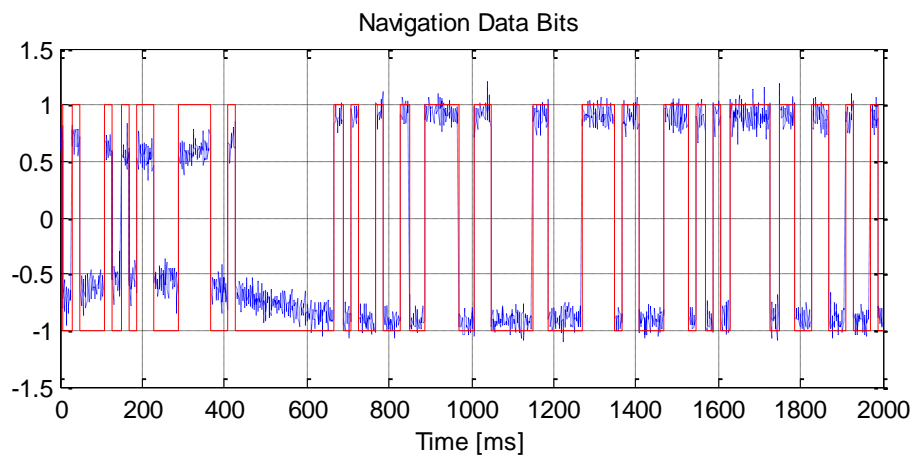
Figure 6.34 - Bit Synchronization Outputs for GPS SVn:19
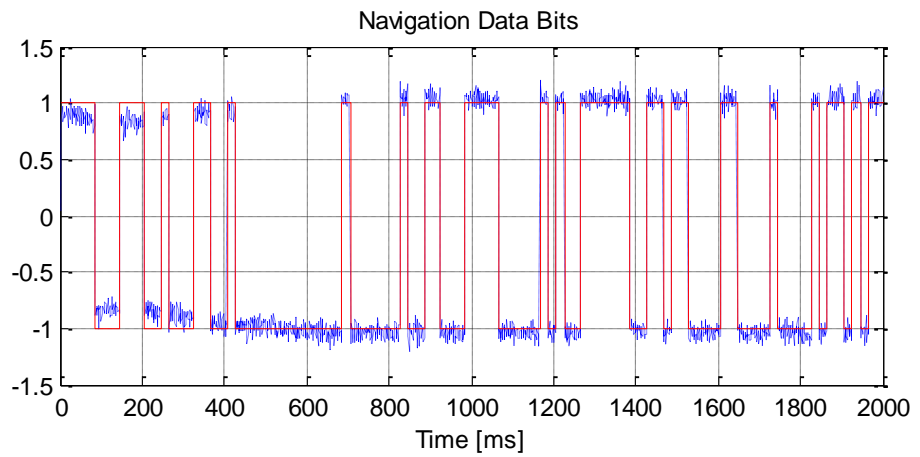
Figure 6.35 - Bit Synchronization Outputs for GPS SVn:22
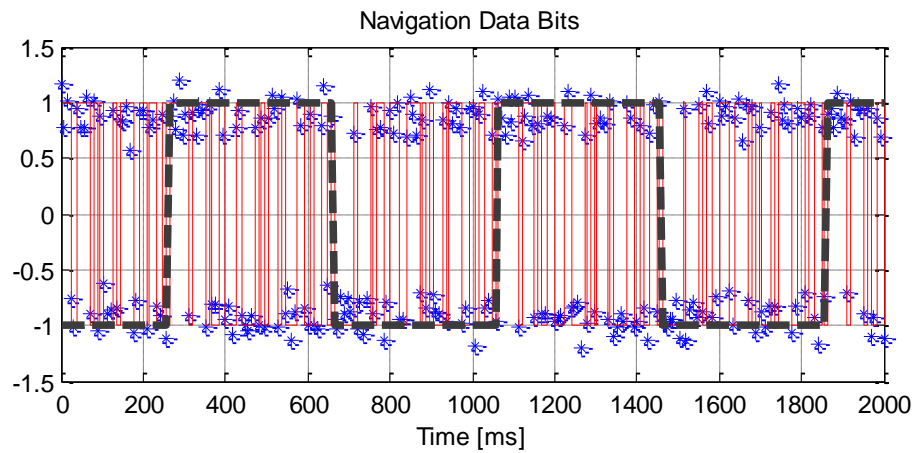
Figure 6.36 - Bit Synchronization Outputs for GIOVE-A

Once the correlator outputs are processed and converted to a binary sequence representing the navigation data bits, it is necessary to synchronize the incoming bit-stream to the local frame. This is done by searching for a pre-determined preamble that is present at the beginning of each sub-frame transmitted by the satellite, as described in Chapter 3. The search is carried out in the form of a correlation operation between the preamble and the incoming bit-stream, for which the results can be seen in Figure 6.37, below. As the preamble is 8 bits long, its location in the decoded bit stream will be identified by a correlation output of 8, which is indicated in the figure with dotted red lines. A line for -8 is also included in the figure, as the incoming bit stream might contain a 180° phase shift, due to the nature of the Costas loops used in the tracking channels.
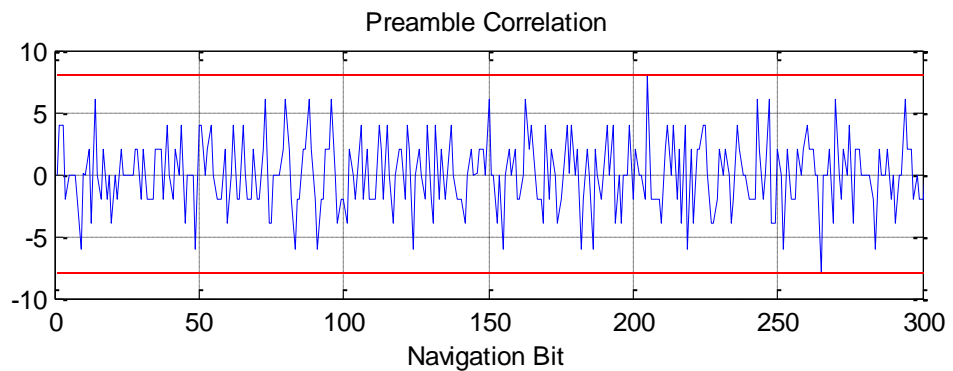
Figure 6.37 - Preamble Search Results

Upon detecting all possible locations for the preamble, a more thorough search is carried out at these possible locations using the TLM and HOW words, and the sub-frame identifiers and CRC codes for the whole navigation frame, as described in Chapter 3. If the bit stream passes these tests, it is passed on to the navigation data extraction block for further processing.

6.3.4 Navigation Data Extraction

The processing that takes place in a GNSS receiver serves two purposes; the first is to make range measurements to the transmitting satellites to determine how far each satellite is from the user, and the second is to calculate the users position using this ranging information in conjunction with parameters transmitted by the satellites that enable the user to calculate each satellites position and correct for errors through perturbation terms. The navigation data extraction handles the task of extracting all these parameters and correction terms from the received bit stream [23]. The template for the data for each navigation system can be found in their respective standards. Since the GIOVE-A satellite was transmitting a test signal at the time of recording of this signal, only the navigation data transmitted by the GPS satellites was used for the data extraction process. A list of these parameters is given in Table 6.4, below, accompanied by a brief description of each parameter.

Table 6.4 - GPS Satellite Parameters and Correction Terms Used in Positioning

Sub-frame Number	Parameter Name	Description
	WN	Week Number
	URA	User Range Accuracy
	Tgd	Group Delay
	ToC	Time of Clock
1	af0	Satellite clock correction term 0
	af1	Satellite clock correction term 1
	af2	Satellite clock correction term 2
	IoDE1	Issue of Data, Ephemeris 1
	ToW	Time of Week

	Crs	Sine correction term for the Radius
	IoDE2	Issue of Data, Ephemeris 2
	IoDE3	Issue of Data, Ephemeris 3
	IoDC	Issue of Data, Clock
2	Dn	Mean Motion Difference
	M0	Mean Anomaly
	Cuc	Cosine correction term for the Argument of Latitude
	e	Eccentricity
	Cus	Sine correction term for the Argument of Latitude
	ToE	Time of Ephemeris
	Cic	Cosine correction term for the Inclination
	OMEGA0	Longitude of the Ascending Node
	Cis	Sine correction term for the Inclination
3	i0	Inclination
	Crc	Cosine correction term for the Radius
	w	Argument of Perigee
	OMEGAdot	Reference rate of Right Ascension
	Idot	Reference rate of Inclination

The extracted values for these parameters and correction terms are listed in Table 6.5, below, for all the acquired GPS satellites, to give an idea of the values to expect. As these sub-frames are all transmitted consecutively, they all share the same week number, time of week, time of ephemeris and time of clock parameters. Inspecting the user range accuracy values for the acquired satellites, it can be seen that there are no issues with the data being transmitted from any of them, and as such, all the signals will be used in the computation of the user position, which will be given in the next section.

Table 6.5 - Extracted Navigation Parameters for the GPS Satellites

Parameter	SVn: 3	SVn: 15	SVn: 16	SVn: 18	SVn: 19	SVn: 22
WN	1364	1364	1364	1364	1364	1364
URA	0	0	0	0	0	0
Tgd	4.19095e-9	-2.32831e-9	-9.77889e-9	-1.02445e-8	-1.44355e-8	-1.81608e-8
ToC	302400	302400	302400	302400	302400	302400
af0	7.8469e-5	5.73427e-4	2.88654e-5	-0.22339e-3	-2.02418e-5	7.23684e-5
af1	2.8421e-12	5.9117e-12	1.9326e-12	-2.0463e-12	1.1368e-12	3.1832e-12
af2	0	0	0	0	0	0
IoDE1	151	143	81	69	66	187
ToW	299628	299628	299628	299628	299628	299628
Crs	72.9063	-17.0938	-96.7188	-64.2813	79.1875	-66.0625
IoDE2	151	143	81	69	66	187
IoDE3	151	143	81	69	66	187
IoDC	151	143	81	69	66	187
Dn	5.26951e-9	5.197e-9	4.5434e-9	4.25089e-9	4.62055e-9	4.25053e-9
M0	1.85883	-0.103142	-1.61371	-1.71834	-3.05044	2.83623
Cuc	3.81656e-6	-1.08592e-6	-4.9863e-6	-3.3658e-6	4.29526e-6	-3.41609e-6
e	0.0078838	0.00946774	0.00322187	0.00675934	0.00319772	0.00481225
Cus	1.29044e-5	3.14415e-6	1.19861e-5	1.21538e-5	1.1513e-5	1.25747e-5
ToE	302400	302400	302400	302400	302400	302400
Cic	-1.8999e-7	5.96046e-8	-4.28408e-8	2.98023e-8	1.28523e-7	5.02914e-8
OMEGA0	0.797585	2.00992	-0.151752	3.02589	0.946326	3.0342
Cis	5.96046e-8	-1.76951e-7	-1.49012e-8	-1.15484e-7	7.63685e-8	2.98023e-8
i0	0.926552	0.957484	0.96254	0.959185	0.958378	0.956701
Crc	112.438	118.438	151.344	145.969	153.688	133.656
w	0.663552	2.55694	-0.936379	-2.69116	-1.34751	-1.56409
OMEGAdot	-8.42357e-9	-8.77572e-9	-8.07391e-9	-7.83283e-9	-8.10319e-9	-7.85426e-9
Idot	4.4537e-10	-2.5751e-10	-4.7287e-10	-4.6966e-10	5.5073e-10	-5.5002e-10

6.3.5 Computation of the Satellite and User Positions

The final stage of receiver processing involves the computation of the satellite and user positions, using the parameters and correction terms given in the previous section along with the pseudo-ranging information provided by the tracking loops. This information is input into the equations provided in Chapter 2, to calculate the satellite positions, correct the initial pseudo-ranging information using the clock bias calculated from the navigation

data, and using these values, calculate the final user position estimation in the ECEF coordinates. The initial pseudo-ranging information for the six GPS satellites that were acquired can be seen in Table 6.6, below. These initial estimations were computed using an average travel time of 68.8 milliseconds for the satellite signals, to provide a good starting point for the iteration procedure.

Table 6.6 - Initial Pseudo-Ranges for the GPS Satellites

Satellite Number	Initial Pseudo-Range
3	20802693.98169 m
15	22795552.76081 m
16	24006005.79402 m
18	23395522.33141 m
19	21981239.00109 m
22	21525002.02768 m

Using these initial pseudo-ranges, the satellite positions were calculated in GNSScope and the initial estimations of the pseudo-ranges were corrected according to the clock bias information provided by the transmitting satellites. The results can be seen in Table 6.7, below, where the satellite coordinates are provided in the ECEF coordinate system.

Table 6.7 - Satellite Positions in the ECEF Coordinate System

Satellite Number	Computed X, Y, Z Coordinates (m)	Corrected Pseudo-Range (m)
3	X = 19239427.55784 Y = 3478161.40170 Z = 17944189.25546	22116498.764863
15	X = 4761827.58405 Y = 17381963.84944 Z = 19210756.66427	24257747.645030
16	X = 26186949.41875 Y = 2485255.36279 Z = -3937462.08371	25304949.583033

18	X = 2602525.01521 Y = 15281176.28262 Z = 21684297.87035	24618846.456769
19	X = 12427590.54291 Y = -9150939.29886 Z = 21714248.40279	23265460.201084
22	X = 16689001.25160 Y = 12364950.10703 Z = 16709744.22839	22836985.028394

The final step of the range processing operations is to use the computed satellite coordinates along with the corrected pseudo-ranges to these satellites, to compute the user position. Once again, this is done using the equations described in Chapter 2, for which the results can be seen in Table 6.8, below. In addition to the coordinates of the receiver in ECEF, the computed clock bias, and the user position in terms of its altitude, latitude and longitude are also provided in the table.

Table 6.8 - User Position in the ECEF Coordinate System

User Position in the ECEF Coordinate System	
Computed User Position (m)	[4472512.56928, 601448.58113, 4492806.78787]
Clock Bias (m)	645143.41970835
Altitude (m)	456.18147937
Latitude	45.06539
Longitude	7.65900

Dilution of Precision for the Computed User Position		
GDOP	: 2.91342	- Geometric Dilution of Precision
PDOP	: 2.55445	- Position Dilution of Precision
HDOP	: 2.20184	- Horizontal Dilution of Precision
VDOP	: 1.48257	- Vertical Dilution of Precision
TDOP	: 1.62705	- Time Dilution of Precision

The second half of the table presents the Dilution of Precision (DOP) values for the computed user position. First used in the Loran-C navigation system, the DOP values provide information regarding the quality of the estimated user coordinates by taking

into account the effects of satellite geometry on the precision of the results. Using the DOP reference values provided in Table 6.9, below, it can be seen that the GNSScope toolbox has provided a positioning solution that is highly accurate using the multitude of techniques introduced in this thesis. A map indicating the user position calculated in this case study can be seen in Figure 6.38, below, using the Google Maps application freely available on the internet. The building that is being pointed to belongs to the Polytechnic University of Torino, where this signal was initially captured and converted to a data file, providing a second indication of the accuracy of the results.

Table 6.9 - Ratings for the Dilution of Precision Values

DOP Value	Rating	Description
< 1	Theoretical	Theoretically possible scenario which may be achieved in the future
1	Ideal	The highest possible accuracy
1 - 2	Excellent	Accurate enough for all but the most demanding applications
2 - 5	Good	The required accuracy for in-route navigation applications
5 - 10	Moderate	Accurate enough to compute a position, but can be greatly improved
10 - 20	Fair	Very low accuracy just enough for a very rough position estimation
> 20	Poor	Accuracy too bad to be used for position calculations
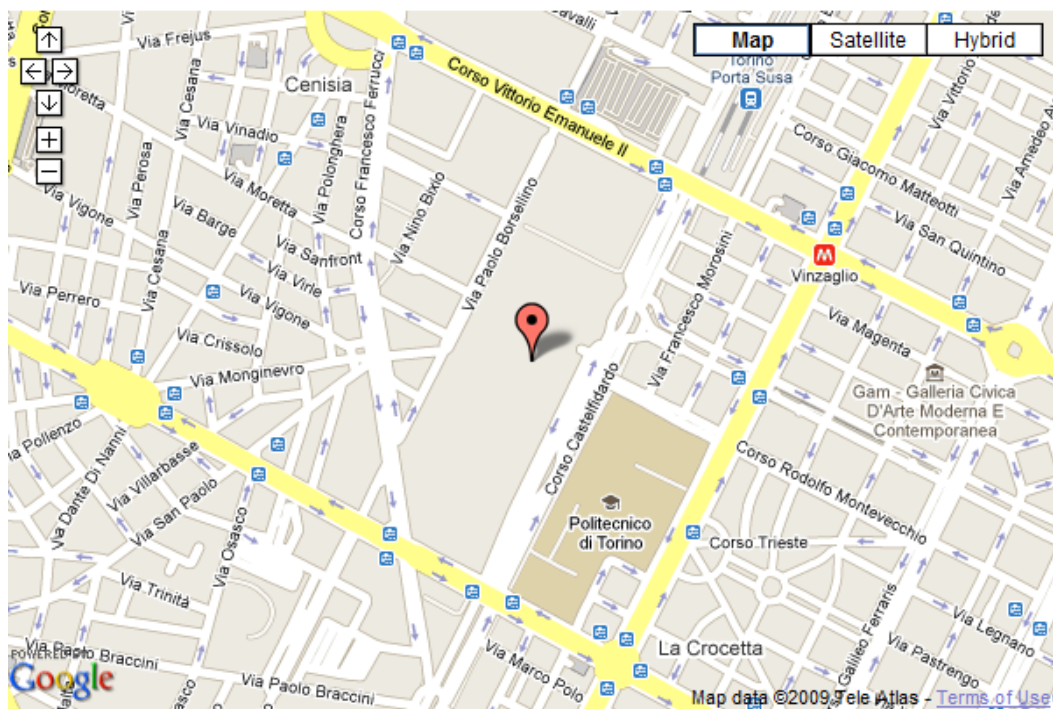
Figure 6.38 - User Coordinates on Google Maps

6.4 Further Analyses

The previous section provided the details of a user positioning case study carried out entirely in the GNSScope toolbox, from the initial acquisition search and tracking the acquired satellite signals, to the frame synchronization, data extraction, and satellite and user position computations. However, one important feature of GNSScope hasn't been discussed in the user positioning case study: the data path word lengths and effects of quantization on the results obtained from the toolbox. As GNSScope is an SDR receiver toolbox designed and implemented in Matlab, it lends itself readily to such analyses, and as such, has built-in quantization settings for each stage of the receiver processing chain to emulate the effects of hardware limitations in receiver designs and to provide a more accurate model of the internal processing taking place in a GNSS receiver. This section will provide an overview of the data path word length and quantization issues present in GNSS receivers [45], and how it affects the results of satellite navigation. The plots presented in the previous section were generated using the floating point operation mode of GNSScope. This section will deal with the more commonly used 8-bit, 4-bit and 2-bit receiver systems and the performance losses that occur from the loss of precision. Plots generated in GNSScope will be used to point out changes in the receivers response to the incoming IF, including the acquisition outputs, carrier PLL and code DLL responses and the resulting decoded satellite signal [5].

The acquisition results for the GPS satellite SVn:3, from the case study presented in the previous section, can be seen in Figure 6.39, below, for the 8-bit, 4-bit and 2-bit quantized receiver analysis, respectively. The results indicate that the acquisition operation is relatively unaffected by the quantization process, due to the fact that each data point is the result of the accumulation of a whole period of the underlying spreading code, and as such, individual errors introduced by the quantization process get filtered out during the acquisition search.
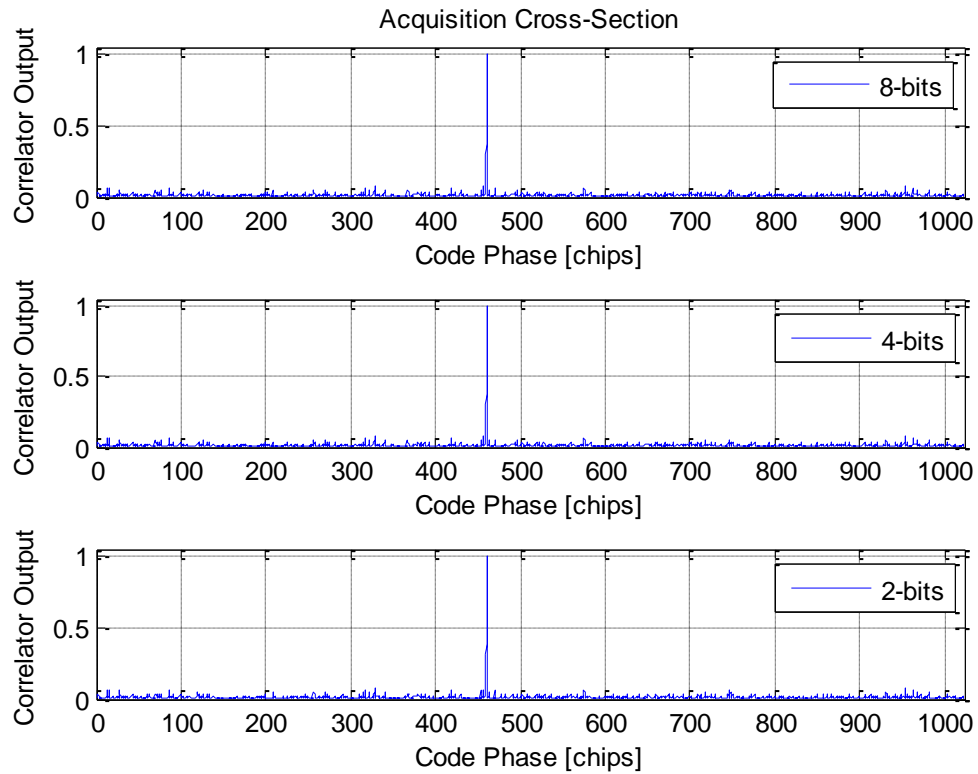
Figure 6.39 - Normalized Acquisition Results for 8-bit, 4-bit and 2-bit Quantization Analysis

The second stage of receiver processing takes place in the tracking loops, where the signal gets processed by the code DLL and carrier PLL to maintain a lock on the acquired parameters of the satellite signal. If these loops fail to perform, the receiver could end up losing the signal, requiring a time consuming re-acquisition stage to continue processing the signal. With that in mind, an analysis of the code and carrier discriminators is given in Figure 6.40 and Figure 6.41, respectively, for the 8-bit, 4-bit and 2-bit quantization of the data path word lengths. Comparing these results with those presented in the previous section for floating point precision, it can be seen that there is virtually no difference between the discriminator responses for floating point and 8-bit quantized operation. Furthermore, although the amount of quantization noise increases, it can be seen that the tracking loops succeed in maintaining a successful lock on the acquired signal for the whole observation time.
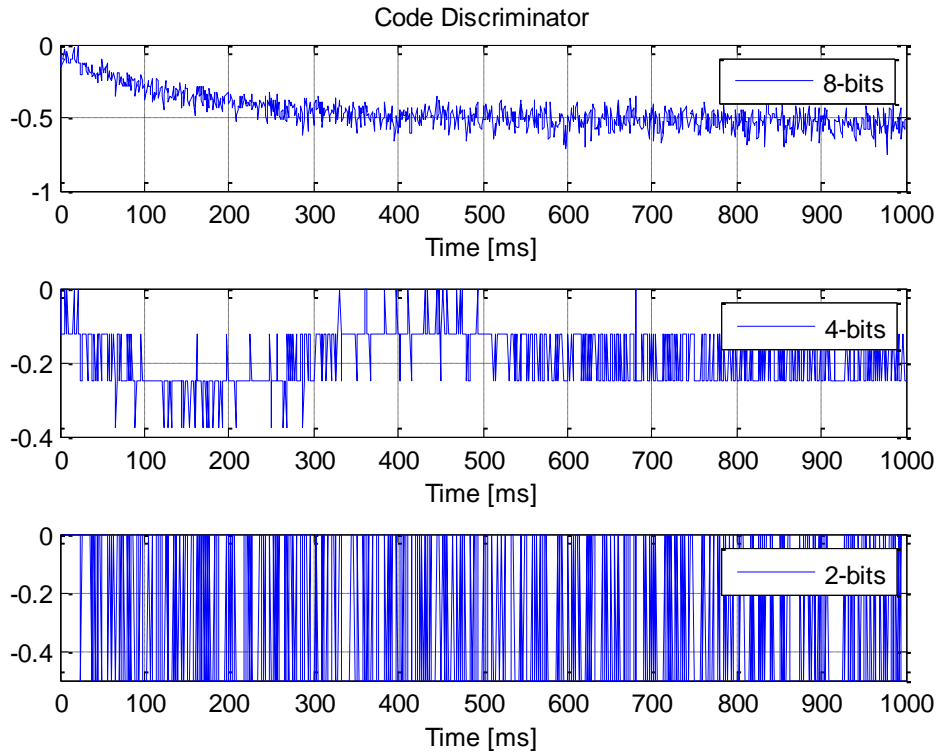
Figure 6.40 - Code Discriminator Analysis for 8-bit, 4-bit and 2-bit Quantization
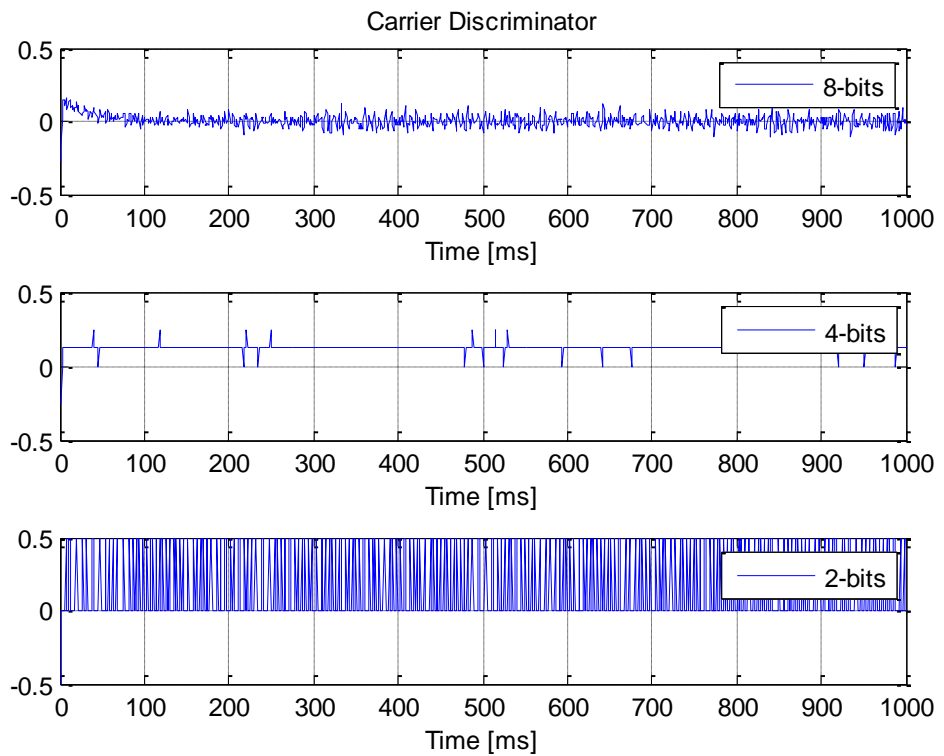
Figure 6.41 - Carrier Discriminator Analysis for 8-bit, 4-bit and 2-bit Quantization

Observing the figures for the 2-bit quantization case, it can be seen that the discriminator responses are oscillatory. However, as these oscillations are not random in nature, they indicate a successful lock on a value that falls between two quantization points, forcing the local signal generators to alternate between two neighboring values. This fact can also be observed in the in-phase correlator outputs that will be used in the satellite and user position computations given in Figure 6.42, below. Although the amount of noise increases as the amount of quantization is increased, the underlying shape of the signal can still be detected, as the noise does not cause any changes in the phase of the correlator outputs.
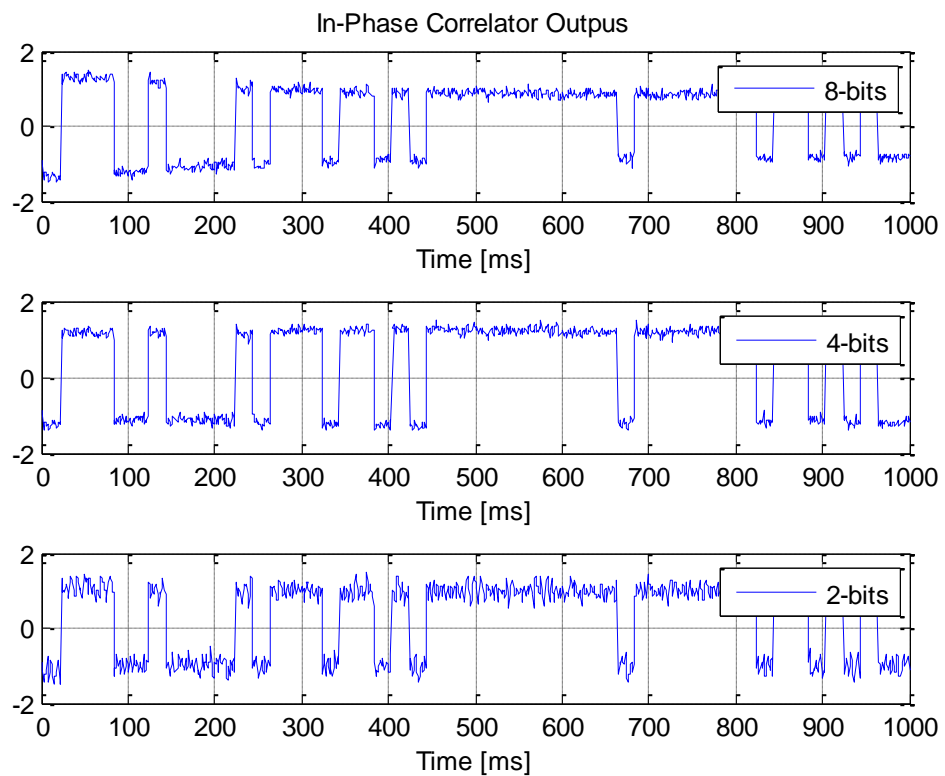
Figure 6.42 - Normalized In-Phase Correlator Output Analysis for 8-bit, 4-bit and 2-bit Quantization

Observing the figures provided in this section, it can be concluded that in all but the most demanding of applications, it is sufficient to use 4-bit word lengths, as the gains of increasing the word lengths beyond this point do not justify the added cost in resources and operation times. As the GNSScope toolbox was designed and implemented in software, this fact is exploited in its default mode of operation, where 2-bit quantization

is used for strong signals, while 4-bit quantization is used for weak signals and signal with high interference. Using shorter word lengths also enables multiple samples to be processed within the same operation, as current commercial computer architectures and the underlying machine codes are based on 64-bit word lengths. This results in significantly reduced operation times, enabling more detailed analyses and more complicated processing techniques to be implemented in the toolbox.

6.5 Conclusions

This chapter has provided a detailed analysis of every aspect of receiver processing taking place in the GNSScope receiver toolbox. Starting with the GUI accompanying the toolbox, this chapter has presented an end-to-end user positioning case study starting with signal acquisition, where signals from GPS satellites were acquired along with the GIOVE-A test signal being transmitted at the time of recording of the signal. This was followed by the tracking loop responses, where the carrier and code discriminators were analyzed in terms of their stability and settling times. Once all available satellite signals were recovered from the received composite IF, the bit extraction and frame synchronization stages were presented, where the correlator outputs obtained from the tracking channels were converted into the navigation data bits transmitted by the satellite. Following the extraction of the navigation data from the recovered signals, the satellite and user positions were calculated, and the results were displayed on a map obtained from the Google Maps application. The final section of this chapter delved into the effects of hardware limitations, specifically the performance losses due to data path quantization. It was shown that successful receiver operation was possible at 2-bit word lengths in GNSScope.

Chapter 7 Conclusions and Future Work

This thesis has provided a detailed overview of the research work carried out in the design and development of a generic SDR GNSS receiver, aptly named the GNSScope toolbox, which is the result of four years of extensive research and development into the current state of the art and future trends in GNSS receiver technologies, capable of dealing with current and upcoming satellite navigation systems and signals in a multiple frequency multiple standard positioning scenario where all available signal content is processed to provide the user with optimal position and timing information. While the toolbox focuses primarily on the frequency domain processing of current and future satellite navigation signals, it acknowledges the efforts being made in the time domain processing of GNSS signals, and as such, provides receiver designers with time domain parameters such as the carrier phase based measurements made in the tracking loops, for further developments in the field. In order to form a coherent understanding of the

work carried out over the course of this project and present the results in an organized manner, the thesis was divided into five main chapters: the principles of satellite based navigation, the characteristics of satellite navigation signals, the strong signal operation of the GNSScope toolbox, weak signals, multipath and multiple access interference in the GNSScope toolbox, and finally, the performance analyses of the GNSScope toolbox chapters.

The first chapter provided a brief introduction into the topics of interest to this research project. Following a brief history of the development of the satellite navigation technology, an overview of the near future of GNSS receivers was given, based on the current trends and ongoing developments in the industry. This was followed by the introduction of the GNSScope toolbox, encompassing all the outcomes of the work carried out throughout the studies. Novel contributions to the state of art were listed for the readers' convenience, with references to publications in the open literature.

The second chapter provided an overview of the basic concepts necessary for solving the user positioning problem introduced by the use of satellite based navigation systems. It was shown through examples that, determining the position of a point in three dimensional space using unsynchronized clocks requires the knowledge of the position of, and distance to at least four beacons in space. As the name suggests, in satellite based navigation systems these beacons are satellites orbiting the Earth. As they aren't stationary, their positions need to be relayed to the user through a message transmitted by each satellite. The parameters contained in this message, were described, along with the equations used in computing the coordinates of the satellites. The user position was then calculated in terms of latitude, longitude, altitude and the receiver clock bias using Keplerian geometry. Further corrections reflecting the effects of the actual geometry of the Earth, were provided at the end of the chapter to calculate the exact user position.

The third chapter provided a brief overview of the signals and modulation schemes currently used in satellite navigation systems. Concepts and definitions fundamental to signals and systems, such as the Fourier transform, filtering and convolution operations, correlation, modulation and multiplexing operations, were explained in order to form a coherent understanding of the signal definitions and mechanisms used to generate them

throughout the thesis. An overview of currently available and upcoming satellite navigation signals and their spectra was given before delving into the details of the GPS and Galileo satellite signals, and the phase-shift keying and binary offset carrier modulation techniques utilized in generating these signals. Finally, a brief overview of current and upcoming ground and space based global and regional navigation signals was given to conclude the chapter.

The fourth chapter introduced GNSScope, a toolbox designed and developed in MATLAB for end-to-end modeling, simulation and analysis of current and upcoming GNSS signals, and outlined the basic operation mode of the receiver, consisting of the processing of strong GNSS signals. First, the operational overview of a GNSS receiver was briefly described, to provide a basis for the contents of the chapter and the organization of the receiver toolbox. Following the overview, basic acquisition techniques implemented in GNSScope were detailed, with examples captured from the toolbox itself showing successful detection and identification of various GNSS signals. Once acquired, the parameters of these satellite signals require tracking over time in order to extract the navigation message encoded within the signal. Before delving into the details of the tracking channels, a brief introduction into the fundamentals of digital PLLs was given to provide a basis for understanding the underlying techniques utilized in these tracking channels. The evolution of the combined Costas code and carrier tracking loop was demonstrated through the principles of individual code and carrier tracking loops. In addition to traditional acquisition and tracking techniques implemented within the receiver, this chapter also described the novel multi frequency, multi modulation acquisition and tracking algorithms built into GNSScope to handle current and future navigation signals utilizing PSK type modulations, including all subclasses of the BOC type modulations. Following successful extraction of the individual satellite signals from the received composite IF signal, it is necessary to decode the message and extract the parameters necessary to compute the satellite and user positions. These stages were described in the range processing section to complete the basic operational overview of the GNSScope toolbox when processing strong satellite signals.

The fifth chapter built onto the fundamentals given in the third chapter, to provide an overview of the advanced signal processing techniques designed and implemented in the GNSScope toolbox including novel algorithms devised over the course of the project. Before delving into the details of these techniques, a brief overview on the issues of weak signals, multipath, and multiple access interference that present in satellite based navigation systems was presented. This was followed by the details of weak signal acquisition and tracking techniques implemented in GNSScope, with novel modifications to ensure higher accuracy in the computed results. In order to provide a basis for the techniques described in this chapter, the successive and parallel interference cancellation techniques were briefly described, with an analysis of their strengths and shortcomings. This was followed by a brief overview of several SIC and PIC based techniques currently in the literature, to provide a comparison for the novel tracking techniques designed and developed during the course of the project, and implemented into the GNSScope toolbox. The final section of the fourth chapter provided the details of these novel algorithms, namely the mirrored channel mitigation technique, the trigonometric interference cancellation technique, and the split chip summation technique. For each of these techniques, case studies were also provided, presenting their performance in the presence of weak signals, multipath, multiple access interference and continuous wave interference, bringing the chapter to an end.

The sixth and final chapter of the thesis provided a detailed analysis of every aspect of receiver processing taking place in the GNSScope receiver toolbox. Starting with the GUI accompanying the toolbox, the chapter presented an end-to-end user positioning case study starting with signal acquisition, where signals from GPS satellites were acquired along with the GIOVE-A test signal being transmitted at the time of recording of the signal. This was followed by the tracking loop responses, where the carrier and code discriminators were analyzed in terms of their stability and settling times. Once all available satellite signals were recovered from the received composite IF, the bit extraction and frame synchronization stages were presented, where the correlator outputs obtained from the tracking channels were converted into the navigation data bits transmitted by the satellite. Following the extraction of the navigation data from the recovered signals, the satellite and user positions were calculated, and the results were

displayed on a map obtained from the Google Maps application. The final section of this chapter delved into the effects of data path word length issues involved in efficient hardware implementations of complex GNSS receiver designs and their limitations, where the received signals and internal computations were heavily quantized to reduce the amount of processing overheads. It was shown through examples, that successful receiver operation was possible at as low as 2-bit resolution, using clever decision making algorithms.

Overall, this doctoral thesis has presented a generic SDR GNSS receiver toolbox capable of handling strong and weak signals, multipath, and cross-correlation interference. In the search to improve the performance of classical techniques and create novel new algorithms to reduce the computational complexity of modern receivers, while enhancing the resolution of the results, most current state of the art technologies in receiver design were also built into the toolbox, including the delayed parallel interference cancellation and binary valued signal modulation compression techniques, forming a strong basis for the comparative analysis of novel new algorithms with the current state of the art. The novelties introduced within the thesis can be summarized as follows;

- The GNSScope Receiver Design and Development Toolbox for the end-to-end modeling, simulation and analysis of GNSS signals, which includes a fully parameterized and reconfigurable generic GNSS receiver offering the following
    - an interactive graphical user interface to control the majority of the algorithms implemented into the toolbox, providing quick and easy access to the processing results of the toolbox
    - acquisition, tracking and range processing blocks capable of producing high accuracy user position and timing results, including supplementary carrier phase and chipping rate information for use in alternative processing techniques
    - in-operation parameter fine tuning through reconfigurable acquisition and tracking loops, offering an increased dynamic range and enhanced performance under low signal-to-noise ratio conditions

- the ability to handle weak signals, signals on the multipath, and multiple access interference on the recorded satellite signals using classical techniques as well as novel techniques developed throughout the course of this project
- multiple frequency / multiple standard operation capable of handling all currently available PSK based satellite navigation signals, including all sub-classes of BOC type modulations and future planned satellite signals

- A fully parameterized generic GNSS acquisition block capable of handling all current and future navigation signals on all frequency bands, including the new modulation schemes being developed for future navigation systems

- A fully parameterized generic GNSS tracking channel model capable of handling all current and future navigation signals on all frequency bands, including the new modulation schemes being developed for future navigation systems

- The Mirrored Channel Mitigation technique, designed as a unified local interference regeneration and removal algorithm, forming the basis for most of the classical communication theory based techniques that were implemented in GNSS receiver designs and the GNSScope toolbox

- The Trigonometric Interference Cancellation technique for the mitigation of continuous wave and cross-correlation interference effects during the acquisition and tracking operations with minimal overheads and high efficiency

- The Split Chip Summation technique used for the detection and identification of deformations in the underlying chipping waveforms of the spreading codes, including multipath and duty cycle imbalance issues, to improve the match rate of the locally generated signals with the received composite IF

Additionally, as the toolbox was designed, developed and implemented in entirely MATLAB, it offers unparalleled modularity, enabling receiver designers to use their own algorithms in conjunction with the provided receiver model to test new technologies. With this in mind, every process within the receiver toolbox was designed as an individual MATLAB function, complete with user documentation compatible with the built-in MATLAB user assistance and help system, enabling receiver designers to build their own receivers using a component oriented design methodology.

7.1 Outcomes of the Research

Over the course of the research project, numerous novel findings were introduced into the literature. The primary outcome of this research project was the GNSScope receiver design and development toolbox for the end-to-end modeling, simulation and analysis of GNSS signals, designed and developed in MATLAB utilizing the flexibility offered by SDR receiver techniques. In contrast to the current state of the art in SDR GNSS receivers which are only able to process C/A code GPS signals transmitted on the L1 frequency band, the GNSScope toolbox was designed to be able to process all current and future navigation signals, including the offset carrier modulated signals being planned for the upcoming satellite navigation systems, in a multiple constellation multiple frequency configuration as described in Chapter 4. In order to accommodate possible changes to the specifications of these upcoming signals, the acquisition and tracking algorithms were fully parameterized to be able to process all known modulation schemes used in satellite navigation systems.

In the search to improve the performance of GNSScope receiver toolbox in the presence of weak signals, multipath, and multiple access interference, classical techniques from the literature were implemented into the toolbox to evaluate their performance under these circumstances. Analysis of these techniques resulted in the design and implementation of several novel algorithms dealing with weak signals, multipath, and multiple access interference. The first of these techniques, referred to as the Mirrored Channel Mitigation technique, was based on the successive, parallel, and delayed parallel interference cancellation techniques to deal with weak signals and multiple access interference in GNSS. Comparative analysis of these techniques revealed that it was possible to reduce the number of additional correlators necessary to carry out the mitigation process by up to a factor of N_s, the number of strong signals being processed by the receiver, resulting in significant reductions in computational complexity. Furthermore, it was shown that through heavy quantization the multipliers used in the reconstruction process for this technique could be replaced by a series of adders, at the cost of reducing the accuracy of the reconstructed interference. However, tests revealed that this quantization noise

could be ignored as long as the reconstructed signal power was below the masking threshold of the acquisition and tracking algorithms.

The next novel signal processing technique introduced into the literature was the Trigonometric Interference Cancellation technique, which exploits the underlying mathematical expressions involved in mitigating a reconstructed interferer from an incoming signal. It was shown that the number of operations involved could be reduced by 25% by rewriting the reconstruction expression, at the cost of introducing noise into the results due to the cosine approximation utilized in the technique. However, further analysis and testing revealed that the noise introduced into the results was always out of phase with the satellite signal under observation, leading to the use of a simple thresholding operation to remove all the effects introduced by the approximations. The thresholding operation was implemented as a simple sign observation to remove out of phase noise components from the results. Additionally, it was shown that this technique could also be used in the mitigation of CW interference by simply taking the PRN code to be unity, at no additional cost.

The final novel signal processing technique introduced into the literature was the Split Chip Summation technique, whereby samples of the received signal are accumulated after being rectified by the polarity of the chipping sequence to obtain a representation of the channel effects and distortions on the positive and negative chip waveform. In contrast to the binary valued signal modulation technique, specific perturbations that affect the two polarities of the chipping waveform differently are preserved rather than being filtered out due to the accumulation process, resulting in a more accurate representation of these perturbations at the cost of an additional accumulator. Furthermore, it was found that using this technique, unbalanced duty cycle errors caused by small variances in the underlying chipping sequence can be detected and compensated, in turn increasing the signal power captured by the correlation process and improving the performance of the acquisition and tracking algorithms.

One aspect of receiver processing that presented itself during the course of the research was discovered during the data path quantization analysis of the GNSScope receiver toolbox. It was shown in the further analyses section of Chapter 6 that the receiver can

produce accurate position and timing information even when the data path was quantized to 2-bit resolution. Furthermore, analysis of the results when the data path was quantized to 1-bit resolution presented an interesting discovery, where the carrier and code loop filters were forming a sigma-delta ($\Sigma\Delta$) modulator, with the output appearing to track the underlying carrier and code frequencies, respectively, although not being able to maintain a stable lock due to not having accurate enough outputs, forming a critically stable system. This resulted in the in-phase correlator outputs to show a residual sinusoid modulating the navigation data, due to the carrier wipe-off process not being able to completely wipe-off the carrier. Although these correlator outputs could be processed by an additional low-pass filter with higher resolution to reveal the underlying navigation data, it would be counter-productive, eliminating the gains obtained from the additional quantization in the processing chain. Rather than introducing more operations into an already complex processing chain, the computational complexity involved with a GNSS receiver can be further simplified by exploiting the fact that the 1-bit quantized tracking loops form $\Sigma\Delta$ modulators that can be redesigned to form stable tracking loops under the expected circumstances. This would result in a simplified architecture, reducing processing times and computational complexity, while at the same time relaxing the constraints placed on the front-end due to the processing limitations of current GNSS receivers.

7.2 Future Work

Although the GNSScope receiver toolbox in itself is a complete end-to-end modeling, simulation and analysis toolbox for GNSS signals, as it operates on a standard PC using the MATLAB software, it comes with many processing overheads not involved with the underlying navigation processing that takes place in a GNSS receiver. However, recent years has witnessed a rapid expansion in the General Purpose Graphics Processing Unit (GPGPU) applications of parallel computing, and the vast processing speed gains that can be gained from using the GPU architecture as opposed to the more general purpose CPU architecture for the implementation of the GNSS processing pipeline. This is due to the way the two processors are designed, where the CPU architecture is composed of a small number of larger processing blocks capable of carrying out a vast array of operations,

while the GPU architecture is composed of a large number of tailor made processing blocks that are optimized for carrying out multiple parallel multiply and accumulate type of operations that form the basis of most modern graphics computing. Recognizing this, and the similarities between the processing pipelines of the tracking channels and the GPU cores, the whole GNSScope receiver toolbox will be ported to be processed as a GPGPU application, also utilizing the on-board high speed memories used in most modern graphics cards to store the large amount of data accumulated during the processing of the incoming IF signal. To this end, the first step will be the implementation of a simple operation to run on the GPU, namely the FFT, as it forms the bottleneck for the processing speed of any GNSS receiver. Following the successful implementation of the correlation operation in the GPU, the remaining digital signal processing can also be ported, where all code written in the MATLAB environment can be processed on the GPU using parallel computing techniques to achieve real-time operation speed on a generic desktop PC. It should be noted that the intention will not be to sever all ties to the MATLAB environment, as it is one of the most widely used mathematical programming environments in academic and industrial research, providing an easy to learn, cross-platform programming environment. By leaving the user interface and custom code entry tools embedded into MATLAB, receiver designers can concentrate on perfecting their designs as opposed to dealing with compatibility and implementation issues that can arise from the use of GPGPU applications and parallel processing techniques.

Finally, even though it is beyond the scope of this project, in order to provide receiver designers with a complete solution covering all aspects of GNSS receiver design, from signal generation and transmission, to the reception and quantization of the signals, and the software and hardware processing of the results, a custom processing platform consisting of Field Programmable Gate Arrays (FPGAs), complex DSP processors and high speed direct memory access can be designed, to accompany the GNSScope toolbox, where the toolbox has full access to all the aspects of the custom processing platform. The FPGA will be used to implement the Costas code and carrier tracking loops, where the correlation operations can be performed in optimized efficient hardware blocks that can be easily reconfigured to reflect new developments [46]. The DSP will be used for the implementation of the loop filters and the associated processing chain. Finally, the use of

high speed on-board memory will greatly improve processing speeds, as it can be accessed by multiple chipsets without being held back by unrelated operations that take place in a general purpose computer. Although similar examples of such boards can be found in the market, commercially available products currently do not offer such a wide solution covering every aspect of receiver design in both software and hardware. Having such a tool would not only lend itself readily to receiver designers and the conception of new novel acquisition and tracking algorithms, but also to the knowledge transfer and education in the field of satellite navigation systems and training of new receiver designers.

Appendices

The authors' publications are provided in this appendix for the readers' convenience, where each new section presents another publication. The publications will be presented in the following order:

A. "GNSScope: A Toolbox for End-to-End Modeling, Simulation and Analysis of GNSS", The Navigation Exhibition, The Royal Institute of Navigation, London, Jun 2008 [4].

B. "Weak Signal and Multipath Analysis Using GNSScope: A Toolbox for End-to-End Modeling, Simulation and Analysis of GNSS", NAV'08 / ILA'37, The Royal Institute of Navigation, London, Oct 2008 [7].

C. "A Low Complexity Cross-Correlation Interference Mitigation Technique for GNSS", European Navigation Conference - Global Navigation Satellite Systems (ENC-GNSS) 2009, Naples, Italy, May 2009 [10].

D. "GNSScope and The Split Chip Summation Technique", European Conference on Circuit Theory and Design (ECCTD) 2009, Antalya, Turkey, Aug 2009 [11].

"GNSScope: A Toolbox for End-to-End Modeling, Simulation and Analysis of GNSS"

The Navigation Exhibition, The Royal Institute of Navigation, London, Jun 2008

GNSScope: Overview of a Toolbox for End-to-End Modeling, Simulation and Analysis of GNSS Systems

Renan Kazazoglu, Ediz Cetin and Izzet Kale

Applied DSP & VLSI Research Group

University of Westminster

London, UK

{r.kazazoglu, e.cetin, kalei}@wmin.ac.uk

With the development of the European navigation system Galileo and the modernization plan for GPS, referred to as GPS III, it is apparent that the civilian navigation signals will be in multiple bands within the next decade offering various applications from roadside assistance to medical services. Therefore, the next generation navigation user terminal will have to be a multi-mode versatile wideband receiver in order to cope with multiple bands and modulation schemes. In such a context, the flexibility offered by software defined radio is expected to become the dominant technology in GNSS receiver development.

This presentation will introduce the Global Navigation System Scope (GNSScope), a transmission and reception model for the GPS L1/L2C and GIOVE-A L1/E5 bands. The Simulink-based model can be divided into five major sections. The signal transmission model covers the generation of the GPS L1/L2C and GIOVE-A L1/E5 signals. The downlink path is characterized as a fading channel which caters for atmospheric delays, Doppler and multipath effects. The RF section is a behavioral model of the low-IF GNSS receiver which is parameterized by the standard RF metrics such as gain, bandwidth, noise figure, second and third-order intercept points, and component mismatches. This is followed by a quadrature ADC and associated DSP chain.

Baseband processing of the model can be divided into three sections; acquisition, tracking and range processing. The resolution of coarse acquisition can be modified by the user through the Doppler search bandwidth and frequency bin size parameters, and the results obtained from coarse acquisition can be further refined through optional configurable post-processing of the acquisition data. A modified Costas loop with multiple

configurable code and carrier discriminators and fully parameterized correlators is implemented for signal tracking. Parameters such as the number of correlators, correlator arm spacing, PLL/DLL configurations, discriminator functions, transient and lock-in mode behavior are fully configurable to optimize receiver behavior. The output of the prompt correlators are fed into the range processing block that converts the data to a unipolar binary representation, extracts the satellite ephemerides and computes the receiver's location using well established orbital mathematics.

GNSScope efficiently integrates RF and baseband sections of the receiver which is actually an effort to relate the RF and DSP metrics in order close the gap between these two disciplines. The resulting simulation environment also provides an accurate signal chain noise analysis and caters for modular discriminators which enable application developers to test and benchmark their own designs. Figure 1 depicts a snapshot of the developed GNSScope.
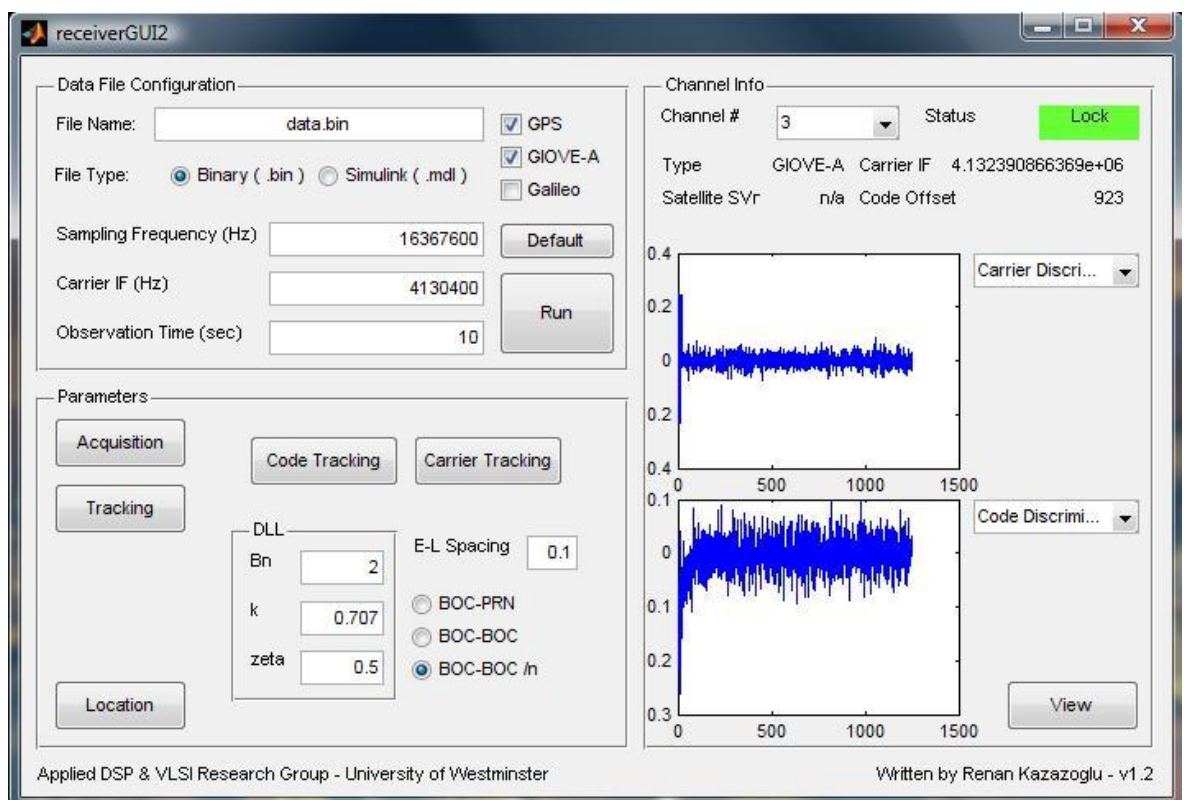
Figure 1. GNSScope

"Weak Signal and Multipath Analysis Using GNSScope: A Toolbox for End-to-End Modeling, Simulation and Analysis of GNSS"

NAV'08 / ILA'37, The Royal Institute of Navigation, London, Oct 2008

Weak Signal and Multipath Analysis Using GNSScope: A Toolbox for End-to-End Modelling, Simulation and Analysis of GNSS

Renan Kazazoglu, Alper Ucar, Ediz Cetin and Izzet Kale

Applied DSP and VLSI Research Group
University of Westminster
115 New Cavendish Street
London W1W 6UW

{r.kazazoglu, ucara, e.cetin, kalei} @ wmin.ac.uk

Abstract: The limited dynamic range of the Pseudo-Random Noise sequences used in Global Navigation Satellite Systems, coupled with the multipath and "near-far" effects caused by the channel characteristics, can result in the loss of visible satellite signals due to cross-correlation interference from stronger satellite signals. In this paper, weak signal and multipath analysis techniques using the Global Navigation System Scope (GNSScope) are presented. A brief background on the Multiple Access Interference problem in spread-spectrum communication and navigation systems is followed by an overview of several cross-correlation mitigation techniques currently used in GNSS. The signal generation, channel modelling and front end capabilities of GNSScope are also presented. The Multiple Access Interference mitigation and multipath recovery capabilities of GNSScope are analysed using simulated signals.

1. Introduction

With the development of the European global navigation system Galileo and the modernization plans for the *Global Positioning System* (GPS), referred to as GPS III, it is apparent that the civilian navigation signals will be in multiple bands within the next decade offering various applications from roadside assistance to medical services [1], [2]. Therefore, the next generation navigation user terminal will have to be a multi-mode versatile wideband receiver in order to cope with multiple bands and modulation schemes. In such a context, the flexibility offered by *Software Defined Radio* (SDR) is expected to become the dominant technology in *Global Navigation Satellite System* (GNSS) receiver development [3], [4].

The Global Navigation System Scope, developed in the Matlab and Simulink platforms, was designed as a complete transmission and reception model for the GPS L1/L2C and GIOVE-A L1/E5 bands. The model can be divided into five major sections, as seen in *Figure 1*. Signal transmission covers generation of the GPS L1/L2C and GIOVE-A L1/E5 signals. The downlink path is characterized as a fading channel which caters for atmospheric delays, Doppler and multipath effects. The RF section is a behavioural model of the low-IF GNSS receiver front-end. This is followed by a quadrature ADC and associated DSP chain. The low-IF receiver model, consisting of the acquisition, tracking, and range and range-rate processing blocks, is fully parameterizable and gives control over important variables such as the number of correlators, correlator spacing, PLL/DLL configurations, discriminator functions, transient and lock-in tracking mode behaviour, multipath handling and strong signal removal for enhanced weak signal processing; as well as allowing users to enter their own designs using built-in and custom blocks to build their receivers. The *Graphical User Interface* (GUI) for GNSScope can be seen in Figure 2.
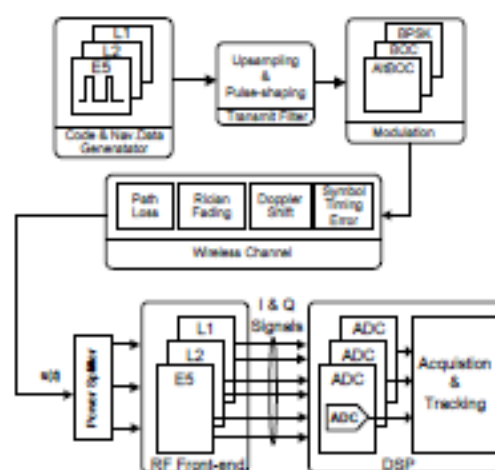
Figure 1 - GNSScope Block Diagram
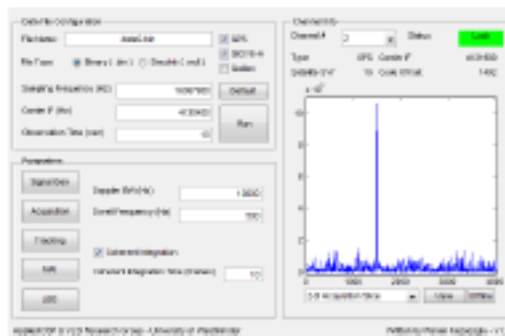
Figure 2 - GNSScope GUI

The paper is organised as follows: In *Section 2* we provide a short review of the weak signal and multipath problem inherent in GNSS, followed by a brief description of several cross-correlation mitigation techniques in *Section 3*. Details regarding signal generation and channel profiles in GNSScope are given in *Section 4*. This is followed by simulation case studies and analyses carried out entirely using GNSScope in *Section 5*. Concluding remarks are given in *Section 6* with an analysis of the results and future plans for GNSScope.

2. Multiple Access Interference

The use of finite length spreading codes in GNSS and random transmission times from different satellites prevent the PRN codes from being completely orthogonal. This limited dynamic range of the PRN codes results in non-zero peaks to be introduced into the cross-correlation characteristics of the spreading codes. *Multiple Access Interference* (MAI) refers to the interference caused when these non-zero cross-correlation peaks become strong enough to mask out the desired satellite signal being tracked [5], [6]. This occurs when the received signal power from one or more of the satellites is much stronger than that of the desired satellite.

In classical *Direct Sequence – Code Division Multiple Access* (DS-CDMA) based communication systems, this issue of varying signal power levels at the receiver is known as the "near-far" problem, which is caused by the variance in the distance between the receiver and the transmitters. However, in GNSS, all transmitting satellites are roughly at the same distance due to their orbits, which should result in similar power levels at the receiver. The so called "near-far" problem in GNSS occurs in the presence of obstructions in the signal path, reducing the received signal power levels of some satellites while not affecting all the satellites in the same manner due to different signal paths. This problem is of particular interest to weak signal

GNSS applications such as E-911, where the receiver typically would be receiving a mix containing reflected, refracted and attenuated signals alongside the direct *Line-of-Sight* (LoS), potentially jamming any weak signals and preventing a position fix from being computed.

3. Cross-Correlation Interference Mitigation

3.1 Successive Interference Cancellation

Successive Interference Cancellation (SIC) is a method of *Cross-Correlation Interference* (CCI) mitigation in which the strongest visible satellite signals are reconstructed and subtracted from the received signal successively, each time re-acquiring to obtain the new strongest visible signal [5], [7]. *Figure 3* shows a basic block diagram representation of the SIC method.
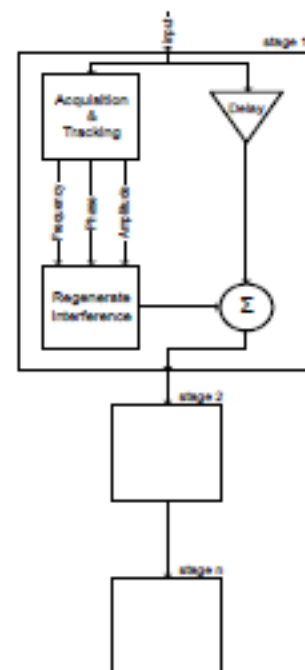
Figure 3 – SIC Block Diagram

Starting the reconstruction process from the strongest signal and working down has the advantage of removing the destructive effects of the strongest interfering signal in each stage, hence reducing MAI in all the following stages. It is important that the reconstruction parameters of code phase, carrier phase, carrier frequency, sign and amplitude are estimated based on the signal with the highest *Signal to Noise Ratio* (SNR) in each stage, as any deviation from actual signal

parameters could cause SIC to further increase the interference on the weak signals. Also, as the SIC method requires re-acquisition in each stage, it is computationally intensive and, in the presence of multiple strong interferers, would result in significantly larger processing times.

3.2 Parallel Interference Cancellation

Parallel Interference Cancellation (PIC) deals with the processing time problem of SIC by processing all the strong interfering signals simultaneously [5]. Once an estimate of all the strong interferers is established, they are all subtracted from the received signal followed by acquisition of the weak signals. This process is repeated until all desired satellite signals are acquired. The trade off for achieving this reduced processing time is in significantly increased hardware complexity, especially when signal power levels vary widely requiring multiple stages to acquire all visible satellites.

3.3 Modified SIC / PIC Algorithms

Both of the above mentioned methods don't come without disadvantages. Whether due to multipath, obstacles on the signal path or fading, the channel profile may change over time, resulting in a change in received signal power levels. The need to process the strongest signal first would require an SIC capable receiver to be reconfigurable. Since this process brings an overhead, a clever decision mechanism is necessary to minimise the amount of changes to the system. The serial nature of processing in SIC results in varying amounts of delay being introduced into the system, increasing the processing time and storage requirements depending on the number of strong interferers in the data. The PIC method was devised mainly to overcome this issue of large delays in the system. In return for increased hardware complexity, it offers fixed delay with reduced processing time as long as the visible satellite constellation doesn't change vastly. However, due to sampling resolution limitations of most GNSS front ends, the subtraction process becomes an issue possibly introducing destructive quantization noise into the system.

Since their introduction into GNSS, several variants of SIC and PIC have been developed. The Delayed Parallel Interference Cancellation (DPIC) method deals with the quantisation noise issue by creating matched correlator channels to track the incoming and reconstructed signals in parallel, then performing subtraction [7], [8]. This method deals with the resolution issue at the cost of added correlator channels. Another method uses the $sinc(\Delta f)$ relationship of the cross-correlation properties of PRN codes to create an estimate of

the strong signal [9]. Although this reduces hardware complexity, it could produce incorrect estimates of the strong signal due to the effects of relative Doppler frequency.

GNSScope has built-in capabilities to perform all the aforementioned methods, including several other techniques developed using GNSScope. These will be published in the near future. Designed in Matlab & Simulink, GNSScope is fully reconfigurable and offers a fast design and prototyping environment. The following section is a brief overview of the signal generation capabilities of GNSScope. It includes details regarding satellite transmission, channel modelling, and multipath and weak signal generation in GNSScope.

4. Signal Generation

In order to study, analyse and evaluate the performance of the receiver, a behavioural GNSS transmission model was developed in Simulink as illustrated in Figure 4.
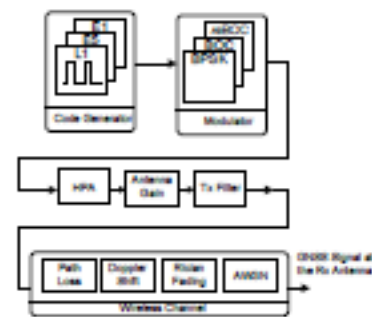
Figure 4 - GNSS Transmission Model

At the highest level, the model can be divided into three main blocks; Code Generation, Modulation, and the Channel. In this model, L1, E1 and E5 Code Generators are fed into the Modulator to generate the desired GNSS signal. This is followed by the transmitter and antenna gain blocks and a raised cosine FIR filter with the impulse response;

$$h(t) = \frac{\sin(\pi t/T)}{\pi t/T} \frac{\cos(\pi Rt/T)}{1 - 4R^2t^2/T^2} \qquad (4.1)$$

where T is the symbol period and R is the filter roll-off factor.

The wireless channel model incorporates a free space path loss block in which the path loss is expressed as;

$$PL(dB) = -10\log\left[\frac{\lambda^2}{(4\pi)^2 d^2}\right] \qquad (4.2)$$

199

where λ is the wavelength of the signal and d is the Tx-Rx separation. Doppler shift is applied to the signal in order to achieve the appropriate frequency offset.

The multipath Rician fading block is implemented in the channel since the transmitted GNSS signal can travel to the receiver along a LoS path in most of the cases. In this scenario, spread multipath components arriving at different angles are superimposed onto the LoS signal [10]. The effect of a LoS signal arriving with many weaker multipath signals gives rise to the Rician distribution. The probability density function of the distribution is given by;

$$p(r) = \begin{cases} \dfrac{r}{\sigma^2} \exp\left[-\dfrac{r^2+A^2}{2\sigma^2}\right] I_0\left(\dfrac{Ar}{\sigma^2}\right), & \text{for } A \geq 0, r \geq 0 \\ 0 & \text{, for } r < 0 \end{cases} \tag{4.3}$$

where r is the received signal voltage, σ is the *Root Mean Square* (RMS) value of r, A is the peak amplitude of the direct-path signal and $I_0(.)$ is the modified Bessel function of the first-kind and zero-order.

The Rician distribution is often described in terms of the *K-factor* parameter which represents the ratio between LoS power and diffused power;

$$K(dB) = 10\log\frac{A^2}{2\sigma^2} \tag{4.4}$$

The multipath is characterised by the *K-factor*, gain and delay factors which specify the gain and propagation delay for each multipath component. *Figure 5* illustrates the output of the transmission model for the Galileo E1 signal.
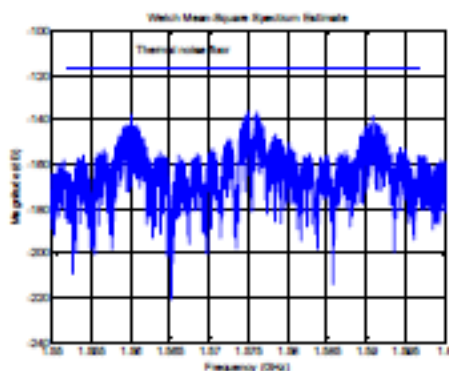
Figure 5 - Galileo E1 Signal at the Rx Antenna

5. Simulation Case Studies & Analyses

We present simulations and analyses performed entirely using GNSScope in this section. For these simulations a data file containing two strong signals and one weak signal was generated. The weak signal was set to be 34dB below the received power level of the two strong signals. *Figures 6 & 7* present the two strong signals used for these simulations in the form of the parallel code phase search acquisition results before and after MAI removal was applied. The plots were organised such that the presence or absence of a peak in the centre of the acquisition plots determines whether there is a detectable signal or not. It can be seen that the two strong signals become undetectable once MAI removal has been applied. The off-centre peaks are the resulting MAI caused by the remaining strong signal in the data file.
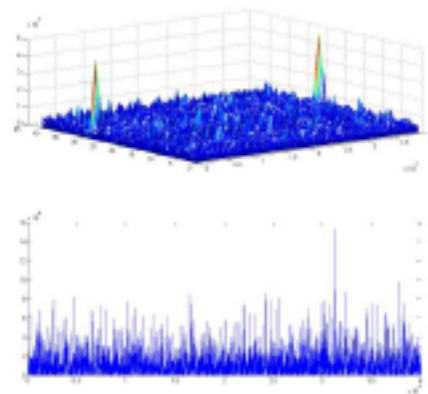
Figure 6 - Strong signal SV1 before and after MAI removal
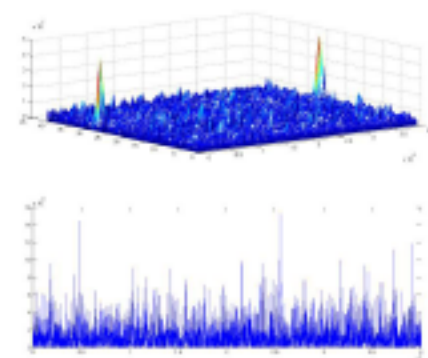
Figure 7 - Strong signal SV2 before and after MAI removal
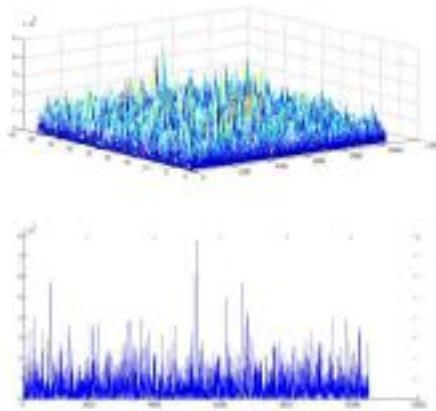
Figure 8 - Weak signal before and after MAI removal (SIC method with no PDI)

Figure 8 shows the weak signal acquisition results after the removal of the MAI from strong signal satellites SV1 & SV2, using the SIC method with no *Post Detection Integration* (PDI) on the acquisition results. The peak in the centre indicates that the weak signal was successfully detected. *Figures 9 & 10* show the weak signal acquisition results using the PIC method without PDI, and the improvements gained from using 10ms PDI on the acquisition results, respectively. Once again, the central peaks indicate successful detection of the weak signal.
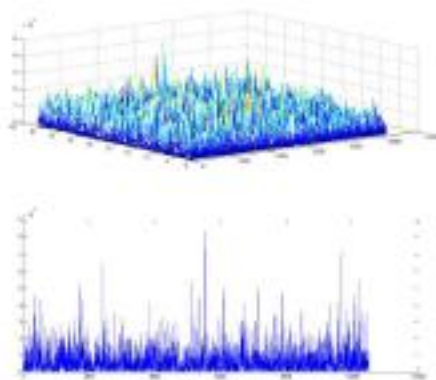
Figure 9 - Weak signal before and after MAI removal (PIC method with no PDI)
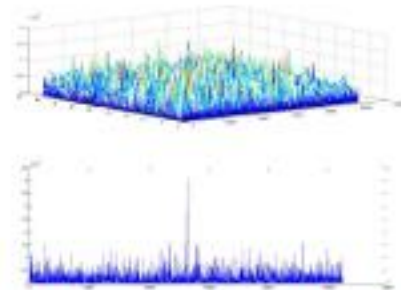
Figure 10 - Weak signal before and after MAI removal (PIC method with PDI)

Figures 11 & 12 show the recovery of signals on the multipath using GNSScope. The simulated file contained the direct LoS along with three multipath components of a single satellite, all equally spaced with gradually decreasing power levels. Two files were generated for -20 dB and -30 dB SNR levels, respectively. It can be seen that the strong direct LoS signal present in the parallel code phase search acquisition plots has been wiped off in both cases to reveal the three signals on the multipath. Both cases present the acquisition results without PDI, and can be improved using PDI over multiple PRN code periods.
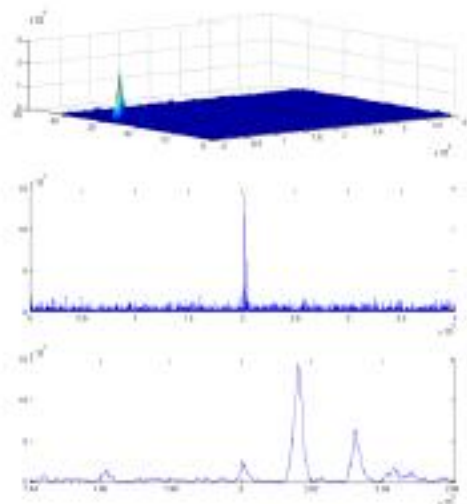
Figure 11 - Acquisition before and after direct LoS signal removal (-20dB SNR)
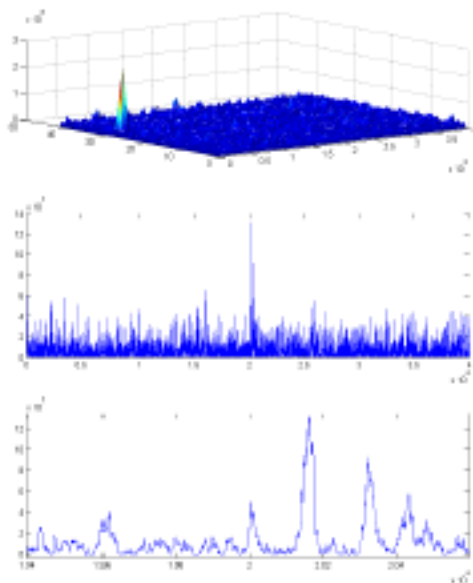
Figure 12 - Acquisition before and after direct LoS signal retrieval (-30dB SNR)

6. Conclusions

Having an end-to-end modelling environment enables designers to accurately simulate weak signal transmission, signals on the multipath and the receivers' response to environmental dynamics. The capability to fine tune every stage of the signal path beginning from satellite transmission through to the receivers position fix to optimize its response enables hardware and software developers to test and benchmark their own designs before new global navigation systems are fully operational. The ability to simulate controlled weak signal conditions provides a better understanding of the receivers' response in obstructed areas. Adding signals on the multipath gives receiver designers the opportunity to analyse the multipath rejection characteristics of their designs.

This paper has provided a brief overview of the capabilities of GNSScope. Several architectures for MAI mitigating receivers have been analysed using controlled signals generated in GNSScope. Simulations have shown that multipath and weak signal detection is possible even at very low power levels, given a good estimate of the strong interferers.

References

[1] Galileo Open Service Signal in Space Interface Control Document, European Space Agency, European GNSS Supervisory Authority, 2008.

[2] Global Positioning System Standard Positioning Service Interface Control Document, GPS Joint Program Office, 2000.

[3] Tsui, J., Fundamentals of Global Positioning System Receivers: A Software Approach, Wiley-Interscience Publications, U.S.A., 2005.

[4] Borre, K., et.al., A Software-Defined GPS and Galileo Receiver: A Single Frequency Approach, Birkhauser, Berlin, Germany, 2007.

[5] Fu, Z. and J. Wang, MAI-Mitigation and Near-Far-Resistance Architectures for GNSS Receivers, Journal of Global Positioning Systems, Vol.2, No.1, p.27-34, 2003.

[6] El-Natour, H.A., et.al., Impact of Multipath and Cross-Correlation on GPS Acquisition in Indoor Environments, ION 2005, San Diego, 2005.

[7] Glennon, E.P. and A.G. Dempster, A Review of GPS Cross Correlation Mitigation Techniques, The 2004 International Symposium on GNSS/GPS, 2004.

[8] Glennon, E.P., et.al., Delayed Parallel Interference Cancellation for GPS C/A Code Receivers, 12th IAIN World Congress and 2006 International Symposium on GPS/GNSS, 2006.

[9] Norman, C.P. and C.R. Cahn, Strong Signal Cancellation to Enhance Processing of Weak Spread Spectrum Signal, U.S.A., 2004.

[10] Wireless Communications, T.S. Rappaport, Prentice Hall Inc, NJ, 2002.

Appendix C

"A Low Complexity Cross-Correlation Interference Mitigation Technique for GNSS"

European Navigation Conference - Global Navigation Satellite Systems (ENC-GNSS)

2009, Naples, Italy, May 2009

A Low Complexity Cross-Correlation Interference Mitigation Technique for GNSS

Renan Kazazoglu, Ediz Cetin and Izzet Kale

{r.kazazoglu, e.cetin, kalei} @ wmin.ac.uk

Applied DSP and VLSI Research Group
University of Westminster
London, UK

Abstract: The finite length Gold codes used in satellite navigation systems limit their dynamic range, resulting in the introduction of unwanted peaks that can mask out signals of interest. In this paper, a novel cross-correlation interference mitigation technique dealing with this issue is introduced. A brief overview of the multiple access interference problem inherent in satellite navigation systems using the code division multiple access technique is followed by the details of the proposed method. Simulation case studies and analyses of the results detailing weak signal scenarios, carried out entirely using the Global Navigation System Scope, are presented. A comparison of the results is given in the conclusions section along with remarks on the performance of the proposed method and future work to be carried out.

Introduction: The finite length Pseudo-Random Noise (PRN) codes used in Global Navigation Satellite Systems (GNSS) limit the dynamic range of operation as they lose orthogonality, resulting in the introduction of unwanted cross-correlation peaks that can mask out certain signals of interest. This effect is referred to as Multiple Access Interference (MAI) and can cause problems during weak signal GNSS operation [1], [2]. Several techniques have been developed that detect this interference and remove it from the received signal to enhance the detection of such weak signals [3]. The Successive Interference Cancellation (SIC) technique is a MAI mitigation method where the strongest signals are iteratively subtracted from the incoming signal, hence removing the detrimental effects from subsequent stages of the processing chain [3]. While this ensures that in each stage the strongest signal is reconstructed with minimal interference, in the presence of multiple strong signals, it can result in significantly increased processing times. The Parallel Interference Cancellation (PIC) technique solves this large processing time issue by processing all strong signals in parallel, reducing the processing time at the cost of significantly increased hardware complexity [3]. However, the one or two-bit Analogue-to-Digital Converters (ADCs) used in most consumer GNSS front-ends introduce issues in subtracting the interferers from the incoming signal [4]. Rather than carrying out operations on the incoming signal, the cross-correlation effects of the interferers could be processed in matched correlator channels and the effects removed at the in-phase and quadrature outputs of these channels, as in the methods described in [5] and [6].

In this paper we propose a method based on the techniques described in [5] and [6]. However, rather than scaling the cross-correlations by a constant sinc(Δf) scale-factor as in [5], resulting in incorrect signal reconstructions possibly degrading the tracking performance, or fully reconstructing the strong interferers as in [6], at the cost of processing overheads being introduced, the proposed method uses an approximation to wipe off the effects of the relative Doppler carrier frequency between the strong and weak signals being tracked.

The following section will briefly describe the proposed method using a single interferer case and extended to multiple interferer cases. This will be followed by simulation case studies and analyses presenting the results obtained using the proposed method. The conclusions section will provide remarks on the effectiveness of the proposed method along with future work to be carried out.

Method: Assuming, for simplicity, that there is one weak signal and one strong interferer, the locally generated replica of the strong interferer being tracked can be expressed as:

$$I_S = Amplitude_S * PRN_S * cos(f_C + Doppler_S)$$

where I_S is the reconstructed in-phase component of the strong signal, $Amplitude_S$ is the amplitude of the strong signal that is being tracked, obtained from the integrate-and-dump filter outputs, PRN_S is the associated Gold code for the strong signal interferer, f_C is the centre frequency and $Doppler_S$ is the Doppler frequency offset of the strong signal interferer. When processed in a standard correlator channel, the in-phase output could be expressed as:

$$I = \{ Amplitude_S * PRN_S * cos(f_C + Doppler_S) \} * \{ PRN_W * cos(f_C + Doppler_W) \}$$

where I is the in-phase correlator output for the weak signal of interest, PRN_W is the associated Gold code of the weak signal and $Doppler_W$ is the Doppler frequency offset of the weak signal of interest. This equation can be re-written as follows:

$$I = Amplitude_S * \{ PRN_S * PRN_W \} * \{ cos(f_C + Doppler_S) * cos(f_C + Doppler_W) \}$$

It can be seen that $Amplitude_S$ is a scale-factor and $PRN_S * PRN_W$ is the cross-correlation of the strong interferer and weak signal of interest PRN codes. This equation can be further simplified using the following trigonometric identity:

$$cos(a) * cos(b) = \{ cos(a-b) + cos(a+b) \} / 2$$

resulting in the following:

$$I = Amplitude_S * \{ PRN_S * PRN_W \} * \{ cos(Doppler_S - Doppler_W) * cos(2*f_C + Doppler_S + Doppler_W) \}$$

Simulation case studies have shown that the high frequency component can be ignored as it will be filtered out by the integrate-and-dump filters of the correlator channels, resulting in the following matched correlator channel equation:

$$I = Amplitude_S * \{ PRN_S * PRN_W \} * cos(Doppler_S - Doppler_W)$$

where the amplitude of the strong signal interferer can be obtained from the associated strong signal tracking channel integrate-and-dump filters, and the cross-correlation of the associated strong and weak signal PRN codes can be stored locally, removing the need to generate the cross-correlations on the fly.

This method trivially extends to n strong signal interferers through n matched correlator channels in the GNSS receiver. As $Amplitude_S$ is obtained from the channel tracking the strong signal interferer, the remaining operation is simply to multiply the cross-correlation of the strong and weak signals with $cos(Doppler_S - Doppler_W)$, removing the necessity to fully reconstruct the strong interferer as in [6], reducing the computational load by 25% for each strong interferer on the weak signal. Also, in contrast to [5], the effect of the relative Doppler frequency is computed for every sample, rather than being approximated to a constant scale factor. This results in a low complexity cross-correlation interference mitigation technique targeting practical complexity reduced real-time GNSS receiver architectures, leading to improved processing efficiency and hence increased receiver performance and reduced power consumption.

In order to evaluate its effectiveness and compare with existing techniques, the proposed technique has been incorporated into our in-house SDR GNSS Receiver analysis and evaluation platform, the Global Navigation System Scope (GNSScope) [7]. The following section will present simulation case studies and analyses carried out entirely using GNSScope.

Simulation Case Studies: Simulation case studies carried out in GNSScope using both real and simulated strong and weak signal conditions show that the technique is successful at identifying and removing strong signal interferers in a variety of cases including weak signal acquisition / tracking, multipath signal wipe-off / recovery and continuous wave interference removal.

The first case study is a weak signal acquisition scenario where the weak signal of interest is masked out by a strong signal interferer. The weak signal was set to be 24dB below the received power level of the strong signal at a relative Doppler frequency of 1kHz, resulting in the weak signal not being detected during initial acquisition, as seen in *Figure 1*. *Figure 2* presents the parallel code phase space search acquisition results for the weak signal of interest following MAI removal using the proposed method. The strong acquisition peak, which can be seen in more detail in the acquisition cross-section presented in *Figure 3*, indicates successful weak

signal acquisition using the proposed method. It can be seen that the acquisition results also provide a good C/N_0, improving the processing gain of subsequent stages.
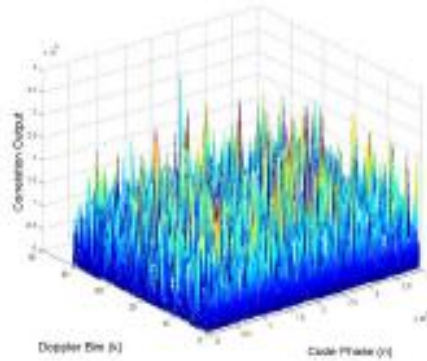
Figure 1 - Weak Signal Parallel Code Phase Space Search Acquisition prior to MAI Removal
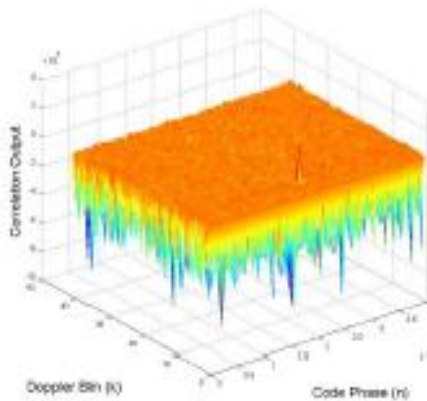
Figure 2 - Weak Signal Parallel Code Phase Space Search Acquisition following MAI Removal

The second case study is a weak signal acquisition scenario where the weak signal of interest is masked out by three strong signal interferers. The weak signal was set to be 34dB below the received power level of the strong signal interferers, each placed at 1kHz Doppler frequency intervals in order to introduce strong interference on the weak signal of interest. The strong acquisition peak present in the weak signal parallel code phase space search

acquisition results in *Figure 4*, and the cross-section results in *Figure 5*, indicate successful acquisition of the weak signal of interest using the proposed method. The results were obtained using 2-bit quantization, showing that the proposed method can be implemented in commercial receiver architectures.
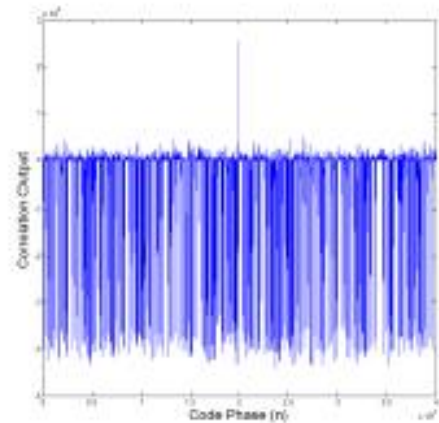
Figure 3 - Cross-Section of the Weak Signal Acquisition Results
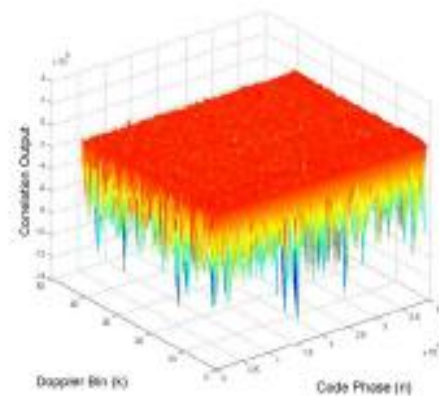
Figure 4 - Weak Signal Parallel Code Phase Space Search Acquisition following MAI Removal
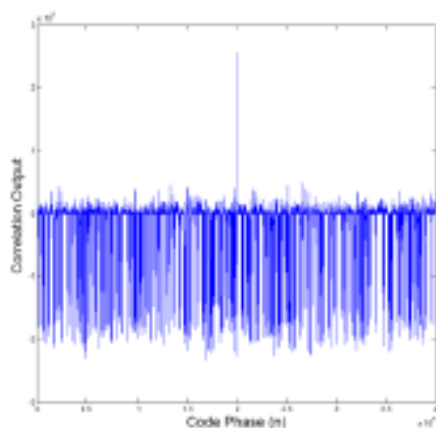
Figure 5 - Cross-Section of the Weak Signal Acquisition Results

Conclusions: This paper has provided a brief overview of a low complexity cross-correlation interference mitigation technique for GNSS, designed and developed using GNSScope. Simulation case studies for the acquisition and tracking of weak signals have been presented using controlled signals generated in GNSScope. The results have shown successful weak signal recovery using the proposed technique. The ability to successfully approximate strong signal interference without having to fully reconstruct the interferers, as in classical MAI mitigation techniques, results in a reduction of the computational complexity. Also, as the approximation caters for the effects of Doppler frequency difference in the time domain, in contrast to the constant scale factor approximation in [5], it results in more accurate signal wipe-off, leading to a practical low complexity MAI mitigation technique, resulting in improved processing efficiency, increased receiver performance and reduced power consumption in practical complexity reduced real-time GNSS receiver architectures.

References:

[1] Moshavi S., *"Multi-User Detection for DS-CDMA Communications"*, IEEE Communications Magazine, pg. 124-136, October 1996.

[2] El-Natour H.A., et.al., *"Impact of Multipath and Cross-Correlation on GPS Acquisition in Indoor Environments"*, ION 2005, San Diego, 2005.

[3] Fu Z. and J. Wang, *"MAI Mitigation and Near-Far-Resistance Architectures for GNSS Receivers"*, Journal of Global Positioning Systems, Vol. 2, No. 1, pg. 27-34, 2003.

[4] Glennon E.P. and A.G. Dempster, *"A Review of GPS Cross Correlation Mitigation Techniques"*, The International Symposium on GNSS/GPS, 2004.

[5] Norman C.P. and C.R. Cahn, *"Strong Signal Cancellation to Enhance Processing of Weak Spread Spectrum Signals"*, USA, 2004.

[6] Glennon E.P., et.al., *"Delayed Parallel Interference Cancellation for GPS C/A Code Receivers"*, The International Symposium on GNSS/GPS, 2006.

[7] Kazazoglu R., et.al., *"Weak Signal and Multipath Analysis Using GNSScope: A Toolbox for End-to-End Modelling, Simulation and Analysis of GNSS"*, NAV'08/ILA'37, London, October 2008.

Appendix D

"GNSScope and The Split Chip Summation Technique"

European Conference on Circuit Theory and Design (ECCTD) 2009, Antalya, Turkey, Aug 2009

GNSScope and The Split Chip Compression Technique

Renan Kazazoglu, Ediz Cetin and Izzet Kale
Applied DSP and VLSI Research Group
University of Westminster
London, UK
{r.kazazoglu, e.cetin, kalei} @ wmin.ac.uk

Abstract— The presence of multipath due to obstructions on the signal path coupled with transmitter and channel based perturbations, can significantly degrade the quality of the received satellite navigation signals, resulting in the non-detection of weaker visible satellites, loss of lock on acquired satellites, and increased pseudo-range errors. In this paper, we present a novel technique based on the binary-valued signal compression method, for the detection, identification and compensation of pseudo ranging code discrepancies and signals on the multipath. Following a brief overview of the system, simulation case studies carried out entirely using the in-house developed satellite navigation receiver development, emulation and analysis platform Global Navigation System Scope (GNSScope) will be presented verifying the results.

I. INTRODUCTION

With the development of the European global navigation system Galileo and the modernization plans for the Global Positioning System (GPS), referred to as GPS III, it is apparent that the civilian navigation signals will be in multiple bands within the next decade offering various applications from roadside assistance to medical services [1], [2]. Therefore, the next generation navigation user terminal will have to be a multi-mode versatile wideband receiver in order to cope with multiple bands and modulation schemes. In such a context, the flexibility offered by Software Defined Radio (SDR) is expected to become the dominant technology in Global Navigation Satellite System (GNSS) receiver development [3], [4].

The Global Navigation System Scope, developed in the Matlab and Simulink platforms, was designed as a complete transmission and reception model for the GPS L1/L2C and GIOVE-A L1/E5 bands. The model can be divided into five major sections, as seen in Fig. 1. Signal transmission covers generation of the GPS L1/L2C and GIOVE-A L1/E5 signals. The downlink path is characterized as a fading channel which caters for atmospheric delays, Doppler and multipath effects. The RF section is a behavioral model of the low-IF GNSS receiver front-end. This is followed by a quadrature ADC and associated DSP chain. The low-IF receiver model, consisting of the acquisition, tracking, and range and range-rate processing blocks, is fully parameterizable and gives control over important variables such as the number of correlators, correlator spacing, PLL/DLL configurations, discriminator functions, transient and lock-in tracking mode behavior, multipath handling and strong signal removal for enhanced weak signal processing; as well as allowing users to enter their own designs using built-in and custom blocks to build their receivers. The Graphical User Interface (GUI) for GNSScope can be seen in Fig. 2
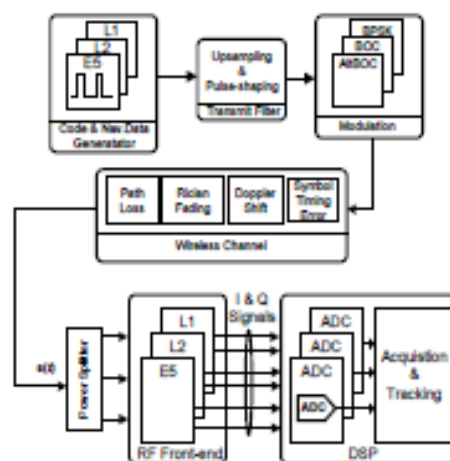
Figure 1. GNSScope Block Diagram
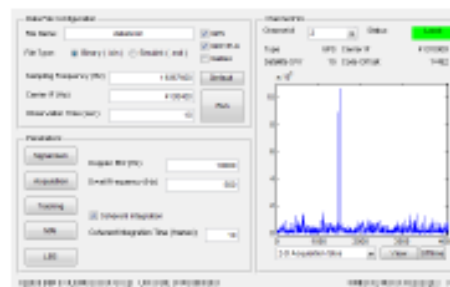
Figure 2. GNSScope GUI

The paper is organized as follows: In Section II we provide a short background on GNSScope and an overview of the binary-valued signal modulation compression method. This will be followed by details of the proposed technique in Section III. Simulation case studies utilizing the proposed method and analyses of the results using GNSScope will be given in Section IV. Concluding remarks and details of further work will be given in Section V.

II. BACKGROUND

A. GNSScope

GNSScope is an end-to-end modeling environment enabling designers to accurately simulate weak signal transmission, signals on the multipath and the receivers' response to environmental dynamics. The capability to fine tune every stage of the signal path beginning from satellite transmission through to the receivers position fix to optimize its response enables hardware and software developers to test and benchmark their own designs before new global navigation systems are fully operational. The ability to simulate controlled weak signal conditions provides a better understanding of the receivers' response in obstructed areas. Adding signals on the multipath gives receiver designers the opportunity to analyze the multipath rejection characteristics of their designs. GNSScope was designed to handle these tasks while giving receiver designers insight into the details of their designs. Having been developed in SDR, it gives receiver designers flexibility and control over every stage of the signal chain.

B. Binary-Valued Signal Modulation Compression

As advances in high-sensitivity GNSS receiver technologies targeting indoor and urban canyon navigation require higher and higher processing speeds for tasks such as multiple access interference mitigation and multipath compensation, the need for improved processing techniques reducing the number of operations for acquisition and tracking is ever increasing [5]. The computational load in these cases can be significantly reduced by the application of the Binary-Valued Signal Modulation Compression for High Speed Cross-Correlation [6] technique. This is accomplished through the summation of the received signal samples rectified by the polarity of the chipping code, resulting in the samples of a single chip of this code. As this technique can be implemented using only simple additions, it greatly reduces the computational complexity while preserving signal range and phase information in the chip waveform. Using this technique, the large number of received signal samples are reduced to a short vector with few samples representing the channel and receiver front-end effects on the chip itself. An example of this, produced using GNSScope, can be seen in Fig. 3 where the compression technique is applied to a generated signal over 100 milliseconds of GPS L1 data containing a multipath component with a 180 degree phase shift with respect to the line of sight signal. The filtering effects along with the multipath signal, are clearly visible.
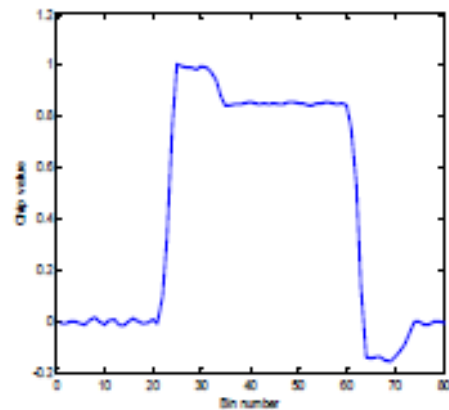
Figure 3. Compressed chip waveform

III. THE SPLIT CHIP COMPRESSION TECHNIQUE

The Split Chip Compression technique is based on the binary-valued signal modulation compression technique, whereby the samples of the received signal are summed after being rectified by the polarity of the chipping code. However, rather than summing all the chips and compressing the waveform into a single chip of the PRN code, losing any information associated with the specific chip polarities, the technique described in this paper splits the chipping code into its positive and negative chips, accumulating them in two separate vectors. This results in increased sensitivity to perturbations on the chipping waveform, as specific perturbations that affect the two polarities of the chipping waveform differently are preserved rather than being integrated, at the cost of a second short vector for the storage of the two separate chips. The two compressed chips represent the effects of the transmitter, channel and receiver front-end on the chipping waveform and can be used in the detection, identification and compensation of distortions such as multipath, unbalanced chipping code duty cycles and filter ringing, which can then be compensated using linearization, curve fitting and parameter extraction techniques.

In order to be able to identify multipath and unbalanced duty cycled effects in the compressed positive and negative chip vector, a simple moving average filter coupled with a thresholding algorithm was also devised. As the thresholding algorithm linearizes the compressed chip waveforms, further work is being carried out to enable the detection of Ionospheric and Tropospheric effects such as dispersion and refraction.

The proposed method has been successfully implemented in MATLAB and integrated into GNSScope. Its uses will be demonstrated in the following section using simulation case studies carried out entirely using GNSScope.

IV. SIMULATION CASE STUDIES

We present simulation case studies and analyses performed entirely using GNSScope in this section. Two case studies are presented. First we present the use of the split chip sum technique in determining the differences in the filtering effects on the positive and negative polarity chips, and how these effects get filtered out during the accumulation process when integrated into a single vector, as in the binary-valued signal modulation compression technique. To this end a simulation file containing a single satellite was generated with 40 megahertz sampling frequency and 5 megahertz center frequency, in order to demonstrate results in high resolution. The signal contains channel and front-end filtering effects that present in typical GNSS receivers. Fig. 4 and Fig. 5 present the compressed positive and negative chips respectively, over an integration period of 200 milliseconds.

When compared to the binary-valued signal modulation compression technique results given in Fig. 6, it can be seen that part of the filtering effects on the chip waveforms have been integrated out and are non-existent. It is apparent from the compressed positive and negative polarity chip waveforms that the leading and trailing edges of these waveforms have also been affected differently, with larger oscillations on the positive chip waveform compared to the negative chip waveform.

The second simulation case study presents the results for an unbalanced duty cycle error condition on the chipping sequence, where the transmitted widths of the positive polarity chips are not equal to those of the negative polarity chips. Fig. 7 and Fig. 8 present the compressed positive and negative chips respectively, computed over an integration period of 100 milliseconds. It can be seen that the split chip compression method is capable of identifying both chip waveforms without any distortions, revealing the 10% duty cycle imbalance and chip specific perturbations while simplifying computations in subsequent stages.

Figure 4. Compressed Positive Polarity Chip
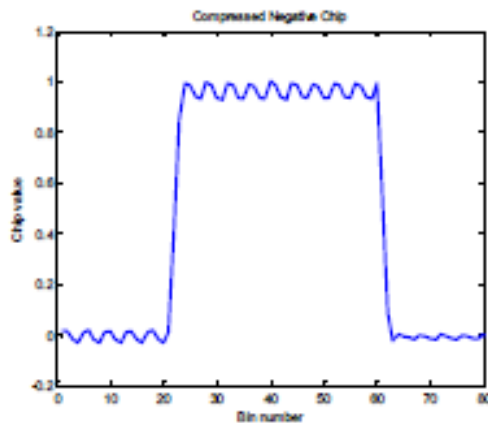
Figure 5. Compressed Negative Polarity Chip
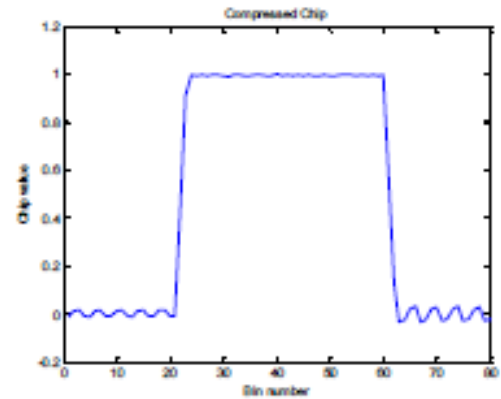
Figure 6. Binary-Valued Signal Modulation Compressed Chip
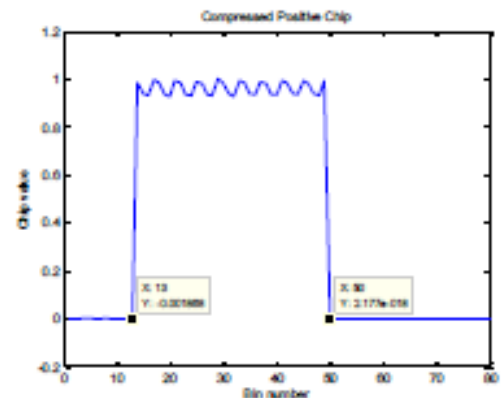
Figure 7. Compressed Positive Polarity Chip
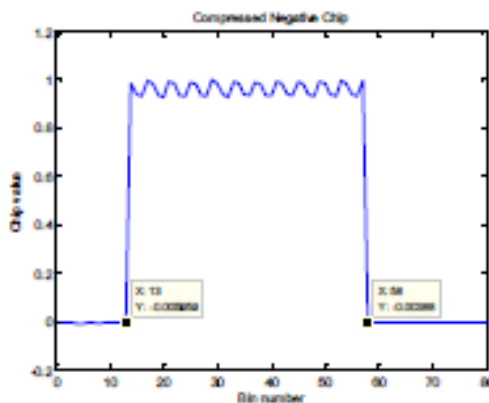
Figure 8. Compressed Negative Polarity Chip

Having knowledge of the duty cycle imbalance, the locally generated PRN code can be modified to compensate for this effect, increasing the SNR of the in-phase and quadrature correlator channel outputs. This results in improved receiver performance in the presence of noise and multipath errors. Fig. 9 presents the compressed chip resulting from the binary-valued signal modulation compression method using the same input file. In the presence of channel based distortions and multipath, the transition region may not be readily detectable, resulting in reduced performance under these conditions.
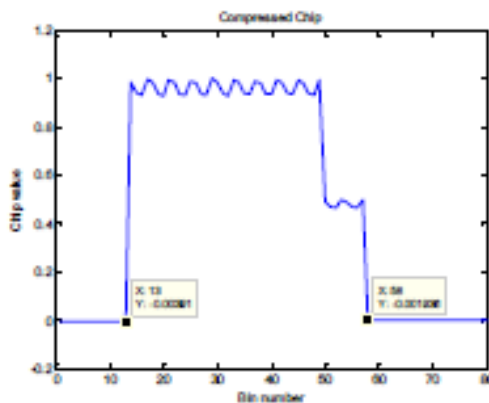
Figure 9. Binary-Valued Signal Modulation Compressed Chip

V. CONCLUSIONS

In this paper we have provided a brief overview of the capabilities of GNSScope and the split chip compression technique. Simulation case studies have been used to demonstrate the techniques' effectiveness under certain threat conditions, and the results have been compared to those of the binary-valued signal compression technique. The method can be used in low complexity high performance GNSS receivers targeting high-sensitivity positioning applications such as indoor or urban canyon navigation.

VI. ACKNOWLEDGEMENTS

REFERENCES

[1] "Galileo Open Service Signal In Space Interface Control Document", European Space Agency, European GNSS Supervisory Authority, 2008.

[2] "Global Positioning System Standard Positioning Service Interface Control Document", GPS Joint Program Office, 2000.

[3] J. Tsui, "Fundamentals of Global Positioning System Receivers: A Software Approach", Wiley-Interscience Publications, USA, 2005.

[4] K. Borre, D.M. Akos, N. Bertelsen, P. Rinder and S.H. Jensen, "A Software-Defined GPS and Galileo Receiver: A Single Frequency Approach", Birkhauser, Berlin, Germany, 2007.

[5] L.R. Weill, "Lightening the Data Processing Load - Signal Compression in GNSS Receivers", InsideGNSS, p. 37-45, Fall 2007.

[6] B. Fisher and L.R. Weill, "Binary Valued Signal Modulation Compression for High Speed Cross-Correlation", United States Patent, Patent No. US 7,403,559 B1, July 22, 2008.

References

[1. **Kaplan, E D.** *Understanding GPS: Principles and Applications.* London : Artech House Inc., 1996.

2. **Tsui, J B Y.** *Fundamentals of Global Positioning System Receivers: A Software Approach.* 2nd. s.l. : Wiley-Interscience, 2005.

3. **Borre, K, et al.** *A Software Defined GPS and Galileo Receiver: A Software Defined Approach.* Boston : Birkhauser, 2007.

4. *GNSScope: A Toolbox for End-to-End Modeling, Simulation and Analysis of GNSS.* **Kazazoglu, R E, Cetin, E and Kale, I.** London : The Royal Institute of Navigation, 2008b. The Navigation Exhibition.

5. *Overview of Software Defined Radio GNSS Receivers using GNSScope: A Toolbox for End-to-End Modeling, Simulation and Analysis of GNSS.* **Kazazoglu, R E, Cetin, E and Kale, I.** London : University of Westminster, 2009b. The GNSS Receiver Designs and Signal Processing Workshop.

6. *The GNSScope Toolbox and Novel Tracking Techniques.* **Kazazoglu, R E, Cetin, E and Kale, I.** London : University of Westminster, 2009c. The ECS Research Conference.

7. *Weak Signal and Multipath Analysis Using GNSScope: A Toolbox for End-to-End Modeling, Simulation and Analysis of GNSS.* **Kazazoglu, R E, Cetin, E and Kale, I.** London : The Royal Institute of Navigation, 2008c. NAV'08 / ILA'37.

8. **Kazazoglu, R E and Kale, I.** *GNSScope: A Toolbox for End-to-End Modeling, Simulation and Analysis of GNSS.* Reading : Thales, 2009d. Presentation.

9. **Kazazoglu, R E, Cetin, E and Kale, I.** *GNSS Receiver Technologies and Novel Acquisition Algorithms.* Korea : s.n., 2007. Presentation.

10. *A Low Complexity Corss-Correlation Interference Mitigation Technique for GNSS.* **Kazazoglu, R E, Cetin, E and Kale, I.** Naples : IEEE, 2009a. ENC-GNSS.

11. *GNSScope and The Split Chip Summation Technique.* **Kazazoglu, R E, Cetin, E and Kale, I.** Antalya : IEEE, 2009. ECCTD.

12. **Kazazoglu, R E, Cetin, E and Kale, I.** *A Single Frequency Reconfigurable GNSS Receiver in SDR.* London : s.n., 2008a. Presentation.

13. *Extending the Applications and Improving the Efficiency of Positioning Through the Exploitation of New GNSS Signals.* **Cross, P, et al.** Naples : IEEE, 2009. ENC-GNSS.

14. **Prasad, R and Ruggieri, M.** *Applied Satellite Navigation Using GPS, Galileo and Augmentation Systems.* s.l. : Artech House Inc, 2005.

15. **Bate, R R, Mueller, D D and White, J E.** *Fundamentals of Astrodynamics.* New York : Dover Publications, 1971.

16. **Spilker, J J and Parkinson, B W.** *Global Positioning System: Theory and Applications.* Washington DC : American Institute of Aeronautics and Astonautics, 1996. Vol. I & II.

17. **GPS Joint Program Office.** *Global Positioning System Standard Positioning Service Signal Specification.* 1995.

18. **European Space Agency.** *Galileo Open Service Signal In Space Interface Control Document.* 2008.

19. **Oppenheim, A V and Schafer, R W.** *Discrete-Time Signal Processing.* New Jersey : Prentice-Hall Inc, 1999.

20. **Mitra, S K.** *Digital Signal Processing.* New York : McGraw-Hill Inc, 2002.

21. **InsideGNSS.** InsideGNSS. *InsideGNSS.* [Online] www.insidegnss.com.

22. *GPS Signal Structure and Performance Characteristics.* **Spilker, J J.** 1978, Navigation, pp. 121-146.

23. *A Complete IF Software GPS Receiver: A Tutorial about the Details.* **Krumvieda, K, et al.** Salt Lake City : Institute of Navigation, 2001. Proceedings of the 14th International Technical Meeting of the Satellite Division of the Institute of Navigation. pp. 789-829.

24. *A 12-Channel Real-Time GPS L1 Software Receiver.* **Ledvina, B M, Powell, S P and Kintner, P M.** s.l. : Institute of Navigation, 2003. Proceedings of the International Technical Meeting of the Satellite Division of the Institute of Navigation.

25. *A Real-Time GPS Civilian L1/L2 Software Receiver.* **Ledvina, B M, et al.** s.l. : Institute of Navigation, 2004. Proceedings of the International Technical Meeting of the Satellite Division of the Institute of Navigation.

26. *GPS Receiver Architectures and Measurements.* **Braasch, M S and Dierendonck, AJ V.** 1999, Proceedings of the IEEE, pp. 48-64.

27. *Galileo Receiver Core Technologies.* **Kovar, P, et al.** 2005, Journal of Global Positioning Systems, pp. 176-183.

28. *An MCMC Algorithm for BOC and AltBOC Signaling Acquisition in Multipath Environments.* **Brahim, F, Chonal, T and Rabaste, O.** s.l. : IEEE, 2008. IEEE Position, Location and Navigation Symposium. pp. 424-432.

29. **Best, Roland E.** *Phase Locked Loops: Design, Simulation and Applications.* New York : McGraw-Hill, 2003.

30. **Ziemer, Rodger E and Peterson, Roger L.** *Digital Communications and Spread Spectrum Systems.* New York : MacMillan, 1985.

31. *Galileo GIOVE-A Acquisition and Tracking Analysis with a New Unambiguous Discriminator.* **Glennon, E P and Dempster, A G.** Sydney : International Global Navigation Satellite Systems Society, 2007b. International Global Navigation Satellite Systems Symposium.

32. *Performance Analysis of MBOC, AltBOC and BOC Modulations in Terms of Multipath Effects on the Carrier Tracking Loop within GNSS Receivers.* **Fantino, F, et al.** Monterey : IEEE, 2008. IEEE Position, Location and Navigation Symposium. pp. 369-376.

33. **Moshavi, S.** Multi-User Detection for DS-CDMA Communications. *IEEE Communications Magazine.* October 1996, pp. 124-136.

34. **Tsui, J B Y, Akos, D M and Stockmaster, M H.** *Block Adjustment of Synchronization Signal for Phase Coded Signal Tracking. 6,195,328* US, February 27, 2001.

35. *MAI Mitigation and Near-Far-Resistance Archictures for GNSS Receivers.* **Fu, Z and Wang, J.** 2003, Journal of Global Positioning Systems, pp. 27-34.

36. *Successive Interference Cancellation Algorithms for Downlink W-CDMA Communications.* **Madkour, M F, Gupta, S C and Wang, YP E.** 2002, IEEE Transactions on Wireless Communications, p. 1690177.

37. *Cross Correlation Mitigation Techniques for Software GPS C/A Code Receivers.* **Glennon, E P and Dempster, A G.** Sydney : International Global Navigation Satellite Systems Society, 2007a. International Global Navigation Satellite Systems Symposium.

38. **Glennon, E P and Dempster, A G.** *Apparatus and Method for Mitigation of Cross Correlation in GPS Systems. 2007/016595* WO, February 8, 2007b.

39. *Delayed Parallel Interference Cancellation for GPS C/A Code Receivers.* **Glennon, E P, Bryant, R C and Dempster, A G.** 2006, International Symposium on GPS/GNSS.

40. **Norman, C P and Cahn, C R.** *Strong Signal Cancellation to Enhance Processing of Weak Spread Spectrum Signal. US 7,116,704 B2* United States, October 3, 2006.

41. **Weill, L and Fisher, B.** *Method for Mitigating Multipath Effects in Radio Systems. 6,370,207* US, April 9, 2002.

42. **Fenton, P C.** *Apparatus for and Method of Making Pulse-Shape Measurements. 2004/093339* WO, October 28, 2004.

43. *Assessment on Low Complexity C/No Estimators Based on M-PSK Signal Model for GNSS Receivers.* **Falletti, E, et al.** s.l. : IEEE, 2008. IEEE Position, Location and Navigation Symposium. pp. 167-172.

44. *CN0 Estimation and Near-Far Mitigation for GNSS Indoor Receivers.* **Lopez-Risueno, G and Seco-Granados, G.** s.l. : IEEE, 2005. Vehicular Technology Conference. pp. 2624-2628.

45. **Ledvina, B M, et al.** *Real-Time Software Receiver. 7,010,060* US, March 7, 2006.

46. *The "System of Systems" Receiver: An Australian Opportunity?* **Dempster, A G.** Sydney : Intenational Global Navigation Satellite Systems Society, 2007. International Global Navigation Satellite Systems Symposium.